

UNCLASSIFIED

AD NUMBER	
AD360457	
CLASSIFICATION CHANGES	
TO:	unclassified
FROM:	confidential
LIMITATION CHANGES	
TO:	Approved for public release, distribution unlimited
FROM:	Distribution authorized to U.S. Gov't. agencies and their contractors; Administrative/Operational Use; 03 MAY 1965. Other requests shall be referred to Defense Atomic Support Agency, Washington, DC 20301.
AUTHORITY	
SECDEF Memo. dtd 2 Aug 1960; DNA ltr dtd 15 Nov 1984	

THIS PAGE IS UNCLASSIFIED

UNCLASSIFIED

AD NUMBER
AD360457
CLASSIFICATION CHANGES
TO
confidential
FROM
secret
AUTHORITY
31 May 1977, Group-3, DoDD 5200.10, per document marking

THIS PAGE IS UNCLASSIFIED

# UNCLASSIFIED

---

*Reproduced  
by the*

ARMED SERVICES TECHNICAL INFORMATION AGENCY  
ARLINGTON HALL STATION  
ARLINGTON 12, VIRGINIA



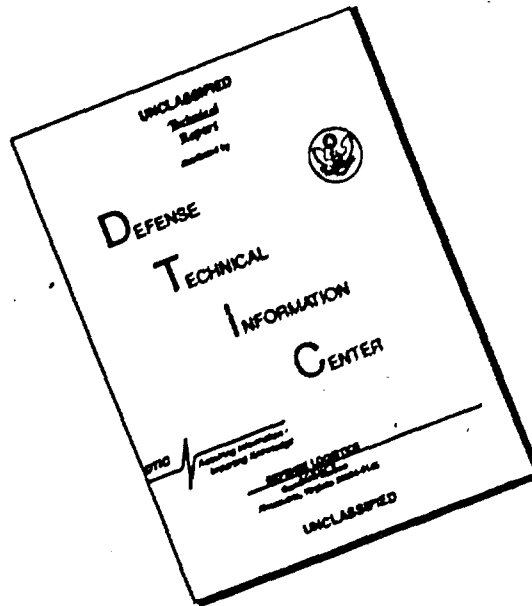
CLASSIFICATION CHANGED  
TO UNCLASSIFIED  
FROM CONFIDENTIAL  
PER AUTHORITY LISTED IN

SEC. OF DEFENSE MEMO. 2 AUG. 60

---

# UNCLASSIFIED

# DISCLAIMER NOTICE



THIS DOCUMENT IS BEST QUALITY AVAILABLE. THE COPY FURNISHED TO DTIC CONTAINED A SIGNIFICANT NUMBER OF PAGES WHICH DO NOT REPRODUCE LEGIBLY.

~~SECRET~~

AD 3 6 0 4 5 7

# DEFENSE DOCUMENTATION CENTER

FOR

SCIENTIFIC AND TECHNICAL INFORMATION

CAMERON STATION, ALEXANDRIA, VIRGINIA



~~SECRET~~

NOTICE: When government or other drawings, specifications or other data are used for any purpose other than in connection with a definitely related government procurement operation, the U. S. Government thereby incurs no responsibility, nor any obligation whatsoever; and the fact that the Government may have formulated, furnished, or in any way supplied the said drawings, specifications, or other data is not to be regarded by implication or otherwise as in any manner licensing the holder or any other person or corporation, or conveying any rights or permission to manufacture, use or sell any patented invention that may in any way be related thereto.

NOTICE:

THIS DOCUMENT CONTAINS INFORMATION  
AFFECTING THE NATIONAL DEFENSE OF  
THE UNITED STATES WITHIN THE MEAN-  
ING OF THE ESPIONAGE LAWS, TITLE 18,  
U.S.C., SECTIONS 793 and 794. THE  
TRANSMISSION OR THE REVELATION OF  
ITS CONTENTS IN ANY MANNER TO AN  
UNAUTHORIZED PERSON IS PROHIBITED  
BY LAW.

360457

CATALOGED BY: DDC

*Operation*

**DOMINIC**

**SH BOWL SERIES**

PROJECT OFFICERS REPORT—PROJECT 6.12

**BACK SATELLITE PACKAGES (U)**

**SECRET**

POR-2031  
(WT-2031)

This document consists of 270 pages  
No. 144 of 276 copies, Series A

DDC  
MAY 25 1965  
TISIA. A

**R. A. Bena, Captain, USAF,  
Project Officer**

Air Force Cambridge Research  
Laboratories  
Bedford, Massachusetts

GROUP-3  
Downgraded at 12 year intervals;  
Not automatically declassified.

This material contains information affecting  
the national defense of the United States  
within the meaning of the espionage laws  
Title 18, U. S. C., Secs. 793 and 794, the  
transmission or revelation of which in any  
manner to an unauthorized person is pro-  
hibited by law.

Qualified requesters may obtain copies of  
this report from DDC.

Issuance Date: May 3, 1965

52185

**SECRET**

Inquiries relative to this report may be made to

Director, Defense Atomic Support Agency  
Washington, D. C. 20301

When no longer required, this document may be  
destroyed in accordance with applicable security  
regulations.

DO NOT RETURN THIS DOCUMENT



SECRET

POR-2031  
(WT-2031)

OPERATION DOMINIC

FISH BOWL SERIES

PROJECT OFFICERS REPORT — PROJECT 6.12

PIGGYBACK SATELLITE PACKAGES (U)

Qualified requesters may obtain copies of  
this report from DDC.

GROUP-3  
Downgraded at 12 year intervals;  
Not automatically declassified.

This material contains information affecting  
the national defense of the United States  
within the meaning of the espionage laws  
Title 18, U. S. C., Secs. 793 and 794, the  
transmission or revelation of which in any  
manner to an unauthorized person is pro-  
hibited by law.

R.A. Bena, Captain, USAF,  
Project Officer

K. Baker  
R. Giacconi  
H. Gursky  
H. Hinteregger  
R. Huguenin  
R. McInerney  
M. Papagiannis  
W. Pfister  
R. Sagalyn  
J. Sandock  
J. Ulwick

Air Force Cambridge Research  
Laboratories  
Bedford, Massachusetts

This document is the author(s) report to the Director,  
Defense Atomic Support Agency, of the results of ex-  
perimentation sponsored by that agency during nuclear  
weapons effects testing. The results and findings in  
this report are those of the author(s) and not neces-  
sarily those of the DOD. Accordingly, reference to  
this material must credit the author(s). This report  
is the property of the Department of Defense and, as  
such, may be reclassified or withdrawn from circula-  
tion as appropriate by the Defense Atomic Support  
Agency.

DEPARTMENT OF DEFENSE  
WASHINGTON, D.C. 20301

3-4

SECRET

SECRET

POR-2031  
(WT-2031)

OPERATION DOMINIC  
FISH BOWL SERIES

PROJECT OFFICERS REPORT — PROJECT 6.12

PIGGYBACK SATELLITE PACKAGES (U)

R.A. Bena, Captain, USAF,  
Project Officer

K. Baker  
R. Giacconi  
H. Gursky  
H. Hinteregger  
R. Huguenin  
R. McInerney  
M. Papagiannis  
W. Pfister  
R. Sagalyn  
J. Sandock  
J. Ulwick

Air Force Cambridge Research  
Laboratories  
Bedford, Massachusetts

Qualified requesters may obtain copies of  
this report from DDC.

GROUP-3  
Downgraded at 12 year intervals;  
Not automatically declassified.

This material contains information affecting  
the national defense of the United States  
within the meaning of the espionage laws  
Title 18, U. S. C., Secs. 793 and 794, the  
transmission or revelation of which in any  
manner to an unauthorized person is pro-  
hibited by law.

This document is the author(s) report to the Director,  
Defense Atomic Support Agency, of the results of ex-  
perimentation sponsored by that agency during nuclear  
weapons effects testing. The results and findings in  
this report are those of the author(s) and not neces-  
sarily those of the DOD. Accordingly, reference to  
this material must credit the author(s). This report  
is the property of the Department of Defense and, as  
such, may be reclassified or withdrawn from circula-  
tion as appropriate by the Defense Atomic Support  
Agency.

DEPARTMENT OF DEFENSE  
WASHINGTON, D.C. 20301

3-4

SECRET

## ABSTRACT

The purpose of the measurements proposed by Project 6.12 was to investigate the spread of fission debris around the globe and its effects on ionization and radio noise.

It was assumed that for the high-altitude shot the fission debris would expand from the detonation point until it was stopped either by the magnetic containment or, in the case of downward-moving debris, by the denser air, causing ionization. A high content of atomic ions is formed in this way around 200 km in height and, due to the low recombination rate, is only slowly removed. The fission products eventually spread around the earth and, if charged, will form a belt. Another belt produced by the trapped fission betas is formed even faster. This belt was expected to emit synchrotron noise.

To make these measurements of the world-wide and long-time effects, Discoverer satellites were instrumented with specially designed research packages.

Because of the difficulties and schedule slippages encountered in attempting the nuclear detonations, this project was not able to obtain data during the time of primary interest. Although the four Discoverer satellites instrumented by Project 6.12 were successfully orbited, they were not operational at the time of the detonation. However, all data transmitted by the satellites will be of interest in defining the ambient conditions prior to the detonation.

## CONTENTS

ABSTRACT-----	5
CHAPTER 1 SATELLITE DESIGN AND OPERATION -----	13
CHAPTER 2 FLUX METERS -----	28
2.1 Objective -----	28
2.2 Background and Theory-----	29
2.3 Instrumentation-----	33
2.4 Data Requirements-----	35
2.5 Results -----	35
2.5.1 Geographic Distribution of Data -----	39
2.5.2 Geomagnetic Distribution Data-----	39
2.5.3 Pitch Angle Distribution of Radiation -----	41
2.6 Discussion -----	42
2.7 Conclusions and Recommendations -----	45
CHAPTER 3 IMPEDANCE PROBE -----	63
3.1 Objective -----	63
3.2 Background and Theory-----	63
3.3 Instrumentation-----	64
3.4 Data Requirements-----	67
3.5 Results -----	68
3.6 Discussion -----	69
3.7 Conclusions -----	74
CHAPTER 4 RADIOMETERS -----	95
4.1 Objective -----	95
4.2 Background and Theory-----	96
4.3 Instrumentation-----	99
4.4 Data Requirements-----	102
4.5 Results -----	102
4.5.1 Flight Test Vehicle 1127 Data -----	102
4.5.2 Flight Test Vehicle 1128 Data -----	103
4.5.3 Flight Test Vehicle 1129 Data -----	104
4.6 Discussion -----	107
4.6.1 Flight Test Vehicle 1127-----	107
4.6.2 Flight Test Vehicle 1128-----	108
4.6.3 Flight Test Vehicle 1129-----	109
4.7 Conclusions -----	112
4.7.1 Flight Test Vehicle 1127-----	112
4.7.2 Flight Test Vehicle 1128-----	112

4.7.3 Flight Test Vehicle 1129-----	113
4.7.4 General Conclusions -----	116
CHAPTER 5 ION TRAP PROBE -----	154
5.1 Objective -----	154
5.2 Background and Theory-----	154
5.2.1 Mode I-----	155
5.2.2 Mode II -----	157
5.2.3 Mode III-----	157
5.3 Instrumentation-----	158
5.3.1 Mode I-----	159
5.3.2 Mode II -----	159
5.3.3 Mode III-----	1
5.4 Data Requirements-----	1
5.5 Results -----	162
5.5.1 FTV 1127 Results -----	163
5.5.2 FTV 1128 Results -----	164
5.5.3 FTV 1129 Results -----	165
5.6 Discussion -----	168
5.7 Conclusions and Recommendations -----	169
CHAPTER 6 RETARDING-POTENTIAL ANALYZER -----	184
6.1 Objective -----	184
6.2 Background and Theory -----	185
6.3 Instrumentation-----	187
6.4 Data Requirements-----	190
6.5 Results -----	192
6.6 Discussion -----	197
6.7 Conclusions -----	199
CHAPTER 7 SUMMARY AND CONCLUSIONS -----	219
APPENDIX A ENGINEERING CHANGE PROPOSAL TO INCORPORATE "N" PAYLOADS INTO DISCOVERER SYSTEM-----	221
APPENDIX B CHECKOUT TEST PROCEDURES -----	230
APPENDIX C "N" DETECTOR PAYLOAD COMMAND SYSTEM CONCEPT -----	247
APPENDIX D INSTRUMENTATION SCHEDULE, FTV 1127 -----	253
REFERENCES-----	267
TABLES	
1.1 Satellite Operational Summary-----	17
2.1 Tabulation of Significant Data-----	47
2.2 Simultaneous Comparison of Beta-1, Beta-2 Sensors-----	55
3.1 Impedance Probe Commutator Assignments, Ring B -----	75

4.1 FTV 1128 Real Time Data -----	119
4.2 FTV 1129 Real Time Data -----	120
5.1 Digitizing Rates for Ion Trap Probe -----	161
6.1 Sensor Element Voltages as Function of Mode and Measurement Number-----	201
6.2 Telemetry Pin Assignments for Retarding-Potential Analyzer-----	202
6.3 Quick-Look Segments for Retarding-Potential Analyzer -----	203
6.4 Tape Format for Retarding-Potential Analyzer -----	203

## FIGURES

1.1 Research module -----	23
1.2 Research module mounted on Agena vehicle -----	24
1.3 In-flight boom and antenna configuration -----	25
1.4 FTV 1127 magnetometer data-----	26
1.5 FTV 1129 magnetometer data-----	27
2.1 Exploded view of radiation experiment-----	56
2.2 Block diagram of radiation experiment -----	57
2.3 Simultaneous playback signal from Beta-1 and Beta-2 lower level discriminators -----	58
2.4 Geographic distribution of observed radiation-----	59
2.5 B-L distribution of observed radiation-----	60
2.6 Magnetic reference system -----	61
2.7 Pitch angle distribution, L = 2 shell -----	62
3.1 Block diagram of impedance probe experiment -----	76
3.2 Satellite antenna network-----	77
3.3 Summary of FTV 1129 data -----	78
3.4 5-Mc result, FTV 1127-----	79
3.5 14.5-Mc result, FTV 1127-----	80
3.6 Orbit 55, 14.5-Mc results, KTS, Orbit 58 readout-----	81
3.7 Orbit 74, 5-Mc results, NHTS, Orbit 77 readout-----	82
3.8 Orbit 78, 5-Mc results, KTS, Orbit 80 readout-----	83
3.9 Orbit 95, 5-Mc results, HTS, Orbit 97 readout-----	84
3.10 Orbit 105, 5-Mc results, VAFB, Orbit 153 readout -----	85
3.11 Orbit 177, 5-Mc results, VAFB, Orbit 185 readout -----	86
3.12 Orbit 193, 5-Mc results, VAFB, Orbit 208 readout -----	87
3.13 Orbit 194, 5-Mc results, KTS, Orbit 208 readout -----	88
3.14 Orbit 209, 5-Mc results, HTS, Orbit 210 readout -----	89
3.15 Orbit 212, 5-Mc results, NHTS, Orbit 215 readout -----	90
3.16 Orbit 215, 5-Mc results, VAFB, Orbit 217 readout -----	91
3.17 Orbit 217, 5-Mc results, KTS, Orbit 219 readout -----	92
3.18 Orbit 225, 5-Mc results, HTS, Orbit 226 readout -----	93
3.19 Orbit 228, 5-Mc results, VAFB, Orbit 231 readout -----	94
4.1 Diurnal spectrum of atmospherics -----	122
4.2 Block diagram for SRP MkIc radiometer -----	123
4.3 Welded module for MkIc radiometer -----	124
4.4 MkIc radiometer package, FTV 1127, FTV 1128, and FTV 1129 -----	124
4.5 Yeiser Type A tape antenna -----	124
4.6 Ambient temperature history, FTV 1128 radiometer package -----	125
4.7 Tape-recorded data, Orbit 61, NHTS, FTV 1128-----	126

4.8	Tape-recorded data, Orbit 63, VAFB, FTV 1128 -----	127
4.9	Tape-recorded data, Orbit 65, HTS, FTV 1128-----	128
4.10	Satellite reception of ground transmitters-----	129
4.11	Ambient temperature history, FTV 1129 radiometer package-----	130
4.12	5-second oscillations on 4.010 Mc only, FTV 1129, Rev. 185, VAFB ---	131
4.13	5-second oscillations on both 4.010 and 6.975 Mc, FTV 1129, Rev. 231, VAFB -----	132
4.14	Tape-recorded data, Orbit 185, VAFB, FTV 1129-----	133
4.15	Polar plot of 4.010- and 6.975-Mc data for Orbit 185, VAFB, FTV 1129--	135
4.16	Tape-recorded data (averages), seven orbits, FTV 1129, 4.010 Mc ----	136
4.17	Tape-recorded data (averages), seven orbits, FTV 1129, 6.975 Mc ----	137
4.18	Tape-recorded data (averages), Orbit 77, NHTS, FTV 1129 -----	138
4.19	Tape-recorded data (averages), Orbit 80, KTS, FTV 1129 -----	139
4.20	Tape-recorded data (averages), Orbit 97, HTS, FTV 1129 -----	140
4.21	Tape-recorded data (averages), Orbit 153, VAFB, FTV 1129 -----	141
4.22	Tape-recorded data (averages), Orbit 185, VAFB, FTV 1129 -----	142
4.23	Tape-recorded data (averages), Orbit 208, KTS and VAFB, FTV 1129 --	143
4.24	Tape-recorded data (averages), Orbit 210, HTS, FTV 1129-----	144
4.25	Tape-recorded data (averages), Orbit 215, NHTS, FTV 1129-----	145
4.26	Tape-recorded data (averages), Orbit 217, VAFB, FTV 1129 -----	146
4.27	Tape-recorded data (averages), Orbit 219, KTS, FTV 1129-----	147
4.28	Tape-recorded data (averages), Orbit 226, HTS, FTV 1129-----	148
4.29	Tape-recorded data (averages), Orbit 231, NHTS, FTV 1129-----	149
4.30	Tape-recorded data, Orbit 9, VAFB, FTV 1127 -----	150
4.31	Discontinuities in the ephemeris, FTV 1129, (latitude)-----	151
4.32	Discontinuities in the ephemeris, FTV 1129, (altitude)-----	152
4.33	Local time of the south-north equator crossing, FTV 1129 -----	153
5.1	Block diagram of ion trap experiment -----	170
5.2	FTV 1127, Orbits 2, 3, and 4, VAFB, recorder playback data -----	171
5.3	FTV 1127, sensor current versus sweep voltage-----	173
5.4	FTV 1128, Orbit 65, VAFB, recorder playback data -----	174
5.5	FTV 1129, Orbits 177 and 178, VAFB, recorder playback data -----	175
5.6	FTV 1129, Orbit 97, HTS, recorder playback data -----	177
5.7	Voltage versus time, Orbit 77, FTV 1129 -----	178
5.8	Ion density versus time, Orbit 77, FTV 1129 -----	179
5.9	FTV 1129, Sensor 1, current versus sweep voltage, 1518 hours -----	180
5.10	FTV 1129, Sensor 1, current versus sweep voltage, 2250 hours-----	181
5.11	FTV 1129, Sensor 1, current versus collector voltage -----	182
5.12	FTV 1129, Sensor 2, current versus collector voltage -----	183
6.1	Schematic of retarding-potential analyzer -----	204
6.2	Detector with the antiperturbation shield removed showing the shroud and $V_0$ grid -----	205
6.3	Positions of retarding-potential analyzer detectors -----	206
6.4	Scale drawing of retarding-potential analyzer detector-----	206
6.5	Sample of Mode I measurement, 81.07 seconds-----	207
6.6	Sample of Mode I measurement, 125.66 seconds -----	208
6.7	Sample of Mode II measurement, 4.54 seconds -----	209
6.8	Sample of Mode II measurement, 77.875 seconds-----	210
6.9	Sample of Mode II measurement, 129.951 seconds -----	211
6.10	Total Mode II measurements -----	212

6.11	Sample of Mode III measurement, 20,516 seconds -----	213
6.12	Sample of Mode III measurement, 0430 hours -----	214
6.13	Sample of Mode III measurement, 0340 hours -----	215
6.14	Sample of Mode III measurement, 1605 hours -----	216
6.15	Total Mode III measurements -----	217
6.16	Comparison of retarding-potential analyzer and impedance probe data--	218



# SECRET

## CHAPTER 1

### SATELLITE DESIGN AND OPERATION

Discoverer satellites were programmed as the instrument carriers for Project 6.12. These satellites are two-stage vehicles which use a Thor as a booster and an Agena rocket as the second stage. The entire second-stage vehicle is placed into orbit. Discoverers were launched from Vandenberg Air Force Base, California, into nearly-circular polar orbits between 200 and 400 km in height.

The following Discoverer satellites were used for this project:

Flight Test Vehicle 1128 launched 30 May 62

Flight Test Vehicle 1127 launched 2 June 62

Flight Test Vehicle 1129 launched 22 June 62

Flight Test Vehicle 1151 launched 27 June 62

Launch dates were coordinated with JTF-8.

The instrumentation for Project 6.12 was mounted on a research module (Figure 1.1) which was then installed on the aft end of the Agena vehicle (Figure 1.2). This module was referred to as the "N" payload by the system contractor — Lockheed Missile and Space Company (LMSC) (Appendix A). After injection into orbit, the payload sensor booms and antennas were extended (Figure 1.3).

Originally three sets of research instrumentation were built—two for flight and one as a spare. The spare instruments were con-

GROUP 3

Downgraded at 12 year intervals; not  
automatically declassified

# SECRET

verted to a flight set, since they were not needed as backups for the first two flights. Because of the tight equipment delivery schedule, it was not possible to install one of the instruments (retarding-potential analyzer) on the third vehicle (1129). The fourth vehicle (1151) was added to the schedule at a later date and did not contain the retarding-potential analyzer or the synchrotron-noise experiment. The check-out test procedures for the instrumented payload are described in Appendix B.

The lifetime of the instrumentation on satellites of this type is limited by either the available power of the batteries or by the actual lifetime of the satellite in orbit before it decays and re-enters the atmosphere.

The power available to the research instrumentation was supplied by a small battery pack and augmented by some excess battery power from the main vehicle supply. This excess power available to the instrumentation payload varied on each satellite, depending upon the power requirements of the primary mission of the Discoverer. In order to conserve battery power, the payloads remained in an inactive mode until turned on by a command receiver system. Selected ground transmitting sites had this command capability. During the period of the inactive operation, some limited data acquisitions were made to check the status of the equipment. Active

or full-time operation of the instrumentation was planned to be initiated 24 hours prior to the scheduled nuclear event in order to obtain world-wide ambient conditions. For a typical operation, a 21-day inactive mode followed by a 6-day active mode was planned. Vehicle 1151 did not have the command capability and performed in active mode for only 56 hours after launch.

The data was recorded on magnetic tape on the satellite with readouts on command at three different ground recording stations (Hawaii, Vandenberg, and New Boston). The commutator for both the tape-recorded and real-time data was a multiple-ring type (Ring A and Ring B). Each ring had 60 points, making a total of 120 informational segments available. The concept of the payload operation and command system is explained in Appendix C. The instrumentation schedule for vehicle 1127 is contained in Appendix D. The instrumentation schedules for other vehicles are similar.

It was planned for the satellite to explore both the pancake region and the trapped-radiation belt many times during its active lifetime. Unfortunately, this objective was not attained. The last satellite (1129) ceased operation on 7 July 62, and the first success in the launch and detonation of the nuclear device took place on 8 July 62.

Figures 1.4 and 1.5 show the output in milligauss as a function of latitude for the X, Y, and Z magnetometers as well as the total field for selected orbits for vehicles 1127 and 1129, respectively. The results for vehicle 1127 are typical for a stabilized vehicle. The results for vehicle 1129, however, show the effects of tumbling. From this data it is noted that there is a good correlation between maximums and minimums of the total field and the latitude. Utilizing this fact it will be possible to obtain a correspondence between geographic position and data in the absence of clock data (as in the case of vehicle 1128). In addition, it will be possible, utilizing the magnetometer data, to determine the aspect of the vehicles.

The operational summary of the four satellites is shown in Table 1.1.

TABLE 1.1 SATELLITE OPERATIONAL SUMMARY

FTV 1128


---

Launch date	30 May 62
Period (minutes)	90.06
Perigee (NM)	104.3
Apogee (NM)	196.0
Inclination (degrees)	74.16
Real-Time Acquisitions (number)	34
Tape-Recorder Acquisitions (number)	29
Real-Time Data (hours)	1.85
Tape-Recorder Data (hours)	11.28
Total Data (hours)	13.13
Last Active Pass	143

FTV 1128 was the first of the N-detector series payloads to be launched. The data received was in the form of digital plots, also referred to as "quick-look strip-charts." These are the telemetry-voltage outputs in a thinned-out form, used mainly to evaluate the performance of the payload and the quality of the data obtained. Subsequently, the satisfactory data is reduced by a computer to the final form (whatever each experiment is set to measure) with the help of preflight calibrations of each payload. The data summary is as follows:

FTV	Flight Test Vehicle
VAFB	Vandenberg Air Force Base
NHTS	New Hampshire (New Boston) Tracking Station
HTS	Hawaii Tracking Station
KTS	Kodiak (Alaska) Tracking Station
TTS	Thule (Greenland) Tracking Station

TABLE 1.1 CONTINUED

<u>Real-Time Data</u>								
Orb.	Sta.	Dur.	Orb.	Sta.	Dur.	Orb.	Sta.	Dur.
9	VAFB	6'00"	79	KTS	4'30"	93	NHTS	4'50"
55	NHTS	6'40"	79	VAFB	1'35"	95	TTS	6'55"
58	HTS	6'15"	81	KTS	0'30"	97	HTS	7'00"
61	NHTS	3'15"	81	HTS	6'05"	106	HTS	6'45"
63	VAFB	3'30"	87	NHTS	6'30"	111	VAFB	15"
65	HTS	3'45"	87	TTS	1'35"	129	HTS	3'20"
71	NHTS	5'10"	89	VAFB	7'00"	143	VAFB	5'15"
77	NHTS	1'30"	90	HTS	8'50"	157	NHTS	4'35"

<u>Tape-Recorded Data</u>								
Orb.	Sta.	Dur.	Orb.	Sta.	Dur.	Orb.	Sta.	Dur.
9	VAFB	2h 38'	58	HTS	1h 12'	63	VAFB	1h 31'
55	NHTS	2h 53'	61	NHTS	1h 26'	65	HTS	1h 37'

One hour and 52 minutes of real time and 11 hours and seven minutes of tape-recorded quick-look data were received in total from this satellite.

Other pertinent systems performed as follows:

Clock: Inoperative.

Magnetometer: Performed satisfactorily.

Ephemeris: The first 66 orbits are covered every minute. Orbits 67, 68, 69 are not covered at all. Orbits 70-200 are covered every five minutes.

TABLE 1.1 CONTINUED

FTV 1127

Launch date	2 June 62
Period (minutes)	90.63
Perigee (NM)	114.9
Apogee (NM)	224.0
Inclination (degrees)	74.26
Real-Time Acquisitions (number)	1
Tape-Recorder Acquisitions (number)	1
Real-Time Data (hours)	0.12
Tape-Recorder Data (hours)	3.2
Total Data (hours)	3.32
Last Active Pass	8

The active life of FTV 1127 was ended prematurely by a failure of the satellite power system, and therefore very little data was actually obtained. The data summary is as follows:

<u>Real-Time Data</u>			<u>Tape-Recorded Data</u>		
Orb.	Sta.	Dur.	Orb.	Sta.	Dur.
9	VAFB	7'20"	9	VAFB	3h 12'

Other pertinent systems performed as follows:

Clock: performance satisfactory.

Magnetometer: performance satisfactory.

Ephemeris: Available, covering the first 66 orbits at one-minute intervals.

TABLE 1.1 CONTINUED

---

<u>FTV 1129</u>	
Launch date	22 June 62
Period (minutes)	89.68
Perigee (NM)	113.10
Apogee (NM)	170.0
Inclination (degrees)	75.1
Real-Time Acquisitions (number)	44
Tape-Recorder Acquisitions (number)	44
Real-Time Data (hours)	1.91
Tape-Recorder Data (hours)	25.7
Total Data (hours)	27.61
Last Active Pass	233

FTV 1129 was the last of the fully instrumented N-detector series. Due to the consecutive postponements of Star Fish, FTV 1129 decayed for approximately three days before the high-altitude nuclear explosion.

The data was originally received in the quick-look form (digital plots) and was subsequently reduced to the final form by computer. The data summary is as follows:



TABLE 1.1 CONTINUED

<u>Real-Time Data</u>								
Orb.	Sta.	Dur.	Orb.	Sta.	Dur.	Orb.	Sta.	Dur.
2	HTS	6'20"	113	HTS	3'30"	209	KTS	2'20"
9	VAFB	6'40"	127	VAFB	0'50"	210	HTS	4'40"
55	NHTS	2'30"	129	HTS	4'20"	215	NHTS	1'40"
55	TTS	4'10"	145	HTS	3'20"	217	VAFB	4'10"
58	KTS	4'00"	153	VAFB	7'20"	219	HTS	3'00"
77	NHTS	4'10"	161	HTS	3'30"	221	NHTS	40"
80	KTS	5'30"	169	VAFB	6'40"	222	NHTS	2'50"
97	HTS	3'00"	185	VAFB	6'40"	224	VAFB	2'10"
105	VAFB	6'30"	208	KTS	2'10"	226	HTS	4'00"
111	VAFB	3'00"	208	VAFB	1'50"	231	NHTS	3'10"

<u>Tape-Recorded Data</u>								
Orb.	Sta.	Dur.	Orb.	Sta.	Dur.	Orb.	Sta.	Dur.
58	KTS	2h 07'	185	VAFB	2h 53'	217	VAFB	1h 47'
77	NHTS	2h 04'	208	VAFB	1h 03'	219	KTS	1h 45'
80	KTS	2h 40'	208	KTS	1h 27'	226	HTS	0h 59'
97	HTS	1h 47'	210	HTS	1h 24'	231	VAFB	1h 18'

One hour and 55 minutes of real time and 25 hours and 42 minutes of tape-recorded reduced data were received in total from the FTV 1129 satellite.

TABLE 1.1 CONTINUED

---

Other pertinent systems performed as follows:

Clock: Worked uninterrupted only after the ejecting of the capsule (~orbit 55).

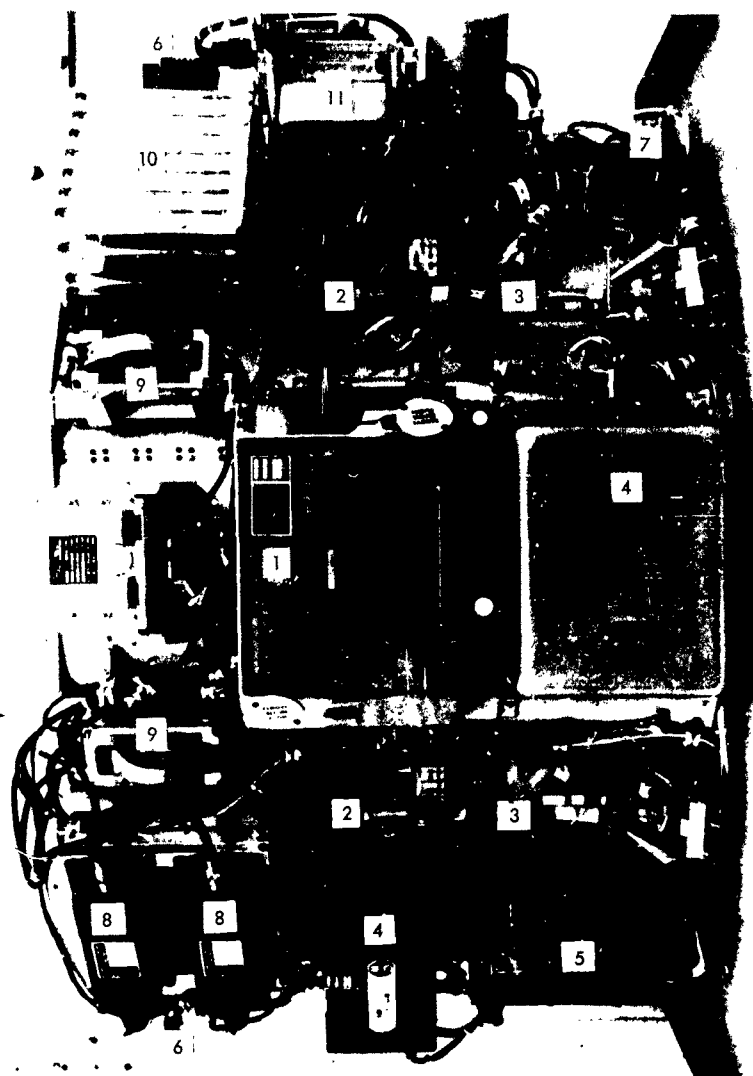
Magnetometer: Performance satisfactory.

Ephemeris: It covers the first 200 orbits at one-minute intervals.  
Orbits over 200 are not covered.

FTV 1151

Launch date	27 June 62
Period (minutes)	93.68
Perigee (NM)	113.0
Apogee (NM)	384.0
Inclination (degrees)	76.06
Real-Time Acquisitions (number)	56
Tape-Recorder Acquisitions (number)	56
Real-Time Data (hours)	3.73
Tape-Recorder Data (hours)	97.0
Total Data (hours)	100.73
Last Active Pass	56

The long delay encountered in obtaining information on this vehicle from the contractor has precluded the inclusion of the results from FTV 1151.



- |  |   |
|--|---|
| 1. Beta-Gamma Detector                 | 6. Impedance Probe Antennas                           |
| 2. Sensor Unit for Ion Trap Probe      | 7. Mounting Bracket for Retarding-Potential Analyzer. |
| 3. Extendible Boom for Ion Trap Sensor | 8. Synchrotron Noise (radiometers)                    |
| 4. Ion Trap Probe Electronics          | 9. Antennas for Synchrotron-Noise Experiment          |
| 5. Impedance Probe                     | 10. Tape Recorder                                     |
|  | 11. System timer                                      |

Figure 1.1 Research module. (AFCRL photo)

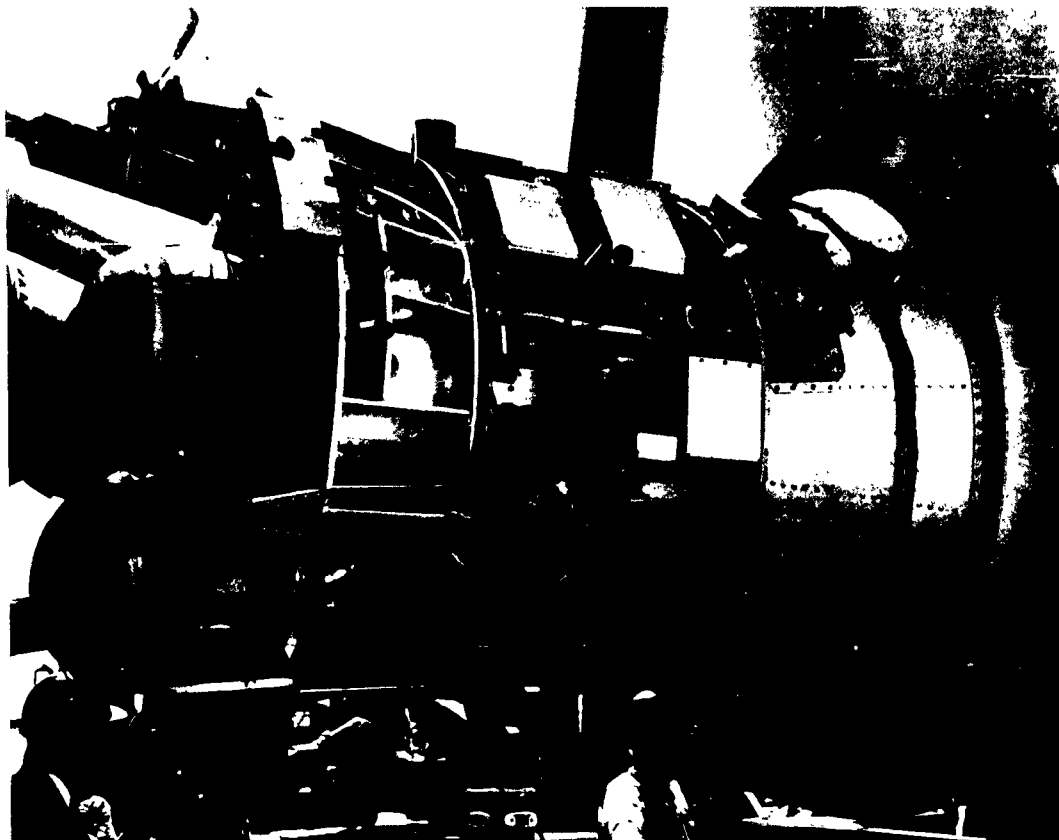
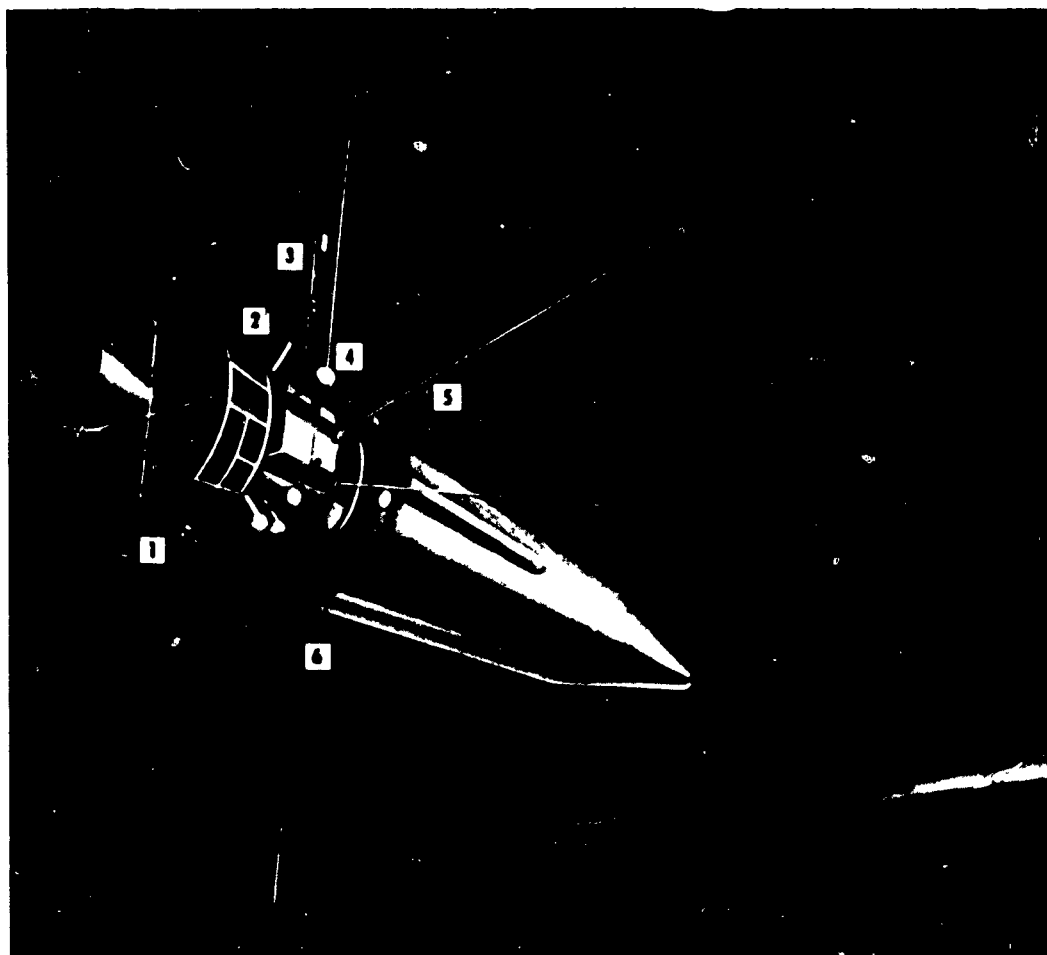


Figure 1.2 Research module mounted on Agena vehicle. (AFCRL photo)



- |                          |                                |
|--------------------------|--------------------------------|
| 1. Aspect Magnetometers  | 4. Ion Trap Sensor (2)         |
| 2. RPA Sensor (2)        | 5. GRF Antenna (2)             |
| 3. Heliflux Magnetometer | 6. Impedance Probe Antenna (2) |

Figure 1.3 In-flight boom and antenna configuration.



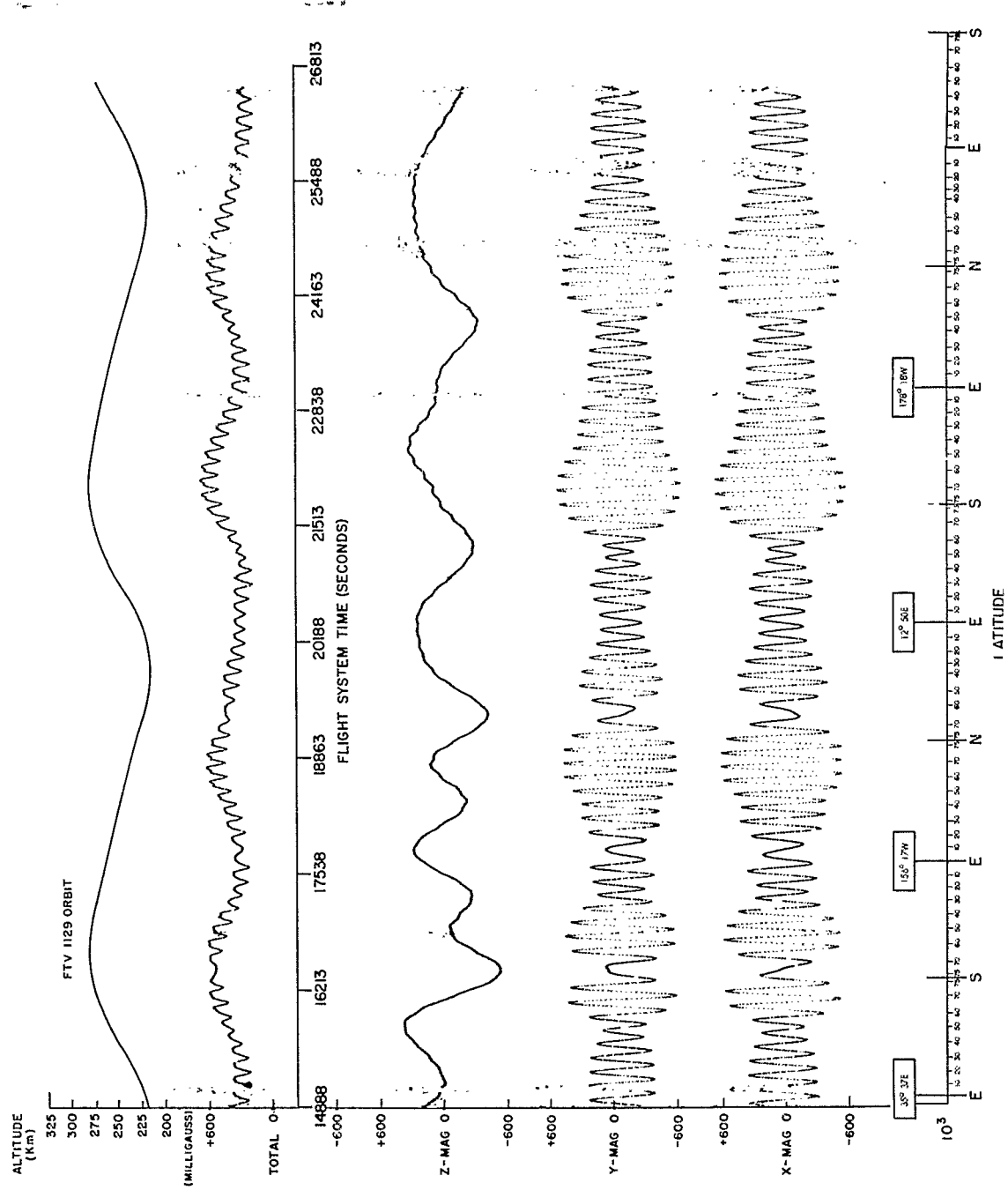


Figure 1.5 FTV 1129 magnetometer data.

## CHAPTER 2

### FLUX METERS

#### 2.1 OBJECTIVE

The objective of this experiment was to perform a world survey from the Discoverer satellite to establish the location of the fission debris and to measure the energetic electrons from fission debris decay produced in the detonations of the Fish Bowl Series. From measurement of the local gamma-ray intensity, the position of the debris pancake could have been determined in successive satellite passes in the vicinity of the test area. This measurement was to be correlated with measurements performed by identical instrumentation carried aloft by rockets flown at the test site. These measurements would have permitted evaluation of the rate of energy deposition in the atmosphere due to gamma rays and electrons from the debris and would have determined the area over which this takes place. These instruments would have measured the intensity, energy spectrum, and pitch angle distribution of the electrons at each passage through the trapped radiation shell. This would have improved the understanding of injection mechanisms and lifetime of the trapped radiation. This knowledge would have, in turn,



contributed to the understanding of the phenomenology of nuclear detonations above the sensible atmosphere.

## 2.2 BACKGROUND AND THEORY

Following the radiative phase of the detonation of a nuclear device, about 25% of the bomb yield remains in the form of hydrodynamic energy of the debris. The debris then expands until brought to rest by the surrounding medium. For lower altitude shots, the fireball and the debris rise and expand. The hydrodynamic streaming of the atmosphere around the fireball causes an upwelling of air at the bottom of the fireball that eventually converts the fireball into a toroid. This interaction imparts a lateral velocity to the fireball and the debris materials and spreads them out horizontally.

The fission debris is, hence, carried to an altitude of about 200 km or more. At these altitudes, beta rays emitted in the upper hemisphere by the radioactive decay of the fission debris can escape the atmosphere. The geomagnetic field will guide these beta rays to the Southern Hemisphere where the majority will be absorbed by scattering in the atmosphere. Those beta rays, which mirror at altitudes above about 200 km, will constitute the trapped fraction of the betas which drift easterly around the earth.

Because of the scattering at these mirror altitudes, the betas may only drift a short distance to the east before they are removed. If the scattering is not too violent, they may drift as far as the South African Anomaly before removal. The beta-ray experiment on the Discoverer satellite would have determined the easterly extension of the trapped shell and, hence, determined the effect which was taking place.

The low atmospheric density in the neighborhood of Shot Star Fish may have permitted the debris to expand to great distances. For example, in the upward direction the major force acting to restrict this expansion is due to the interaction of the charged debris with the geomagnetic field. As a consequence, this expansion may continue until the debris is (1) brought to rest (its energy having been converted to magnetic energy and stored in the compressed field); (2) guided along the magnetic field from the magnetic bottle to the Southern Hemisphere; (3) deionized and its subsequent trajectory determined by the gravitational force and by the position and velocity of the particle at time of deionization. Any additional beta decay of this debris atom will reionize it, and thence its trajectory will be determined by the geomagnetic field; or (4) broken up into separate blobs as the expansion becomes turbulent.

The expansion in the downward direction is controlled principally by the exponentially increasing atmosphere. The debris ions lose energy, probably, in fair agreement with the Bohr-Nielsen theory of range-energy loss of heavy ions. The ions come to rest at an altitude of 100 to 200 km.

In Shot Teak of Operation Hardtack I, the debris pancake extended for hundreds of miles, and the gamma rays and beta rays from fission debris decay produced local ionization in sufficient amount to cause blackout phenomena.

In Shot Star Fish the debris, which expanded in the upward direction, efficiently injected beta rays from the fission debris into the geomagnetic field. A fraction of the electrons from fission debris decay as well as a fraction of the ionized debris can be trapped in the geomagnetic field to form a radiation belt identical to the belt of artificially injected particles from Shots Argus I, II, and III. Decay electrons produced at high altitude in the geomagnetic field spiral along the magnetic field lines and will mirror at an altitude which depends on their pitch angle at injection. Electrons that mirror deep in the atmosphere are lost by scattering and collision, while electrons that mirror sufficiently high in the atmosphere at an altitude greater than about 300 km will have a lifetime in excess of a few minutes. These electrons will drift in

an easterly direction until they form a closed shell around the world. The time for this shell to close is a function of the electron energy. Electrons of 0.5 Mev will, on the average, complete 1 revolution in approximately 1 hour whereas electrons of 2.0-Mev energy will complete 1 revolution in approximately 20 minutes. The ionized debris will drift in a westerly direction and will complete 1 revolution in approximately 1 day.

A polar-orbiting satellite will cross this artificially created belt twice per orbit, provided the orbital altitude is sufficiently high as is the case for the Discoverer satellite, and provided electron and debris injection occurs at a sufficiently high altitude which is the case for Shot Star Fish. It should be emphasized that Shot Star Fish had approximately one thousand times the nominal yield of Shots Argus I, II, and III so that a copious injection of electrons occurred. The shell extended with different lifetimes and intensity from a few hundred kilometers to thousands of kilometers. It was hoped that by measuring the extension of the shell and the characteristics of the radiation composing it, namely, intensity and energy spectra as well as pitch angle distribution at one altitude, it would have been possible to infer the phenomenology of the event as a whole. It was hoped that significant scientific data could have been acquired

which would have furthered the understanding of the dynamics of the distribution of the fission debris in the Van Allen radiation belt.

### 2.3 INSTRUMENTATION

The instrumentation flown on the Discoverer satellite was designed to detect gamma rays and beta rays, both from natural and artificial sources.

As shown in Figures 2.1 and 2.2, the instrument package contained one gamma-ray detector and two beta-ray detectors disposed along perpendicular axes. This geometric configuration will allow rough measurements of angular distributions to be performed and correlated with magnetic aspect.

The beta-ray detector consists of a plastic scintillator which is covered by a thin aluminum shield and is viewed by a ruggedized photomultiplier. The aluminum shield prevents visible light from impinging on the scintillator and establishes a minimum energy for beta rays that enter the scintillator. The chosen thickness of  $6.8 \text{ mg/cm}^2$  corresponds to the practical range of electrons of 70 kev. The thickness of the plastic scintillator, approximately  $0.31 \text{ g/cm}^2$ , corresponds to the practical range of 0.8-Mev electrons, and is therefore sufficient to stop a large fraction of the electrons from debris decay. The detector is exposed to the ambient through a hole in the instrument package.

The field of view of this sensor is approximately 1 steradian. The detector is one hundred and fifty times more sensitive to electrons than to gamma rays. The range of sensitivity of this detector is from approximately  $10$  to  $10^9$  electrons/cm<sup>2</sup> sec.

The pulse rate and the total current from the detector are measured. A two-channel pulse-height analyzer is used to furnish crude spectral information for pulse rates from  $10$  to  $10^5$  pulses/sec. The maximum pulse rate is determined by the fixed dead time of the counter of  $10$   $\mu$ sec. The pulse rates measure the number of pulses of energy greater than the threshold energy.

The current monitor measures the rate of energy deposition in the crystal. It is capable of measuring currents equivalent to energy deposition rates from approximately  $10^4$  Mev/sec to approximately  $10^9$  Mev/sec.

The gamma-ray detector consists of a cesium iodide-thallium activated [CsI(Tl)] crystal scintillator of approximately 4-g weight covered by a 0.3-g/cm<sup>2</sup> aluminum shield and viewed by a ruggedized photomultiplier. This detector is embedded in a foaming compound which is used to support the various components in the instrument package. The detector is therefore shielded from the ambient by composite materials roughly equivalent to at least 2 g/cm<sup>2</sup> of aluminum. This scintillator is therefore

relatively insensitive to electrons of energy lower than a few Mev. The detector is sensitive to gamma rays of energy greater than about 100 kev over  $4\pi$  steradians. The range of sensitivity of this detector is from approximately  $10$  to  $10^9$  gamma rays/cm<sup>2</sup> sec. This dynamic range is obtained, as in the case of the electron detectors, by use of pulse and current measurements.

#### 2.4 DATA REQUIREMENTS

The data from this experiment was furnished to a commutator wired in accordance with Inter-Range Instrumentation Group (IRIG) standard. This allows decommutation and digital presentation of the data received by ground stations and stored on magnetic tape. Processing of these tapes will provide: (1) analog quick-look data; (2) analog decommutated data; (3) tabulated digital decommutated data; (4) trajectory data; and (5) magnetic aspect data. It is understood that full orbit data will be furnished by use of a magnetic tape recorder provided by the payload integrator.

#### 2.5 RESULTS

Of the instruments flown in this program, only two—those flown on satellites 1128 and 1129—have yielded data that has been reduced at this time. One acquisition from an instrument on vehicle 1127 was obscured by light leaks in our sensors. Of the remaining flights, only limited data was received because of various combinations of failures in the satellite system and in our instruments and has not yet been

reduced. On 1151, indications are that our equipment malfunctioned shortly after the beginning of the flight.

The nature of this data is shown in Figure 2.3 which is a reproduction of the analog record received from two of the sensors during a pass over the Hawaii tracking station. The data was telemetered back from the on-board tape recorder and represents the record of one full orbit. The playback is 26 times faster than the recording time, and the time scale shown in the figure is the elapsed time of the playback. The telemetered signal in volts is logarithmically proportional to the counting rate which is shown on the right-hand scale. The start of the recording was determined to be 23 hr 24 min GMT, and the ephemeris gave the vehicle position to be as noted on the top scale of the figure. As shown, the vehicle was close to the equator at 66°E longitude and moving North at the beginning of the record. Large fluxes of radiation are encountered at the North polar regions and the Equator is again crossed at 105 seconds, this time at 125°W longitude and moving South. Radiation is again recorded in the South polar region, but this time the radiation extends close to the Equator. From 180 to 200 sec the vehicle is crossing the South Atlantic Anomaly which is that region of the Earth where the geomagnetic field is the weakest for any given magnetic latitude. Consistently, in all the data we have received the radiation levels are highest in this region of the world.



The differences in the appearance of the record for the two beta sensors can be ascribed to the fact that the sensors are oriented at right angles with respect to each other and, in general, have different orientations with respect to geomagnetic field. The fine structure which shows up in the data should be ascribed to a modulation induced by the roll of the vehicle causing short-term variations of the angle between the magnetic field and the axis of the sensors. For example, a large peak is evident in Beta-1 at 53 sec, while in Beta-2 peaks appear at 50 and 70 sec. The magnetometer data indicates that the orientation of the magnetic field and the sensor (pitch angle) changes in the following manner.

t = 50 sec	$\theta B-1 = 30^\circ$	flux = 300	counts/sec
	$\theta B-2 = 81^\circ$	flux = $6 \times 10^3$	counts/sec
t = 53 sec	$\theta B-1 = 82^\circ$	flux = $7 \times 10^3$	counts/sec
	$\theta B-2 = 20^\circ$	flux = 300	counts/sec
t = 57 sec	$\theta B-1 = 15^\circ$	flux = 600	counts/sec
	$\theta B-2 = 82^\circ$	flux = 2300	counts/sec

Where the peaks occur the magnetic field is nearly normal to the sensor, and the flux values are minimum when the field is most nearly along the sensor axis. At times when  $\theta B-1 = \theta B-2$ , the flux levels in the two sensors are equal. Similarly throughout the data the observations indicate that particles are most abundant at  $90^\circ$  pitch angles and least abundant at  $0^\circ$  pitch angles.

The gamma sensor did not respond significantly during any of the records and has not been included in any of the data reduction in this report. The real-time records do not generally show the presence of any radiation, since they are mostly acquired from low-latitude stations. These records have not been included in the results of this report.

The above description of a single data record indicates how the data is analysed; namely, according to its distribution in geographic coordinates, the pitch angle distribution of the radiation, and the distribution in B-L coordinates. The latter, a magnetic coordinate system introduced by McIlwain<sup>1</sup>, depends on particles being trapped in a magnetic shell. The quantity B is just the magnitude of the magnetic field. The advantage of the B-L representation is that on a given L shell the flux of trapped radiation should be a function only of B and should not depend on geographic coordinates.

The analysis of the data utilizes not only the record of the sensors as shown in Figure 2.3, but simultaneous magnetometer readings and various monitors, as well as accurate timing and ephemeris information. For vehicle 1128 the on-board clock failed, and the timing information was obtained by utilizing magnetometer data and knowledge of the vehicle command system, as well as the sensor data itself. For vehicle 1127 some of the timing is inaccurate because of erratic behavior of the clock.

#### 2.5.1 Geographic Distribution of Data.

The geographic distribution of data from vehicle 1129 is shown in Figure 2.4 and listed in Table 2.1. The data from 1128 has not been incorporated into this data reduction, since for that vehicle we do not have the timing information necessary to correlate the data with the ephemeris. The 1128 data is listed in Table 2.1 but only as a function of tape time. Each point is the geographic position of a maximum that appears on the data as well as the recorded flux level. The North data appears along a line that lies between 60 and 70° latitude; in the South the data is more spread out in latitude except in the region of the South Atlantic Anomaly centered at 0° longitude.

The data represents the accumulation from fourteen acquisitions of vehicle 1129 and not all regions of the Earth were observed, explaining some gaps in the data. Some of the gaps are probably real; for example, in the North between 80E and 80W longitude, and in the South, there is a significant slot between 50° and 70°S latitude around 0° longitude. The absence of any recorded flux between 30°S and 50°N is quite real. This distribution will become more understandable following the next discussion.

#### 2.5.2 Geomagnetic Distribution Data.

The accumulated data from vehicle 1129 has been correlated with the local B-L parameters where significant flux levels are recorded. This data is plotted in Figure 2.5. Since calculation of B and L depend on knowledge of geographic coordinates, it has not been

possible to make this correlation for the data from vehicle 1128. Because of the time resolution in the available data and uncertainties in the ephemeris, it has not been possible to assign L designations more exactly than shown; namely,  $L=2, 4, 5$ . Flux levels are plotted for every opportunity; that is, the absence of radiation is recorded as well as its presence. On a given pass the satellite will cross an L shell four times, although at different B values. The general features of these curves can be understood by reference to the  $L = 2$  curve. At B greater than 0.4 gauss the bulk of the observations indicate that little, if any, radiation is present (the threshold of the detectors is about 300 counts/second). At B less than 0.35 gauss the observations indicate that the counting rate rises very sharply as B continues to decrease. In terms of trapped radiation this indicates that the particles in the  $L = 2$  shell have such pitch angle distribution that the bulk of them mirror at B values of 0.35 gauss and less; in fact, it would seem that most of the distribution has mirrored at  $B = 0.3$  gauss. In the  $L = 4$  shell, there seems to be a component of trapped radiation at B less than about 0.45 gauss, at least at B greater than 0.45 about half the observations indicate little flux. In the  $L = 5$  shell, there seems to be no clear indication of trapped and untrapped radiation.

It should be noted that much of the observed scatter may be due to inaccurate ephemeris data which places observations at an incorrect B-L position. Also, there can be considerable structure within what we call  $L = 4$  or 5.

### 2.5.3 Pitch Angle Distribution of Radiation.

It should be noted that the magnetometers allow fixing the orientation of the sensors with respect to the Earth's magnetic field, but not with respect to the Earth itself. It is possible, depending on the location, to ascribe up or down to the sensors or North or South. Assuming that the radiation which we measure are charged particles, the only angular distributions allowable are symmetric with respect to the magnetic field, i. e., charged particles spiral around the field and can move along the field. The geometry is shown in Figure 2.6. The sensor is shown making an angle  $\theta$  with respect to the magnetic field. It will detect charged particles whose plane of spiraling makes the same angle  $\theta$  with respect to the field, but independent of the azimuth of the particle around B. The angle  $\theta$  is the pitch angle. It has been possible to make correlations with the magnetic field for that portion of the 1128 data where we have the complete magnetometer record and data from both beta sensors. The angular distribution of some of the  $L = 2$  shell data is shown in Figure 2.7 which shows that the bulk of the radiation is at large angles with respect to the magnetic field. Considerably more data must be reduced before an accurate distribution can be obtained. The large field of view of the detectors ( $90^\circ$  total) causes a spread in the data, and other variables must be considered; namely, the value of B at the observation point and within the  $L = 2$  shell.

The distinction between large and small pitch angles is more obvious when simultaneous data from the two beta sensors is noted as is done in Table 2.2. In this way gross time variations are eliminated as well as the effect of crude resolution in L and B. In every case where this comparison is possible significantly higher flux levels are encountered when the sensors are at large angles with respect to the magnetic field than at small angles.

## 2.6 DISCUSSION

The results noted above give a fairly clear, if not yet detailed, picture of the radiation levels at from 250 - 350 km above the Earth's surface. By radiation we mean electrons with energies greater than 100 kev. The beta sensors utilized three modes of measurements; lower level discriminator, counting pulse corresponding to particles of energy greater than 0.5 Mev; upper level discriminator corresponding to particles of energy greater than 1 Mev; and log current monitor which measured the total energy deposited in the crystal. The minimum energy particle to which the sensor was sensitive was determined by the entrance window of the scintillation crystal. For electrons the minimum energy was about 100 kev and for protons about 1 Mev. The response of the sensors in these three modes indicates that the bulk of this radiation is electrons since the lower level discriminator is typically some ten times greater than the upper level discriminator rate; if protons were present in great number the two modes should indicate approximately the same pulse rate.

Electron fluxes are observed with a maximum intensity of about  $10^4 \text{ sec}^{-1} \text{ cm}^{-2} \text{ sterad}^{-1}$  between  $60^\circ - 70^\circ$  latitude, both North and South corresponding to  $L = 4$  to  $L = 5$ . Additional radiation is observed at lower latitude in the South extending from about  $40^\circ \text{W}$  to  $40^\circ \text{E}$  longitudes corresponding to the  $L = 2$  shell. The angular distribution is one in which the bulk of the radiation makes large angles with respect to the magnetic field lines. These results are similar to ones reported by other groups with instruments on similar satellites. 2, 3, 4.

The angular distributions suggest that much of the radiation we measured is trapped at least for times comparable to period of measurement; however, most of the radiation observed in the  $L = 4$  and the  $L = 5$  shells cannot be trapped for any long period of time. We can consider the extreme case that all the radiation we measure is reflected at the altitude (250-300 km) of the observation. This radiation then reflects again in the opposite hemisphere at about the same longitude and at an altitude corresponding to the same magnetic field. This process cannot go on indefinitely, since inhomogeneities in the magnetic field cause particles to drift East or West in longitude depending on the sign of the charge. Electrons of 0.5 Mev in the  $L = 4$  or 5 shells will drift completely around the Earth in about 20 minutes, always mirroring at the same magnetic field value. Thus, at that part of the Earth where the field is strong, particles tend to mirror at higher altitudes than at the part of the Earth where the field is weak. The minimum altitude to

which particles can descend during this drift and still not be absorbed in the atmosphere is between 100 - 200 km. Particles mirroring at these altitudes in the South Atlantic where the Earth's field is a minimum will mirror at high altitudes elsewhere. This explains the presence of radiation in the  $L = 2$  shell occurring only near the South Atlantic Anomaly at other parts of the Earth the same radiation mirrors at considerably higher altitudes and is not observed at the satellite.

Conversely, particles mirroring at low altitudes at regions far from the South Atlantic where the field is high will drive farther into the atmosphere as they approach the South Atlantic where the field is low and will be lost. On this basis we can assign a maximum  $B$  value for a given  $L$  such that one can observe no trapped radiation on this  $L$  shell at higher values of  $B$ . This value of  $B$  is just the smallest value of  $B$  observed for a given  $L$  at about 100-km altitude, and it will occur in the South Atlantic. For  $L = 4$ ,  $B_{\max} = 0.38$  gauss, and for  $L = 5$ ,  $B_{\max} = 0.41$  gauss. The  $B$ - $L$  distributions for  $L = 4$  and  $L = 5$  in Figure 2.5 indicate considerable radiation at higher  $B$  values. This radiation must have been lost to the atmosphere within minutes or hours of the observation. The intensity of lost radiation is between  $10^3$  and  $10^4$   $\text{cm}^{-2} \text{sec}^{-1}$ . O'Brien<sup>5</sup> reports losses of about  $10^5$   $\text{cm}^{-2} \text{sec}^{-1}$  between  $L = 4$  and  $L = 5.6$ . O'Brien's measurements were made at 1000 km for electrons of 40 kev. Estimates of losses were made by using the pitch angle distribution of the radiation and indicated considerable radiation loss down to  $L = 2$ . We do not observe these losses at lower altitudes,



but this may be due to a softening of the energy spectrum with a corresponding reduction in flux at 0.5 Mev.

For the  $L = 2$  shell,  $B_{\max} = 0.30$  gauss, and our observed B-L distribution indicates that above 0.3 gauss the radiation fall of very sharply.

It is probably no coincidence that the geographic distribution of radiation which we see, particularly the  $L = 4$  and  $L = 5$  data, coincides closely to the zone of maximum auroral intensity, and the flux levels which the satellite encountered can account for a modest amount of auroral activity. The maximum counting rates observed (about  $10^4 \text{ cm}^{-2} \text{ sec}^{-1}$  of 0.5-Mev electrons) corresponds to an energy flux of about  $10^{-2} \text{ ergs cm}^{-2} \text{ sec}^{-1}$ . Since an incident energy of several  $\text{ergs cm}^{-2} \text{ sec}^{-1}$  is necessary to account for the weakest aurora, the radiation we measure can account for only a small fraction of the energy in an aurora.<sup>6</sup> Since 0.5-Mev electrons can penetrate to 70 km, we can account for the portion of an auroral display that extends to such low altitudes. Balloon and rocket observations of auroral zone precipitation indicate that, except during periods of solar disturbances, electrons with energy less than 100 kev provide the bulk of the energy input, but our sensors were not sensitive to such particles.<sup>7, 8.</sup>

## 2.7 CONCLUSIONS AND RECOMMENDATIONS

The data has not yet been analyzed with sufficient precision to allow more than qualitative conclusions to be made. These are:

1. Trapped radiation from the  $L = 2$  shell is observed.

2. Radiation is observed in the  $L = 4$  and  $L = 5$  shells which can not be trapped for periods more than perhaps an hour. This radiation can account for some auroral activity.

3. Pitch angle distributions are such that particles are more intense at  $90^\circ$  with respect to the magnetic field than at small angles.

The analysis of the data is still continuing and a particular effort is being made to eliminate magnetometer and timing errors to permit accurate B-L assignments. The analysis so far has indicated the usefulness of radiation measurements from satellites with these orbital parameters, particularly in the following respects. At such low altitudes the bulk of the trapped radiation is not present, and much of what remains represents loss from the radiation belts. These observations thus set limits on the lifetime of the normally trapped radiation. Auroral zone precipitations are clearly indicated except that measurements must be extended to lower energy particles to observe the bulk of the radiation responsible for auroras. Extending the sensitivity of the detectors to smaller fluxes could yield significant results regarding the lifetimes of particles in  $L$  shells smaller than 2. The dynamics of the radiation belts show up more clearly at low altitudes than at higher altitudes where they tend to be masked by the normal complement of long-term trapped radiation.

TABLE 2.1 TABULATION OF SIGNIFICANT DATA

Read out Orbit	Tape Time	GMT	Beta-2 Lower level	Beta-2 Upper level	Lat.	Long.
<u>FTV 1129</u>						
58	63 sec	39408 sec	0.4	Th	15 S	87 E
	79	39899	1.0	0.4	43 S	95 E
	141	41511	0.4	0.3	26 S	113 W
	215	43435	0.35	Th	72 N	12 E
	246	44241	.35	.25	25 N	55 E
77	21 sec	54011 sec	3.5	2.35	62 N	11 W
	82	55597	1.2	.45	41 S	25 E
	86	55701	0.55	Th	45 S	27 E
	95	55935	3.3	2.0	60 S	37 E
	127	56767	.55	Th	57 S	163 E
	198	58613	1.2	0.55	60 N	154 W
	202	58717	0.6	Th	66 N	146 W
	228	59393	3.5	0.85	60 N	31 W
	285	60875	1.5	0.95	35 S	0 E
	290	61005	2.0	0.6	42 S	2 E
80	21 sec	74886 sec	2.1	0.70	68 N	150 E
	24	74964	1.5	0.65	71 N	158 E
	27	75043	1.0	0.55	75 N	178 W

TABLE 2.1 CONTINUED

Read out Orbit	Tape Time	GMT	Beta-2 Lower level	Beta-2 Upper level	Lat.	Long.
<u>FTV 1129</u>						
80	32 sec	75172 sec	0.5	0.5	75 N	147 W
	51	75666	1.65	0.6	52 N	91 W
	105	77070	0.5	Th	40 S	65 W
	110	77200	0.4	Th	49 S	62 W
	115	77330	3.1	1.4	56 S	56 W
	119	77434	2.2	0.5	60 S	53 W
	129	77694	3.0	1.1	74 S	16 W
	132	77772	0.65	Th	75 S	2 W
	151	78266	1.05	0.5	58 S	72 E
	154	78344	2.2	0.5	51 S	78 E
	227	80242	2.2	0.8	67 N	126 E
	231	80346	2.0	0.5	72 N	140 E
	253	80918	2.6	1.2	57 N	118 W
	319	82634	1.1	0.5	50 S	83 W
	323	82738	2.8	0.6	58 S	77 W
	327	82842	0.8	Th	64 S	70 W
	333	82998	0.8	Th	70 S	55 W
	337	83102	3.1	2.0	75 S	32 W
	342	83232	2.5	0.7	75 S	1 W

TABLE 2 1 CONTINUED

Read out Orbit	Tape Time	GMT	Beta-2 Lower level	Beta-2 Upper level	Lat.	Long.
<u>FTV 1129</u>						
97	54	85124	2.6	1.9	70 N	112 E
	58	85228	2.4	0.8	73 N	122 E
	61	85306	3.0	0.7	85 N	150 E
	66	85436	1.45	0.5	74 N	180 E
	71	85566	3.5	1.8	69 N	160 W
	75	85670	3.3	2.6	62 N	148 W
	145	1090	2.4	0.8	53 S	106 W
	149	1194	1.3	Th	60 S	100 W
	154	1324	0.7	Th	66 S	90 W
	161	1506	2.7	Th	74 S	63 W
	165	1610	3.3	2.5	76 S	33 W
	170	1740	3.3	3.0	73 S	5 W
	174	1844	3.2	2.5	68 S	12 E
	178	1948	2.4	0.95	64 S	18 E
	183	2078	0.65	Th	55 S	29 E
	187	2182	0.55	Th	50 S	32 E
	190	2260	0.55	Th	44 S	36 E
153	25 sec	49123	0.5	Th	41 S	45 E
	28	49201	0.6	Th	44 S	47 E

TABLE 2.1 CONTINUED

Read out Orbit	Tape Time	GMT	Beta-2 Lower level	Beta-2 Upper level	Lat.	Long.
<u>FTV 1129</u>						
153	34	49357	2.5	N.R.	52 S	51 E
	36	49409	3.0	2.3	57 S	54 E
	39	49487	2.3	1.0	62 S	61 E
	67	50215	2.5	1.7	62 S	179 E
	70	50293	2.0	0.7	58 S	177 W
	72	50340	0.5	Th	55 S	174 W
	140	52113	2.7	1.6	59 N	134 W
	143	52191	2.5	1.3	63 N	130 W
	229	54427	0.6	Th	35 S	21 E
	232	54505	1.1	Th	39 S	22 E
	235	54583	0.9	Th	47 S	26 E
	243	54791	3.0	1.7	58 S	33 E
	245	54843	3.3	3.0	61 S	37 E
	247	54895	2.2	0.8	64 S	42 E
	276	55649	3.1	1.0	60 S	159 E
	348	57521	0.7	Th	61 N	154 W
	350	57573	1.4	0.4	65 N	150 W
	434	59757	0.75	Th	34 S	1 W
	437	59835	1.1	Th	38 S	0

TABLE 2.1 CONTINUED

Read out Orbit	Tape Time	GMT	Beta-2 Lower level	Beta-2 Upper level	Lat.	Long.
FTV 1129						
153	440 sec	59913	0.6	Th	41 S	0
185	40 sec	86299	1.6	0.9	73 N	103 E
	53	237	1.9	1.55	62 N	167 W
	118	1927	0.9	0.7	41 S	132 W
	131	2265	0.6	Th	62 S	117 W
	146	2655	1.3	0.9	72 S	59 W
	169	3253	1.5	Th	48 S	12 E
	242	5151	1.2	0.6	71 N	72 E
	251	5385	1.5	Th	74 N	129 E
	256	5515	1.4	0.8	70 N	152 E
	347	7881	2.6	2.2	73 S	107 W
	373	8557	3.0	1.6	68 S	33 W
208	20	1472	1.85	1.2	75 S	44 W
	40	1992	0.9	0.4	52 S	10 E
	44	2096	1.1	0.4	45 S	16 E
	115	3942	3.05	1.35	70 N	72 E
	125	4202	3.0	0.8	74 N	129 E
	132	4364	1.7	Th	68 N	161 E
208	25	7335	3.0	1.6	50 S	10 W

TABLE 2.1 CONTINUED

Read out Orbit	Tape Time	GMT	Beta-2 Lower level	Beta-2 Upper level	Lat.	Long.
<u>FTV 1129</u>						
208	192	4992	1.2	1.1	53 S	170 W
210	47	86122	0.9	Th	67 S	105 W
	65	190	3.1	2.6	70 S	10 W
	88	788	0.8	Th	34 S	23 E
	156	2556	2.4	1.5	75 N	105 E
	173	2998	2.3	1.3	61 N	176 E
215	Too Noisy For Analysis					
217	17	32007	2.4	1.6	67 S	137 W
	88	33853	2.3	1.3	52 N	86 W
	117	34607	2.0	0.8	67 N	32 E
	191	36531	2.0	1.4	56 S	85 E
	230	37545	2.5	1.5	50 S	140 E
219	44	42674	0.9	1.2	61 S	178 E
	116	44546	1.7	1.6	59 N	125 W
	208	46938	0.7	0.7	44 S	34 E
	221	47276	3.3	2.5	66 S	53 E
	250	48030	1.2	0.9	56 S	172 E
226	73	84713	1.9	1.2	69 S	3 W



TABLE 2.1 CONTINUED

Read out Orbit	Tape Time	GMT	Beta-2 Lower level	Beta-2 Upper level	Lat.	Long.
<u>F IV 1128</u>						
9	43 sec		0.5	Th		
	111		1.0	.5		
	125		1.1	0.5		
	250		1.1	0.5		
	319		1.4	0.6		
	334		1.6	0.6		
58	22		1.7	0.4		
	97		3.0	2.0		
61	12		1.6	0.3		
	29		2.9	2.0		
	132		2.5	1.8		
	160		0.4	Th		
63	16		3.2	2.2		
	19		3.0	1.4		
	112		1.2	.4		
	127		3.1	2.6		
	144		2.3	1.4		
65	48		0.8	Th		
	53		2.4	1.4		

TABLE 2.1 CONTINUED

Read out Orbit	Tape Time	GMT	Beta-2 Lower level	Beta-2 Upper level	Lat.	Long.
<u>FTV 1128</u>						
65	62		1.6	.5		
	68		3.0	1.7		

Tape Time. Time on record from beginning of record

GMT Greenwich mean time in seconds.

Th Voltage indicated threshold value.

Data from 1128 listed versus tape time only and was not included in geographic distribution.

TABLE 2.2 SIMULTANEOUS COMPARISON OF BETA-1, BETA-2 SENSORS

Simultaneous comparison of Beta-1, Beta-2 sensors.  $\theta$  = angle of sensor with respect to the magnetic field,  $\beta$  = response of sensor in volts (logarithmically proportional to counting rate.)

Acquisition & Time		$\theta_1$	$\beta_1$	$\theta_2$	$\beta_2$
$\phi 58$	22sec.	$79^\circ$	1.8v	$19^\circ$	0
	97.5	$84^\circ$	2.9	$14^\circ$	.4
	95.5	$50^\circ$	1.7	$62^\circ$	1.4
$\phi 65$	48.5	$60^\circ$	.8	$52^\circ$	.6
	50.5	$32^\circ$	.4	$82^\circ$	2.6
	52	$52^\circ$	1.6	$48^\circ$	1.6
	53	$81^\circ$	2.6	$20^\circ$	.4
$\phi 65$	57	$14^\circ$	.3	$82^\circ$	2.0
	65	$71^\circ$	2.4	$90^\circ$	2.5
	66.5	$87^\circ$	1.7	$85^\circ$	1.7
	68	$88^\circ$	1.2	$80^\circ$	1.2
	71.5	$84^\circ$	3.1	$52^\circ$	1.8
	73	$57^\circ$	2.2	$57^\circ$	2.2
	172.5	$90^\circ$	3.2	$40^\circ$	0
	175	$17^\circ$	0	$79^\circ$	1.6
$\phi 62$	26.5	$18^\circ$	0	$79^\circ$	2.7
	28	$53^\circ$	2.0	$46^\circ$	2.0
	29	$68^\circ$	2.9	$44^\circ$	1.0
	131.5	$61^\circ$	2.4	$77^\circ$	2.5
	133	$56^\circ$	2.5	$62^\circ$	1.5
$\phi 9$	111.5	$52^\circ$	1.0	$41^\circ$	.4

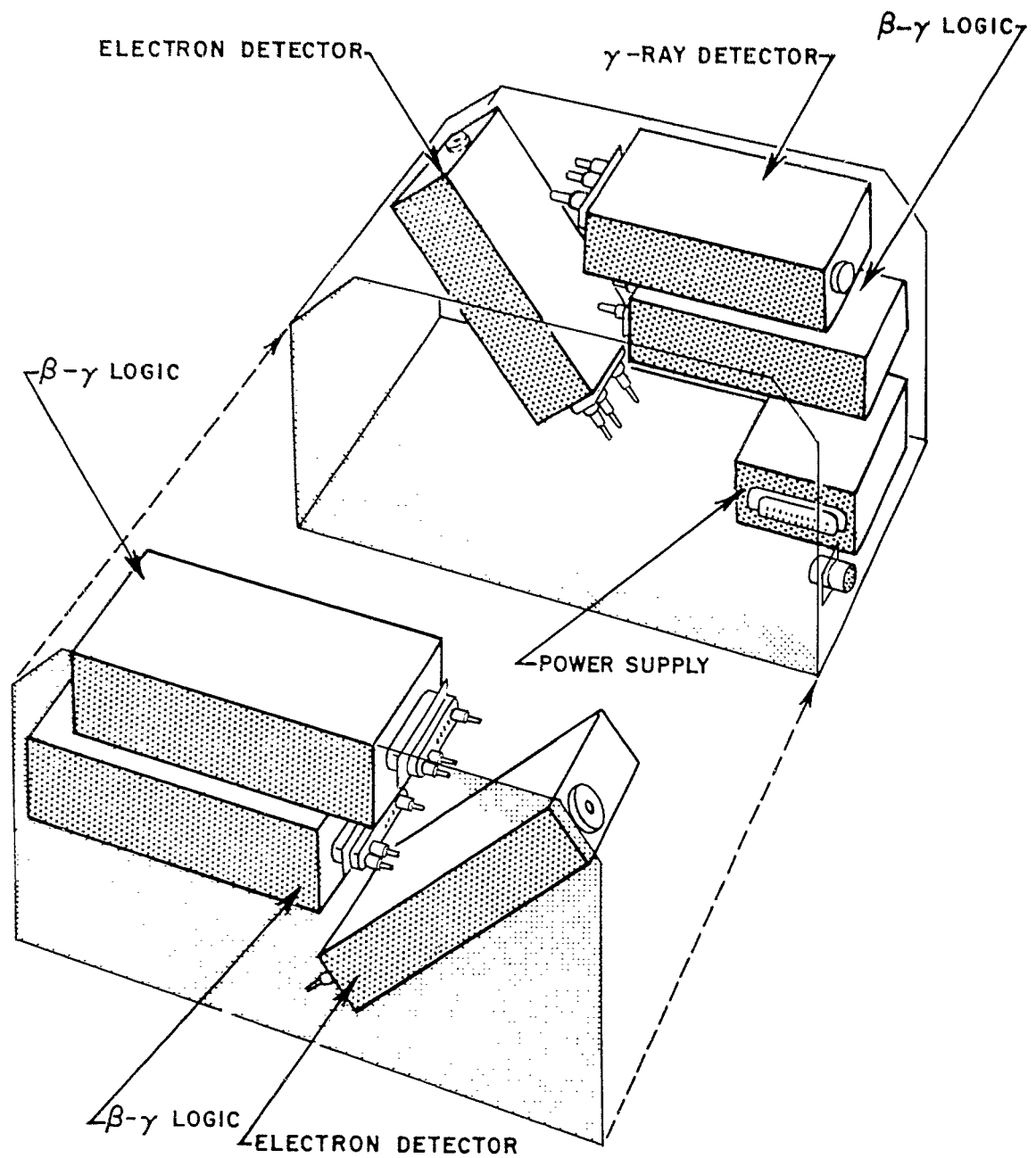


Figure 2.1 Exploded view of radiation experiment.

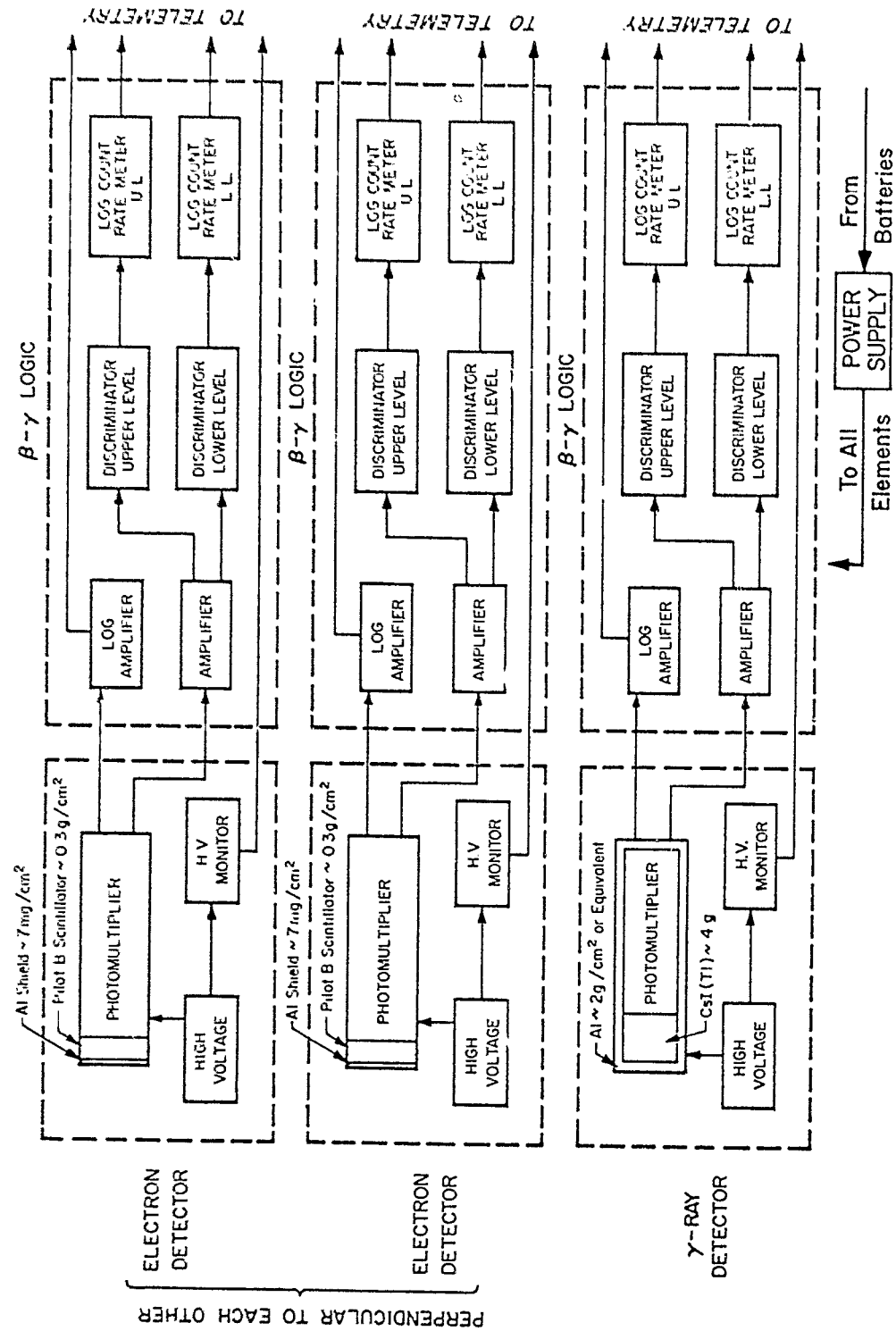


Figure 2.2 Block diagram of radiation experiment.

SECRET

58

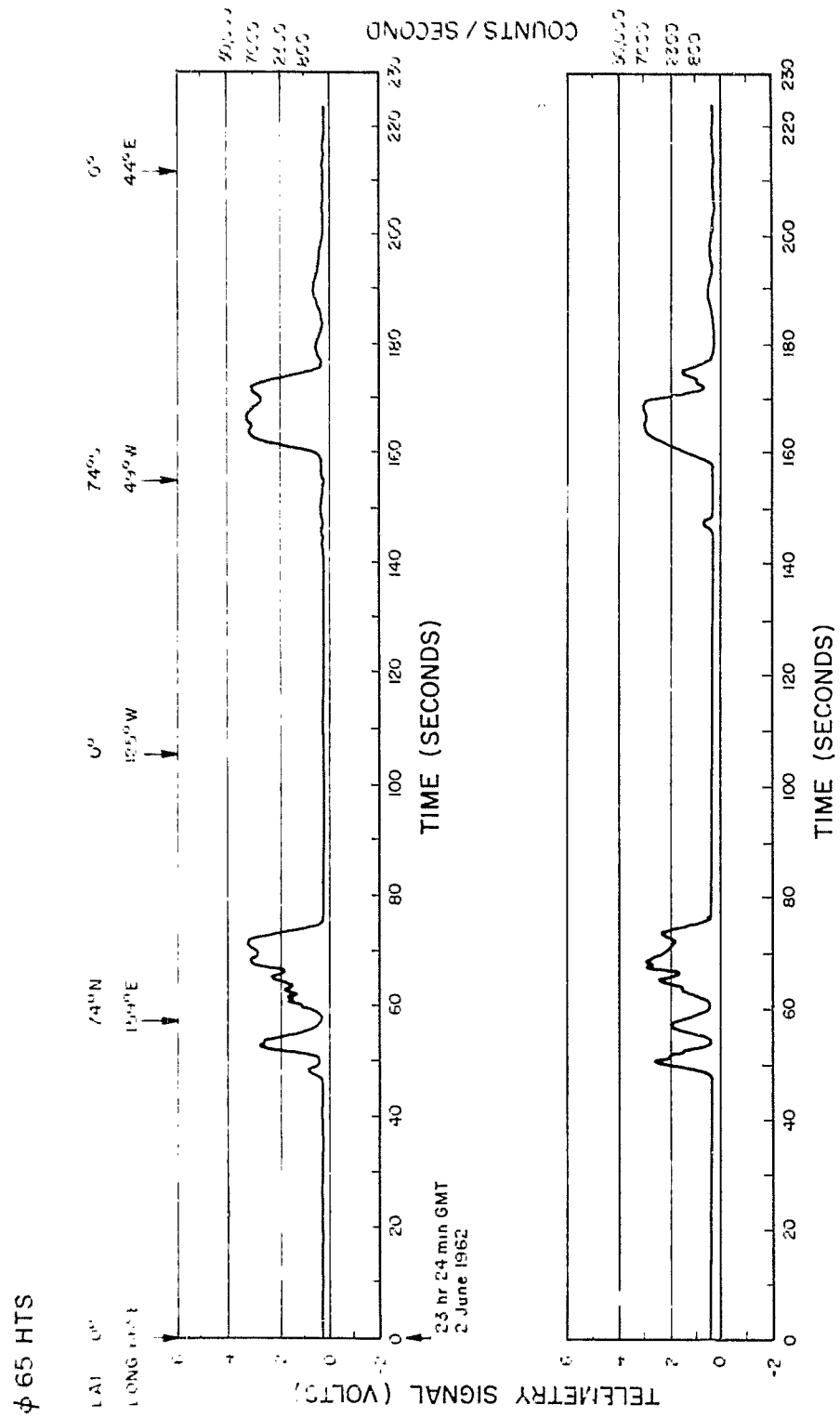


Figure 2.3 Simultaneous playback signal from Beta-1 and Beta-2 lower level discriminators.

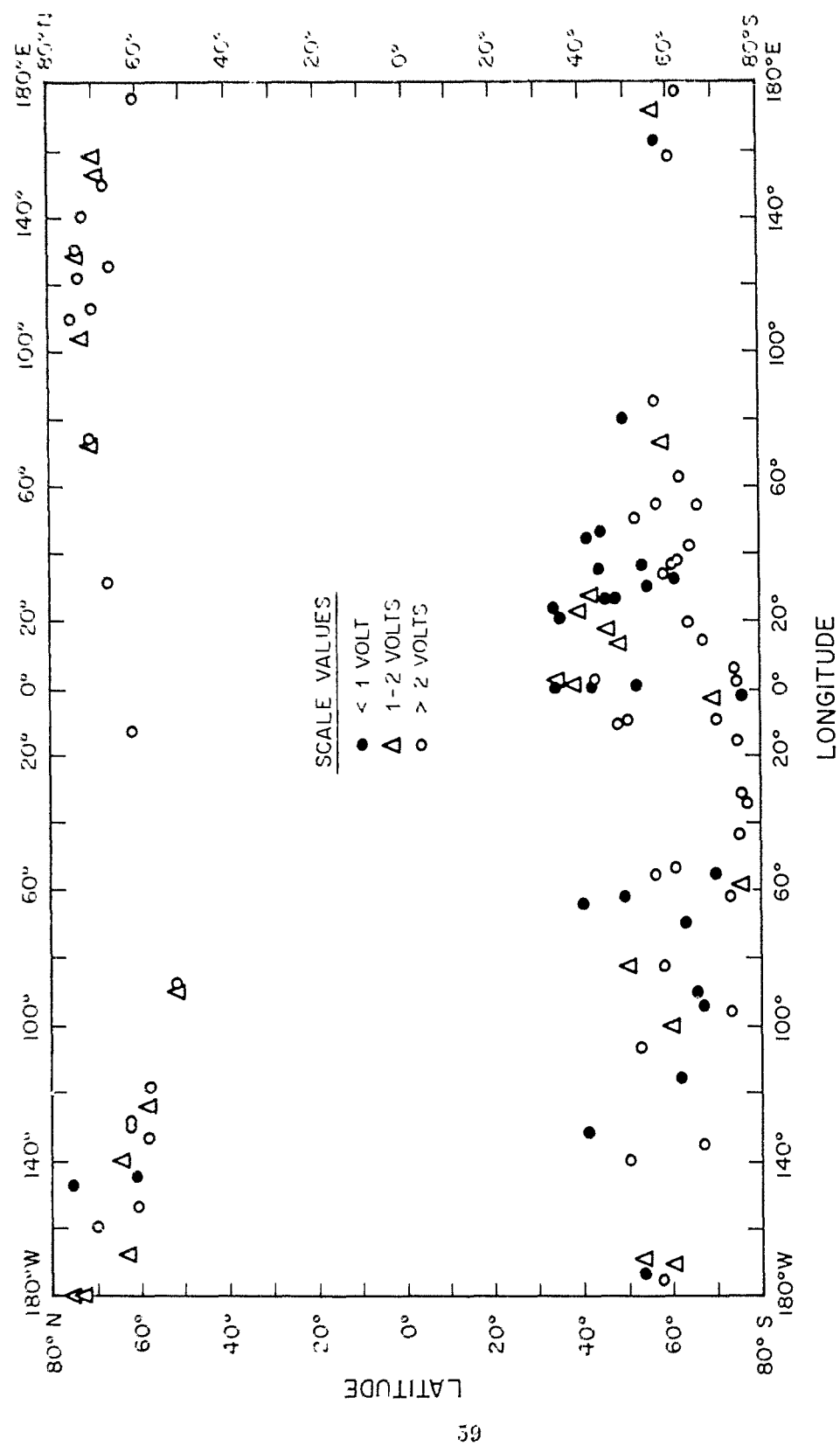


Figure 2.4 Geographic distribution of observed radiation.

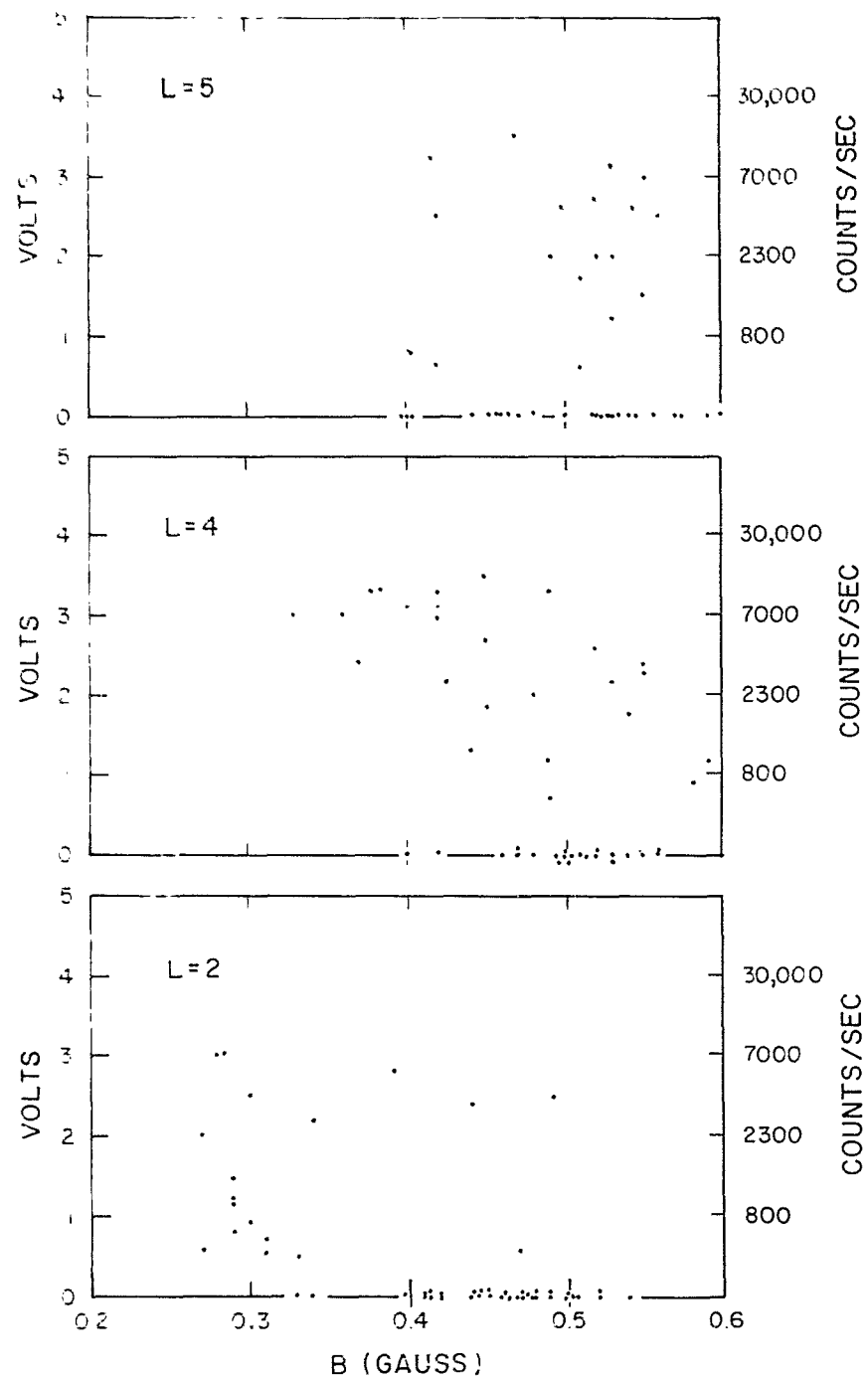


Figure 2.5 B-L distribution of observed radiation.



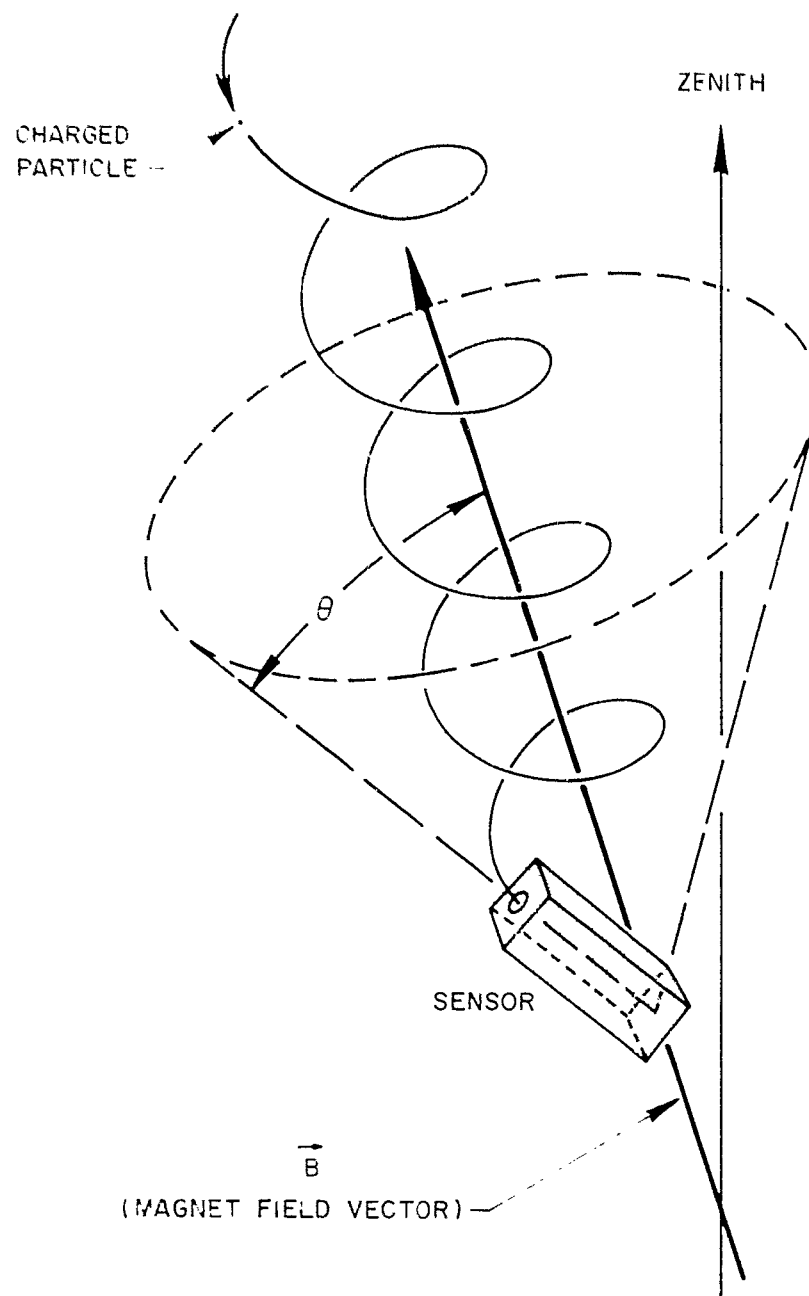


Figure 2.6 Magnetic reference system.

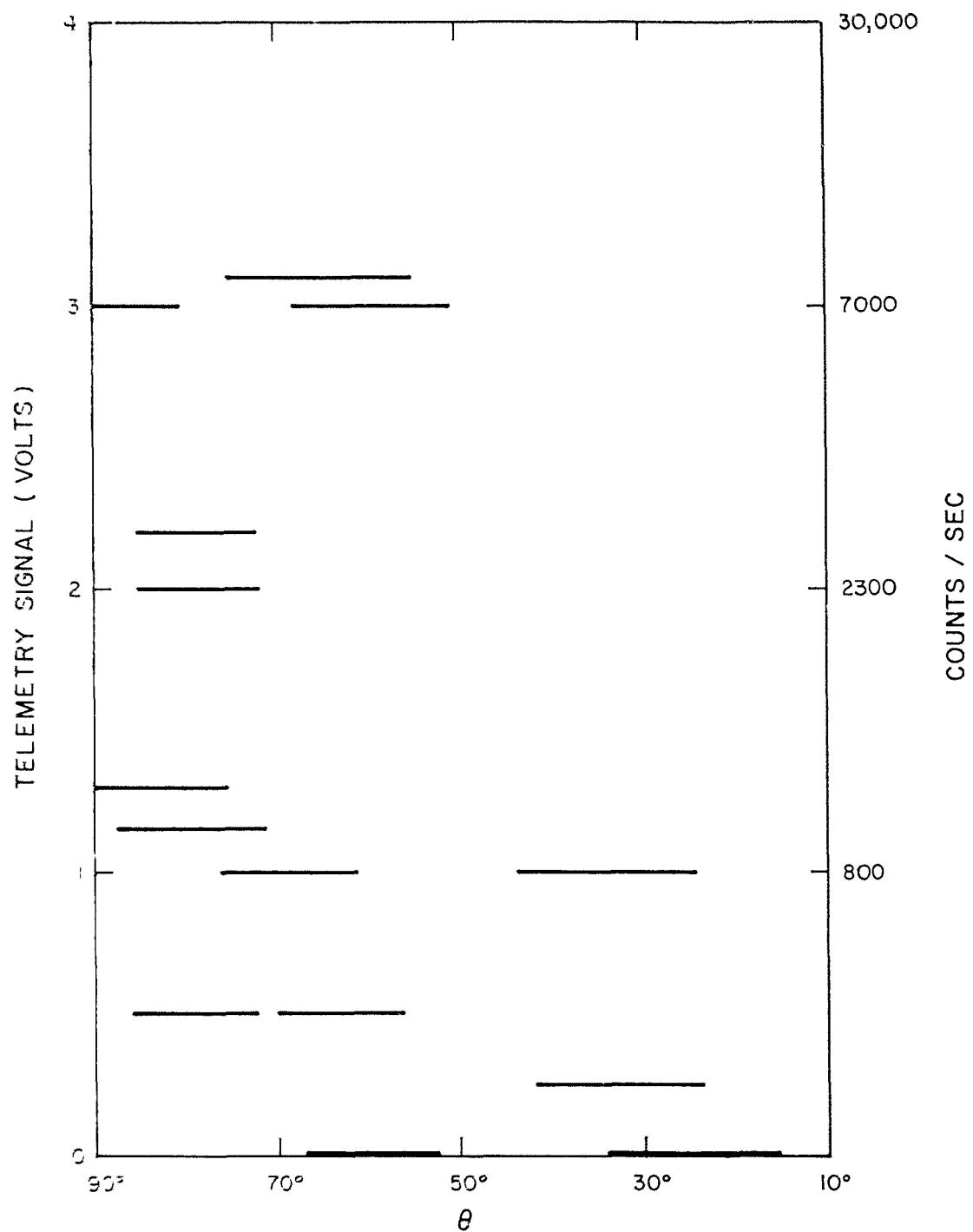


Figure 2.7 Pitch angle distribution, L = 2 shell.

## CHAPTER 3

### IMPEDANCE PROBE

#### 3.1 OBJECTIVE

The objective of the standing-wave impedance probe on the Discoverer was to measure the change in electron density in the F-region of the ionosphere resulting from a nuclear explosion. Measurements were to be made in the immediate vicinity of the satellite and in the range from  $10^3$  to  $10^9$  electrons/cm<sup>3</sup>.

#### 3.2 BACKGROUND AND THEORY

The impedance of an antenna is modified when it is immersed in a medium containing a significant quantity of free electrons. It was proposed to determine the electron concentration of the plasma by measuring these impedance changes on a dipole antenna mounted on an earth satellite passing through the region of interest. The lower the measuring frequency, the greater will be the impedance change for a given electron density. In order to measure the range of values expected and yet remain in the measurement range of the instruments, 24-foot dipole antennas were mounted on the Discoverer satellites and their impedance measured at 5 and 14.5 Mc.

The standing-wave impedance probe developed by the University of Utah for the Air Force has been flown successfully on a number of rockets and more recently on two Discoverer satellites.<sup>9, 10, 11</sup> On one Discoverer satellite, data was obtained from the tape recorder output at seventeen tape-readout stations with coverage varying from one-half to two orbits. Programs for high-speed computers have been written such that the digitalized information of the standing waves on magnetic tape may be converted to impedance values and then to electron densities automatically.

### 3.3 INSTRUMENTATION

The impedance-measuring system is shown in Figure 3.1. This system consists essentially of two RF oscillators, artificial transmission lines, and the dipole antenna. The 5- and 14.5-Mc balanced crystal oscillators are alternately connected to the dipole antenna through the sections of artificial line. The two lines, together with short lengths of coaxial cable, are electrically equivalent; one is used to feed each element of the dipole antenna, thus providing a balanced system. The RF voltages on six of the 23 sections of one of the artificial lines are rectified and then applied to the commutator in the telemetry package. The standing wave existing on the line connecting the oscillator

to antenna is recreated on the ground from these six telemetry points. This standing-wave pattern is sufficient to uniquely define the driving-point impedance of the antenna.

Measurement of the electron densities by the impedance-probe method necessitates using frequencies on the order of the expected plasma frequencies. This requirement dictates the use of frequencies from about 1 to 15 Mc. Achieving an efficient antenna at these frequencies poses a difficult problem for small rockets; however, antennas of satisfactory size on the satellite were obtained by use of thin flat 3/4-inch-wide metal tape. The tape is coiled into a roll and stored in a mechanism approximately 1 by 3 by  $3\frac{1}{2}$  inches. When the satellite was stabilized in orbit at a height where there is essentially no air drag, the coil was released and unrolled to a length of 12 feet. Two such antenna elements were mounted diametrically opposite on a cylindrical section of satellite body to form a 24-foot balanced dipole.

At the operating frequencies of 5 and 14.5 Mc, the element length is considerably less than a quarter wavelength, and therefore, the free-space impedance of the antenna has a small resistive component and relatively large capacitive reactance. The standing wave on a transmission line terminated by such an impedance is extremely high, and consequently, it is difficult to

detect changes in the impedance. Furthermore, the effect of electron motion on the antenna impedance is such as to make it increase in negative reactance. It was desirable, therefore, to reduce the magnitude of the initial standing wave on the line and to cancel the negative reactance of the free-space antenna impedance, since in the plasma it will change in the negative direction. Consequently, a series network was added near the antenna terminals that transformed the initial impedance to  $75 + j100$  at the two operating frequencies. This impedance presented a respectable initial standing wave on the balanced 100-ohm transmission lines, and the larger resistive component allowed the reactance to change quite radically before the standing wave increased out of the range of measurement.

The artificial transmission lines were 23-section, 50-ohm lumped-circuit lines designed to be just over half a wavelength at the lower frequency. One of the two equivalent lines had six tap points from equally spaced sections brought out to diode-capacitor rectifiers. These rectifiers transformed the RF voltages on the order of  $\frac{1}{2}$ -volt rms level to the standard telemetry range of 0 to +5 volts. The tap points were designated as VSWR 1 through 6 and are shown in Table 3.1.

Periodically, the impedance probe system was calibrated by switching a known impedance across the lines in place of the antenna. This impedance and the actual switching were in the antenna units. Figure 3.2 shows the antenna network flown on these satellites.

The 5- and 14.5-Mc oscillators were transistorized crystal-controlled units that developed balanced outputs of  $\frac{1}{2}$  volt rms into each line of the balanced 100-ohm system when the lines were terminated.

#### 3.4 DATA REQUIREMENTS

The standing-wave impedance-probe data consisted of voltages in the range 0 to 5 volts on thirteen pins of the commutator. The data was recorded on the tape recorder in the satellite. On Ring B the impedance probe segments were as follows: Positions 13 through 18 and 46 through 50 define two complete measurements of the impedance at one frequency. Pin 51 was at the 0 calibration level with pin 52, the mode pin indicator, varying between 4 and 3-1/2 volts indicating operation at 14.5 and 5 Mc, respectively. For data reduction, the following is required: (1) digitalized plots for each readout for each segment; (2) analog strip charts of both sets of six pins in sequence with the master pulse calibration pins; a speed of 40 in/sec and a minimum deflection of 2 inches for full scale; (3) a low-density binary tape

with the digital values (in volts) of each group of six pins and the associated time words; (4) a two-ply listing of all tapes; (5) complete ephemeris of the satellite; (6) altitude, yield, time of detonation, and geocentric latitude and longitude of the nuclear device; and (7) ionosonde data from as broad a coverage of the satellite orbit as possible.

### 3.5 RESULTS

The standing-wave impedance probe functioned on two satellites, 1127 and 1129, and failed on 1128. The data from 1128 shows a constant standing wave on the antennas throughout the lifetime of the satellite for both the 5-Mc and 14.5-Mc frequencies. This indicates that all the electronics functioned properly, but that the antenna release mechanism either failed or was not activated. Since limited telemetry was available, this function could not be monitored to determine the exact nature of the malfunction.

The impedance probe functioned properly on 1127, but only two complete orbits of data are available because of the failure in the Lockheed data recording-transmitting system. Data from both frequencies, 5 Mc and 14.5 Mc, were available and analyzed. The low-frequency probe was flown for the measurement of the normal ionosphere, while the high frequency was flown to measure the expected extreme increases in electron density due to weapons test effects. Since there were no weapons tests while 1127 and 1129 were in orbit, the 14.5-Mc data is mainly useful for comparison with the 5-Mc results.



The impedance probe on 1129 functioned throughout the lifetime of the satellite in the low-frequency mode but failed in the high-frequency mode on orbit 77. It is impossible to determine the exact nature of the failure, but it was in the oscillator circuit. There was sufficient high-frequency data available, however, for calibration and comparison purposes of the low-frequency probe. A total of approximately 17 orbits of low-frequency data were available for analysis. Figure 3.3 shows the amount of data available, plotted as a function of geographic latitude with the longitude of the equator crossings noted. The orbits in which the data begin are also noted.

Figures 3.4 and 3.5 show the electron density, the altitude of the satellite, and the X magnetometer (vertical orientated) as a function of latitude for FTV 1127 for low and high frequency, respectively. Figures 3.6 through 3.19 are similar representations of the 1129 results.

### 3.6 DISCUSSION

The standing-wave impedance probe data was digitalized and stored on high-density computer tapes by Lockheed. We further processed the data on an IBM 7090 computer system utilizing programs developed for the analysis of the data. The outputs from this computer, electron density as a function of recording time, were listed

and stored on BCD low-density tapes. From these tapes we were able to obtain complete graphical representation of the data using the Electronic Associates, Inc. (EAI) automatic plotting system. Thus, the complete system of transmitting, recording, digitalizing, processing, and representing the data is done automatically.

In the analysis of the data the collision frequency effects at satellite altitudes are negligible and neglected. The effect of the earth's magnetic field is also neglected based on previous rocket and satellite results. On FTV 1117 no apparent effect was evident although the vehicle had a very slow tumble rate after orbit number 10. Finally, although both the real and reactive components of the impedance are calculated from the voltage standing-wave ratio and the phase of the standing wave and either can be used for the case of an operating frequency well above the plasma frequency, only the reactive component was used in the analysis because of its greater sensitivity to the electron density changes. In addition the reactive component can be calculated from the phase measurements even when the standing-wave ratio cannot be determined as in the case where the plasma frequency is near, at, or greater than the operating frequency.

The electron density can be calculated from the measured change in reactance according to the following:

$$N = \frac{f^2 \text{Mc}}{80.6} \times \frac{C_0}{C_1} \times \frac{\Delta X}{\Delta X + \frac{1}{\omega C_0}}$$

where

$$\omega = 2 \pi f$$

$$f = \text{operating frequency}$$

$$C_0 = C_1 + C_2$$

$$C_1 = \text{effective capacitance of the antenna}$$

$$C_2 = \text{shunt capacitance of the antenna}$$

$$X = X_{FS} - X_1$$

$$X_{FS} = \text{reactance of antenna in free space}$$

$$X_1 = \text{reactance of antenna in the ionosphere}$$

In general, we tune the antennas, which are short dipoles, to a free-space value of j100 ohms at a special facility constructed for this purpose. For these three satellites the antennas were tuned and the effective and shunt capacitance measured on a mock-up shell of an Agena vehicle.

In the analysis of the data we had two problems. The impedance measurements for the 5-Mc data gave a much higher effective capacitance than measured. This was explained, however, by the presence

during flight of several protruding objects (the heliflux magnetometer, two GRF antennas, and two ion trap probes) that were not present when the effective capacitance was measured. With a change in this value and knowledge of the ionosphere we were able to analyze the 5-Mc data.

The other problem was in the analysis of the 14.5-Mc data. In order to have results that corresponded to those from the 5-Mc data, we had to add a fixed phase to all the measurements of the standing wave. This meant that a longer cable connecting the lumped transmission line to the antenna was flown than was used in the calculations. We could not verify this, but the results of Figures 3.4 and 3.5 show the very excellent agreement between the 5- and 14.5-Mc probe results.

Since this vehicle was stabilized (this is shown in the X magnetometer output), the small changes in density evident throughout the flight in Figures 3.4 and 3.5 are fine structure measurements of the ionosphere. Even when the satellite is going through the F-layer, where the density is the highest, detailed fluctuations in density are present and quite noticeable. The expected dip in density at the magnetic equator, which for these orbits is essentially the geographic equator, are evident. Quite large changes in density around the southernmost part of the orbit in the auroral zone are shown on both orbits. The satellite has gone through the F-layer and in fact is at an altitude above 350 km. Of interest is the fact that not only is there an increase in density (the peak at 70° south for

both orbits) but that two and three very sharp minimums, lower than any other nighttime values, are evident.

The results of 1129 are shown in Figures 3.6 through 3.19. Only in orbit 55, where only a small amount of data was available, was the vehicle stabilized. Figure 3.7, the first readout after the satellite became unstable, shows this effect on the electron density results. The X magnetometer output is shown for comparison purposes. If the data is examined carefully, it can be seen that sometimes the peaks in density are in phase with the magnetometer output and sometimes not. The changes in density are not due to effects of the earth's magnetic field with respect to the antenna. The change is associated with the spin of the vehicle and is probably a measurement of the electron density in and out of the wake of the vehicle. We have observed this effect also on FTV 1117.

Orbit 177 (orbit 185 readout) shows a much faster spin rate than on the earlier results. The effect of the spin on the electron density measurements is not nearly so severe. The measurements of electron density at two ground recording stations (Adak and Hawaii) are shown on the data. There is an excellent agreement between the two results.

The last two orbit readouts, Figures 3.18 and 3.19, are interesting. The satellite is now at a low altitude and is experiencing the heating effects due to friction with the air. The low electron density values present in all previous orbits are a constant higher value

for these orbits. This is explained as a loss of a small part of the antenna due to the heating effects. In the Figure 3.19 where now the satellite has a very slow tumble rate shown on the X magnetometer data, the effect of the wake is more evident since the antenna is in the wake for longer periods of time.

### 3.7 CONCLUSIONS

The standing-wave impedance probe measures the electron density of the ionosphere very well. In a stabilized vehicle, fine structure measurements of the ionosphere can be made. If the vehicle is spinning, a spin rate of 1 revolution per minute or greater is desirable for more detailed measurements. It is important that the two frequency impedance probes be flown, not only for the greater range, but to provide a comparison and calibration in case the flight conditions of the probes are not as anticipated.

TABLE 3.1 IMPEDANCE PROBE COMMUTATOR ASSIGNMENTS, RING B

<u>Position</u>	<u>Output</u>	<u>Measurement</u>	<u>Telemetry</u>
01	Cal 0	Cal	-
13	IP-1**	VSWR 1	X109
14	IP-2	VSWR 2	X110
15	IP-3	VSWR 3	X111
16	IP-4	VSWR 4	X112
17	IP-5	VSWR 5	X113
18	IP-6	VSWR 6	X114
30	Cal 5	Cal	-
46	IP-1	VSWR 1	X213
47	IP-2	VSWR 2	X214
48	IP-3	VSWR 3	X215
49	IP-4	VSWR 4	X216
50	IP-5	VSWR 5	X217
51	Cal 0	Reference	X218
52	IP-7*	Mode	X219
57	Cal 6	Cal	-
53,59,60	Sync		

\*Output number IP-7 is mode control which indicates the frequency and mode of the system. The frequency is switched whenever the commutator passes this segment.

\*\*Impedance probe.

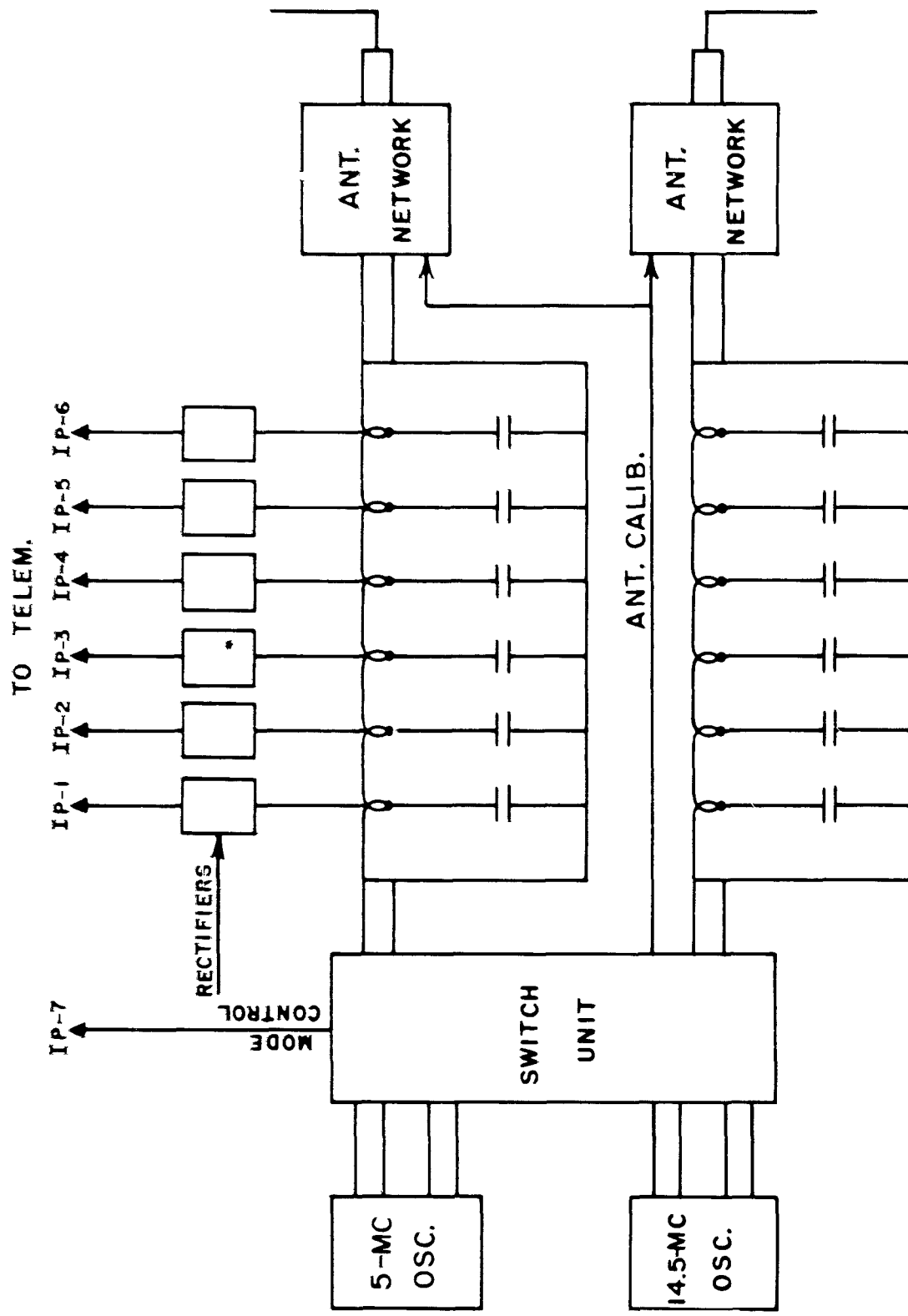


Figure 3.1 Block diagram of impedance probe experiment.



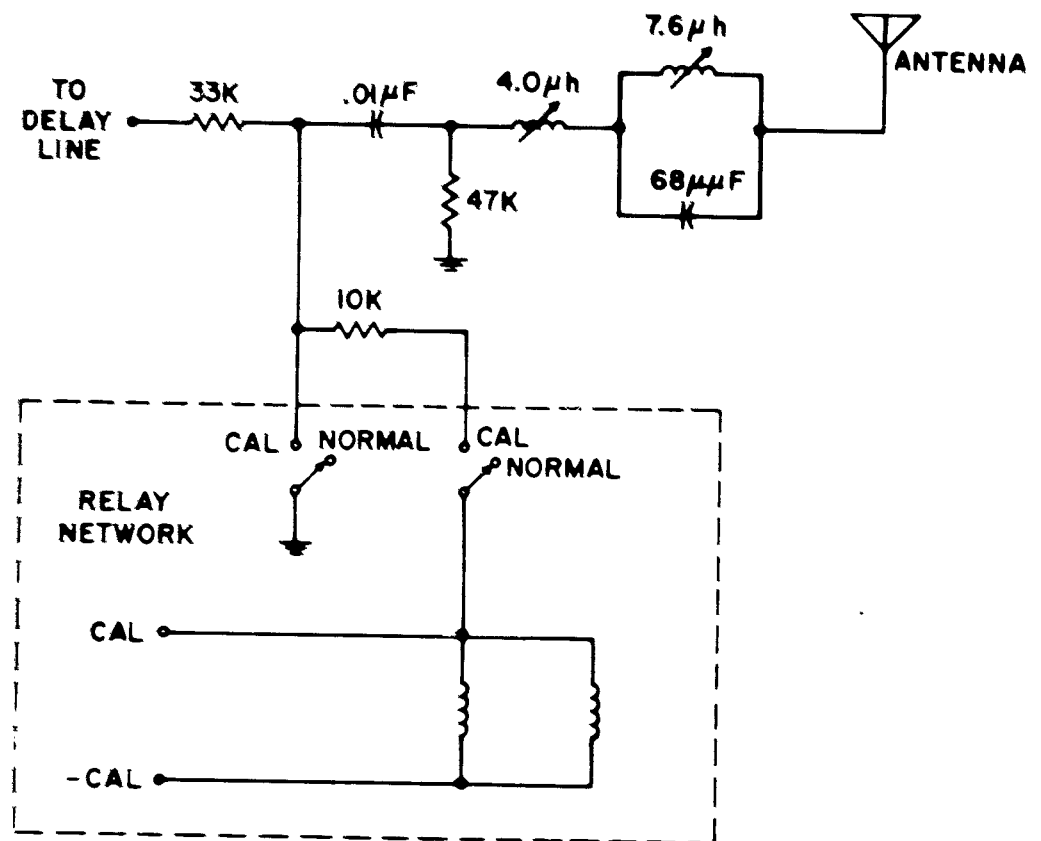


Figure 3.2 Satellite antenna network.

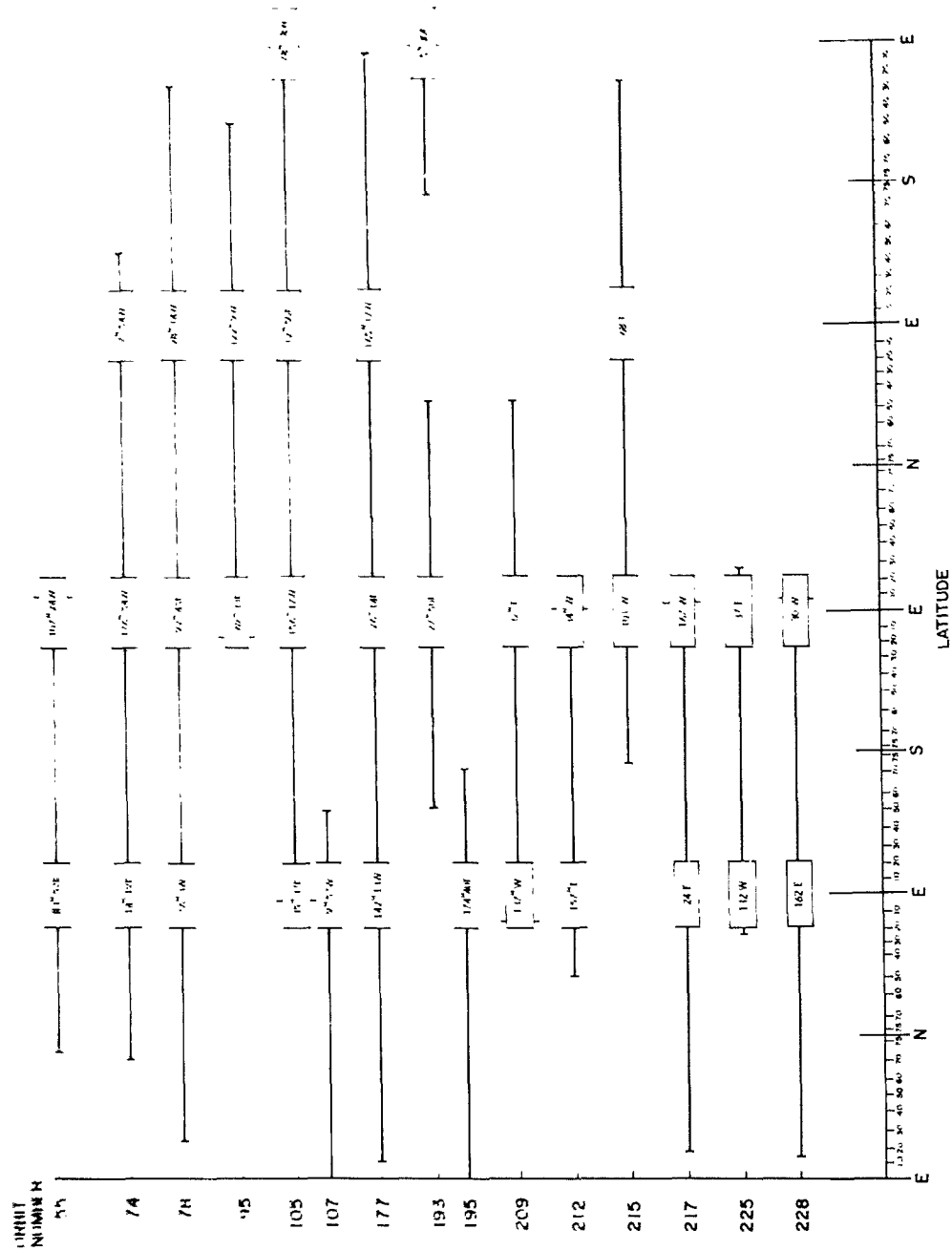


Figure 3.3 Summary of FTV 1129 data.

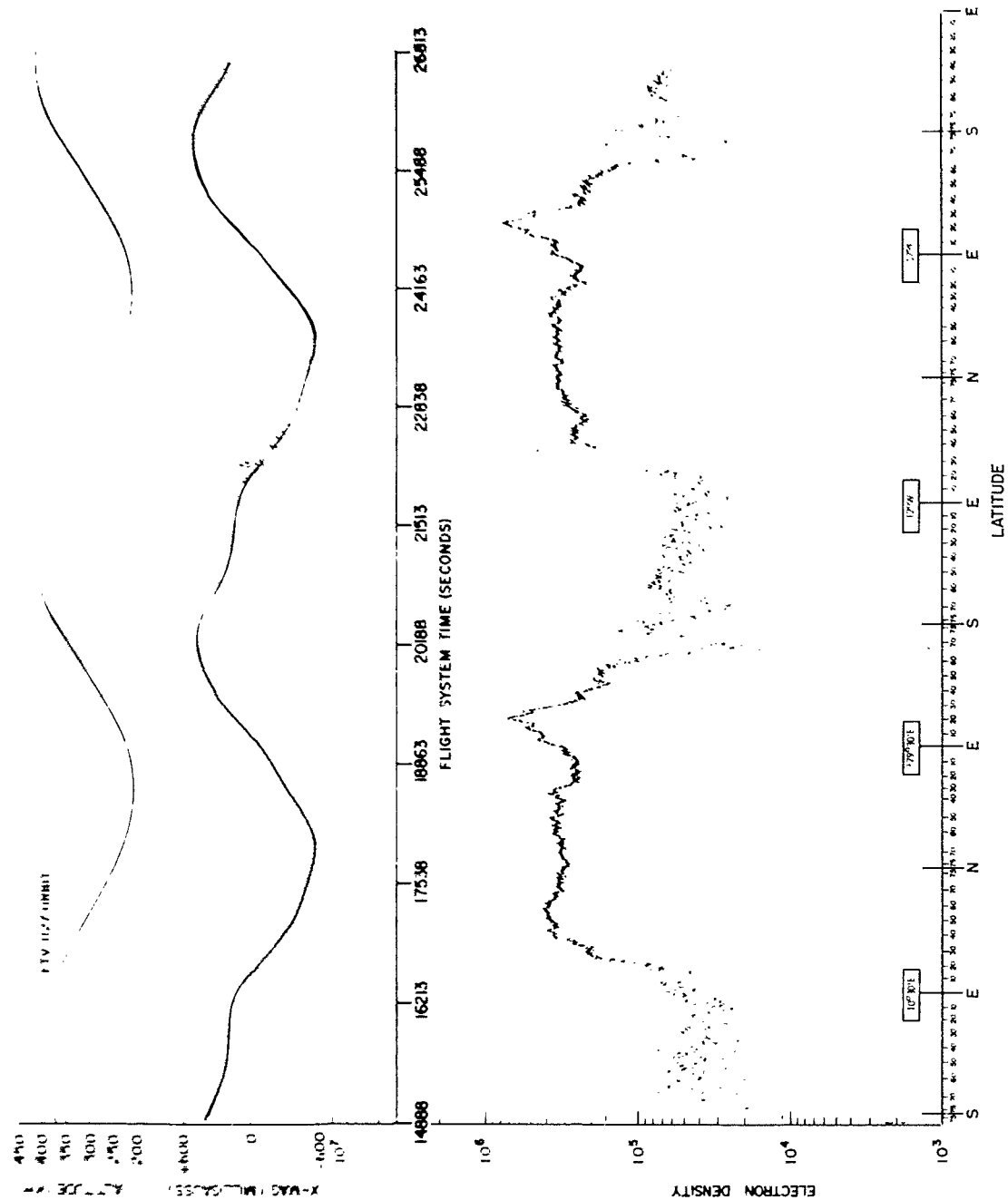


Figure 3.4 5-Mc result, FTV 1127.

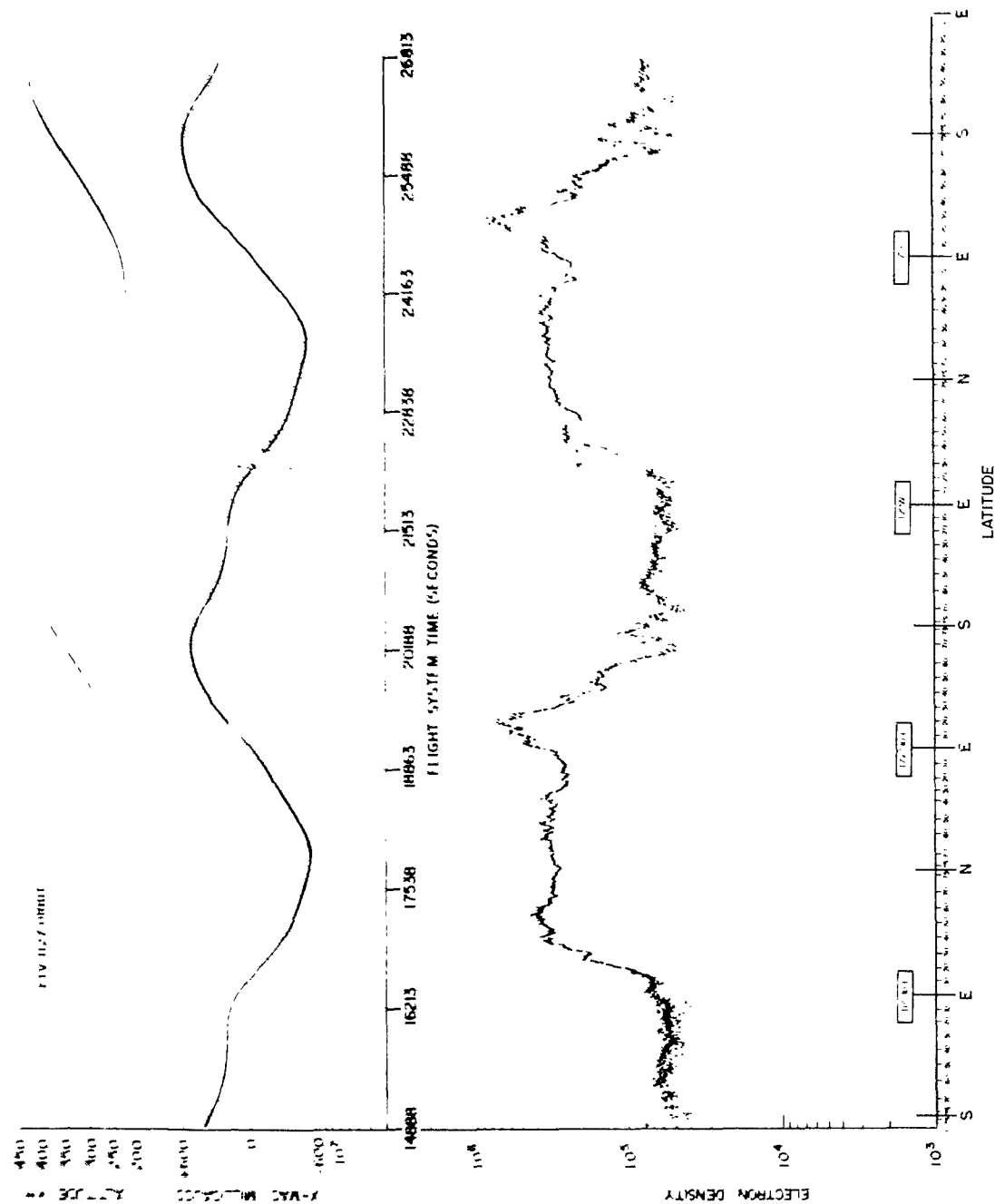


Figure 3.5 14.5-Mc result, FTV 1127.

SECRET

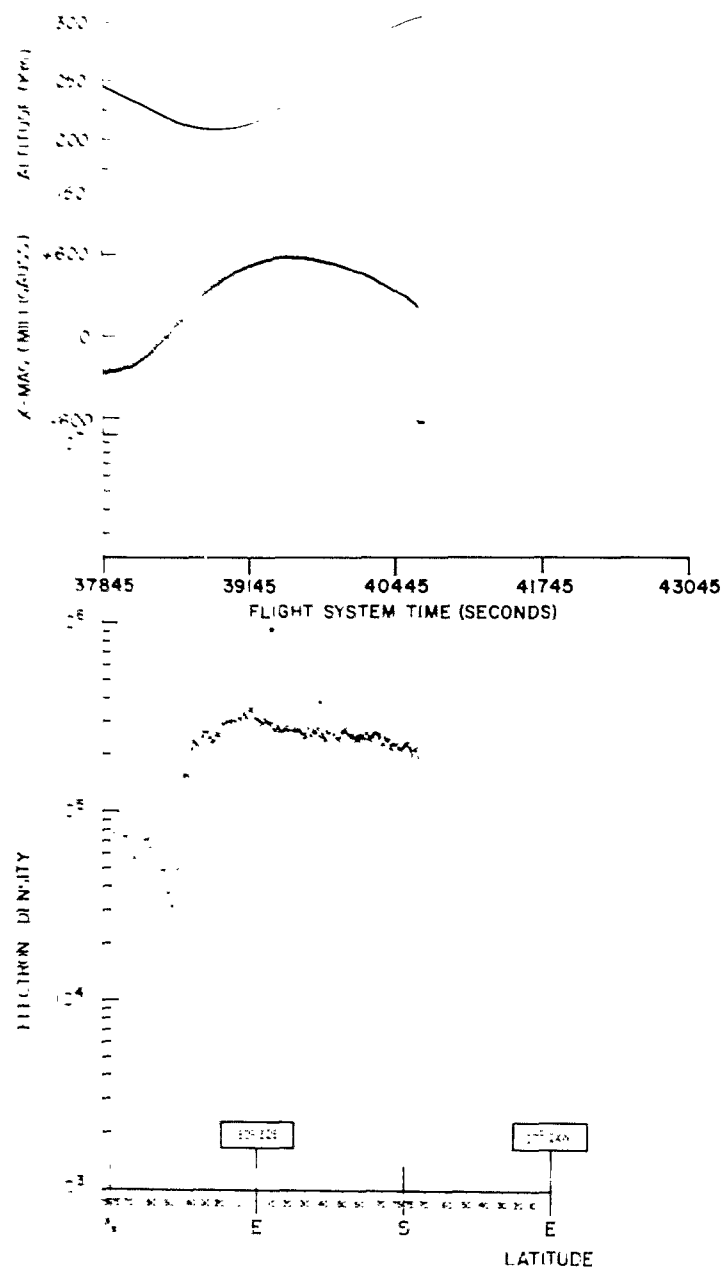


Figure 3.6 Orbit 55, 14.5-Mc results, KTS, Orbit 58 readout.

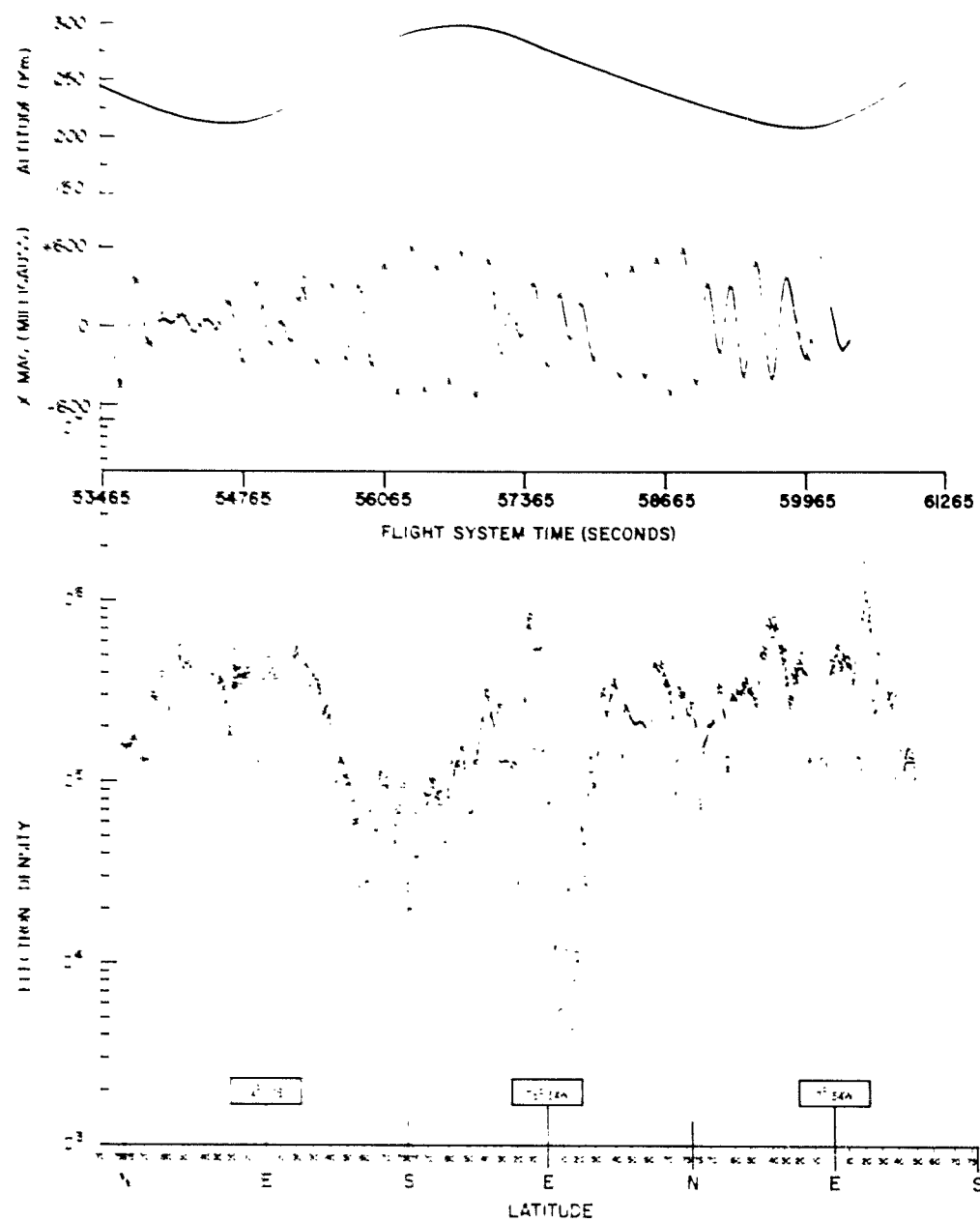


Figure 3.7 Orbit 74, 5-Mc results, NHTS, Orbit 77 readout.

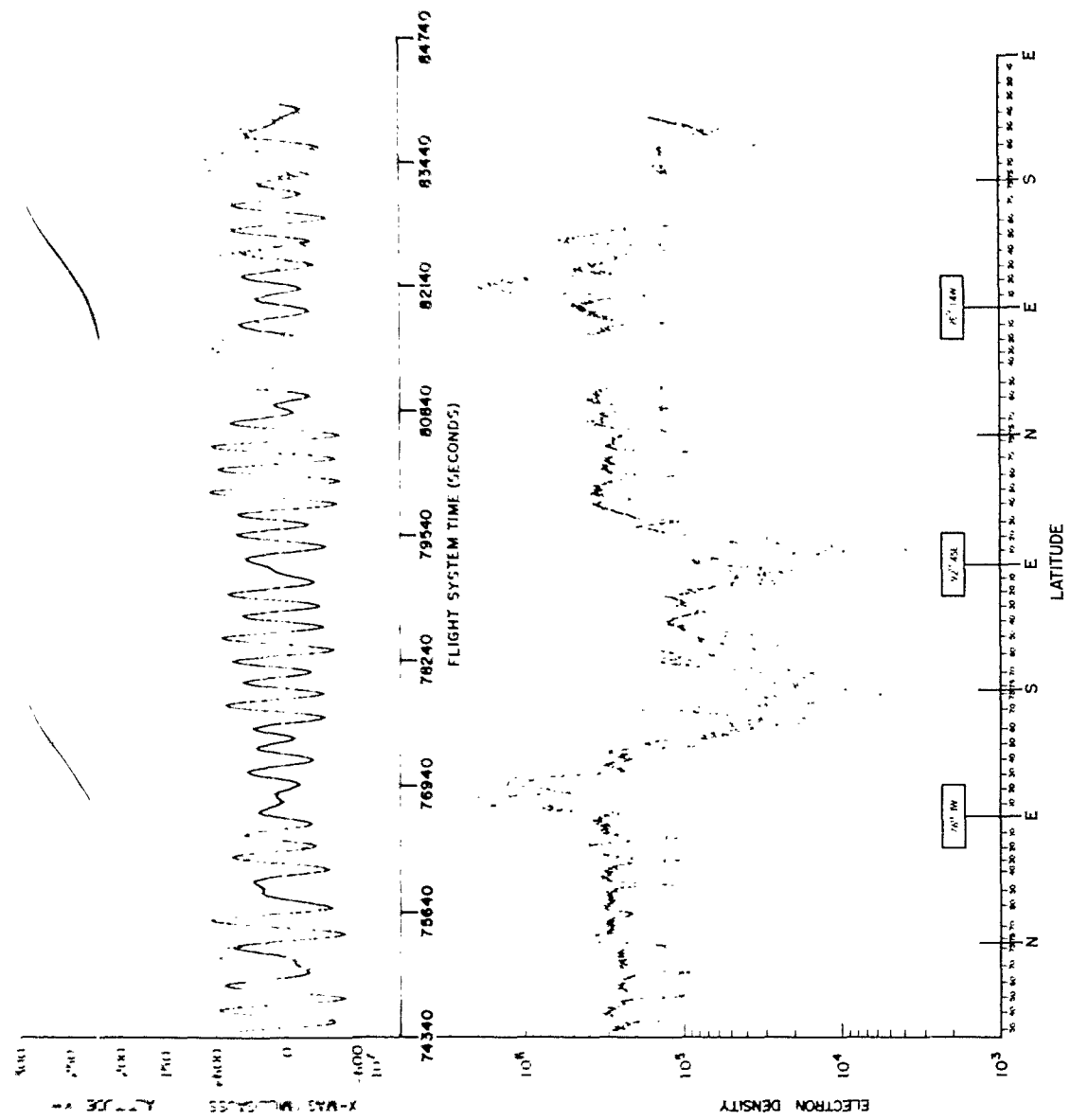


Figure 3.8 Orbit 78, 5-Mc results, KTS, Orbit 80 readout.

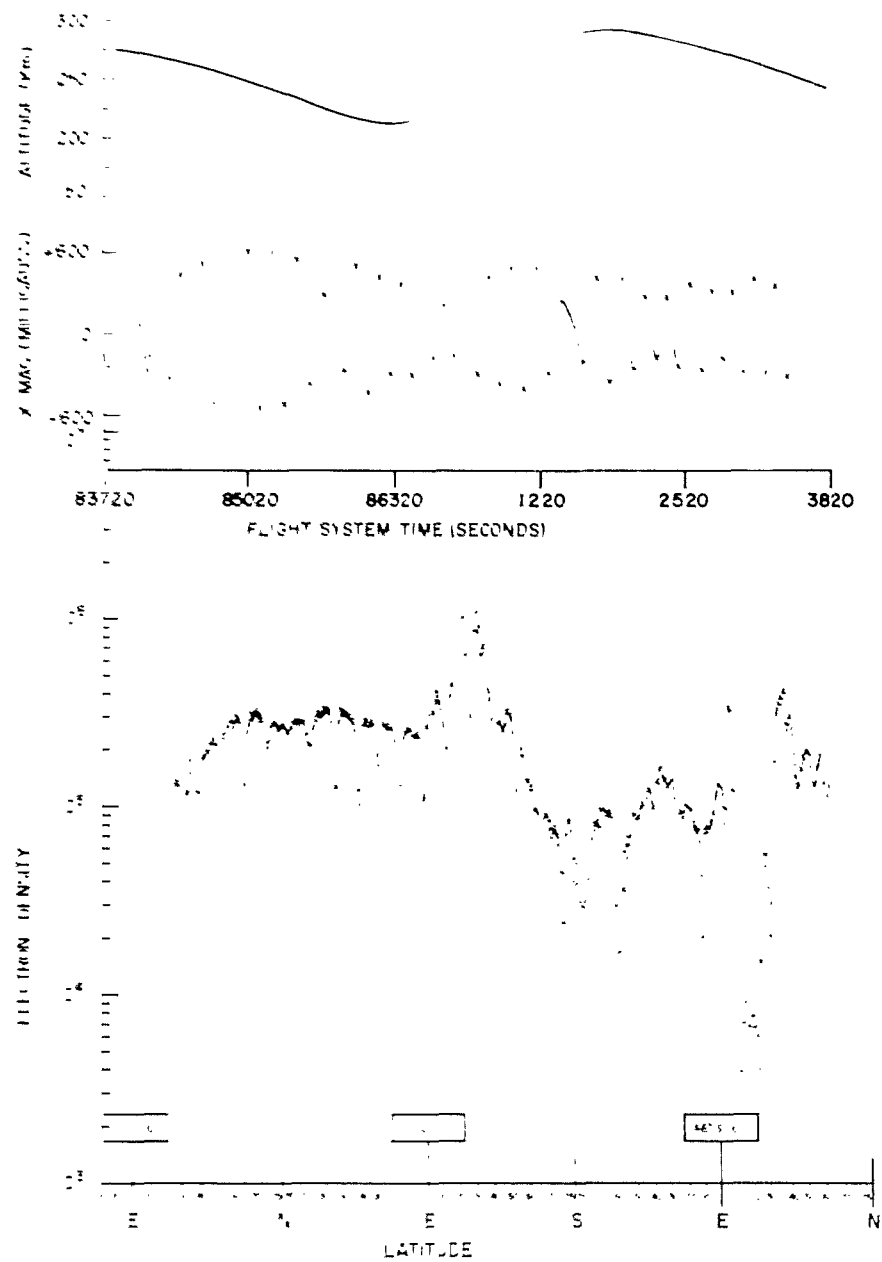


Figure 3.9 Orbit 95, 5-Mc results, HTS, Orbit 97 readout.





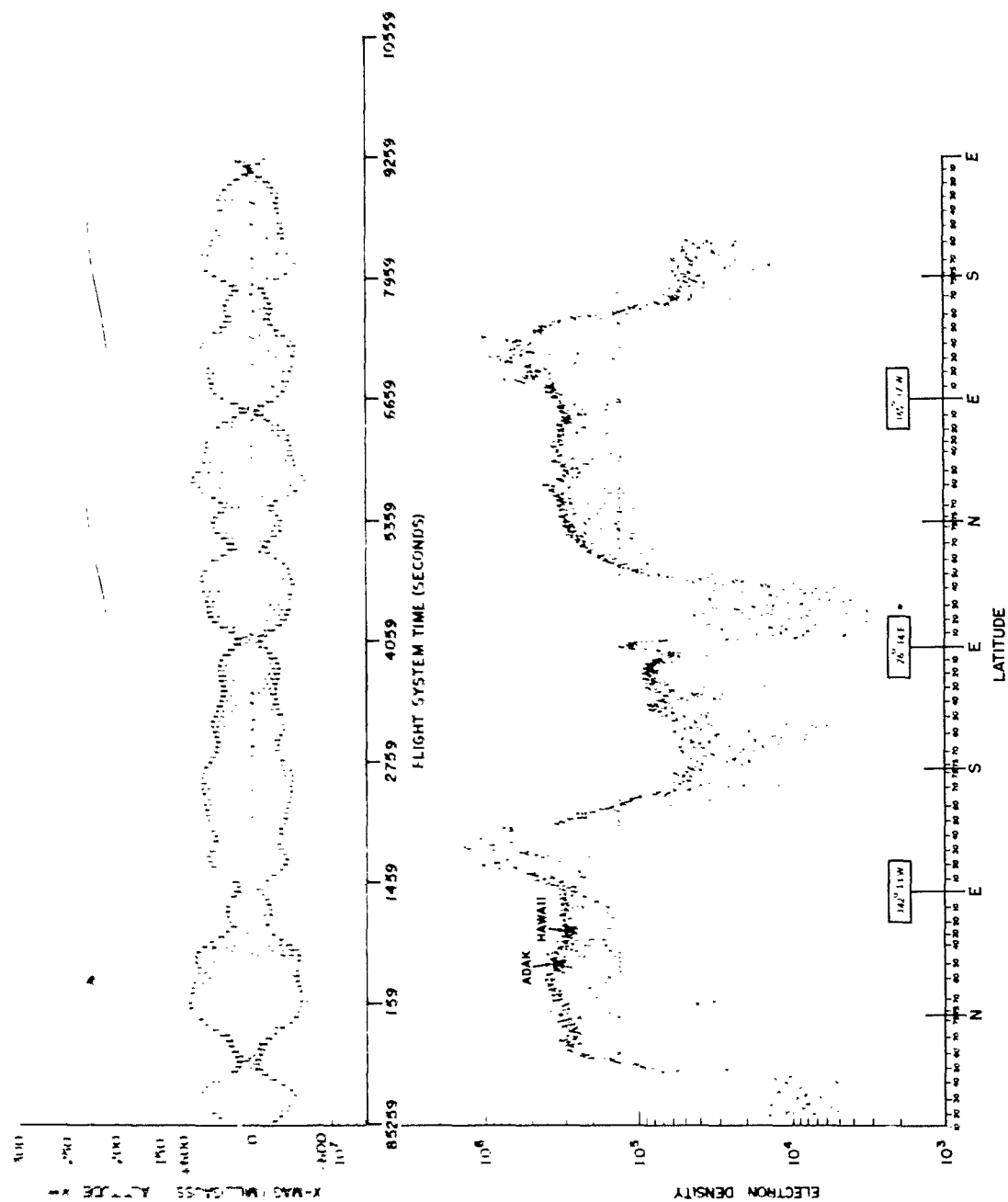


Figure 3.11 Orbit 177, 5-Mc results, VAFB, Orbit 185 readout.

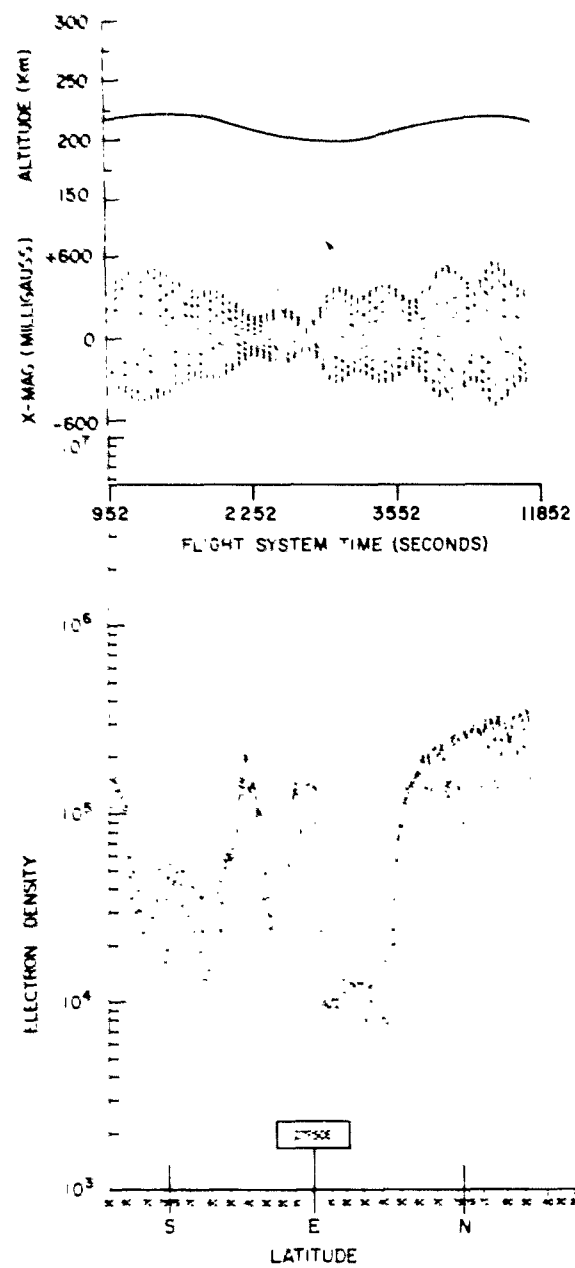


Figure 3.12 Orbit 193, 5-Mc results, VAFB, Orbit 208 readout.

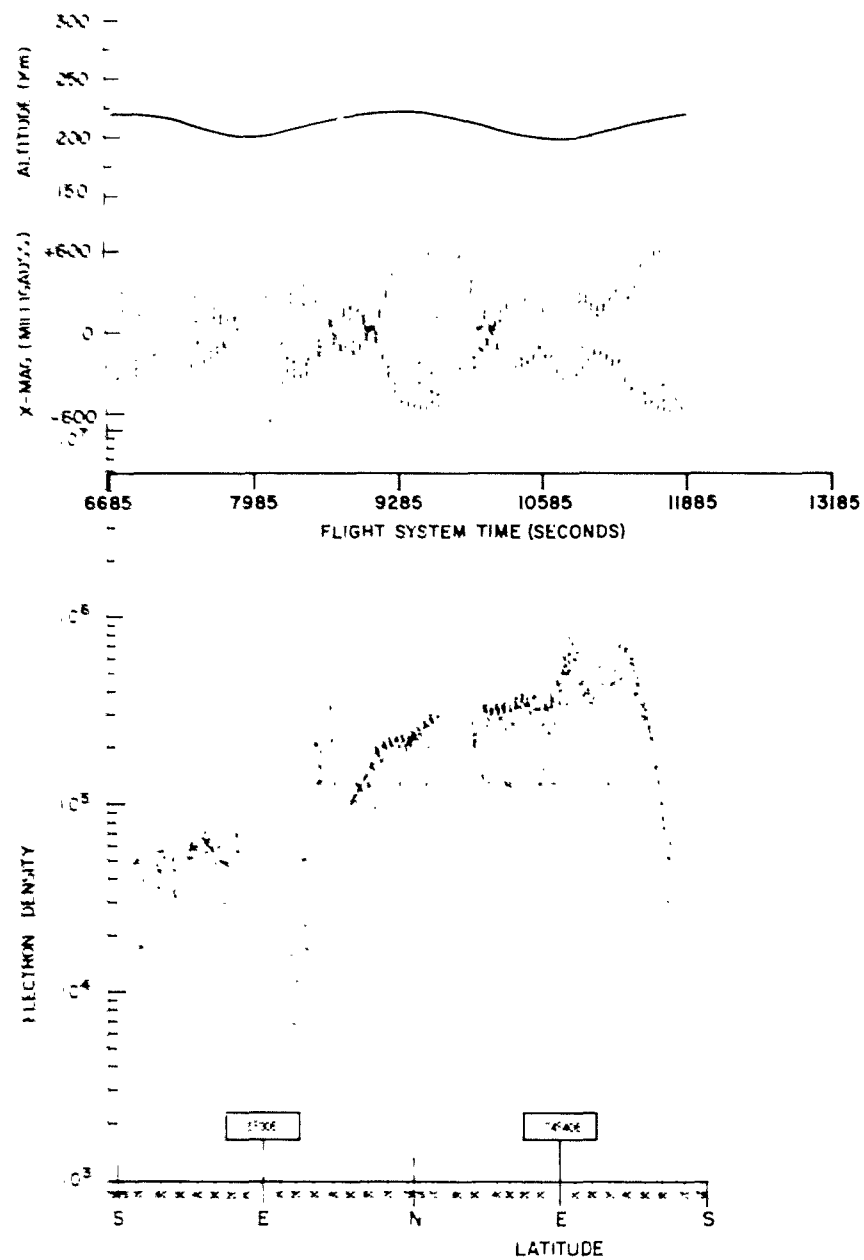


Figure 3.13 Orbit 194, 5-Mc results, KTS, Orbit 208 readout.

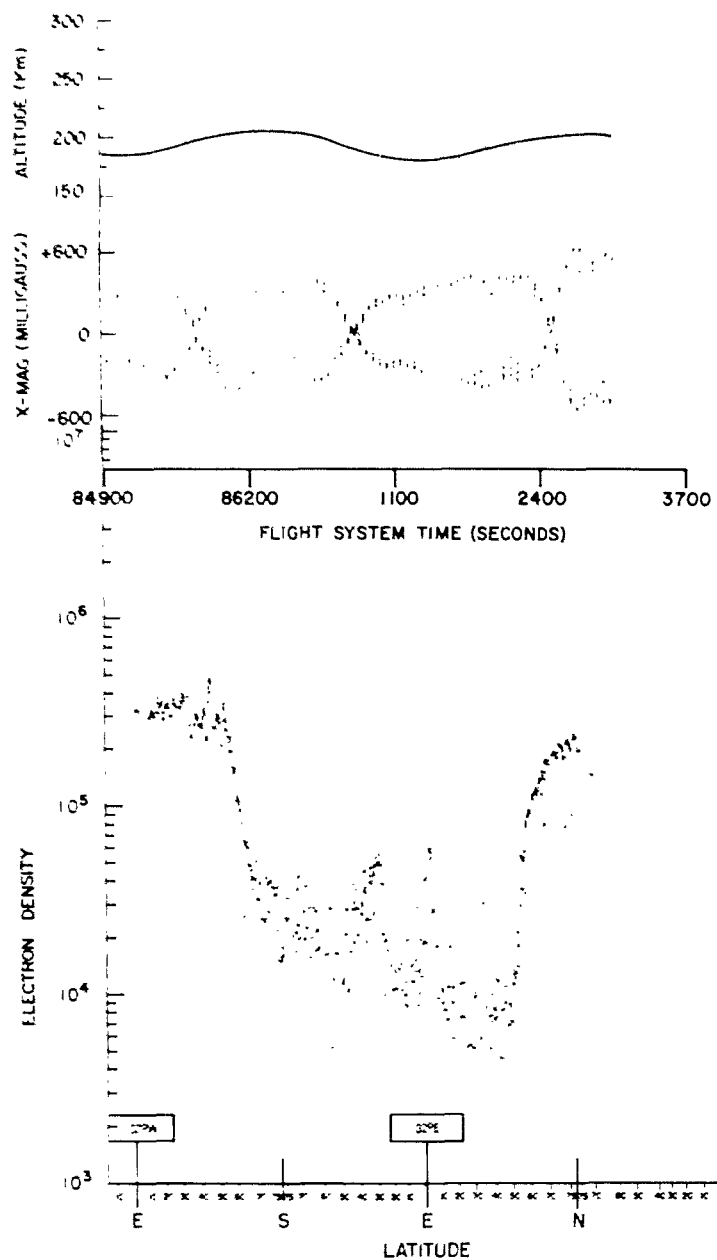


Figure 3.14 Orbit 209, 5-Mc results, HTS, Orbit 210 readout.

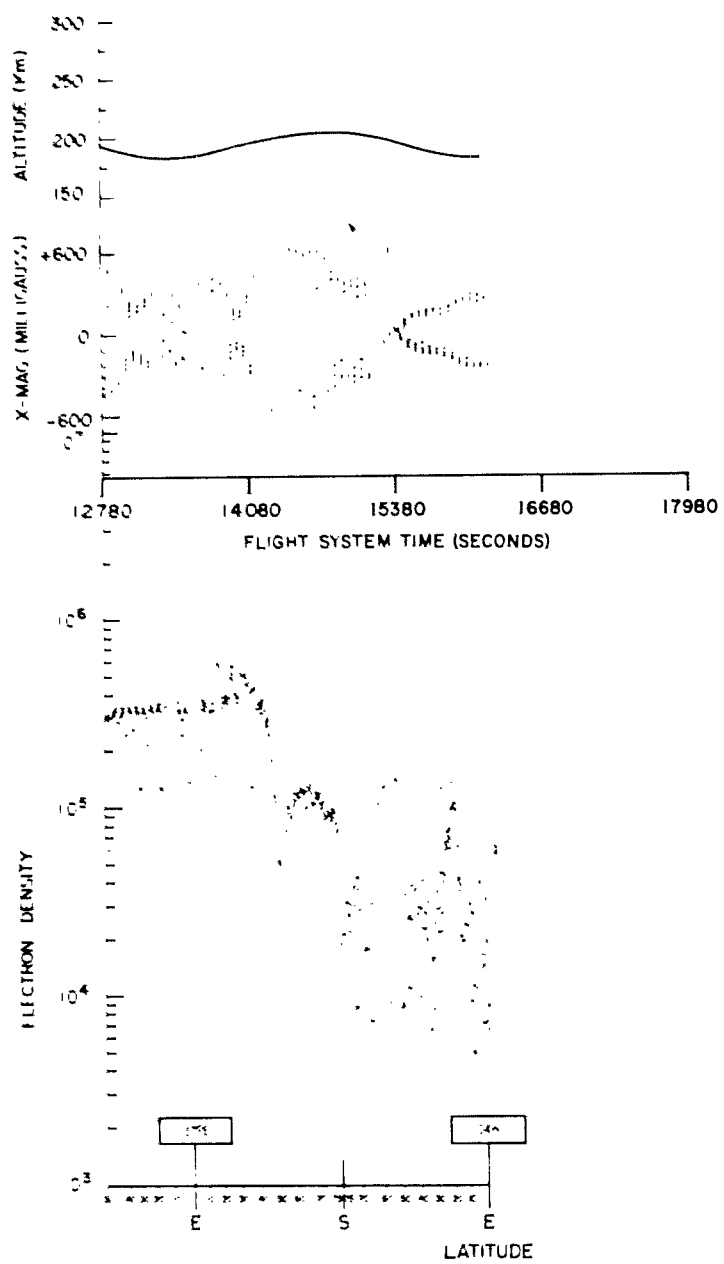


Figure 3.15 Orbit 212, 5-Mc results, NHTS, Orbit 215 readout.

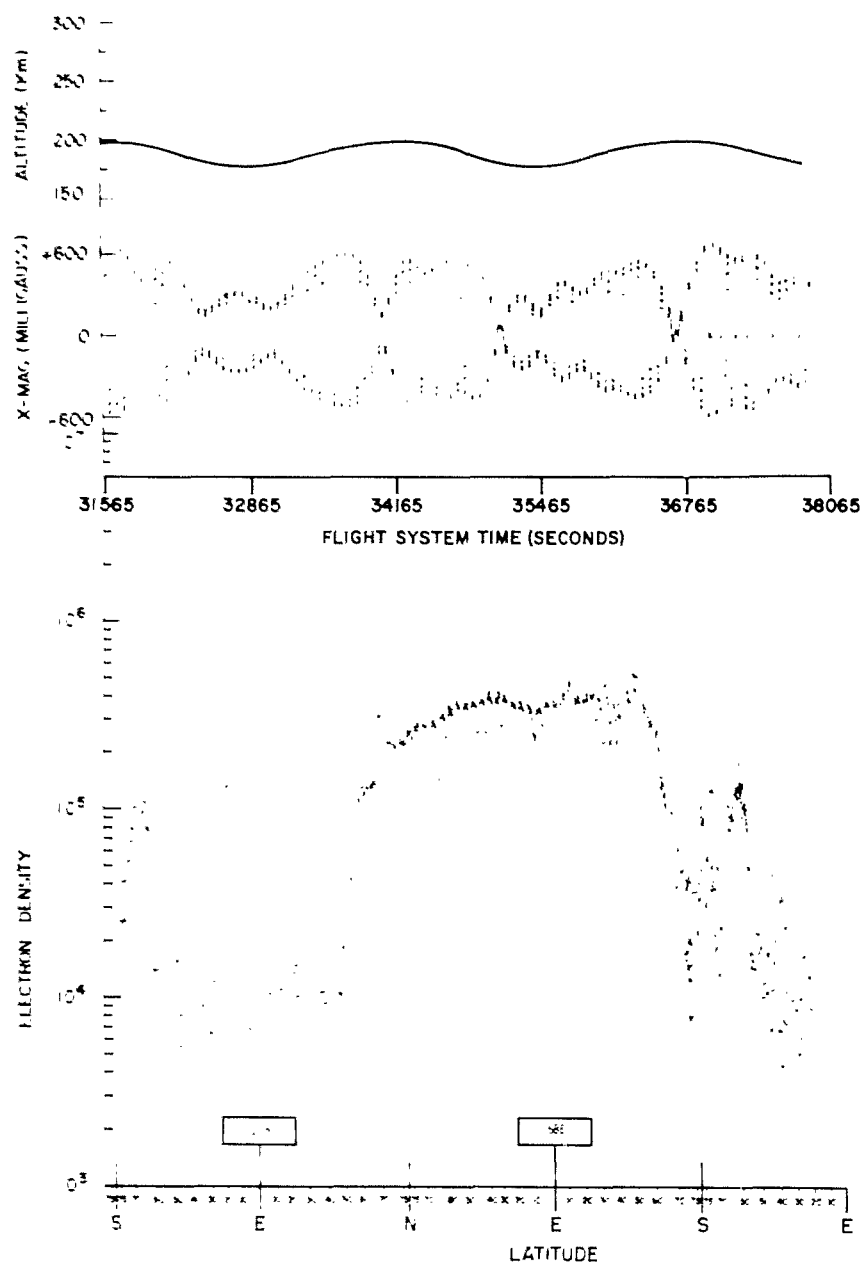


Figure 3.16 Orbit 215, 5-Mc results, VAFB, Orbit 217 readout.

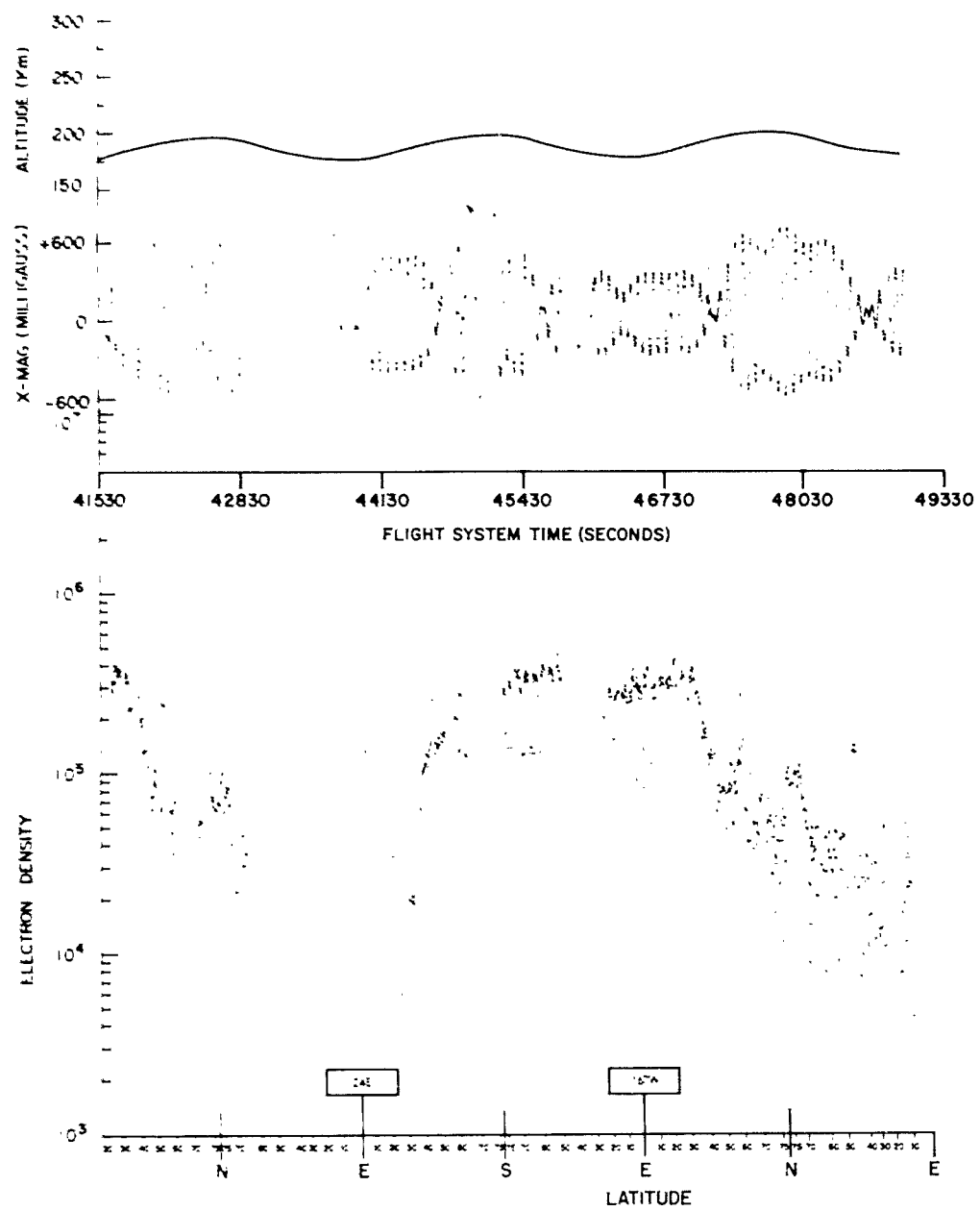


Figure 3.17 Orbit 217, 5-Mc results, KTS, Orbit 219 readout.



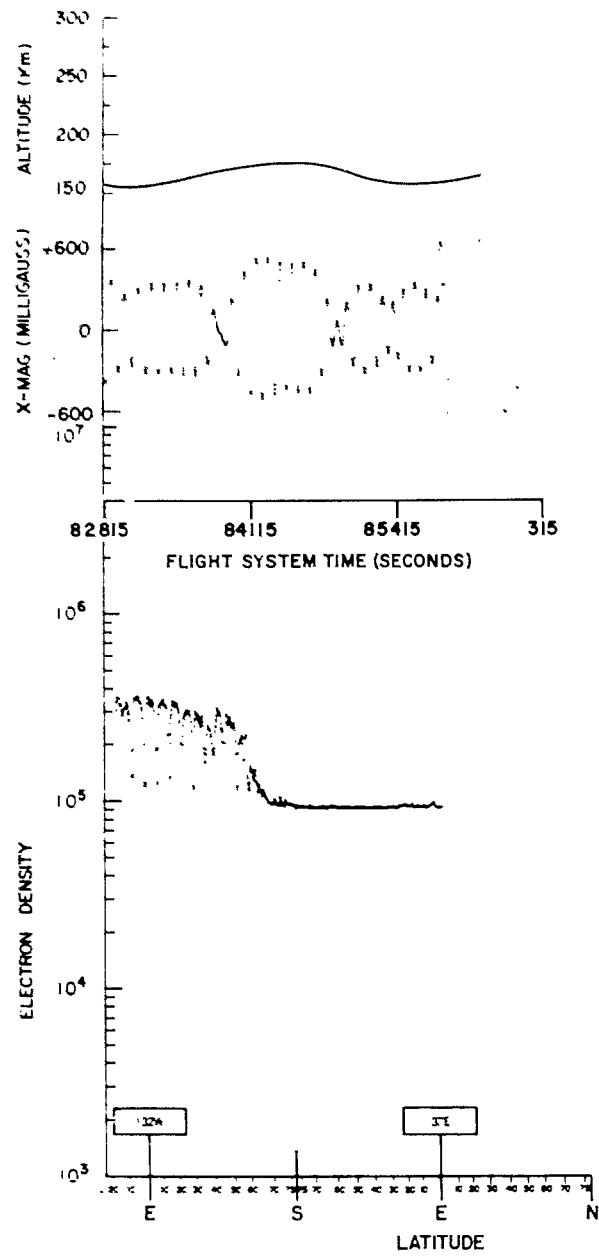


Figure 3.18 Orbit 225, 5-Mc results, HTS, Orbit 226 readout.

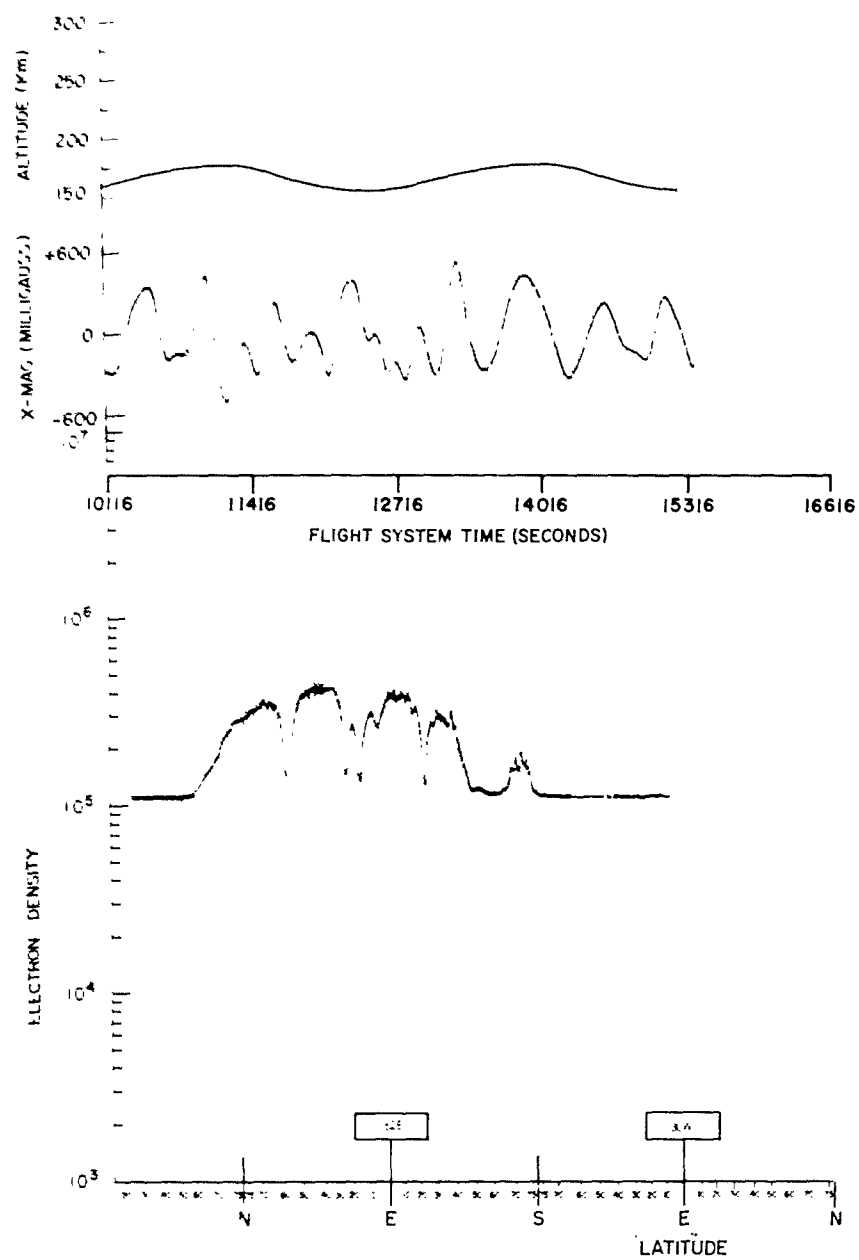


Figure 3.19 Orbit 228, 5-Mc results, VAFB, Orbit 231 readout.

## CHAPTER 4

### RADIOMETERS

#### 4.1 OBJECTIVE

The objective of this experiment was to measure the radio environment before, during, and after the Star Fish event. Measurements before the event would establish the existing natural radio background, thus allowing an absolute evaluation of the Star Fish effects. Measurements after the event would estimate the rate at which conditions were returning to normal. The work was undertaken by the Space Radio Project (SRP) of the Harvard College Observatory

The natural radio noise background is generated largely by the following processes:

1. Magnetobremssstrahlung (gyro-radiation) generated both by electrons trapped in the terrestrial magnetic field (the horns of the Van Allen belt have been detected as low as 300 km above the surface of the earth) and by precipitation of untrapped electrons, believed responsible for the auroras and possibly the night-glow. Conventionally, the gyro-radiation is divided into cyclotron (nonrelativistic energies) and synchrotron (relativistic energies) radiation, in which the harmonics of the cyclotron frequency become important,

2. Electromagnetic radiation scattered by magnetic field and inhomogeneities from plasma waves generated by the Cerenkov and two-stream processes in the ionosphere. The steep electron density

gradient ( $dN/dR$ ) of the lower ionosphere, however, does not favor the production of intense plasma waves.

3. Galactic radio radiation due to synchrotron radiation. This is expected to be substantially different along the galactic plane and toward the galactic halo. Possible contributions from discrete radio sources (Sun, Jupiter, Cassiopeia) should also be considered.

4. Natural terrestrial noise background due to local and propagating atmospherics. The intensity of this noise at low frequencies is modified by the propagation conditions and displays a diurnal variation shown in Figure 4.1.

5. Man-made noise, especially over densely populated areas. This noise is expected to be, in general, narrow-band in contrast to the mostly wide-band atmospherics.

From the above extensive but probably still incomplete list of potential radio noise sources, one can appreciate how complex, but also how necessary, are the measurements of the natural radio background, especially when the effects of an artificial event of similar nature are to be evaluated.

#### 4.2 BACKGROUND AND THEORY

This project has been engaged in a theoretical and experimental program to predict and measure the long-wavelength radio environment that is unobservable on the surface of the earth because of the shielding of the terrestrial ionosphere. The

frequency range of primary interest has been roughly from 10 Mc to 10 kc. To date, the project has prepared instrumentation for several satellites and probes in the Discoverer, MIDAS, and Blue Scout programs.

The results of the Argus and Jason projects in injecting and measuring beta decay electrons trapped in the terrestrial electromagnetic field has led to consideration of the various radio-environmental effects caused by this band of trapped electrons. The synchrotron radiation of these trapped electrons in the geomagnetic field will be peaked in the megacycle region of the spectrum which is unobservable on the surface of the earth. In addition, there is great interest in the electromagnetic pulse generated by the explosion itself.

The radioactive debris of a high-altitude nuclear explosion ejects beta decay electrons into the surrounding terrestrial magnetic field, producing synchrotron radiation. The most probable energy of electrons emitted is assumed to be 1 Mev. For evaluation, it is further assumed that the major energy radiated by these beta decay electrons falls into a rather small frequency interval around a frequency of maximum radiation. The

frequency of maximum radiation is given as:

$$\nu_{\max} = 1.4 \overline{H} \text{ gauss } (E/m_0 c^2)^2 \text{ Mc} \quad (4.1)$$

where:  $\nu_{\max}$  = frequency of maximum radiation, Mc

H = magnetic field, gauss

E = energy of electron, Mev

$m_0$  = rest mass of particle, Mev

c = velocity of light, m/sec

For E = 1 Mev,  $(E/m_0 c^2)^2$  becomes 4; thus the expression may be written as:

$$\nu_{\max} = 5.6 \overline{H} \text{ Mc} \quad (4.2)$$

At 400 km above the earth's surface,  $\overline{H}$  is roughly 0.25 gauss; therefore, for 1-Mev electrons the frequency of maximum radiation falls in the megacycle range. Measurements made on the electron spectrum resulting from the Argus project show a considerable number of electrons at 2 Mev and above, so that synchrotron radiation should be intense up to 10 Mc.

The effective temperature of such a cloud produced in the Argus project is:

$$T_e \approx 2 \times 10^8 / \overline{H} \text{ } ^\circ\text{K/Mt} \quad (4.3)$$

or roughly at the altitude of interest:

$$T_e \approx 10^9 \text{ } ^\circ\text{K/Mt} \quad (4.4)$$

This should be compared with a maximum cosmic radio background temperature of  $10^7$  °K at 4 Mc.

The synchrotron radiation is polarized and therefore could have possibly been detected as a modulation at the tumble period of the Discoverer satellite. The polarization of the synchrotron radiation would enable its detection at only a few percent of the cosmic background.

The experiment frequencies of 4.010- and 6.975-Mc are below the  $F_2$  ionospheric-region critical frequency over considerable portions of the satellite orbit. During those periods when the satellite was above the  $h_{\max} F_2$ , there still existed a possibility of leakage of terrestrially generated radio-frequency signals through the ionosphere. The project had, at Harvard University, a series of ground-based transmitters and receivers operating on the satellite frequencies. These transmitters sent out a coded sequence of pulses during times when the satellite passed over the Cambridge area. Time correlations of this pulse code, with the telemetry data, have been made to determine the local ionospheric attenuation at frequencies below the  $F_2$  critical frequency.

#### 4.3 INSTRUMENTATION

A large dynamic range, 80 db, was selected for the N-detectors (designated MkIc) to avoid the saturation which we had experienced

with previous satellite radiometers. Each payload included two radiometers operating at frequencies 6.975 Mc and 4.010 Mc. The bandwidth of both radiometers was  $\sim 10$  kc, and the post detection time constant was set at 2.5 seconds by the telemetry sampling rate.

The radiometers basically were crystal-controlled superheterodyne total power receivers with an intermediate frequency of 310 kc. The power drain was a modest 600 mw, including the voltage regulator. The radiometer input impedance was  $50\Omega$ . The performance of the receiver was continuously monitored in flight by switching periodically between the antenna ( $15 \text{ sec} \cong 6\tau$ ) and an internal load ( $5 \text{ sec} \cong 2\tau$ ). A block diagram of the MkIc radiometer is shown in Figure 4.2.

The MkIc radiometer was constructed of welded modules encapsulated in Stycast 1090H. One such module is shown in Figure 4.3. After the modules were assembled and tuned, the entire package and harness were also embedded in Stycast. The weight of each completed radiometer was 1.35 pounds. The payload in its final form is shown in Figure 4.4. The radiometers were calibrated at temperatures from  $-65^{\circ}\text{C}$  to  $+60^{\circ}\text{C}$ . An ambient temperature monitor was included in the payload, and its output was received along with the other telemetered data. As we will see in section 4.5 results, this humble monitor gave us some very useful information in an area where it was least expected but badly needed—on the satellite local time.



The antennas employed, one of which is shown in Figure 4.5, were Yeiser Laboratories 25-foot tape antennas and were used as monopoles because of the severe space and weight limitations of the satellites. Each antenna was power matched for free space, using a base loading inductance and a matching transformer.

Given the stringent space, weight, power, and telemetry limitations imposed on the radiometers and the tight time schedule for their bread-boarding, construction, and testing, SRP feels quite proud of their on-time delivery and their subsequent successful performance.

The lack of an ionospheric sounding station of continuous operation in the Boston area prompted the SRP to construct (as fast as it could) a simple ionospheric sounder to complement the N-detector observations. This would enable us to check the ionosphere for leakage of ground noise and at the same time evaluate the ionospheric conditions for wave propagation. The leakage test was performed by transmitting a coded signal from the SRP ground station at Harvard College Observatory to the satellite during its passage over the Boston area. After the completion of the sounder (it was ready only for one of the Discoverer satellites, Flight Test Vehicle (FTV) 1129), an ionogram was taken before and after each Boston passage of the satellite.

In addition to the sounder, two receivers were also operated at the same frequencies as the satellite radiometers (6.975 Mc and 4.010 Mc) to monitor the local activity at those frequencies. Operation of the

sounder, the transmitters, and the monitors required a group of three people on practically an around-the-clock schedule.

#### 4.4 DATA REQUIREMENTS

The data requirements for the reduction of the experimental results are: (1) complete ephemeris of the Discoverer satellite; (2) altitude, yield, time of detonation, and geocentric latitude and longitude of the nuclear device; (3) an indication of the energy and number of electrons trapped by the geomagnetic field as determined by other detectors on the Discoverer payload; (4) analog oscillographs of the decommutated telemetry with system times and pre- and post-calibrations clearly marked; (5) digital magnetic tape of the decommutated telemetry data in standard format for the IBM 7090 digital computer; (6) ionosonde data from as broad a coverage of the satellite orbit as possible; and (7) data from the Discoverer magnetometer for tumble and spin results.

#### 4.5 RESULTS

##### 4.5.1 Flight Test Vehicle 1127 Data.

The data obtained from our radiometers were not of good quality because the temperature environment immediately after ejection of the capsule was too low for optimum operation of our equipment. Until the satellite could start rotating and equalize the temperature (about orbit 50), the vehicle was completely stabilized, and our radiometers, mounted on the Agena airframe and directly exposed to space, were on

the cold (shadowed) side of the vehicle. These radiometers had been designed to operate most efficiently at room temperature, and this condition was never achieved by Flight Test Vehicle 1127. Operating temperatures were very low ( $\sim 30^{\circ}\text{C}$ ), so the sensitivity of the instruments was greatly reduced.

#### 4.5.2 Flight Test Vehicle 1128 Data.

The received quick-look data of Flight Test Vehicle (FTV) 1128 have indicated that our radiometers performed satisfactorily after orbit 55, i.e. after the temperature was stabilized around  $10^{\circ}\text{C}$ . A complete thermal history of our payload is shown in Figure 4.6, and from it one can see why the radiometers of FTV 1127 ran into difficulties during the early orbits.

Partial restrictions and priorities on data processing at Lockheed have curtailed the reduction of the tape-recorded data from FTV 1128 to their final form (brightness temperature or radio noise flux). However, we have undertaken to reduce the tape-recorded data by eye and hand from the available quick-look strip charts. This is a hard and slow process, and the accuracy obtained in this manner is much inferior to that of a computer reducing the data from the original magnetic tapes. However, it is hoped that in the future a proper and accurate reduction of the data can be made.

Some of the tape-recorded data of FTV 1128, reduced in the above-mentioned manner, are plotted in Figures 4.7, 4.8, and 4.9,

along with total magnetic field and the payload temperature. The necessity of using the magnetometer and the temperature data will be explained below. A summary of the FTV 1128 real time data, the only ones reduced in the computer, is given in Table 4.1. In this table, Rev is the satellite revolution, UT and LT are universal and local time, respectively.  $T_b$  is brightness temperature, and S is flux.

Transmissions to measure ionospheric leakage were made from Harvard Observatory during the active life of the satellite. We operated for the total of 46 passes over the Boston area. It is anticipated, however, that the leakage results will be inconclusive because of the satellite's low altitude.

#### 4.5.3 Flight Test Vehicle 1129 Data.

The originally received quick-look data indicated that our radiometers performed satisfactorily, and this was confirmed by the subsequently received reduced data.

The ionospheric sounder was completed in time for the Flight Test Vehicle (FTV) 1129 satellite. Ionograms were taken preceding and following each passage of the satellite over the Boston area. In addition, ionograms taken at other different parts of the day established the diurnal variation of the ionosphere during the satellite flight. An example of the transmission operation and the results obtained is shown in Figure 4.10.

Most of the records indicate that the transmitter (5-second pulses) is clearly picked up by the satellite radiometers, but these results are not conclusive because of the very low orbit of the satellite.

The thermal history of the FTV 1129 payload, shown in Figure 4.11, displays the same features evident in the record of FTV 1128. A summary of the real time observations from the reduced real time data is given in Table 4.2. In this table, Rev is the satellite revolution, UT and LT are universal and local time, respectively.  $T_b$  is brightness temperature, and S is flux. A more elaborate analysis was reserved for the extended tape recorded data.

The logs of the maximum, the minimum, and the average of every observational cycle, each one having a duration of 20 seconds divided into 15 seconds on the antenna and 5 seconds on the internal calibration, were tabulated and plotted vs universal time. In practically all the records, a large difference between the maxima and the minima appeared in certain sections of the orbit; this separation occasionally reached several orders of magnitude. A more detailed analysis of all the points within each observing period revealed that the apparent separation was due to a  $\sim 5.1$ -second-period oscillation of the noise level. A closer search through all the records showed these oscillations to be more frequent at 4.010 Mc than at 6.975 Mc. An expanded picture of the oscillations is shown in Figures 4.12 and 4.13. Figure 4.12 shows the oscillations appearing at 4.010 Mc but not at

6.975. In Figure 4.13 the oscillations appear simultaneously on both frequencies. The cause of these oscillations is not exactly clear. We will discuss this phenomenon again in the conclusion.

In addition to plotting the logs of the maxima, minima, and averages, we also plotted the difference for the two frequencies (4.010 Mc and 6.975 Mc) against time for all available orbits. The differences of these logs is the log of ratio of the maximum, minimum, and average radio noise level at the two frequencies, and is indicative of the slope of the spectral index in the region of the above mentioned frequencies. A typical long orbit (No. 185 recorded at Vandenberg Air Force Base) where all these plots are included is shown in Figure 4.14.

Polar diagrams of the averages at 4.010 Mc and 6.975 Mc were also made to evaluate the latitude dependence of the received radio noise. Orbit 185 (Vandenberg) is diagrammed in Figure 4.15. Figure 4.16 displays the averages at 4.010 Mc from seven different orbits (No. 80, recorded at Kodiak; 97, Hawaii; 153, Vandenberg; 185, Vandenberg; 210, Hawaii; 217, Vandenberg; 231, Vandenberg), and Figure 4.17 shows the averages at 6.975 Mc for the same orbits. This combined representation was chosen to demonstrate the repetition of some typical features from orbit to orbit, and also to show the progressive emergence in the later orbits of a characteristic pattern.

Finally in Figures 4.18 to 4.29 the averages of the two frequencies are shown together for all the 12 available orbits (there are

at least 300 such average points in each diagram, corresponding to the 300 or more 20-second observational periods included in each tape-recording). This representation demonstrates the similarity of the patterns obtained at the two frequencies. It also shows some small but significant differences that the two patterns exhibit. One such difference is that the radio noise level rises and falls more smoothly at 6.975 Mc than it does at 4.010 Mc; another is that the 6.975 Mc pattern rises ahead and falls after the one at 4.010 Mc. These features hint that there is a strong dependence of the radio noise level on the ionospheric electron density. These results will be discussed further in the conclusion.

#### 4.6 DISCUSSION

##### 4.6.1 Flight Test Vehicle 1127.

The magnetometer and the electron density probe performed rather normally during the early orbits. The formula suggested by Lockheed (letter of July 27, 1962),

$$t = 13563 + 26.5 T$$

where  $t$  = systems time

$T$  = plot time

rendered completely incompatible results for all the data. However, from the few available clock data, we were able to reduce a new time formula:

$$t = 14786 + 26.0 T$$

and this produced the anticipated over-the-earth pattern for the total magnetic field and the electron density. These are shown along with our data in Figure 4.30.

Because the finality of the satellite power system failure was uncertain, the transmissions to measure ionospheric leakage were continued until orbit 101, i. e. a total of 25 passes over the Boston area. Unfortunately the satellite did not recover.

#### 4.6.2 Flight Test Vehicle 1128.

The ephemeris of Flight Test Vehicle (FTV) 1128 was satisfactory but incomplete. A jump (increase) of about 15 km takes place in the interface of the two ephemeris sections, due presumably to computer extrapolations.

The major problem with the tape recorder data analysis was presented by the failure of the satellite clock and the failure of the electron density probe. The only data that would help place the orbit were from the magnetometer (which could place to a rather good approximation the crossing of the equator as well as the northernmost and southernmost latitudes of the orbit — the NPT and SPT) and from the ambient temperature monitor of our equipment.

The temperature monitor could be of help in the following manner. From our previous experiments we had observed that the temperature would reach minimum around sunrise. This minimum point could be located to a rather good approximation on our records. On the other



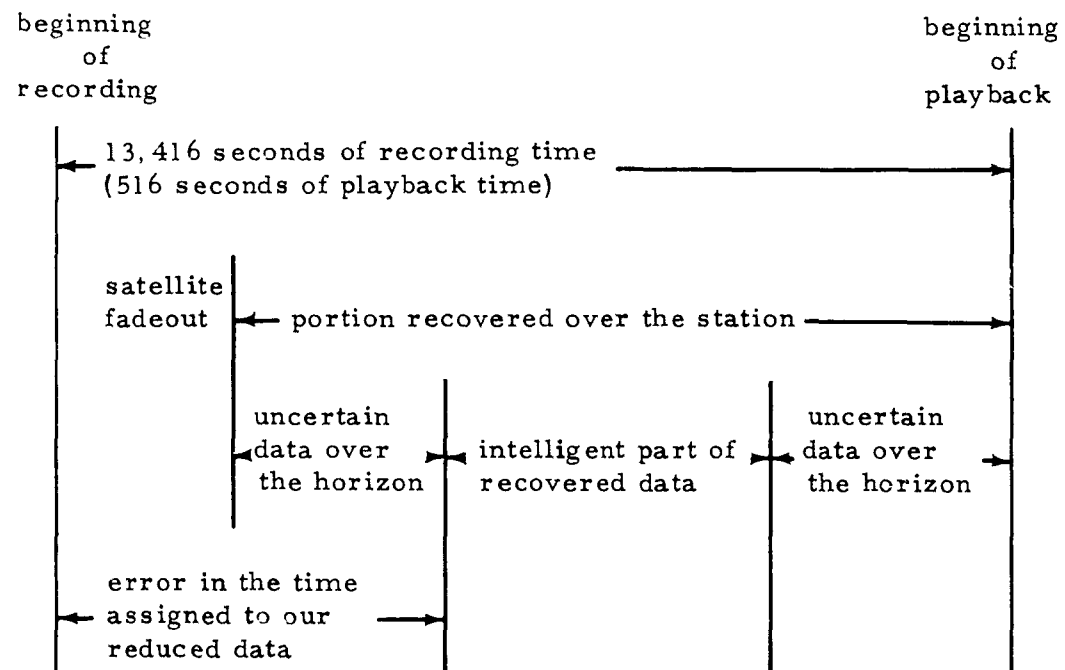
hand, the ephemeris gives the universal time and longitude and hence the local time of each segment of the orbit. In this manner the point of the orbit where we have local sunrise could be found and associated with the corresponding point on our records, and thus the orbit could be placed. The fact that the two methods (magnetometer and temperature monitor) are independent, and also that one usually has more than one such encounter for each tape record, allowed us to place the orbits with considerable confidence.

One might think that the orbit could be placed from the log books of the telemetry stations that operate the tape recorder. As we will see in the analysis of the FTV 1129 data, this unfortunately is not possible.

#### 4.6.3 Flight Test Vehicle 1129.

The digital listings of the reduced data received from Lockheed had printed on the side (according to our request) the corresponding universal time. When the data were plotted using this time list, a very puzzling pattern emerged. To resolve this problem we decided on a trip to Lockheed to have a first-hand contact with their computer staff. There we found that Lockheed, due to a misunderstanding between the computer staff and the tracking staff, had assigned to the beginning of our data the beginning of the recording time. This is not correct for the following reason.

The satellite can store approximately 13,416 seconds of data. This can be played back at a ratio of 260.1, i.e. in 516 seconds. The satellite, however, fades out beyond the tracking station before it has the opportunity to play back the whole record. The portion lost (at least 100 seconds of playback time, i.e. at least 2,600 seconds of actual recording) corresponds to the beginning of the recording, because the tape recorder plays back the data in reverse order. In addition an undertermined amount of data is lost on both sides of the station because of bad reception conditions when the satellite is close to the horizon. The following diagram illustrates the situation.



Because of the uncertainty concerning the actual amount of lost data, it is impossible to place the orbit from the log books of

the tracking stations. It must be remembered that a 12-second mistake in the playback time corresponds to a mistake of more than 20 degrees on the satellite orbit. For this reason, this method could not be used in placing the orbits of FTV 1128.

From the existing AFCRL clock data for FTV 1129, we were subsequently able to reduce the actual times of the tape records, which we also made available to all the other participants in the FTV 1129 satellite program.

Another difficulty encountered in reducing the FTV 1129 data was the inadequacy of the provided ephemeris. This ephemeris was composed of three completely mismatched sections, due presumably to over-the-border extrapolations of the computer. The fact that the satellite did not have a beacon after orbit 55, and the ephemeris had to be based only on tracking angles, could account for the computer error. The mismatching of the three ephemeris sections is shown in Figures 4.31 and 4.32. In addition to the mismatching problem, the ephemeris did not cover orbits over 200, where practically 50% of the data is located. Realizing the inefficiency of this ephemeris, Lockheed agreed to run a new one. However, this was not done because no funds were available.

Subsequently, we were able to obtain some SPADATS bulletins for the FTV 1129 satellite (officially called Alpha-Beta 1). Using these bulletins and the existing real time data, we constructed an ephemeris

for the orbits over 200, and using it, we were able to examine the large amount of data included in these orbits. At the time of this writing, we are still trying to produce a new ephemeris through SPADATS.

#### 4.7 CONCLUSIONS

##### 4.7.1 Flight Test Vehicle 1127.

The very limited amount of data obtained, coupled with the reduced sensitivity of our radiometers, made it practically impossible to draw any substantial conclusions from the Flight Test Vehicle satellite data.

##### 4.7.2 Flight Test Vehicle 1128,

The preliminary hand reduction of the Flight Test Vehicle (FTV) 1128 data has produced a latitude- and local-time-dependent pattern with average fluxes of the order of  $10^{-20}$  watt  $m^{-2}$  (cps) $^{-1}$  (see Table 4.1). The relatively short life of the satellite does not allow a clear separation of dependence on latitude and local time, because the satellite always reaches a certain latitude at approximately the same local time. A strong correlation of the 4- and 7-Mc data was observed, indicating a rather broad banded noise source.

A very striking feature of the tape-recorded data (see Figures 4.7, 4.8, and 4.9) is the very large dynamic range of radio noise level encountered over an orbit. The explanation could probably be found in the ionospheric propagation conditions and on the latitude and local time dependence of the radio noise level. This phenomenon which has not

yet been fully understood could be very significant in many space operations.

A more detailed analysis of the FTV 1128 data, including ionospheric leakage results, will be undertaken as soon as the data are properly reduced by the computer.

#### 4.7.3 Flight Test Vehicle 1129.

To obtain conclusive results (positive or negative) on the problem of ionospheric leakage, the satellite must be clearly above the  $F_2$  max, and the critical frequency of the ionosphere must be higher than the frequency of the coded signals transmitted to the satellite. The orbit of Flight Test Vehicle (FTV) 1129 was unfortunately much lower than originally anticipated. In fact, the satellite was never clearly above the  $F_2$  max over Boston, and therefore the obtained results cannot be conclusive. All the passes over the Boston area for which data are available show that the ground signal is recognized by the satellite. This confirms the basic principal of the experiment but does not answer the leakage problem, because of the low altitude of the orbit. Accurate measurements of the galactic radio noise were also precluded for the same reason.

The 5.1-second oscillations observed in our data seem to be caused by the fact that there is a second commutator of period 2.55 seconds on board the satellite. Each observational cycle of the electron density probe is made up of two periods of this commutator, i.e.,

a total of 5.1 seconds. During the first period, the low frequency (5 Mc) is in operation, and the mode monitor reads  $\sim 3.85$  volts. During the next period, the higher frequency (14.5 Mc) is used, and the mode monitor is at 2.8 volts. Through some coupling, which is not yet fully understood, this periodic alternation is imposed on our receivers, producing the observed 5.1-second oscillations. The puzzling part of the problem is that these oscillations appear only during certain sections of the orbit and not always on both frequencies. One explanation could be that the interference is regulated by the antenna impedance, and hence by the local electron density. A more detailed comparison of our data with that of the electron density probe, which hopefully will resolve this problem, has not been possible yet because of the different time listing of the two data.

The most striking feature of our data is the very large dynamic range of the received radio noise encountered over each orbit. The profile of the FTV 1129 orbit (Figures 4.18 to 4.29), especially of the later ones, is strikingly similar to the diurnal variation pattern of atmospheric noise as observed from the ground. This observation is not surprising in view of the low orbit of the FTV 1129 satellite. The local time dependence of the observed pattern (high during the night, low during the day, with steep changes at sunrise and sunset) is clearly shown in Figure 4.15.

A latitude effect was also observed with more pronounced signals

received around  $\pm 40^\circ$  latitude where most of the storm activity takes place. In the early orbits, as can be seen from Figure 4.33, the south-north crossing of the equator occurred at approximately 4:30 am local time, and the latitude and local time effects were to some extent opposing each other. This resulted in a not very clear pattern for these orbits (e.g., orbit 77 observed in New Hampshire, Figure 4.18). In the later ones the S-N crossing of the equator occurred at around 2:30 am local time, and the two effects seem to align together and produce a typical clear pattern (e.g., orbit 185 observed at Vandenberg, Figure 4.22).

An altitude dependence could not be established because of the practically circular orbit of FTV 1129, and also because there is some uncertainty regarding the reliability of the available altitude information.

No obvious longitudinal dependence was observed. However, some special features recurred from orbit to orbit for which no apparent geophysical correlation could be established because of lack of more extensive observations.

A comparison of the obtained flux patterns with the corresponding electron density profiles for the same orbits indicated very strongly the existence of the inverse correlation between the local plasma frequency and the observed radio noise fluxes.

The strength of the received radio noise will definitely depend on the ionospheric propagation conditions, especially in the lower ionosphere where the collision frequency is still high. Therefore the observed inverse correlation with the electron density is very much in line with what one would expect, and to a great extent explains the observed latitude and local time dependence of our data. A close correlation between the two frequencies was apparent, indicating the broad-banded nature of the noise source.

Though all the noise sources mentioned in Objectives, Section 4.1, may be present, the very large observed fluxes and their distribution suggest strongly that the predominant source is the atmospheric noise. If this is the case, then satellite observations such as those made by FTV 1129 (low-frequency radio noise measurements) will allow a rapid and complete earth coverage of atmospheric activity and storm centers.

#### 4.7.4 General Conclusions.

One of the two objectives of the N-detector satellites, the measurement of the Star Fish effects, has not been accomplished because of several postponements of the high-altitude nuclear detonation. The other objective, however, the evaluation of the ionospheric environment, has been carried out successfully for all the experiments on board. The electron density, the positive and negative ion densities, the magnetic field, the  $\beta$  and  $\gamma$ -ray fluxes, and the radio noise flux have been measured simultaneously for several orbits. This should provide quite



a complete picture of the encountered environment and its variations. In our case a very strong radio noise flux was measured, with substantial latitude and local time dependence. These unexpectedly high radio noise levels could have important repercussions on such vital areas as space telecommunications, ballistic missile guidance, radio navigation, etc. These experiments have also indicated that the atmospheric activity over the entire earth could be adequately monitored by a satellite-borne low-frequency radiometer. The detected radio noise levels in FTV 1128 were a little lower than the ones observed in FTV 1129. This could indicate an altitude dependence of the received radio noise, because FTV 1128 had a somewhat higher orbit.

The early failure of the FTV 1127 satellite and the rather low orbits of FTV 1128 and FTV 1129 have precluded any conclusive measurements on ionospheric leakage and galactic radio noise. This brings us to the recommendations for the future.

The existence of very strong radio noise fluxes below the  $F_2$  max should be more fully investigated in order to establish clearly its latitude, longitude, altitude, local time dependence, and correlation to other geophysical phenomena. A further investigation of natural and man-made radio noise leakage through the  $F_2$  layer has now become more pressing because of the very strong fluxes observed.

The ideal way to establish the global pattern of the radio noise below the  $F_2$  max and check for its possible leakage through it is to

use a sweep-frequency radiometer ( $\sim 1$  to 10 Mc) on an elliptical orbit satellite ( $\sim 200$ -km perigee,  $\sim 800$ -km apogee) with a long life expectancy and accurate ephemeris and clock information.

We hope that such an opportunity will arise in the future and that the valuable experience gained from the N-detector satellite will allow us to carry out this task successfully.

TABLE 4.1 FTV 1128 REAL TIME DATA

Rev	Sta*	UT	LT	4.010 log T <sub>b</sub>	4.010 log S	6.975 log T <sub>b</sub>	6.975 log S	ALT km	Comments
9	VAFB	1306	0506	5.3	-20.2	6.1	-18.9	346	Regular
55	NHTS	1005	0505	6.2	-19.3	9.0	-16.0	308	7 varies
58	HTS	1430	0430	6.2	-19.3	6.5	-18.5	321	4 offset
61	NHTS	1929	1429	6.2	-19.3	6.2	-18.8	202	7 quiet 4 varies
63	VAFB	2230	1430	5.3	-20.2	6.2	-18.8	198	Very good 7
65	HTS	0132	1532	5.0	-20.5	6.0	-19.0	191	4 noisy
71	NHTS	1005	0505	6.2	-19.3	6.5	-18.5	315	7 slope assypt.
77	NHTS	1927	1427	6.0	-19.5	6.8	-18.2	210	7 slope
79	KTS	2217	1217	5.5	-20.0	5.3	-19.7	245	Good
79	VAFB	2223	1423	5.3	-20.2	6.1	-18.9	220	7 noisy
81	HTS	0127	1527	5.3	-20.2	5.5	-19.5	198	Slopes
81	KTS	0124	1524	5.2	-20.3	5.8	-19.2	221	Very short
87	NHTS	0958	0458	6.2	-19.3	7.5	-17.5	317	7 noisy
87	TTS	1006	0506	5.0	-20.5	6.0	-19.0	301	4 poor
89	VAFB	1255	0455	8.0	-17.5	7.5	-17.5	324	Source
106	HTS	0120	1520	6.0	-19.5	6.3	-18.7	(250)	Begins well
129	HTS	0104	1504	5.5	-20.0	6.5	-18.5	250	Poor
143	VAFB	2147	1347	6.3	-19.2	6.5	-18.5	291	Poor
157	NHTS	1831	1331	6.0	-19.5	-	-	317	No data 7
*	VAFB	Vandenberg Air Force Base.							
	NHTS	New Hampshire (New Boston) Tracking Station.							
	HTS	Hawaii Tracking Station.							
	KTS	Kodiak (Alaska) Tracking Station.							
	TTS	Thule (Greenland) Tracking Station.							

TABLE 4.2 FTV 1129 REAL TIME DATA

Rev	Sta*	UT	LT	4.010 log T <sub>b</sub>	4.010 log S	6.975 log T <sub>b</sub>	6.975 log S	ALT km	Comments
77	NHTS	1935	1435	6.0	-19.5	6.7	-18.3	215	4 & 7 noisy
80	KTS	0000	1400	5.5	-20.0	-	-	240	Pulse
97	HTS	0135	1535	5.3	-20.2	6.2	-18.8	215	Quiet
105	VAFB	1255	0455	9	-16.5	12	-13	262	Very noisy
111	VAFB	2215	1415	5.3	-20.2	5.8	-19.2	216	Quiet
113	HTS	0120	1520	5.2	-20.3	6.2	-18.8	215	Quiet
127	VAFB	2205	1405	5.2	-20.3	6.1	-18.9	216	Quiet
129	HTS	0105	1505	5.2	-20.3	6.2	-18.8	215	Quiet
145	HTS	0050	1450	5.0	-20.5	6.0	-19.0	214	Quiet
153	VAFB	1215	0415	10	-15.5	12	-13	233	Very noisy
161	HTS	0035	1435	5.1	-20.4	6.2	-18.8	214	Quiet
169	VAFB	1200	0400	10	-15.5	12	-13	225	Very noisy
185	VAFB	1140	0340	11	-14.5	12	-13	218	Very noisy
208	KTS	2155	1155	5.0	-20.5	5.0	-20.5	220	Very quiet
208	VAFB	2200	1400	5.5	-20.0	6.0	-19.0	210	Quiet
209	KTS	2320	1320	4.8	-20.7	5.4	-19.6	220	Quiet
210	HTS	0000	1400	4.9	-20.6	5.4	-19.6	200	Quiet
215	NHTS	0750	0250	10	-15.5	12.6	-12.4	205	Poor

\* VAFB Vandenberg Air Force Base  
 NHTS New Hampshire (New Boston) Tracking Station  
 HTS Hawaii Tracking Station  
 KTS Kodiak (Alaska) Tracking Station

TABLE 4.2 CONTINUED

Rev	Sta*	UT	LT	4.010 log $T_b$	4.010 log S	6.975 log $T_b$	6.975 log S	ALT km	Comments
217	VAFB	1050	0250	9	-16.5	11	-14	200	Pulse
219	HTS	1340	0340	9	-16.5	11	-14	192	Pulse
221	NHTS	1705	1205	5.3	-20.2	6.2	-18.8	205	Spike
222	NHTS	1835	1335	5.7	-19.8	7.2	-17.8	205	Quiet
224	VAFB	2130	1330	6.0	-19.5	6.2	-18.8	200	Quite good
226	HTS	0030	1430	5.0	-20.5	5.5	-19.5	192	7 slope
231	NHTS	0720	0220	11	-14.5	-	-	160	No 7 Mc

\*      VAFB    Vandenberg Air Force Base.  
          NHTS    New Hampshire (New Boston) Tracking Station.  
          HTS     Hawaii Tracking Station.  
          KTS     Kodiak (Alaska) Tracking Station.

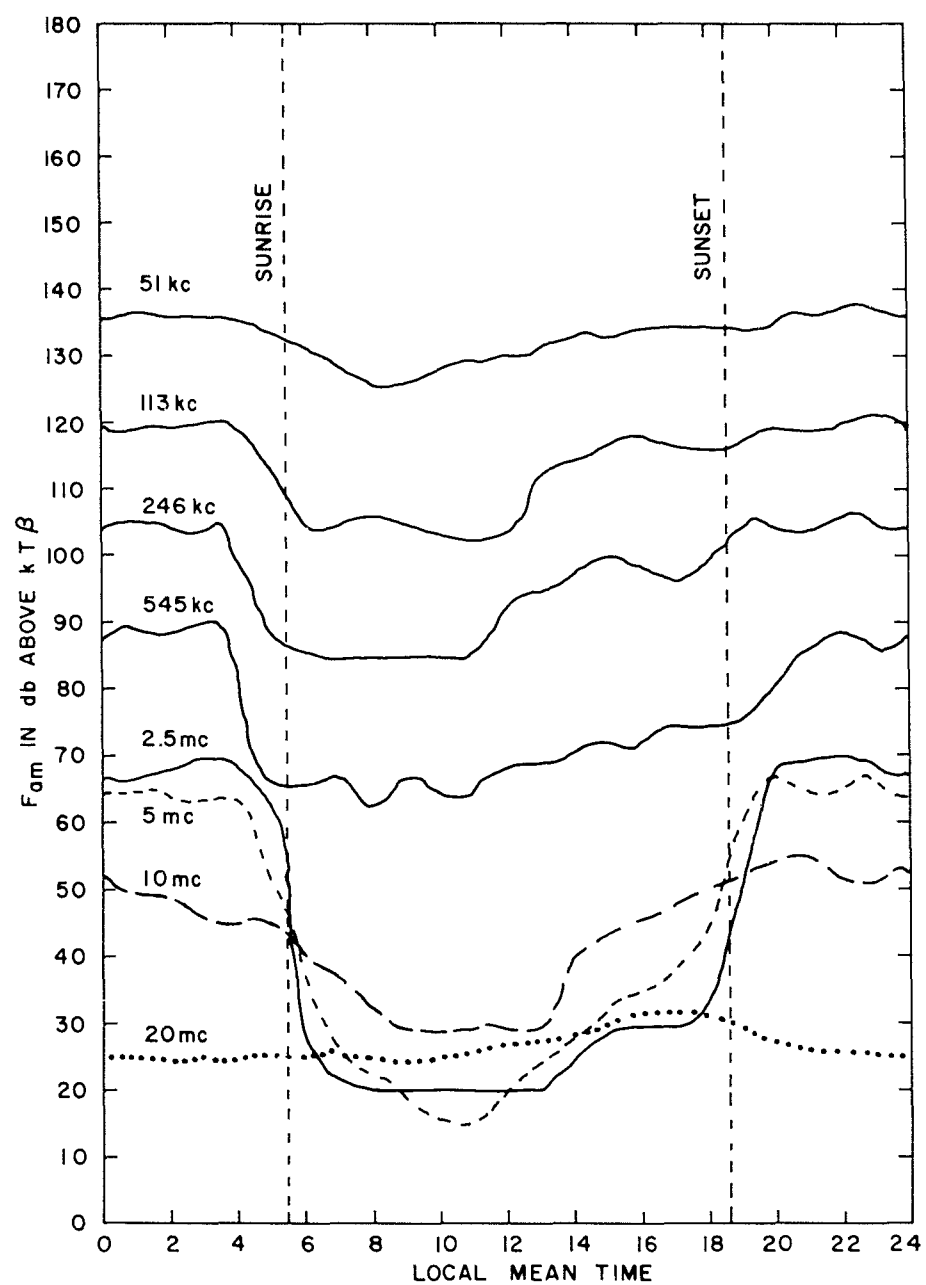


Figure 4.1 Diurnal spectrum of atmospherics.

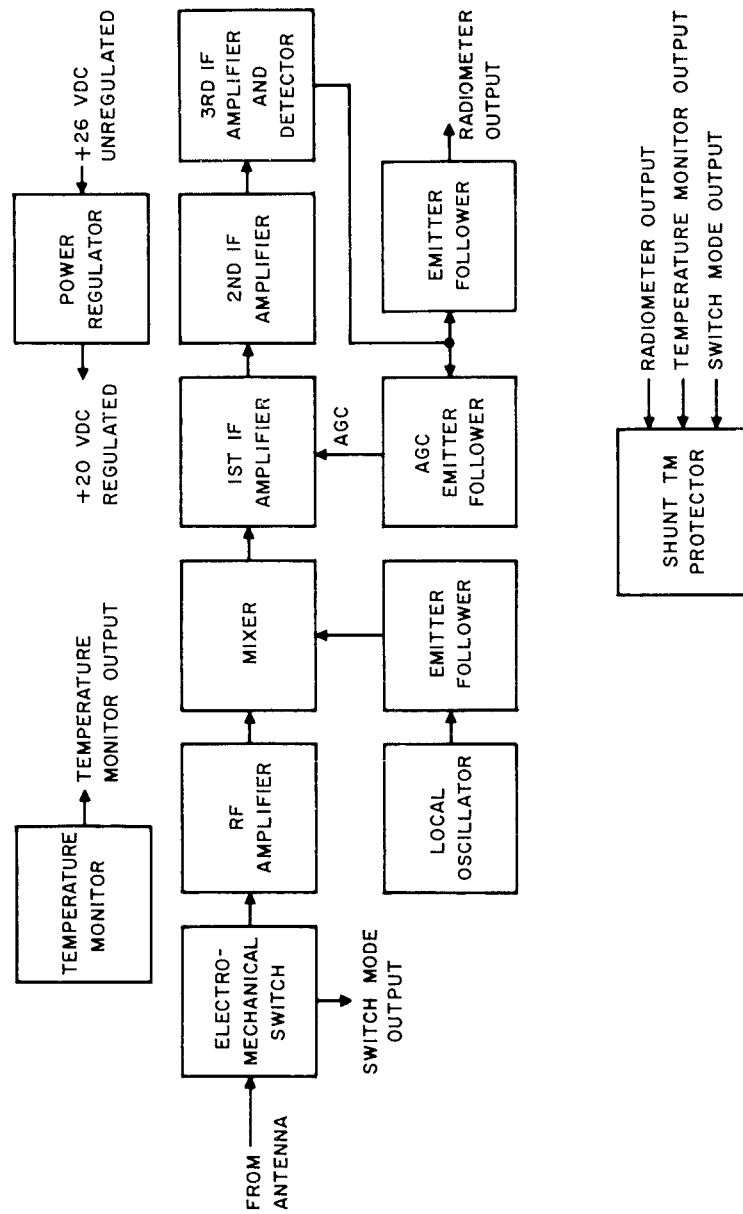


Figure 4.2 Block diagram for SRP MkIc radiometer.



Figure 4.3 Welded module for MkIc radiometer.

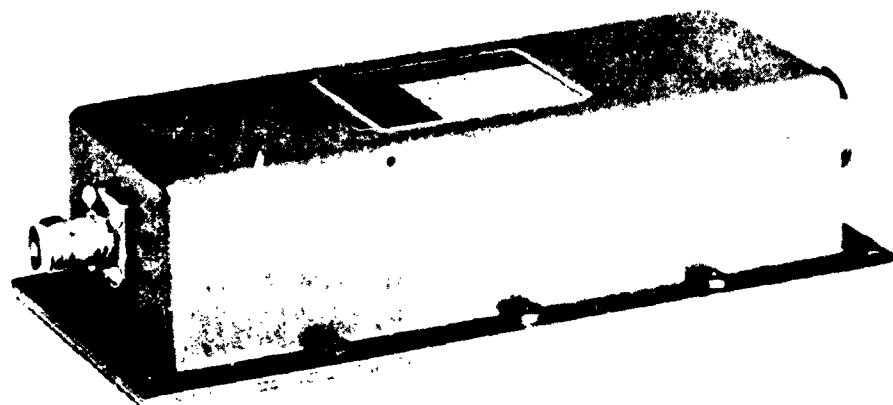


Figure 4.4 MkIc radiometer package, FTV 1127, FTV 1128, and FTV 1129.

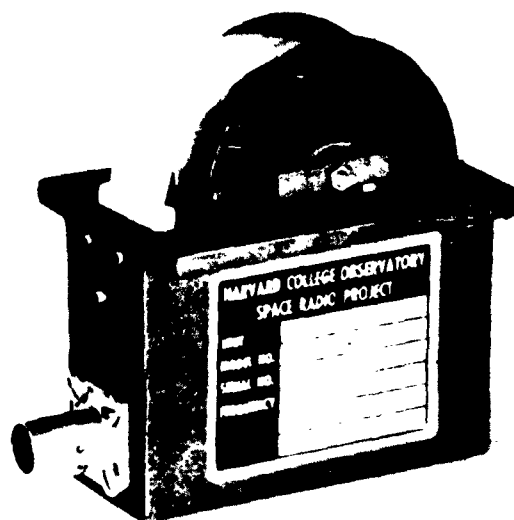


Figure 4.5 Yeiser Type A tape antenna.



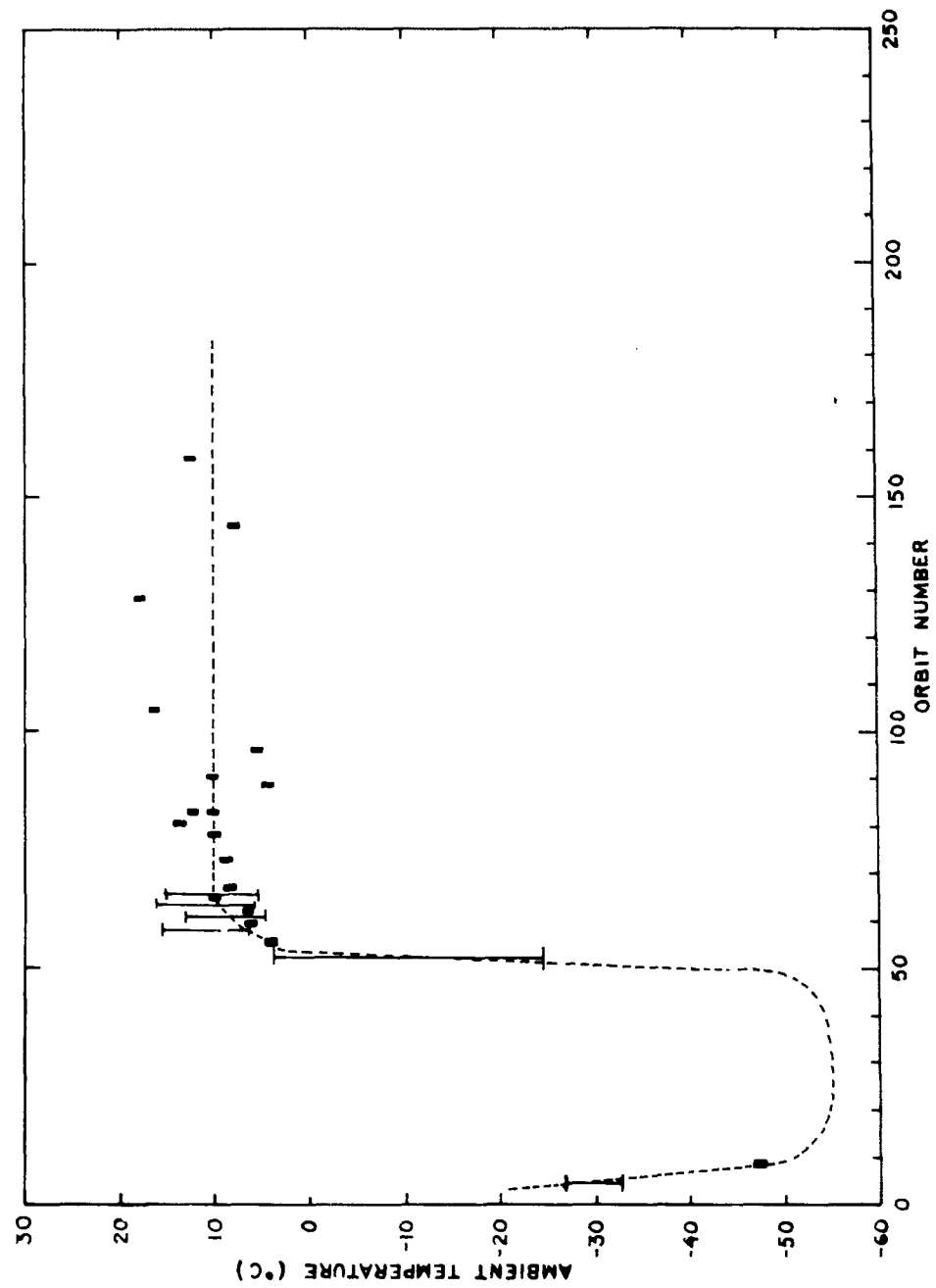


Figure 4.6 Ambient temperature history, FTV 1128 radiometer package.

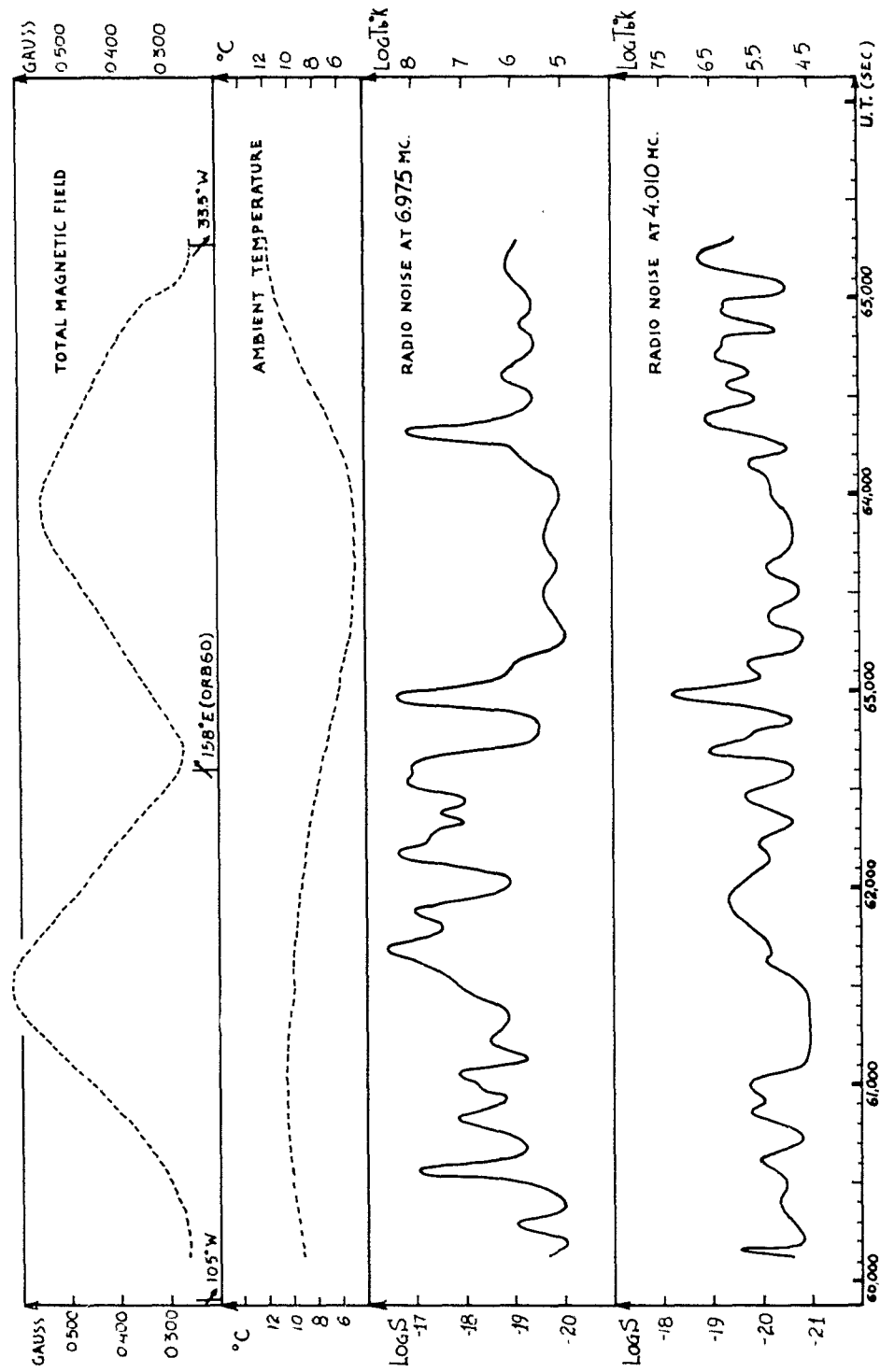


Figure 4.7 Tape-recorded data, Orbit 61, NHTS, FTV 1128.

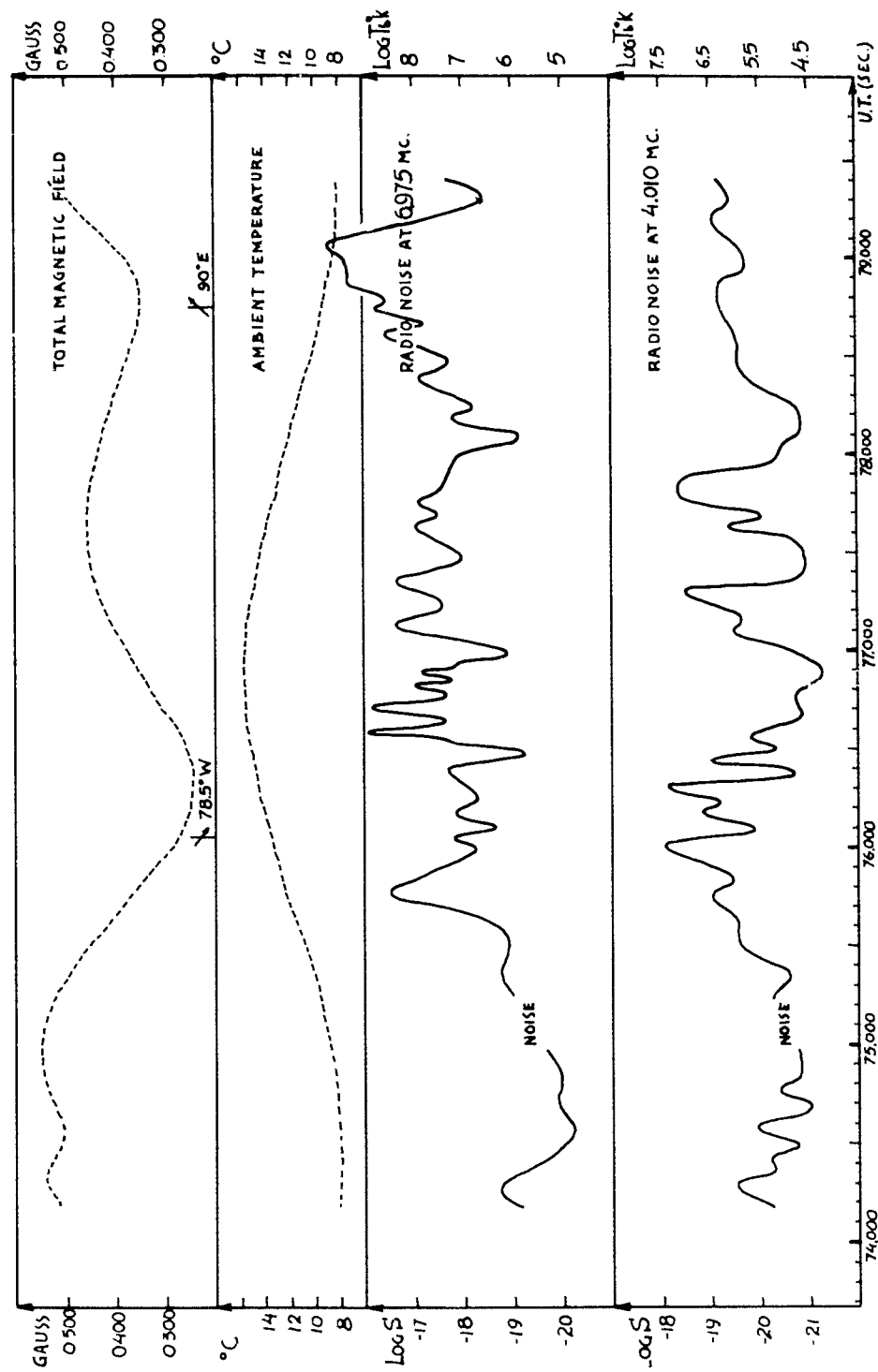


Figure 4.8 Tape-recorded data, Orbit 63, VAFB, FTV 1128.

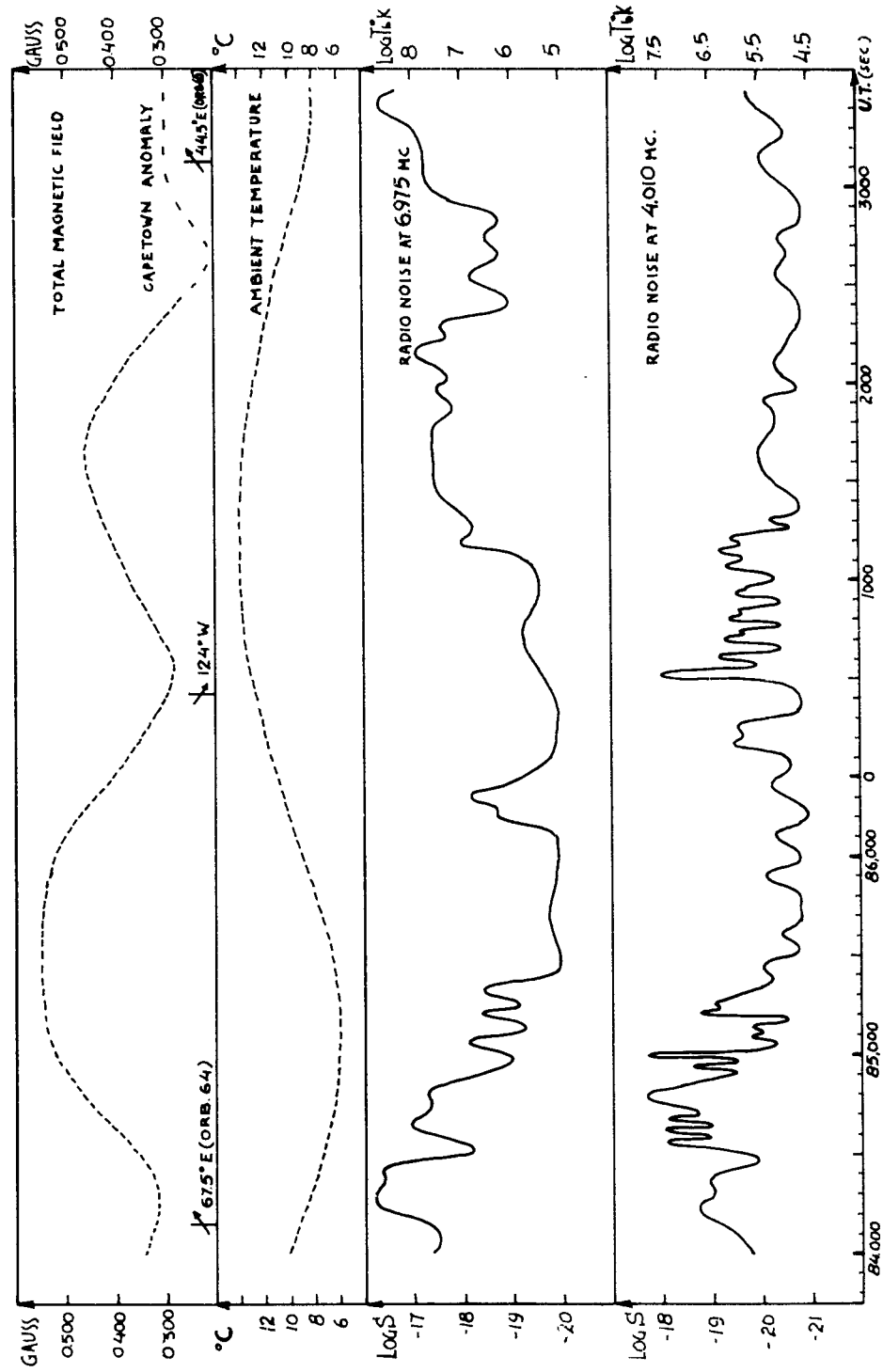


Figure 4.9 Tape-recorded data, Orbit 65, HTS, FTV 1128.

# IONOSPHERIC CONDITIONS

$h'F_2 \sim 230 \text{ Km}$        $f_o F_2 \sim 4.4 \text{ Mc}$

$h'F_1 \sim 200 \text{ Km}$        $f_o F_1 \sim 4.1 \text{ Mc}$

STRONG E-REGION AT  $\sim 135 \text{ Km}$ .

# SATELLITE DATA

FTV 1129, REV. 77, NEW BOSTON

HEIGHT  $\sim 260 \text{ Km}$ . MAX. ELEVATION  $\sim 36^\circ$

OPERATING FREQUENCY 4.010 Mc

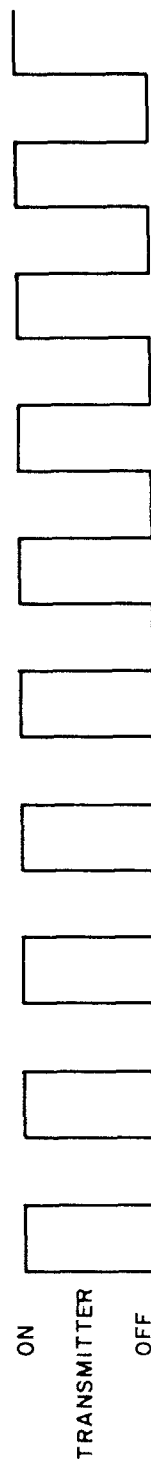
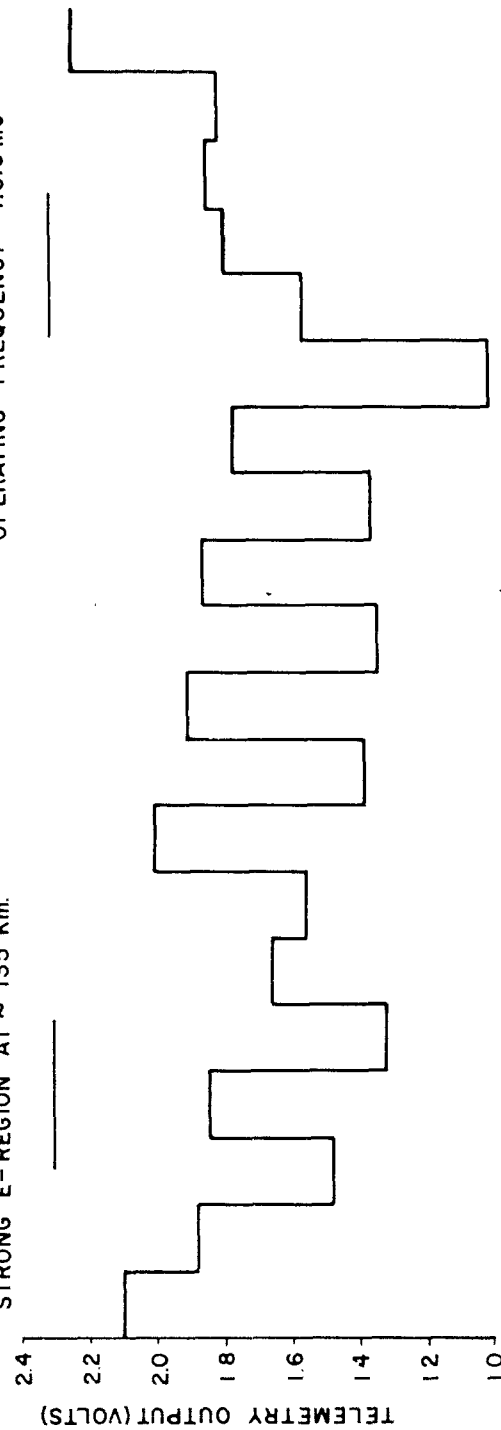


Figure 4.10 Satellite reception of ground transmitters.

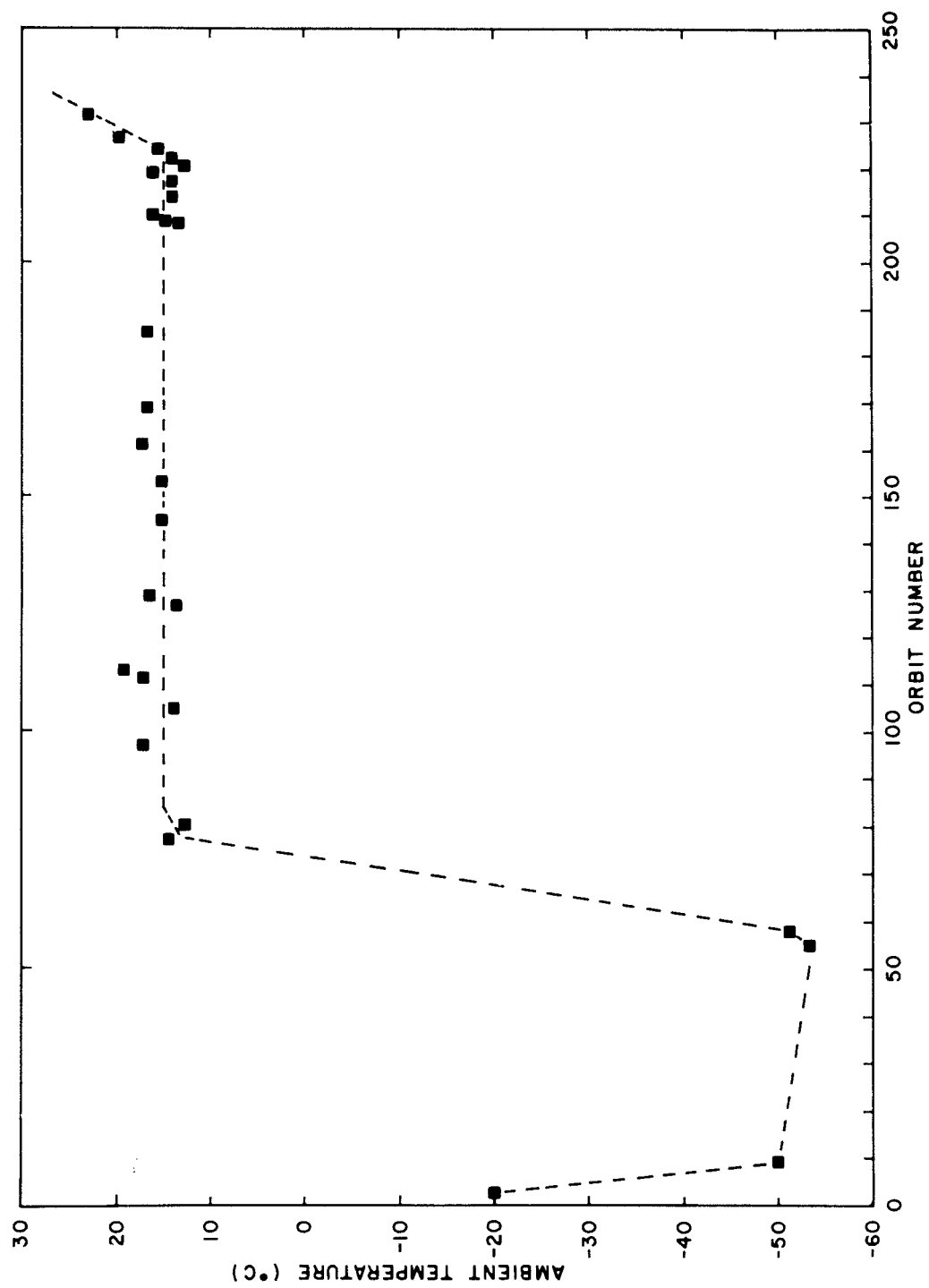


Figure 4.11 Ambient temperature history, FTV 1129 radiometer package.

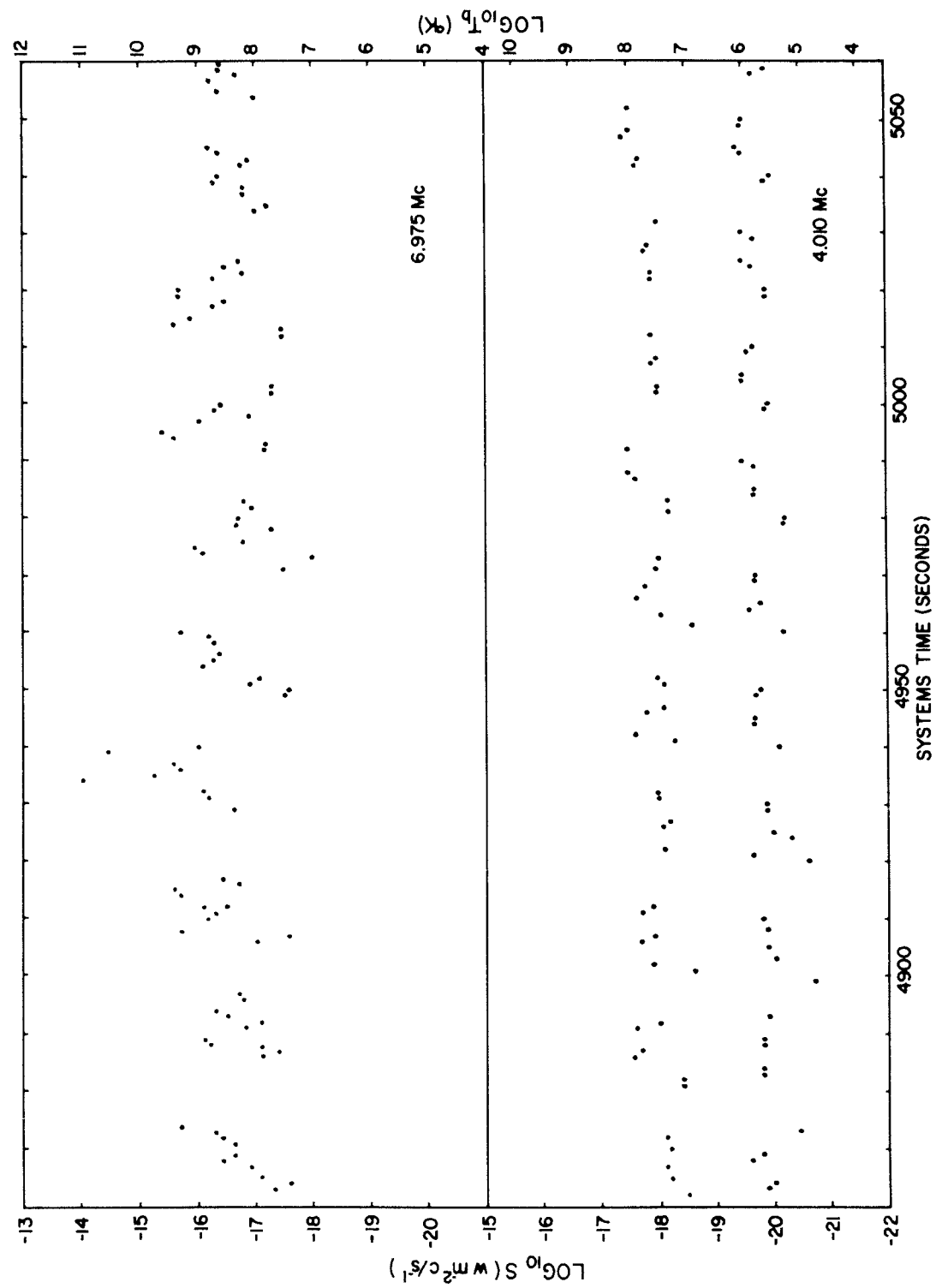


Figure 4.12 5-second oscillations on 4.010 Mc only, FTV 1129, Rev. 185, VAFB.

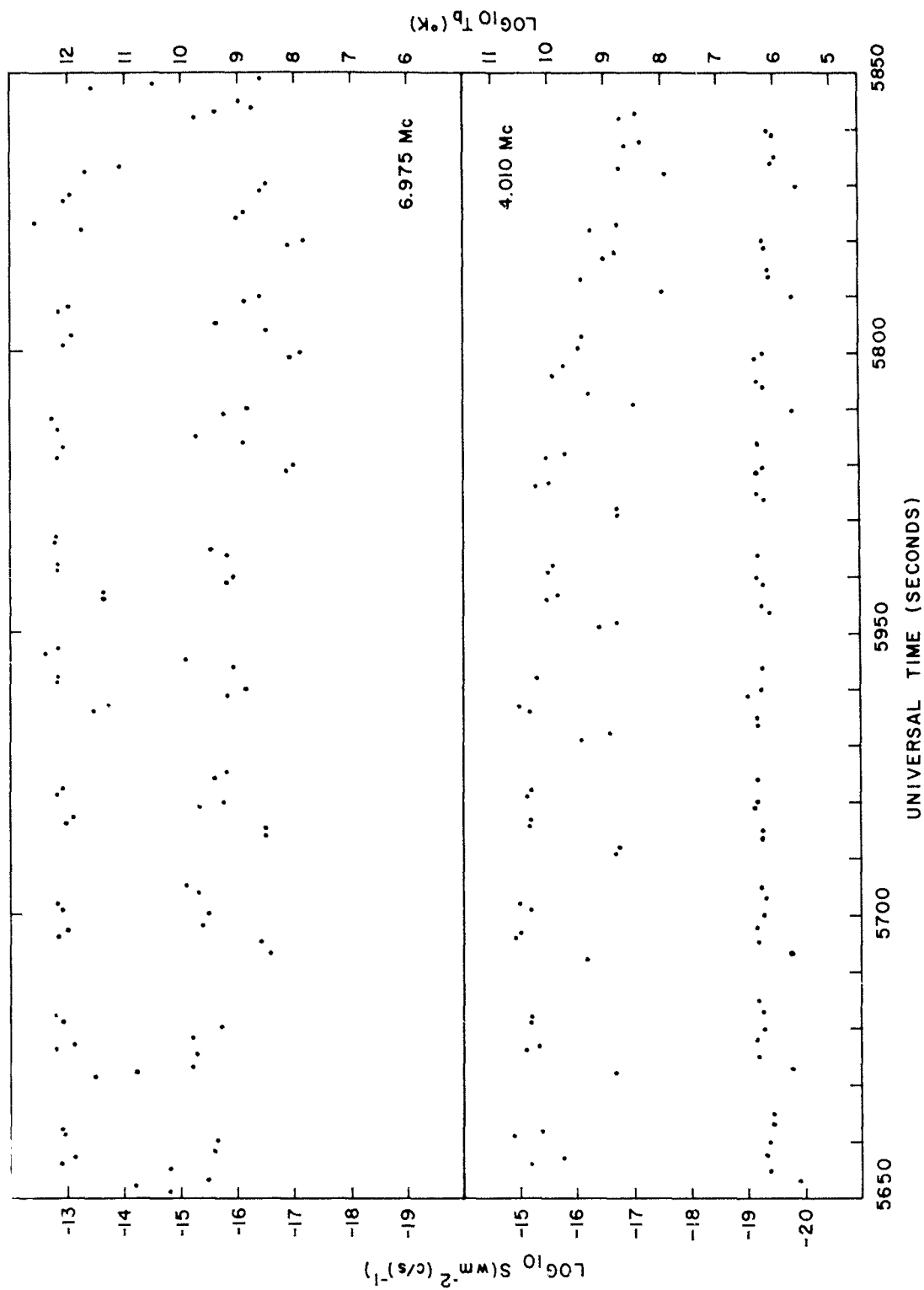


Figure 4.13 5-second oscillations on both 4.010 and 6.975 Mc, FTV 1129, Rev. 231, VAFB.



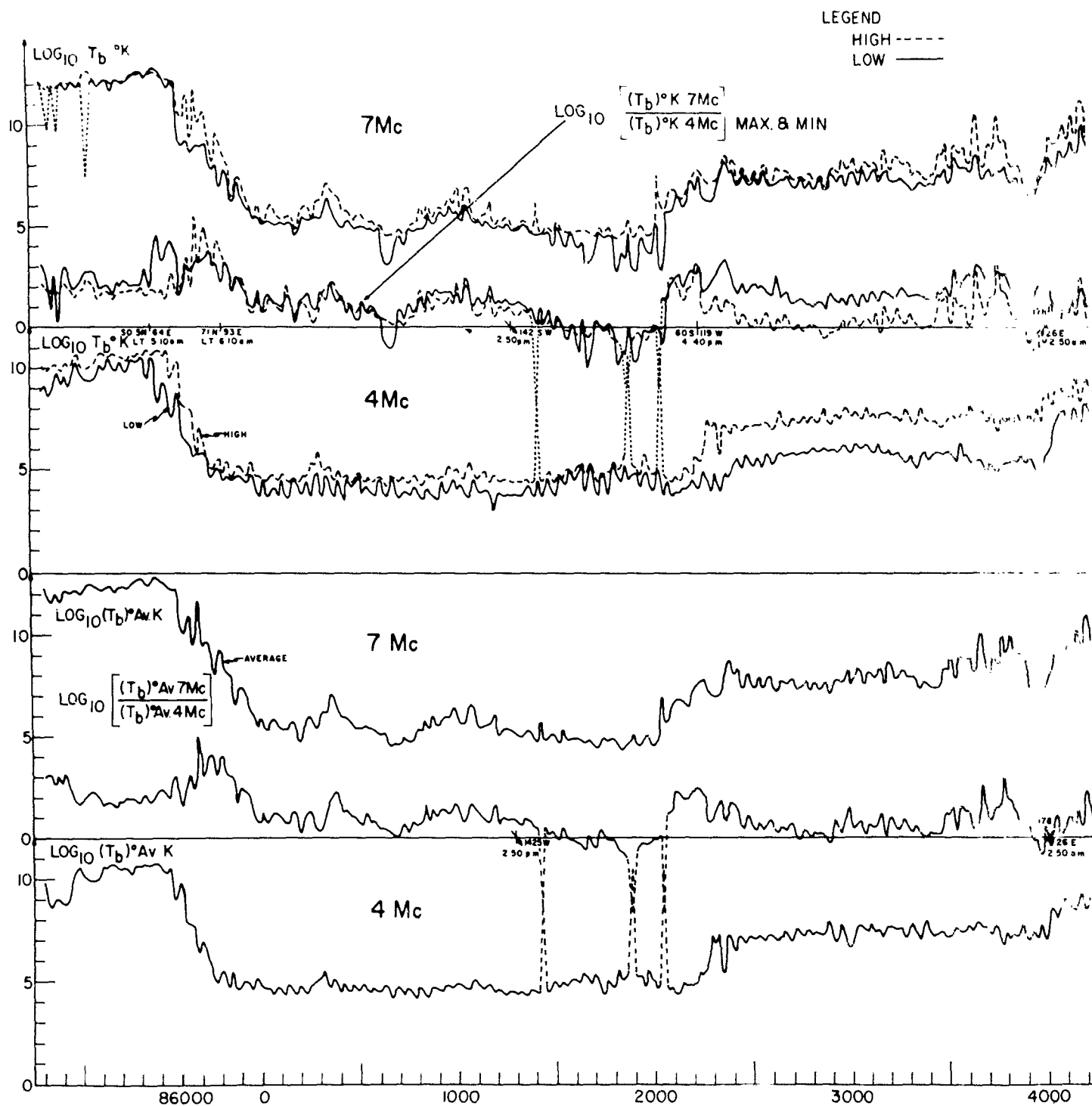


Figure 4.14 Tape-recorded data

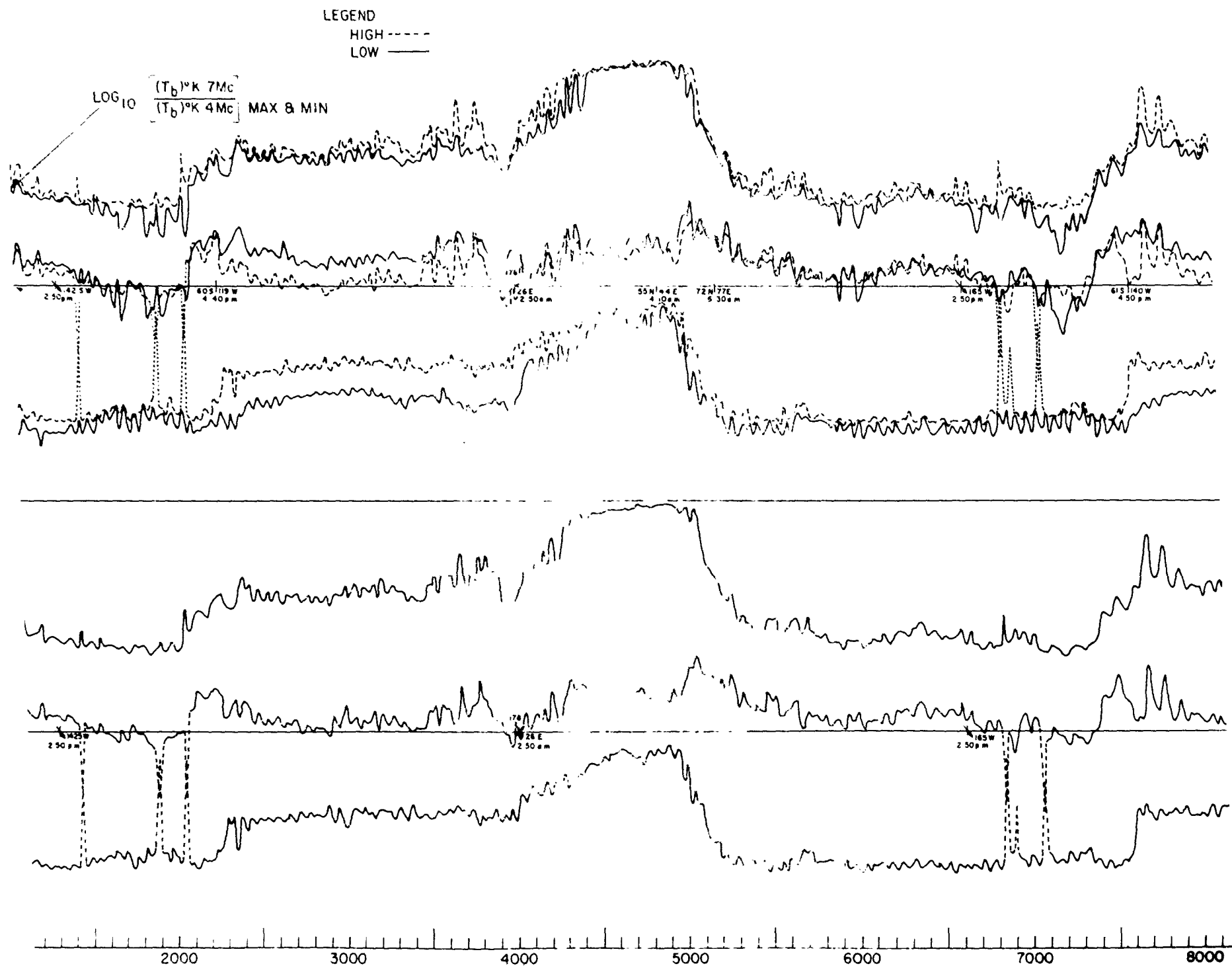
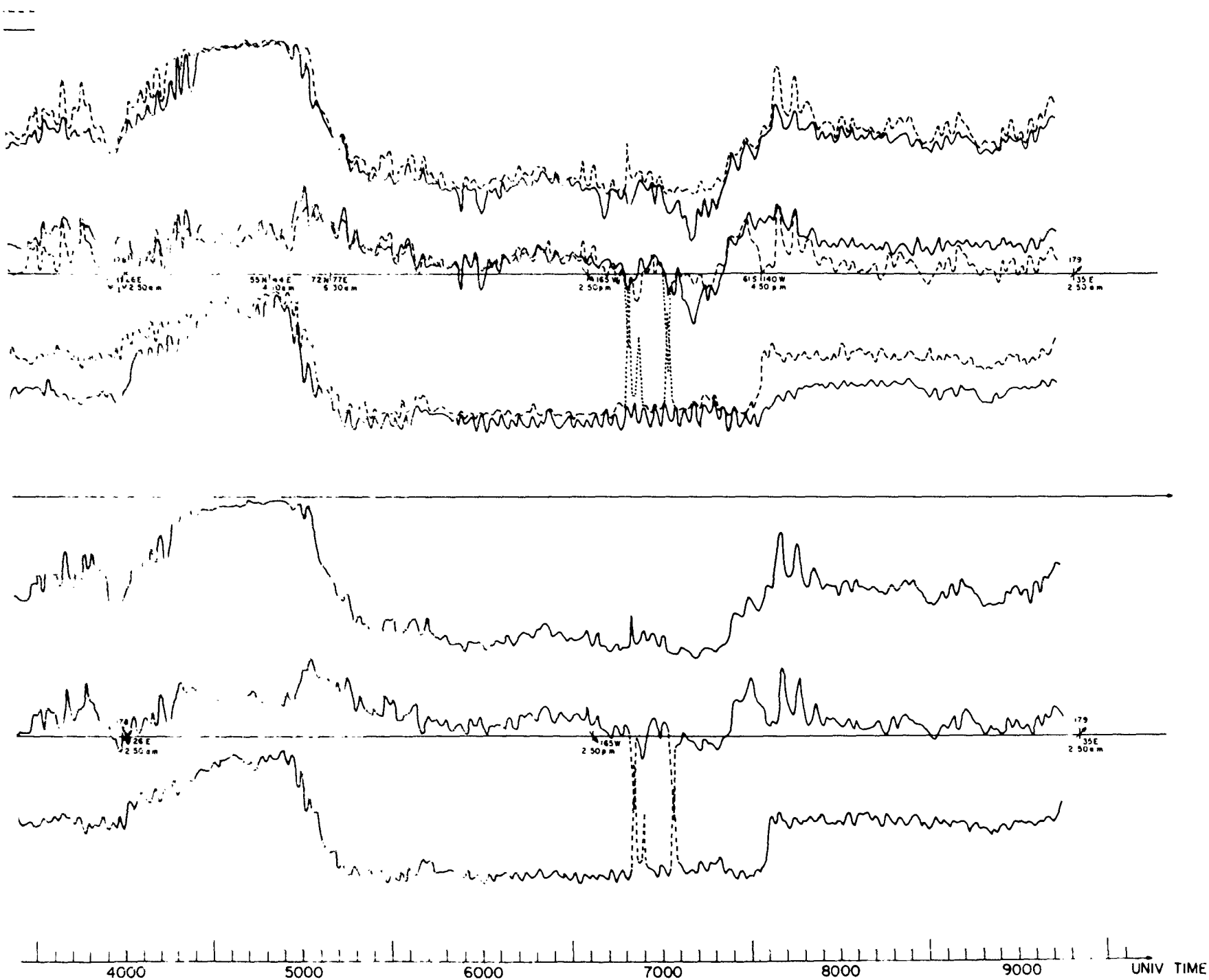


Figure 4.14 Tape-recorded data, Orbit 185, VAFB, FTV 1129.

133-134

SECRET

2



ape-recorded data, Orbit 185, VAFB, FTV 1129.

133-134

**SECRET**

**3**

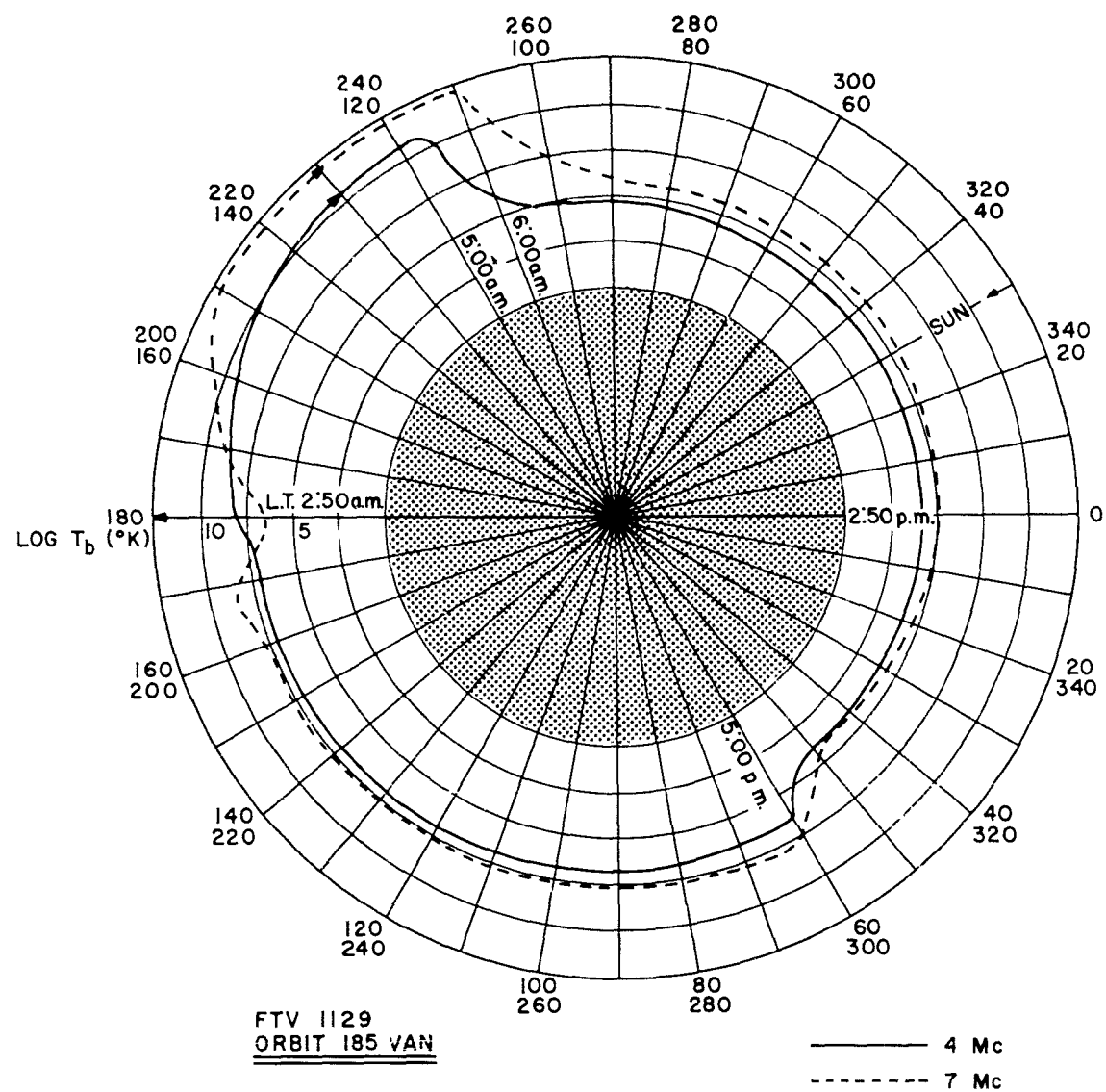


Figure 4.15 Polar plot of 4.010- and 6.975-Mc data for Orbit 185, VAFB, FTV 1129.

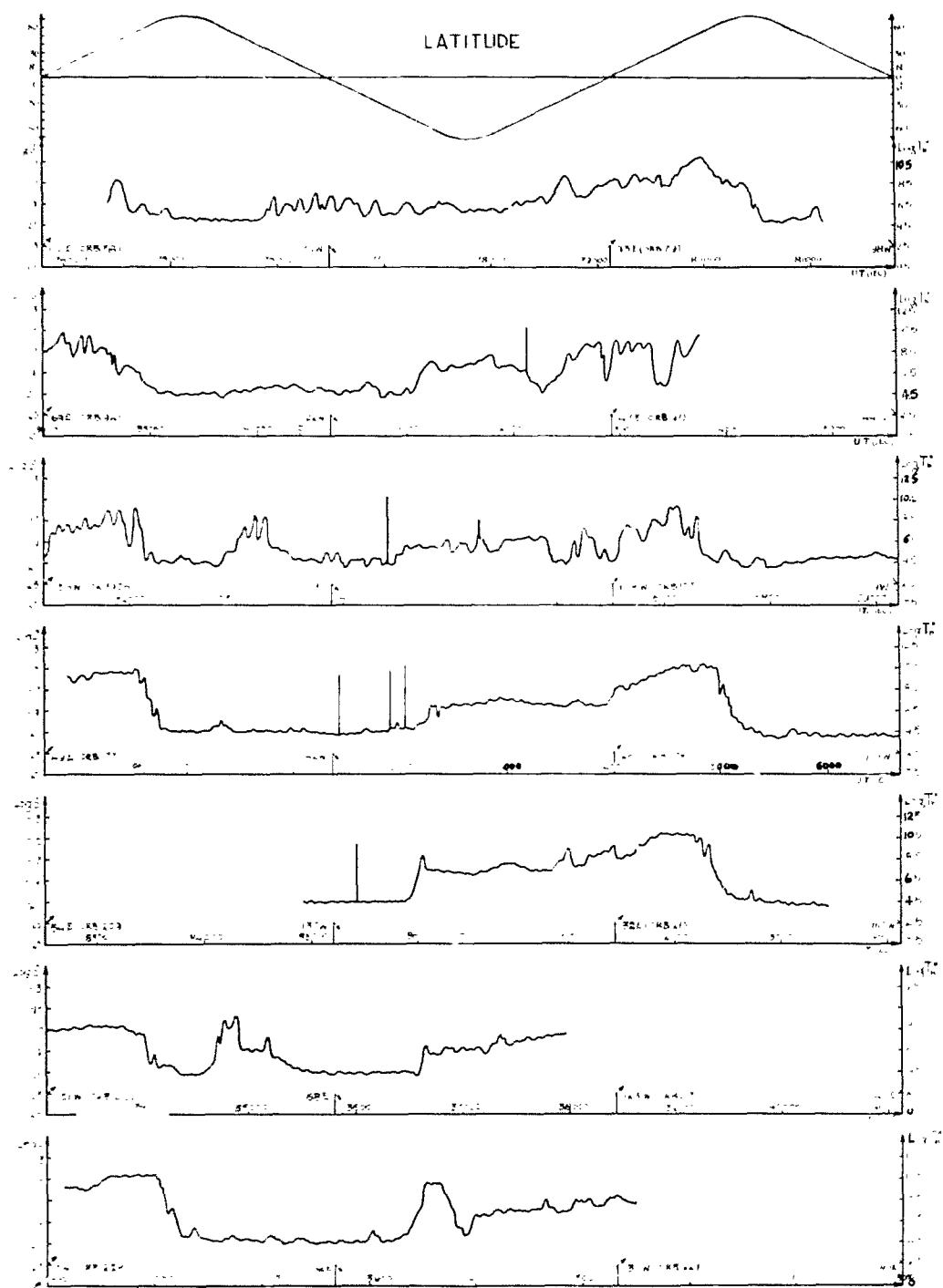


Figure 4.16 Tape-recorded data (averages), seven orbits, FTV 1129, 4.010 Mc.

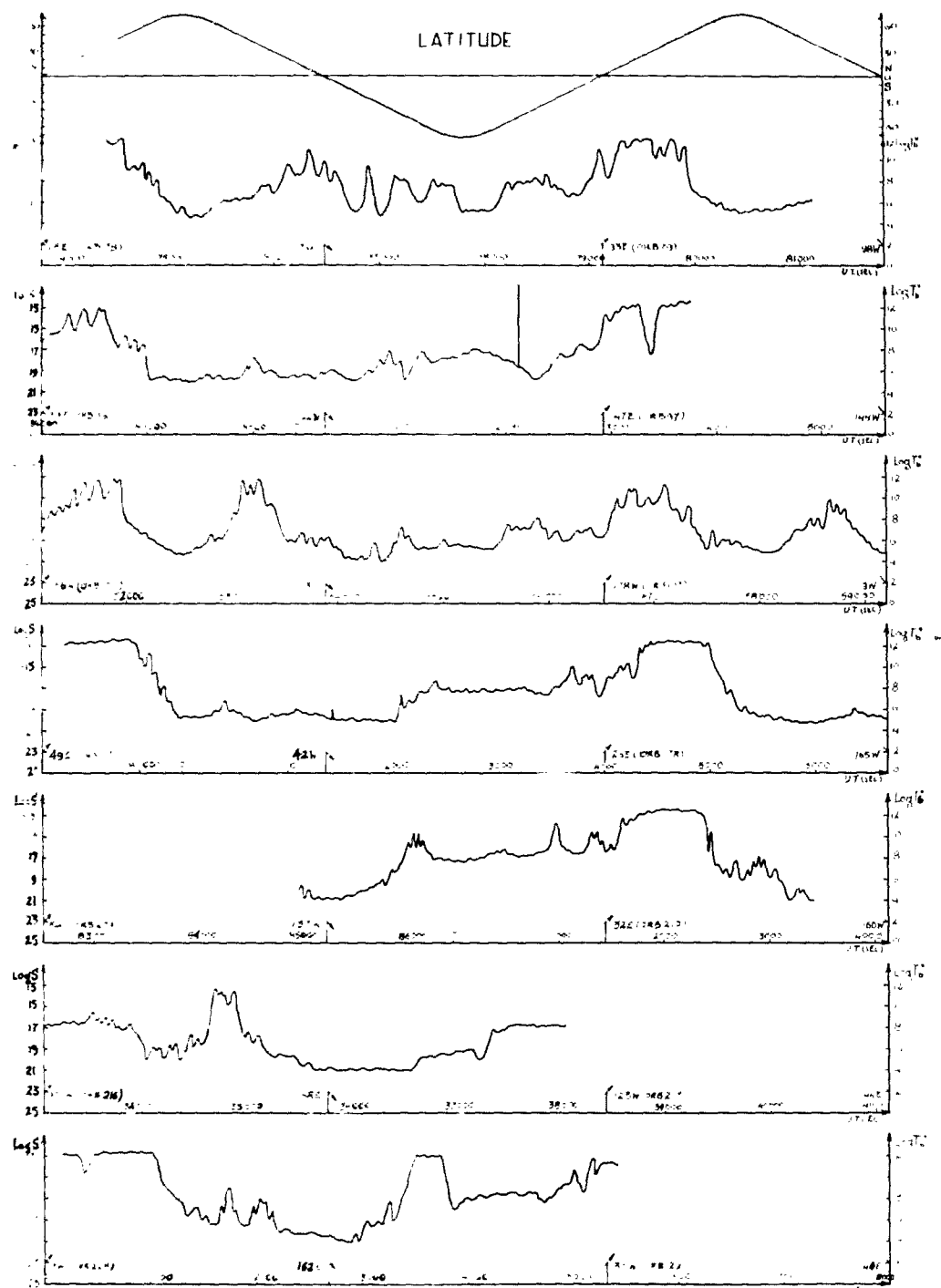


Figure 4.17 Tape-recorded data (averages), seven orbits, FTV 1129, 6.975 Mc.

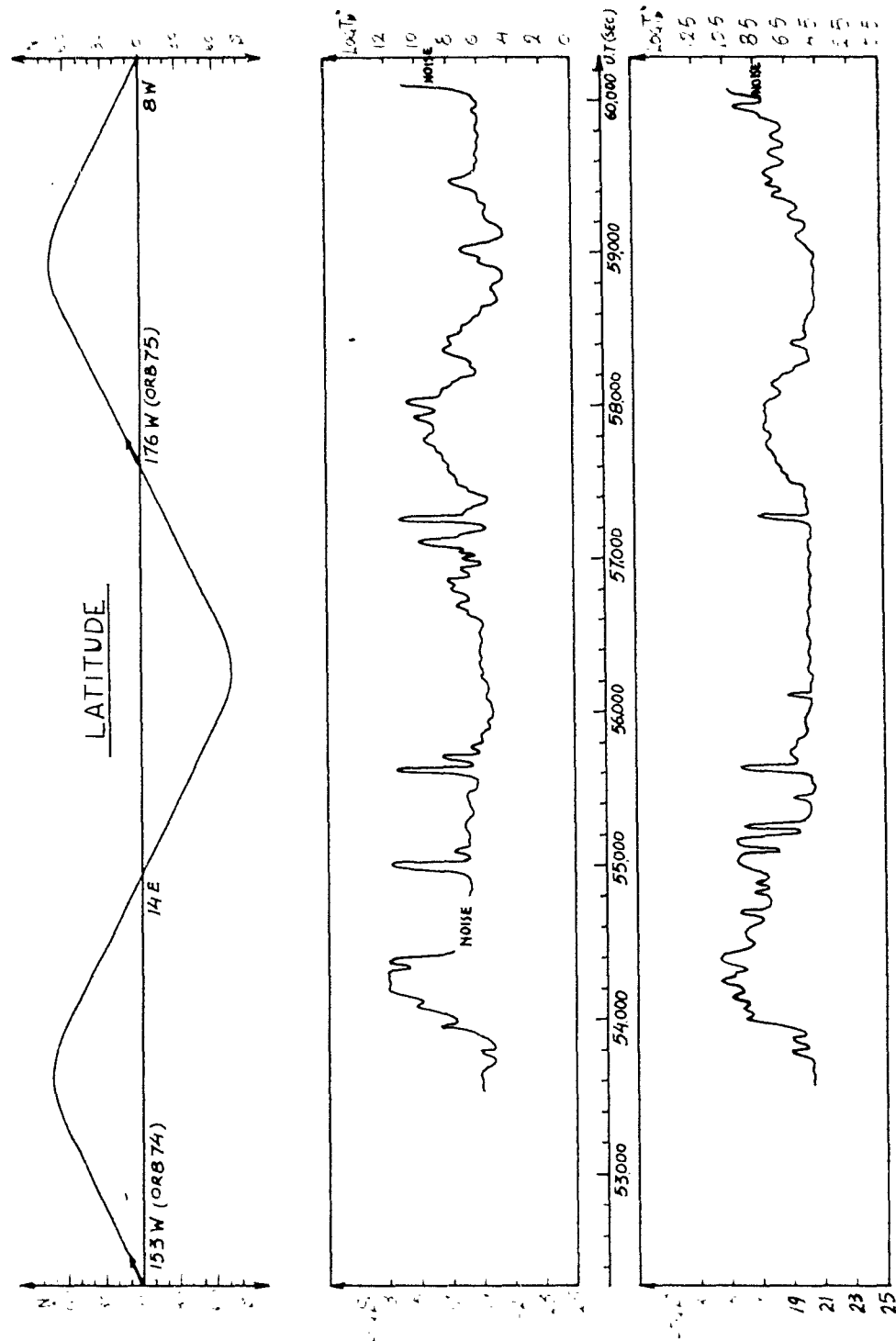


Figure 4.18 Tape-recorded data (averages), Orbit 77, NHTS, FTV 1129.

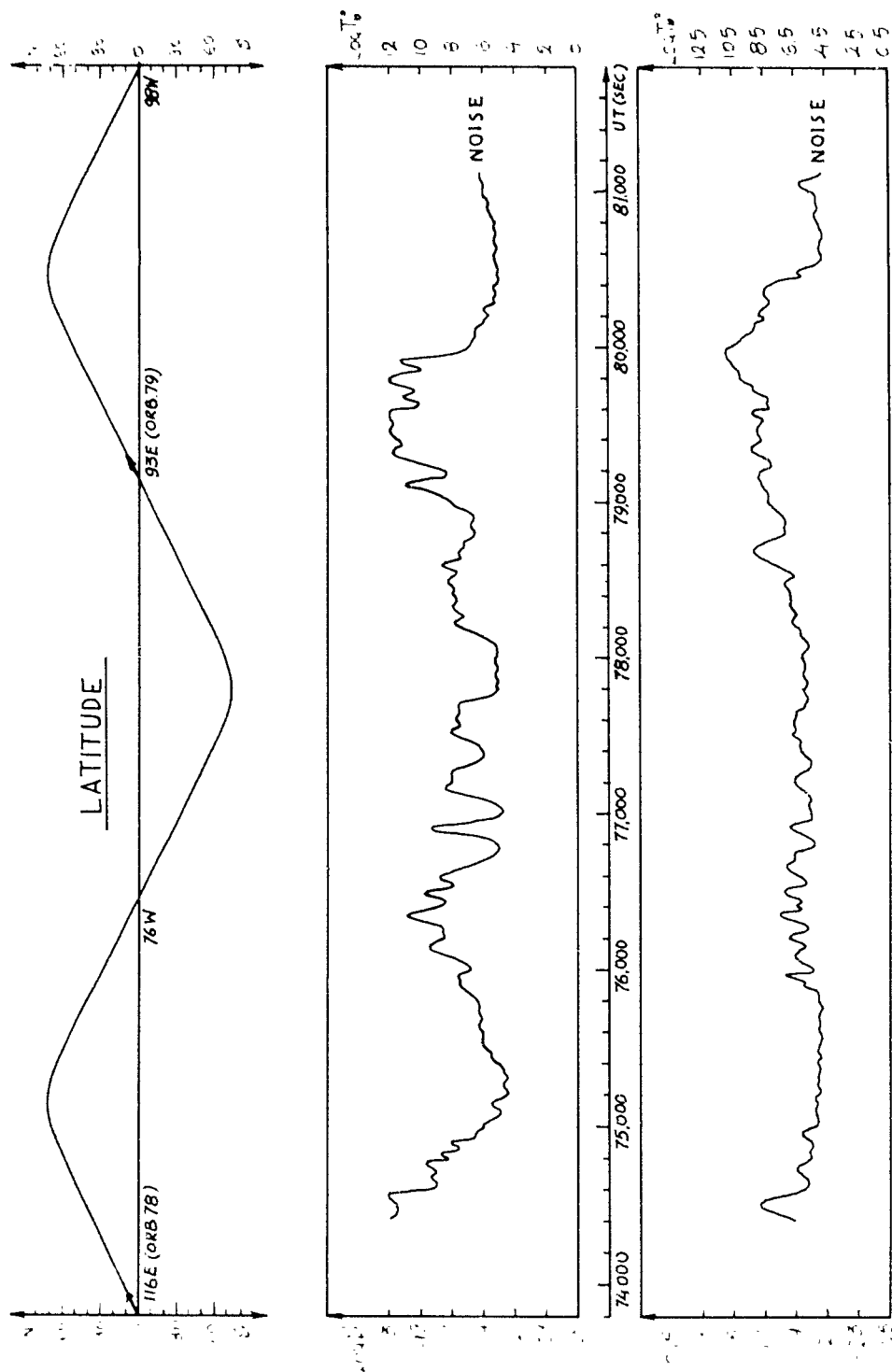


Figure 4.19 Tape-recorded data (averages), Orbit 80, KTS, FTV 1129.



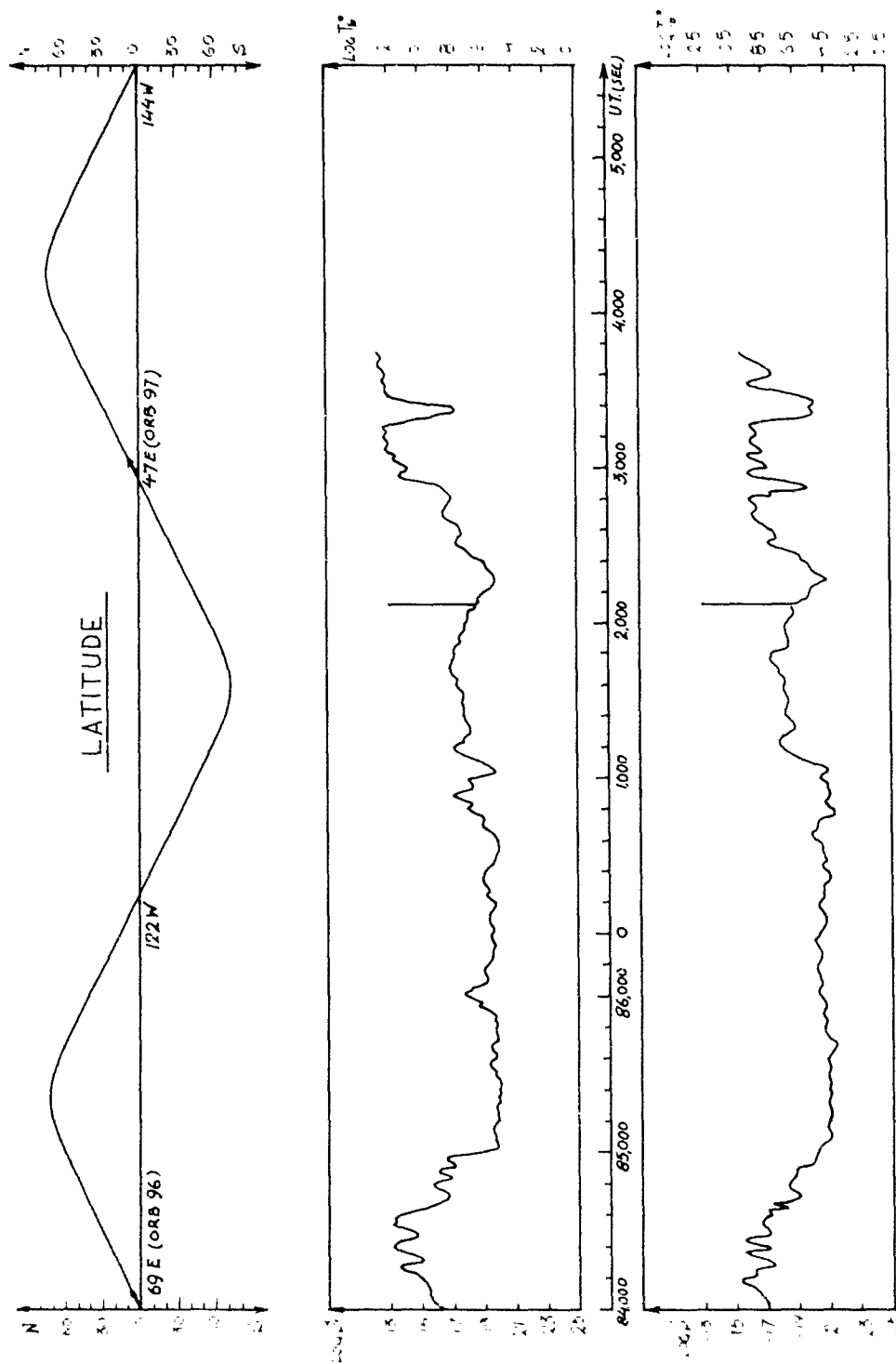


Figure 4.20 Tape-recorded data (averages), Orbit 97, HTS, FTV 1129.

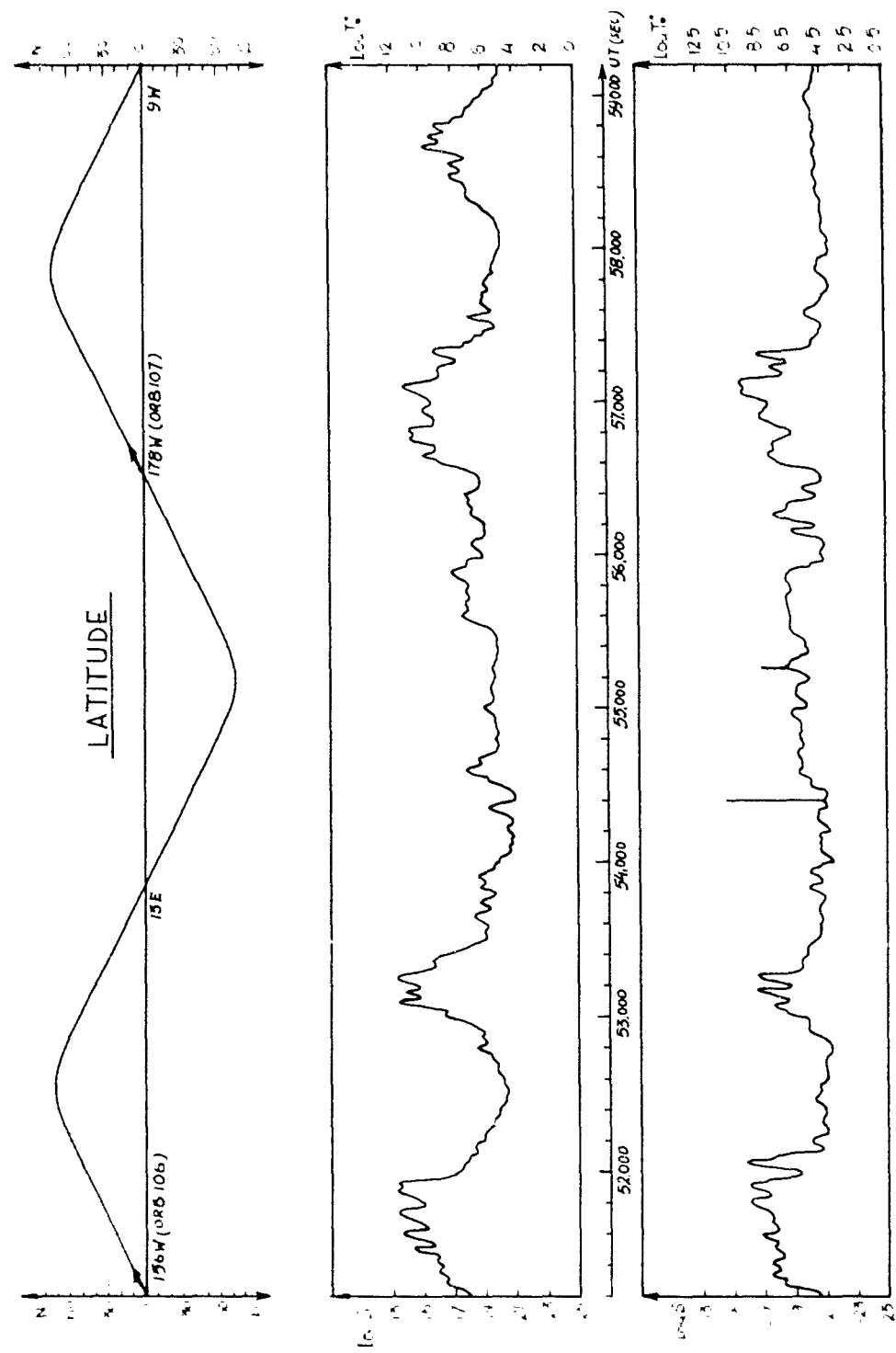


Figure 4.21 Tape-recorded data (averages), Orbit 153, VAFB, FTV 1129.

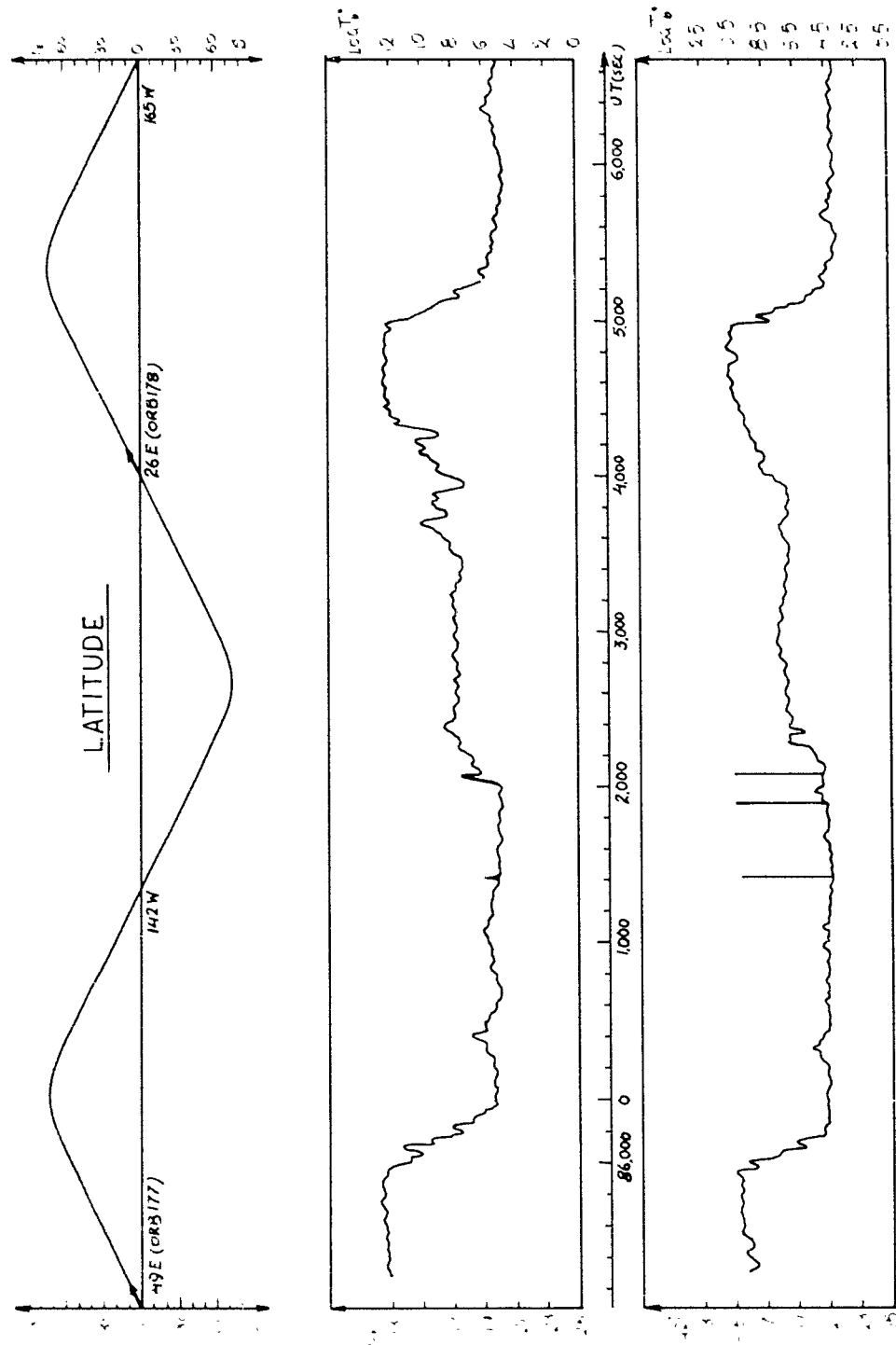


Figure 4.22 Tape-recorded data (averages), Orbit 185, VAFB, FTV 1129.

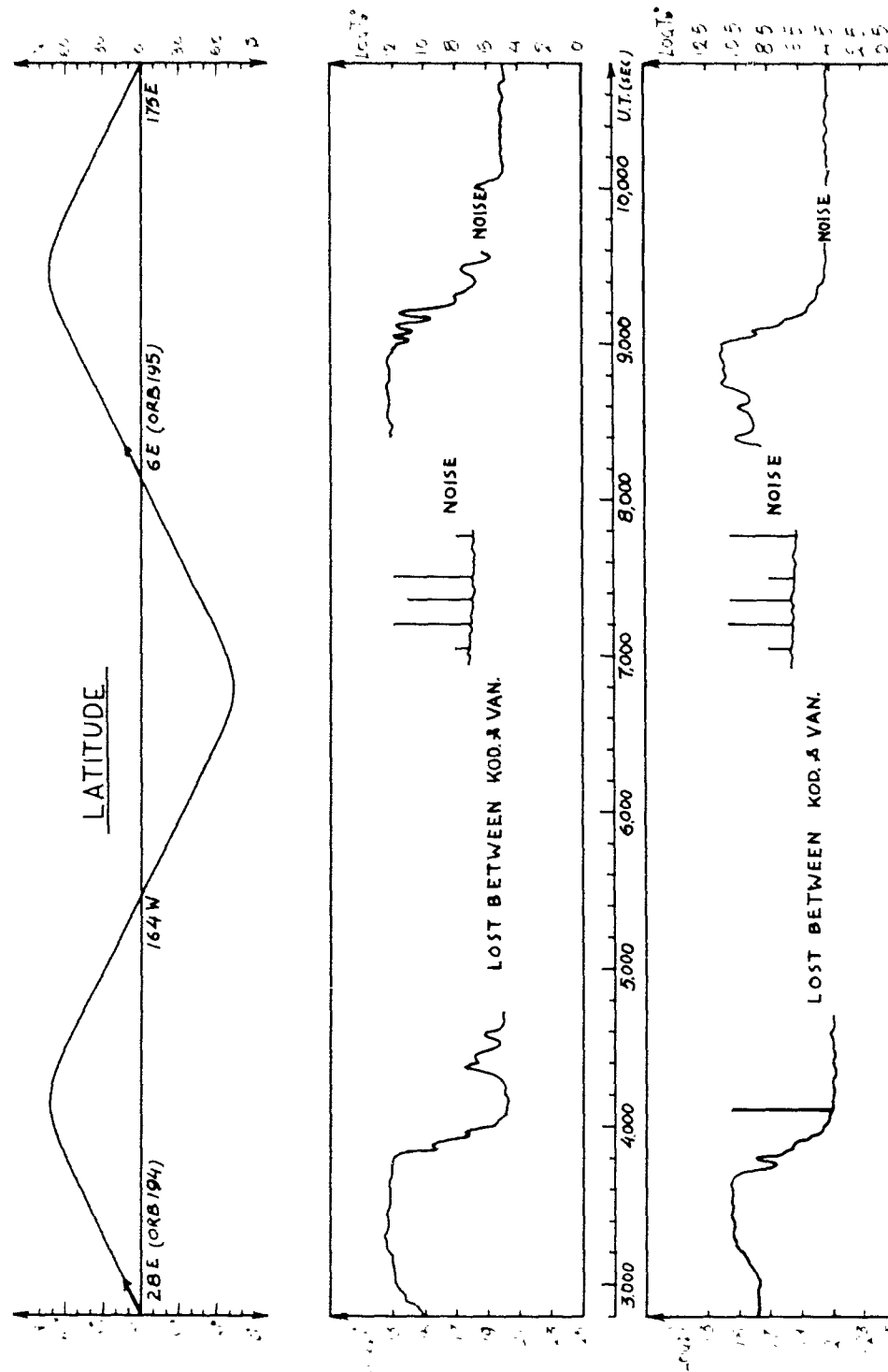


Figure 4.23 Tape-recorded data (averages), Orbit 208, KTS and VAFB, FTV 1129.

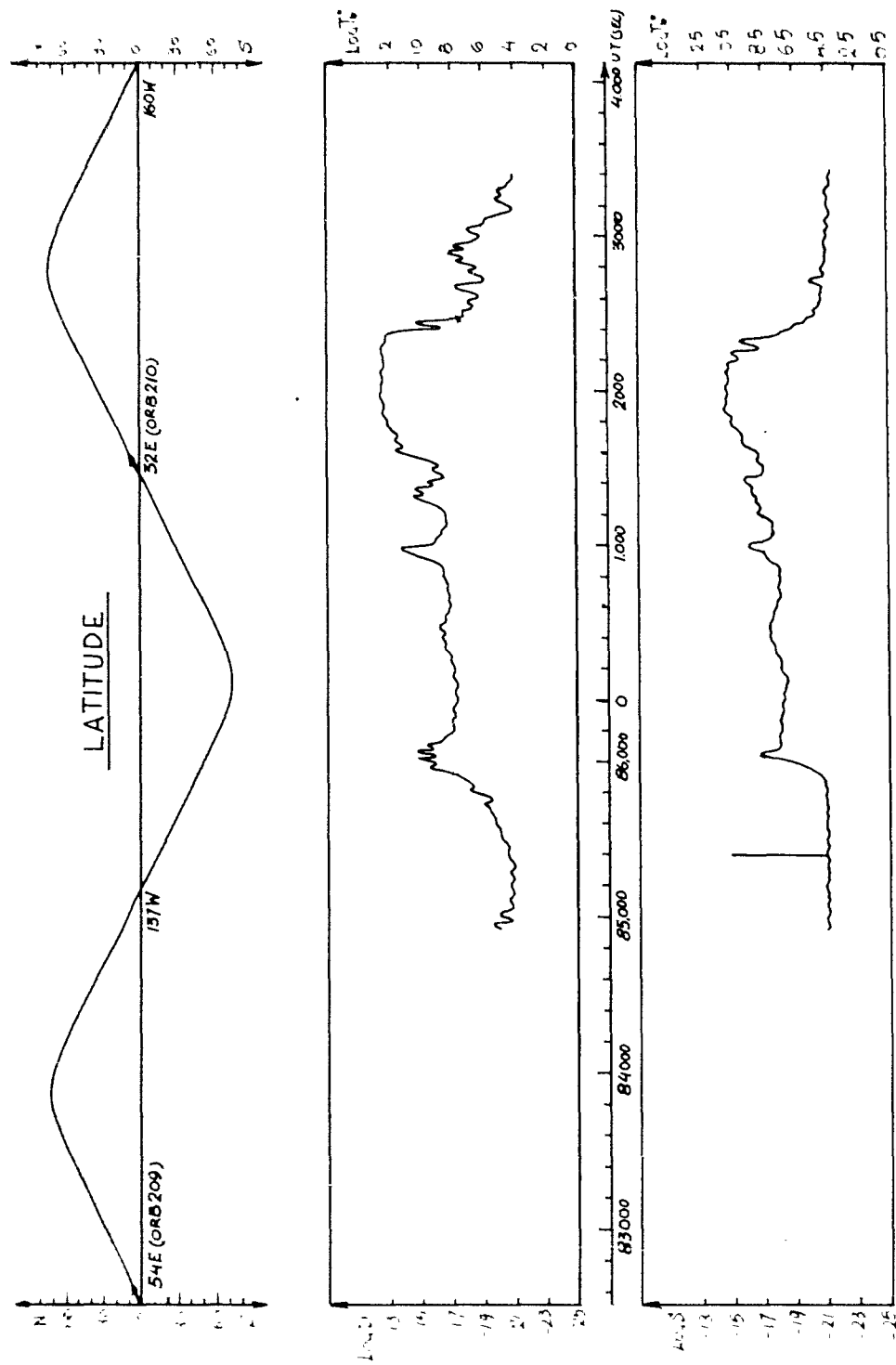


Figure 4.24 Tape-recorded data (averages), Orbit 210, HTS, FTV 1129.

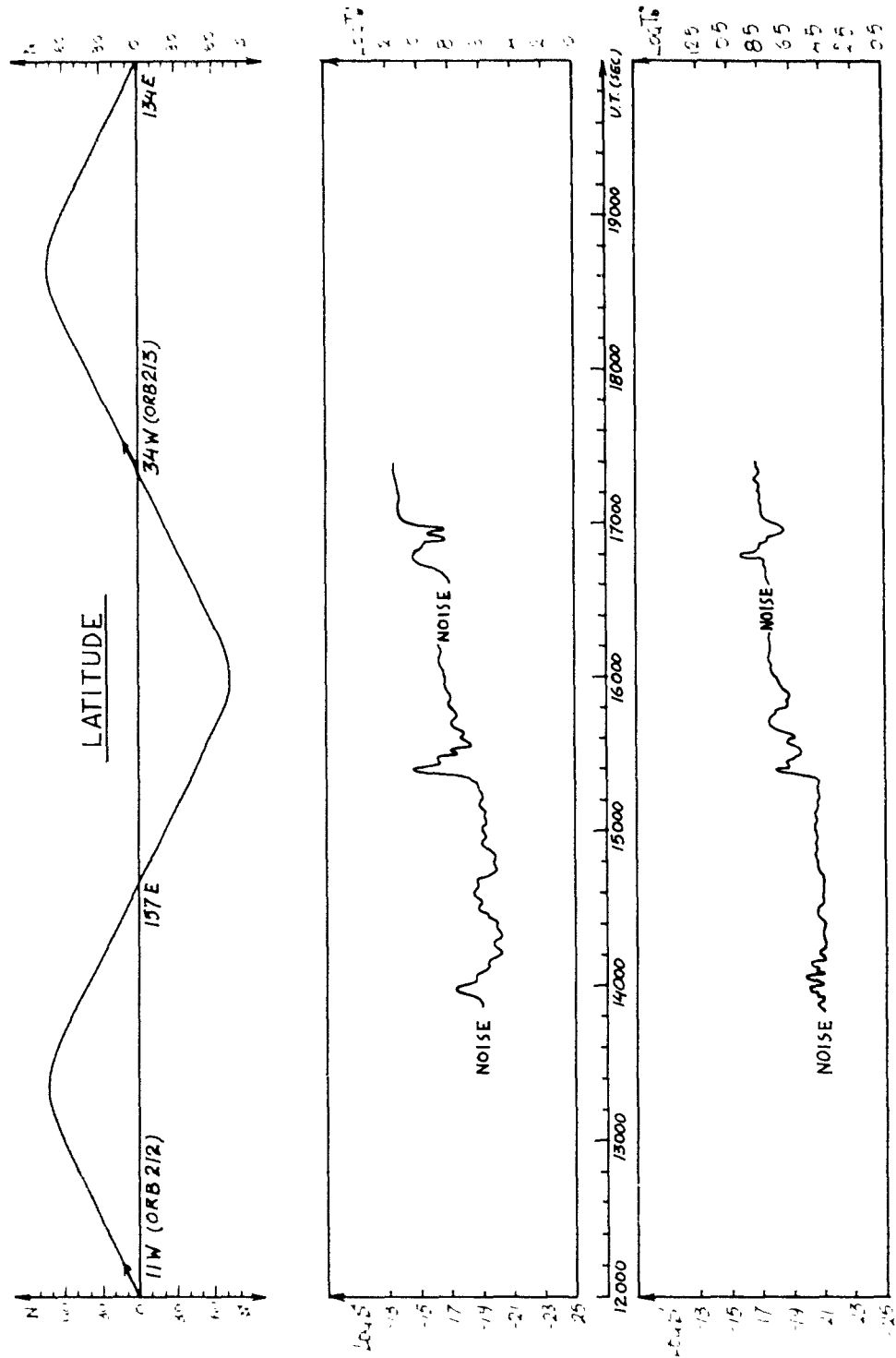


Figure 4.25 Tape-recorded data (averages), Orbit 215, NHTS, FTV 1129.

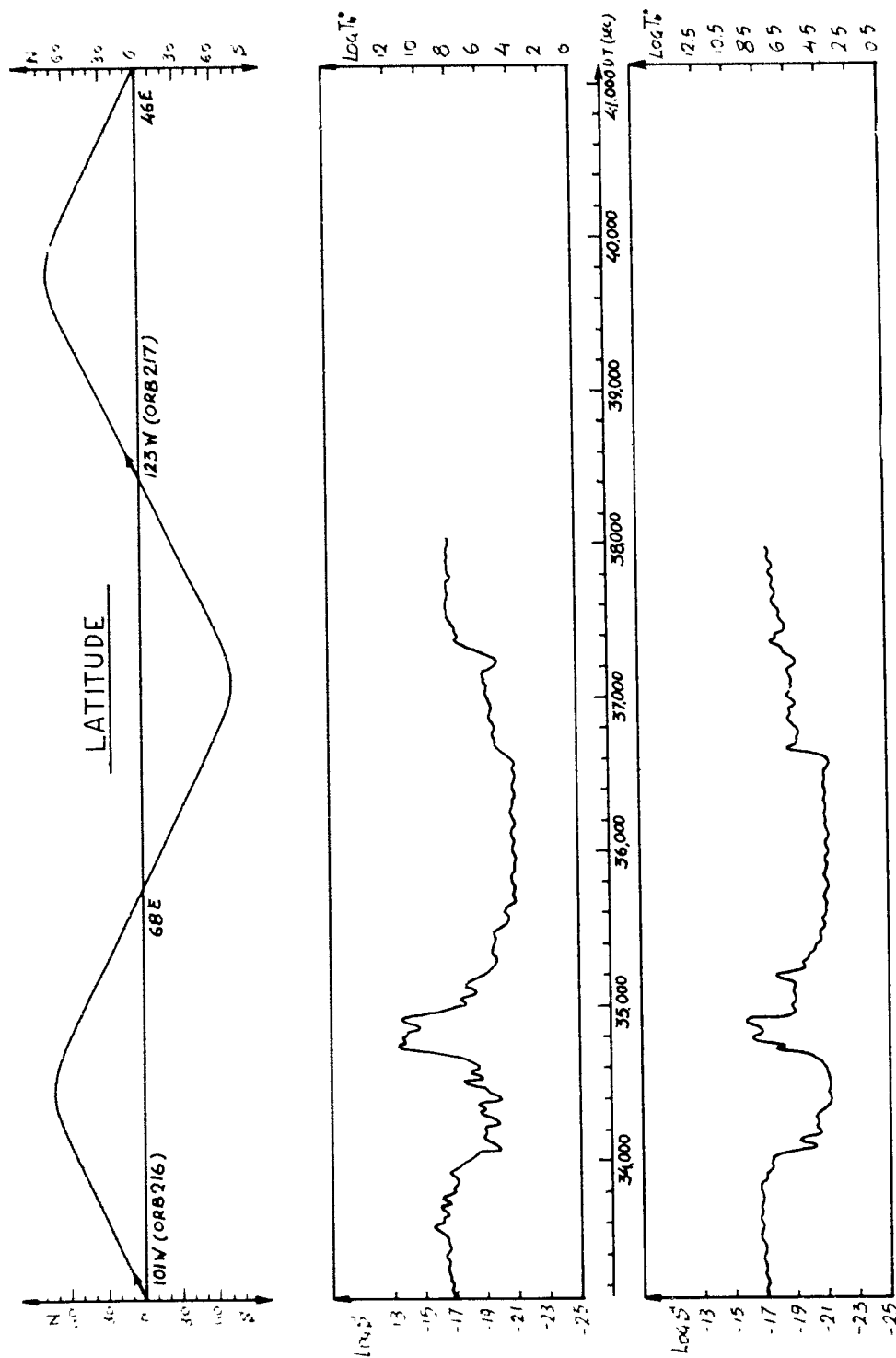


Figure 4.26 Tape-recorded data (averages), Orbit 217, VAFB, FTV 1129.

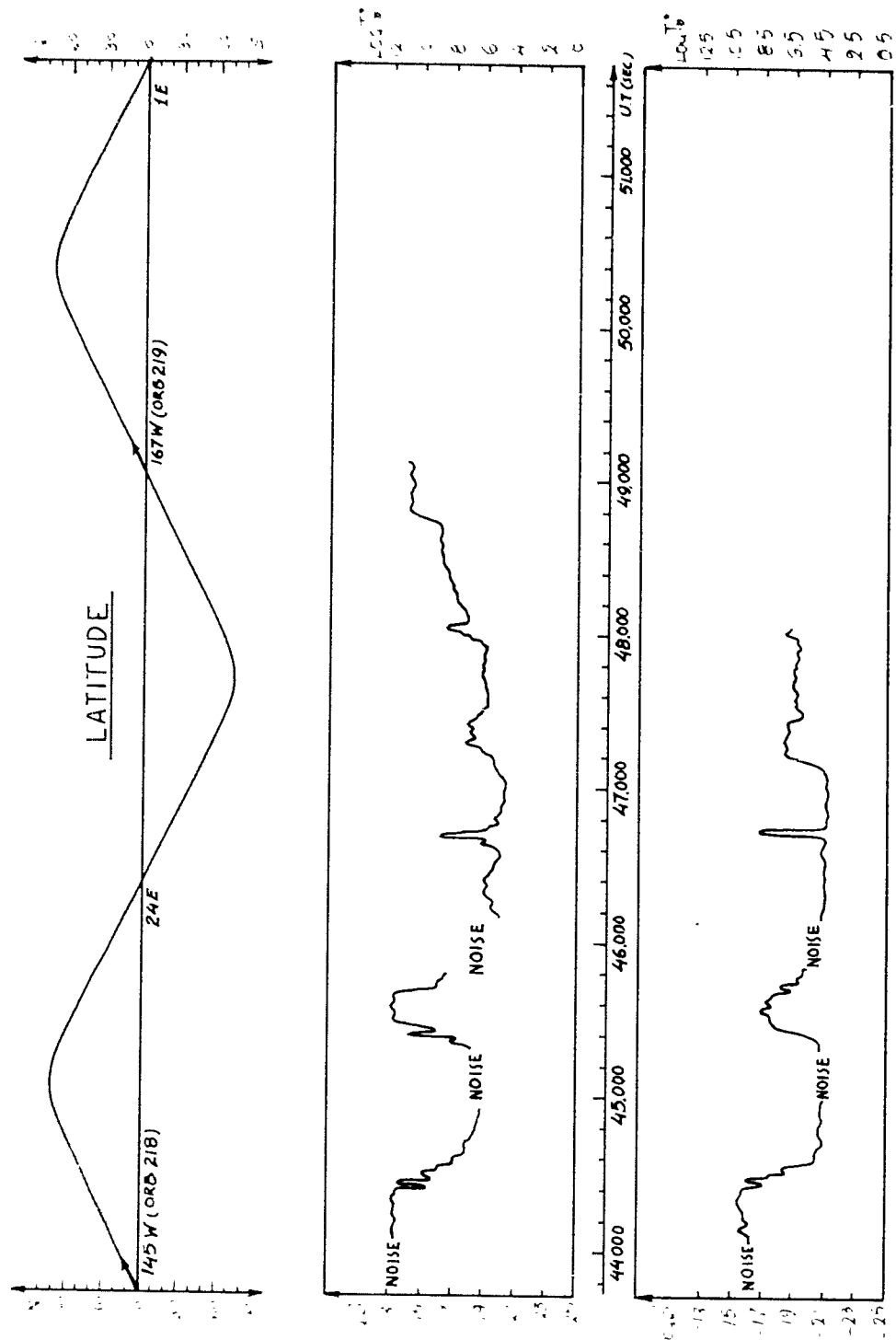


Figure 4.27 Tape-recorded data (averages), Orbit 219, KTS, FTV 1129.



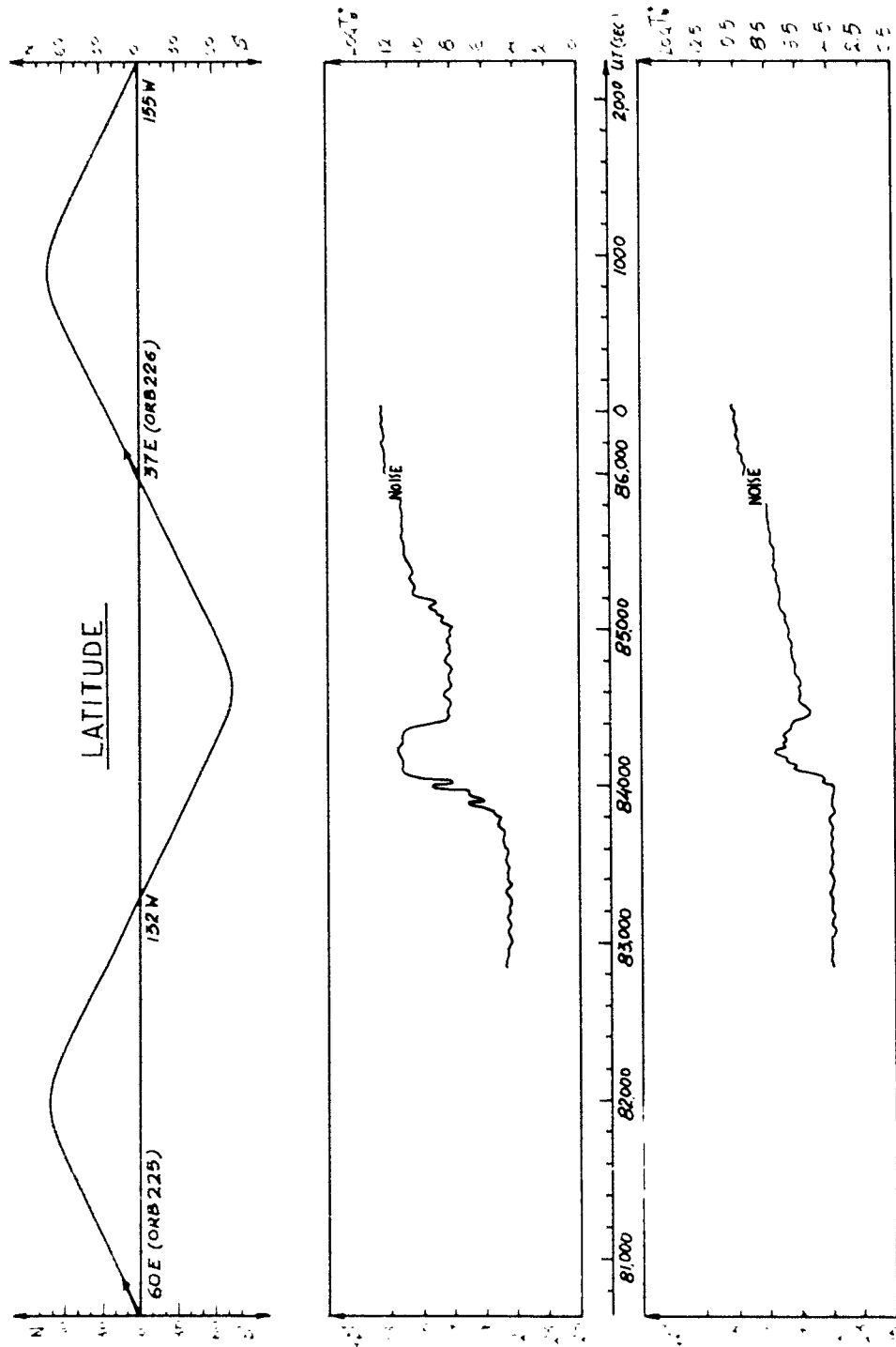


Figure 4.28 Tape-recorded data (averages), Orbit 226, HTS, FTV 1129.

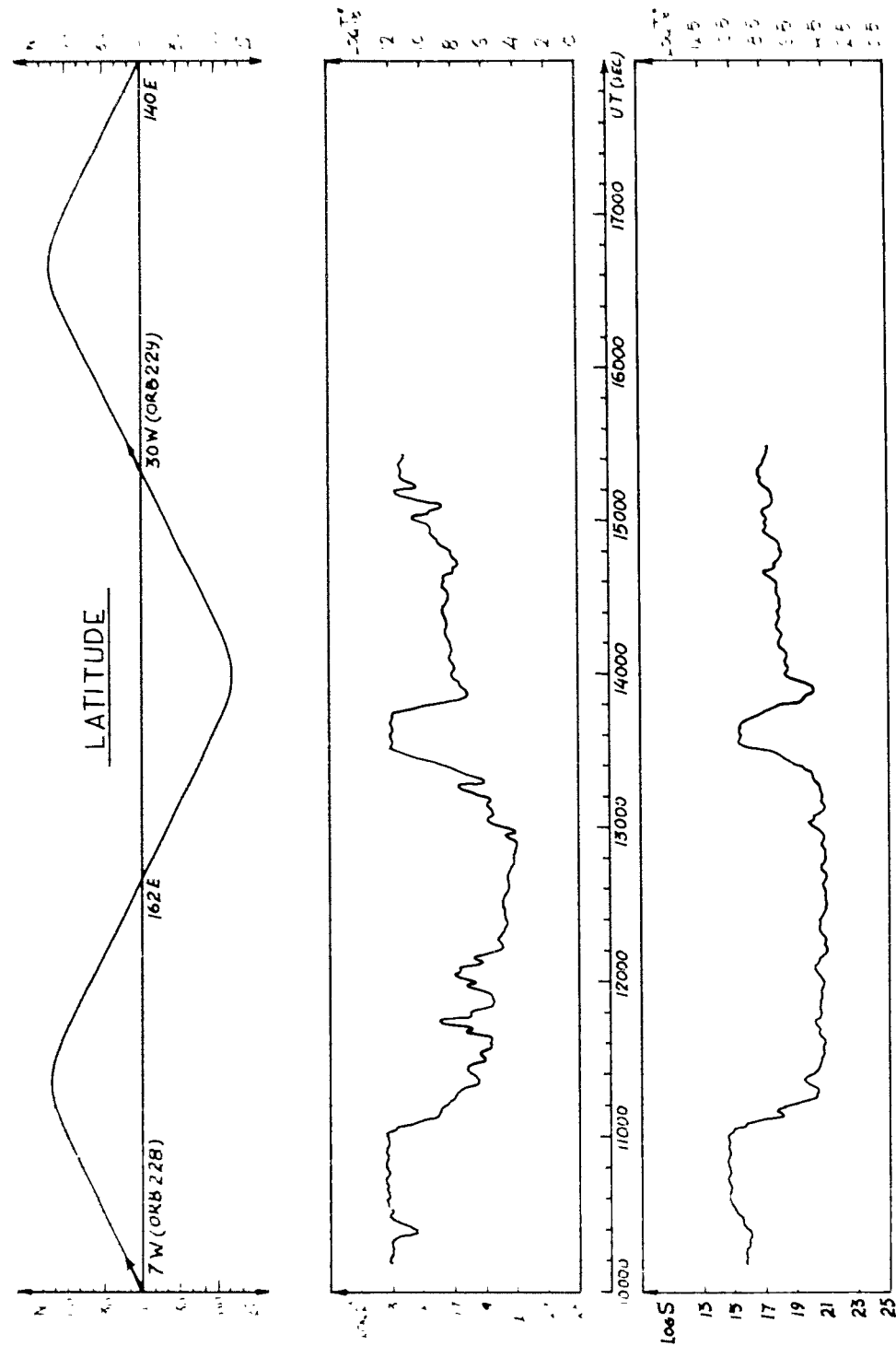


Figure 4.29 Tape-recorded data (averages), Orbit 231, NHTS, FTV 1129.

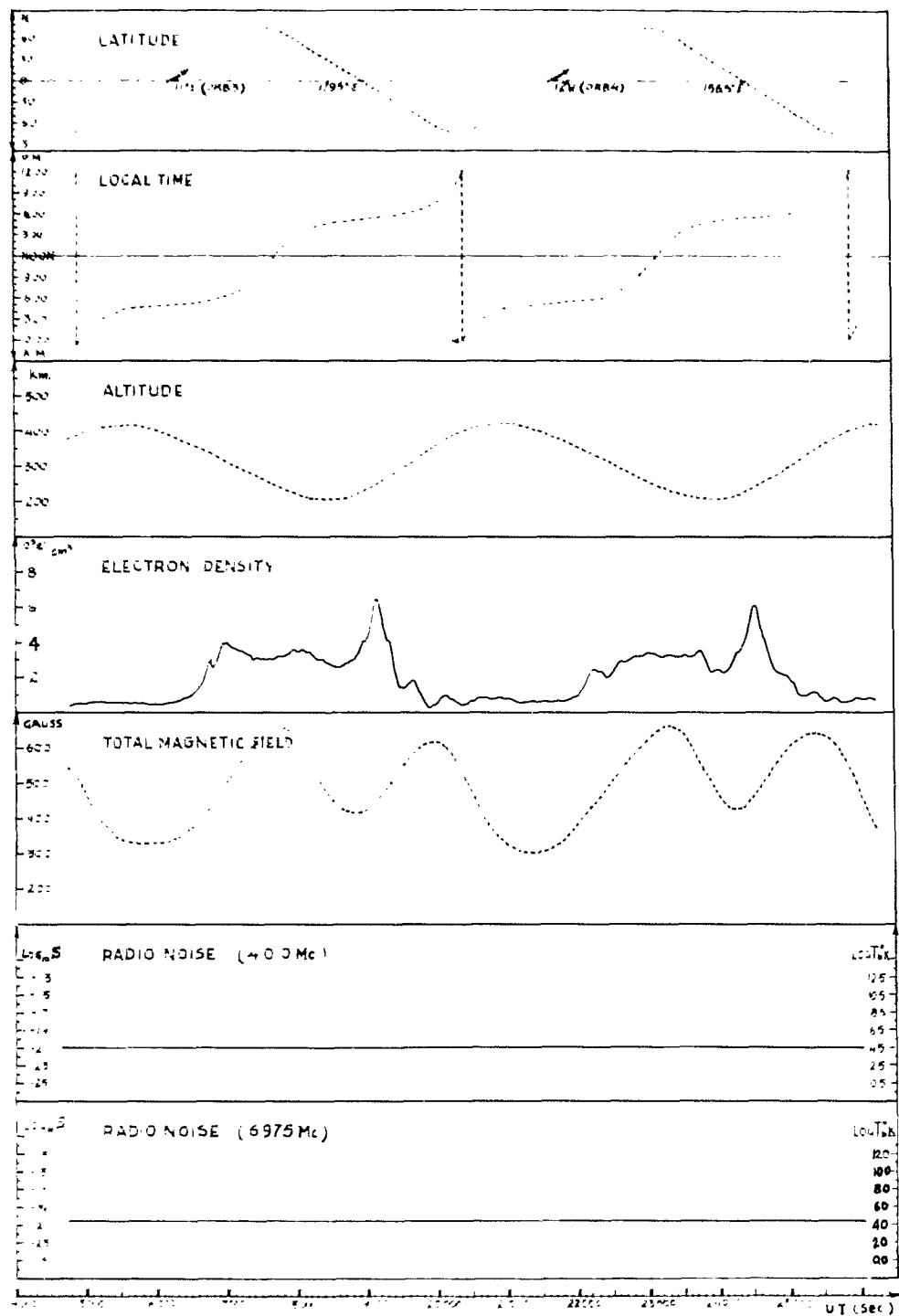


Figure 4.30 Tape-recorded data, Orbit 9, VAFB, FTV 1127.

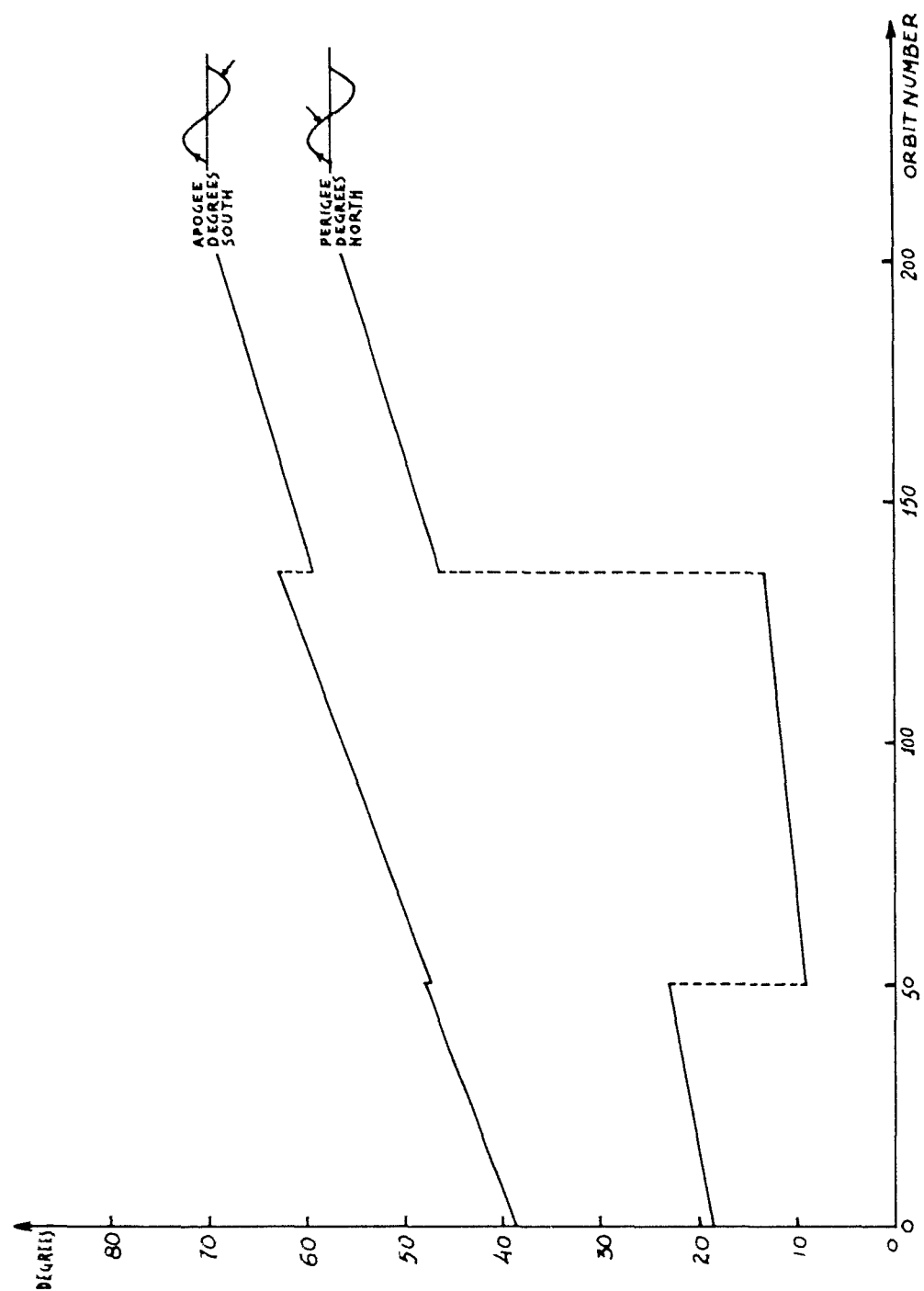


Figure 4.31 Discontinuities in the ephemeris, FTV 1129, (latitude).

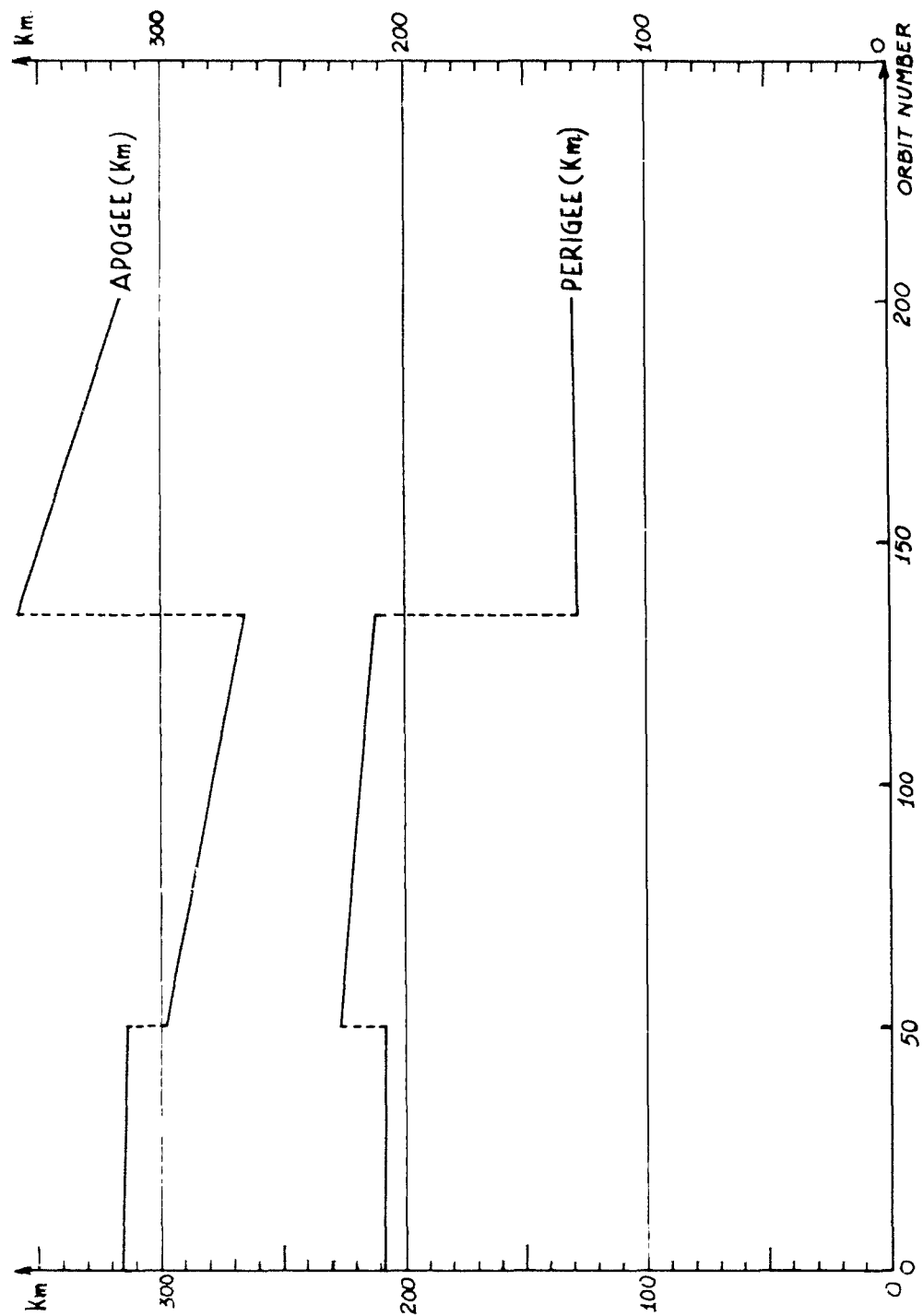


Figure 4.32 Discontinuities in the ephemeris, FTV 1129, (altitude).

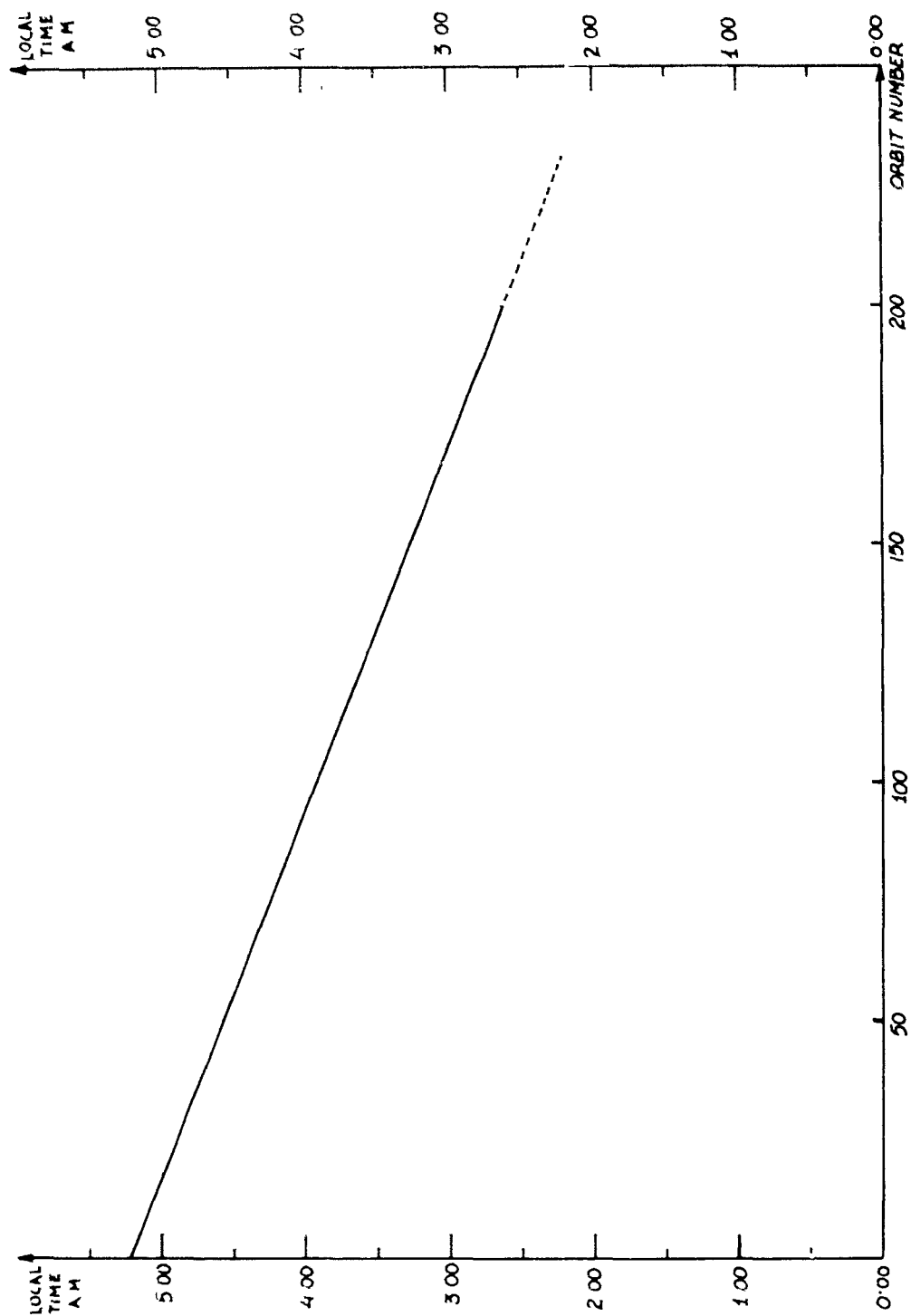


Figure 4.33 Local time of the south-north equator crossing, FTV 1129.

## CHAPTER 5

### ION TRAP PROBE

#### 5.1 OBJECTIVE

The objective of this experiment was to study the variations with latitude and longitude at an approximately constant altitude near the peak of the F-region (300 km): (1) positive ion and electron densities in the range 10 to  $10^{10}$  particles/cm<sup>3</sup>; (2) energy distributions of charged particles in the range 0 to 100 ev; and (3) vehicle potential due to vehicle-plasma interaction.

The study of these properties and their global distribution before, during, and after a high-altitude atomic burst would reveal important facts on the extent and nature of the disturbance caused by such an event, relating to photochemical processes, RF propagation, radar tracking of rockets and satellites, etc.

#### 5.2 BACKGROUND AND THEORY

Instruments to measure charged particle densities, temperature, and energy distribution have been flown in the past three years on vertical probe rockets and satellites. The objective of such flights was to study these electrical properties, their absolute values and time, altitude and positional variations leading to a better understanding of the basic properties of the ionosphere and

interplanetary plasma. Such properties as the dissociation, ionization and recombination processes operating in the undisturbed plasma, vehicle-plasma interaction in the light of how the presence of the vehicle modifies the plasma, and how vehicle potential is influenced by the plasma are being studied and their physical significance evaluated.

The theory is discussed with reference to the three modes of instrument operation (Sections 5.2.1 through 5.2.3).

#### 5.2.1 Mode I,

A voltage is applied between the two electrodes sufficient to collect all charged particles entering the electrode system given by:

$$V = \frac{m v^2}{2 q} \left( \frac{b^2}{a^2} - 1 \right) \quad (5.1)$$

where: a = radius of inner sphere, cm

b = radius of outer sphere, cm

v = velocity of particle relative to vehicle, cm/sec

m = mass of heaviest particle expected to be collected, gm

q = particle charge, coulombs

V = applied volts



$v$  in this formula can be expressed as:

$$|v| = |v_T| + |v_v| \quad (5.2)$$

where:  $v_T$  = maximum velocity of particle in a Maxwellian gas

$v_v$  = vehicle velocity

so, considering the vehicle (rocket or satellite) employed and

whether the instrument is collecting positive or negative

particles  $|v_T| \gg |v_v|$  or  $|v_T| \ll |v_v|$ ; hence, one or the

other can be neglected, e.g., for  $a = 1.27$  cm,  $b = 5.7$  cm,

$v_v = 8 \times 10^5$  cm/sec, and considering singly charged  $\text{NO}^+$  ions,

then -192 volts are required to collect all ions entering collection

since  $v_v \gg v_T$ . Taking the case now where  $v_v \gg v_T$ , then it

is easily seen that the probe sweeps out a volume of:

$$v_v \times A = v_v \times \pi r^2 \text{ cm}^3/\text{sec} \quad (5.3)$$

where:  $v_v$  = vehicle velocity

$A$  = cross-sectional area of probe

$r$  = outer radius of probe

If now the ion density in the volume swept out is  $n_+/\text{cm}^3$ , then the

current flow to the center electrode is given by:

$$i = n_+ e_x v_v \pi r^2 \times f(v) \quad (5.4)$$

where:  $i$  = current flow to center electrode  
 $n_+$  = ion density (number/cm<sup>3</sup>)  
 $e_x$  = charge per particle  
 $v_v$  = vehicle velocity  
 $\bar{\epsilon}$  = experimentally determined transmission factor for  
outer electrode

The value of the function  $f(v)$  depends on the potential of the outer sphere with respect to the undisturbed environment.

#### 5.2.2 Mode II.

For electrons the theory is identical to standard Langmuir-probe theory which may be found in standard texts. From analysis of the current-voltage curves, (electron) temperature, vehicle potential, and the form of  $f(v)$  to be used in Equation 5.4 are easily determined.

The simple Langmuir-probe theory must be modified for ions to take into account vehicle velocities of the same order of magnitude as random thermal-ion velocities.

#### 5.2.3 Mode III.

Plotting the second derivative of the current against voltage gives a typical form of Maxwellian (or other) energy-distribution diagram.

### 5.3 INSTRUMENTATION

Two experiments were involved—one for negative particles and one for positive particles. A sensor, a bias box, and an amplifier were provided for each. Both experiments derived timed functions and voltages from a common timer box. A block diagram of the instrumentation is shown in Figure 5.1.

The sensors consisted of a set of two concentric spherical electrodes. The outer electrode was 3 inches in diameter and perforated to give a high transmission of particles; the inner electrode was solid and of 1-inch diameter. Both were tungsten coated to reduce photo and secondary electron emission. The sensor was mounted at the end of a boom which was erected perpendicular to the vehicle surface when conditions of zero drag and zero g were attained. The boom was made long enough to place the sensor outside any vehicle influence such as solar shadow, vehicle plasma, and vehicle wake.

A series of programmed voltages were applied to both electrodes from the timer box and bias box.

A description of one unit applies to both, so attention will be given to the positive ion unit. Potentials are reversed on the electron sensor.

#### 5.3.1 Mode I.

A fixed negative potential is applied to the center sphere from the bias box, the outer sphere being kept at vehicle potential. The bias supply is in series with the center electrode and the logarithmic dc amplifier, the input terminal of the latter being at vehicle potential and so acting as a zero impedance device.

As explained previously, the probe sweeps out a cylindrical path through the plasma: hence, the current measured is proportional to ion density. A voltage proportional to the log of the current in the range 0 to 5 volts is telemetered on a continuous channel with a frequency response minimum of 100 cps.

#### 5.3.2 Mode II.

With a fixed potential applied to the inner electrode, a sweep voltage in the range +20 to -20 is applied to the outer electrode, thus operating the sensor in a Langmuir-probe mode. By means of a calibrated analog voltage telemetered on a commutated channel, a plot of current produced against voltage applied will give vehicle potential and an ion temperature measurement.

#### 5.3.3 Mode III.

The outer sphere is kept at vehicle potential; the inner electrode voltage is varied between zero and maximum (voltage applied in Mode I) by means of the bias supply. Again, an analog

voltage telemetered on a commutated channel gives a measure of applied voltage to be plotted against current produced, giving an energy-distribution diagram.

In addition to programing the mode of operation, the timer box also provides an analog voltage (telemetered) on a commutated channel, giving an indication of the mode in use at all times.

The two sensor units consisted of the spherical electrode assembly, mounting assembly, and boom assembly. The boom was 3 feet long with a uniform diameter of 1 inch. The booms weighed  $1\frac{1}{2}$  pounds each. The two bias supplies were mounted in as close a proximity to the respective sensor booms as possible. The bias supply boxes were approximately 4 by 4 by 5 inches and weighed 2 pounds each. Two amplifiers were mounted as close as possible to the respective bias boxes. The amplifiers were approximately 9 by 4 by 2 inches and weighed 2 pounds each. The timer box was mounted in a convenient location. Its size was 9 by 5 by 4 inches and weighed  $3\frac{1}{2}$  pounds.

The total power consumption had an average value of 3 watts with a peak of 8 watts and a minimum of  $1\frac{1}{2}$  watts, all at +28-volts dc. The instrument had a telemetry output of six pieces of data to be commutated.

#### 5.4 DATA REQUIREMENTS

The immediate post-flight requirement is for a paper strip chart of appropriate commutator (Ring B) —Visicorder type—at a chart speed of 10 in/sec. Post-flight data reduction requires the commutated channel decommutated and digitized at the rates shown in Table 5.1. All information is to be corrected for drift, etc., and put on magnetic tape in standard IBM format and also to be tabulated. Complete ephemeris data including time, latitude, longitude, radial altitude above the earth's surface, and resultant velocity (absolute velocity) are also to be put on tape and tabulated.

TABLE 5.1 DIGITIZING RATES FOR ION TRAP PROBE

<u>Output</u>	<u>Post Numbers</u>	<u>Digitizing Rate</u> samples/sec
ES-1*	02, 19, 31, 43	10
ES-2	03, 20, 32, 44	10
ES-3	04, 21, 33	$7\frac{1}{2}$
ES-4	05, 29, 45	$7\frac{1}{2}$
ES-5	34	$2\frac{1}{2}$
ES-6	42	$2\frac{1}{2}$

\*ES = Electric structure, ion trap

## 5.5 RESULTS

Two spherical electrostatic analyzers were successfully flown on each of the Discoverer satellites 1127, 1128, and 1129. Sensor 1 was used to measure the density, energy, and temperature of negative ions and electrons; sensor 2 was used to measure the density, energy, and temperature of positive ions. Most of the data were obtained in the altitude region from 180 to 425 km.

The results given in this report have been obtained from strip charts, since the magnetic tapes for the experiment (all outputs) were received in the latter part of April 1963. This did not allow time to include machine-processed data. As a result, much of the charge density fine structure along the satellite trajectory is not shown on the experimental curves.

The reduction of the results has been further complicated by inadequate ephemeris and satellite clock data. For example, the original ephemeris for FTV 1129 showed the apogee and perigee altitudes increasing after orbit 134. An improved ephemeris was finally obtained through SPACETRACK in early May. The satellite clock did not work on FTV 1128. The clock data is necessary to relate the experimental outputs to the ephemeris. The magnetometer data which gives crude geographical position was received in May 1963. For this reason the experimental outputs are given with respect to system time.

#### 5.5.1 FTV 1127 Results.

The experiments worked well for approximately 2 orbits. All experiments then terminated due to a command failure. The variation of positive ion and electron densities with geographic latitude is shown in Figure 5.2. The flight was carried out at a time of Arctic Summer and Antarctic Winter.

As shown in Figure 5.2 the positive ion and electron values agree within the experimental error during the day and show a significant difference beginning at about ionospheric sunset.

The electron density becomes less than the positive ion and remains less until after sunrise. The negative ion concentration is found to exceed the electron density at night. As can be seen from Figure 5.2 the position of the sun has a dominant influence on the magnitude of the charge densities. At night, the time of minimum densities, the vehicle reaches its maximum altitude of approximately 415 km.

Mode II. From the Mode II current voltage curves, see for example Figure 5.3, the satellite potential may be determined (Sagalyn, Smiddy, Wisnia, 1963). Because of the poor resolution of the strip chart data, the Mode II current voltage data could not be reduced. Curves obtained from real-time acquisitions gave small values of satellite potential, (-0.1 to -0.5 volt ). The average energy of the ambient charged particles varied between 0.16 and 0.20 ev. The corresponding ambient temperatures varied between  $1000^{\circ}\text{K}$  and  $2000^{\circ}\text{K}$ . Periodic measure-



ments of energy, temperature and satellite potential can be obtained when the magnetic tape data is analyzed.

Mode III. The experiment did not operate in Mode III during the real-time acquisition periods. This data can also be obtained when the magnetic tape data is analyzed.

#### 5.5.2 FTV 1128 Results.

Results were obtained from six tape-recorded orbits and 23 real-time acquisitions from FTV 1128. The vehicle clock did not operate, so that crude position must be obtained from the magnetometer results. The magnetometer data was received during the second week of May 1963; this did not allow time to correlate the experimental outputs with the magnetic field.

Positive ion and electron densities obtained from the tape read-out on the sixty-fifth orbit is shown as a function of system time in Figure 5.4. The ion and electron densities are approximately equal when the charge densities are high. From a comparison of these results with those obtained on satellites 1127 and 1129 one can estimate that the values obtained between 20 and 130 seconds correspond to daytime conditions. At about 143 seconds, which probably corresponds to local ionospheric sunset, there is a sharp decrease in the charge densities. At this time the electron density becomes less than the positive ion density. This is in agreement with results obtained on vehicles 1127 and 1129, showing the presence of negative ions in the nighttime ionosphere.

The Mode II and III data have not yet been reduced. This, together with the machined processed Mode I results, will be given in a report to be prepared at the Air Force Cambridge Research Laboratories.

#### 5.5.3 FIV 1129 Results.

Experimental results were obtained from fifteen tape recorded orbits and twenty-three real time acquisitions on vehicle 1129. As the magnetic tape outputs were not received until the end of April 1963, only hand-processed strip chart data will be given in this report. Because of the inadequacy of the original ephemeris, inconsistencies appeared in the orbital data. For example, after orbit number 134 the apogee altitude suddenly increased. New orbital elements were obtained and a new ephemeris derived by SPACETRACK.

The variation of charge densities, positive ions, and electrons with latitude obtained on orbits 177 and 178 are shown in Figure 5.5.

The altitude variations are small during this period; apogee is 230 km and perigee is 210 km. The overall pattern of the latitudinal variations is similar to that observed on vehicles 1127 and 1128.

A rapid increase in charge density is observed shortly after ionospheric sunrise. Normal daytime magnitudes are reached a few hours later. During the day, the density variations are small. Shortly before ionospheric sunset the charge densities decrease, reaching a minimum a few hours after sunset. At night between 0100 and 1230 hours local

time a secondary maximum is observed at  $20^{\circ}$  to  $25^{\circ}$  south. A nighttime increase in electron densities is often observed around midnight by ionosonde stations near the equator.

The positive ion and electron densities are approximately equal during the day. At night the positive ions are a factor of 1.5 to 5 greater than the electron densities.

While the pattern just described was observed on most orbital records received from vehicle 1129, on certain of the orbits, significant differences occurred. For example, on orbit 97, as shown in Figure 5.6, the charge densities during the nighttime reach to almost the daytime values. At this time, the electron and positive ion densities are nearly equal. This will be discussed further in the next section.

The spin and tumble rate of vehicle 1129 varied considerably during the data acquisition period. This motion is easily determined from the experiment outputs as the sensors move in and out of the vehicle wake. The effect on the measurement is shown in Figure 5.7; this reproduction of a portion of the flight record illustrates the decrease in the positive ion measurement when sensor 2 enters the vehicle wake. Both the electron and ion densities were found to decrease almost an order of magnitude in the shadow of the vehicle, three to five feet behind the satellite. A comparison of the ion densities values obtained over a portion of an orbit with the sensors in and out of the satellite wake is given in Figure 5.8.

Mode II. Only real-time Mode II data has been reduced at this time. The electron current voltage curves give temperatures ranging between 1200° and 2100°K. Examples of Mode II electron sweep curves obtained during the flight of FTV 1129 are shown in Figures 5.9 and 5.10. The vehicle potential was measured to be -1.0 to 0.5 volt. The temperature is calculated to be 1534°K from Figure 5.9 and 1830°K from the data given in Figure 5.10.

Mode III. Examples of collector current vs collector voltage curves obtained from sensors 1 and 2 are shown in Figures 5.11 and 5.12. This data was obtained at 340 km and a local time of 0542 hours. Saturation is reached at a collector voltage of 75 volts. This corresponds to a charged particle energy of 9 ev. Assuming a vehicle potential of 1 ev, this corresponds to positive ions of 8-ev energy; the calculated ion mass is 30 amu. This indicates that the mass of the majority of the positive ions present is less than 30 amu.

The electron sensor curve in Figure 5.11 shows that over 90% of the charged particles are collected for an applied voltage of 10 volts. This corresponds to the voltage required for the collection of ambient electrons. Most of the electron sensor current voltage

curves show a small increase up to 40 or 50 volts. This increased current may be due to the presence of higher energy electrons or to negative ions.

Periodic Mode III measurements along each orbit will be obtained from the machine-processed data.

#### 5.6 DISCUSSION

The latitudinal variations of charge densities obtained on polar orbiting vehicles 1127, 1128, and 1129 show certain general persistent features. These include a sharp decrease in the ion and electron densities around sunset, a secondary maximum of varying relative intensity at night, a minimum in density before sunrise, a rapid increase in density after sunrise. The electron densities are usually lower than the positive ions during the night hours. Significant number of negative ions are observed below 300 km at night.

The daytime variations with latitude and solar position are small; this is partly due to the fact that the effects of the solar position and altitude variations tend to cancel one another on the orbits chosen for vehicles 1127, 1128, and 1129.

Changes in longitude do not have a major effect on the latitudinal variations. However, the data shows that the relative magnitudes of the maxima and minimum are effected by change in longitude.

Significant modifications of the general latitudinal pattern do occur. As pointed out earlier, the results of vehicle 1129 show large changes in the magnitudes of the nighttime maxima. Examination of the solar and magnetic

data for this period shows increased solar activity. This relation will be examined in some detail as part of the analysis of these results.

These three satellites were launched in the same season; a period of Antarctic Winter and Arctic Summer. The charge densities change from one to three orders of magnitude between the light and dark regions of the ionosphere. It would be very desirable to carry out similar measurements in the altitude region 200 to 400 km, in the months of October and February, to obtain seasonal variations in the ionospheric charge densities over the earth.

It is unfortunate that the temperature and energies of the charged particles could be reduced for only the real-time acquisition. Any effect of latitude, longitude, altitude, and local time on these properties could not be determined. It will be possible to obtain this information from the machine-processed data.

#### 5.7 CONCLUSIONS AND RECOMMENDATIONS

The variations of ambient positive and negative ions and electrons have been obtained as a function of local time, latitude, and longitude, in an altitude region 200 to 400 km. The energies and temperatures of these particles have also been measured periodically during each orbit. The results show the solar position as dominant influence on the results. The launching of vehicles with similar payload during each season of the year would therefore be highly desirable. The machine processing of the vehicle data continues. This data will be included in a report on the analysis and interpretation of the results.

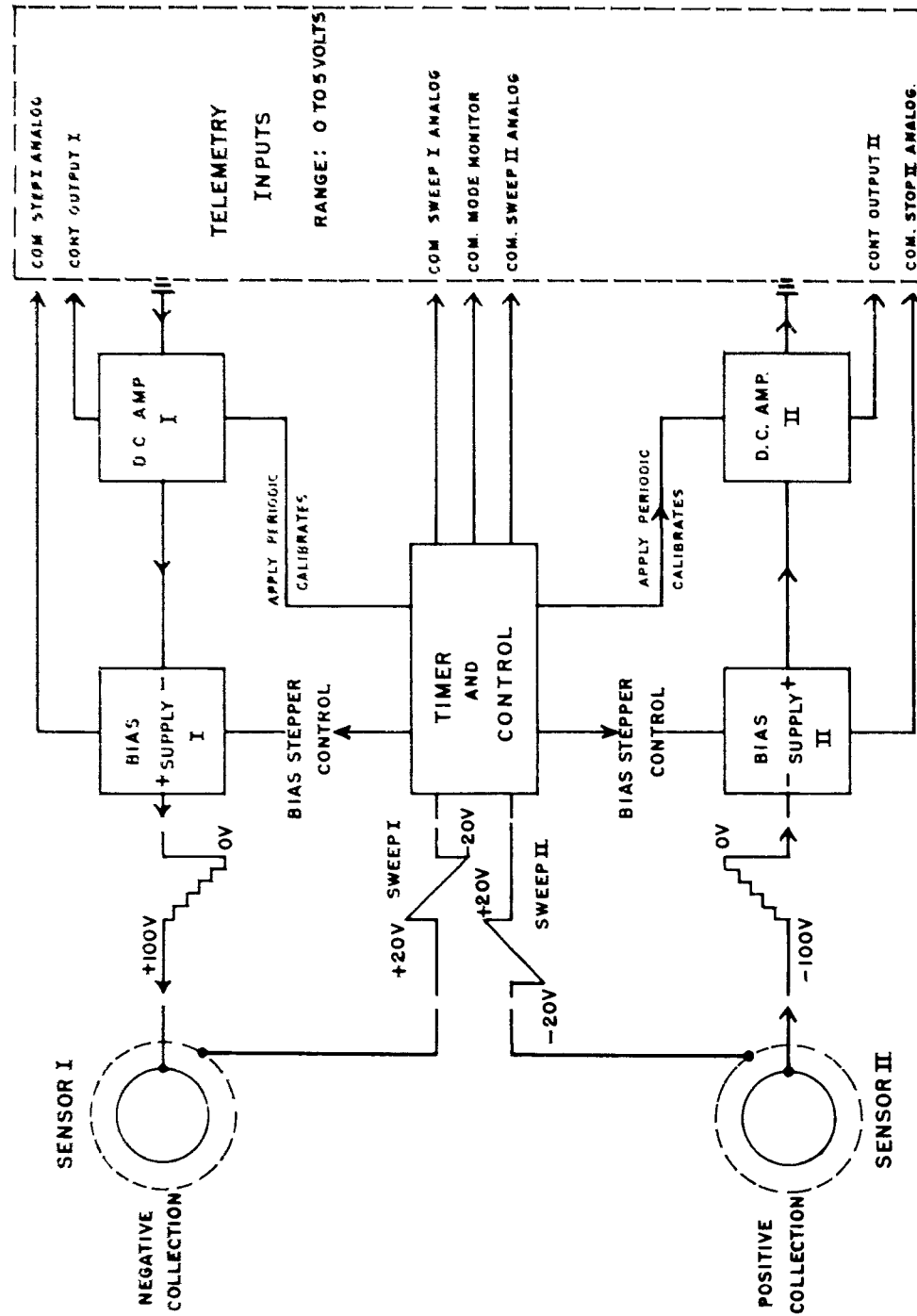
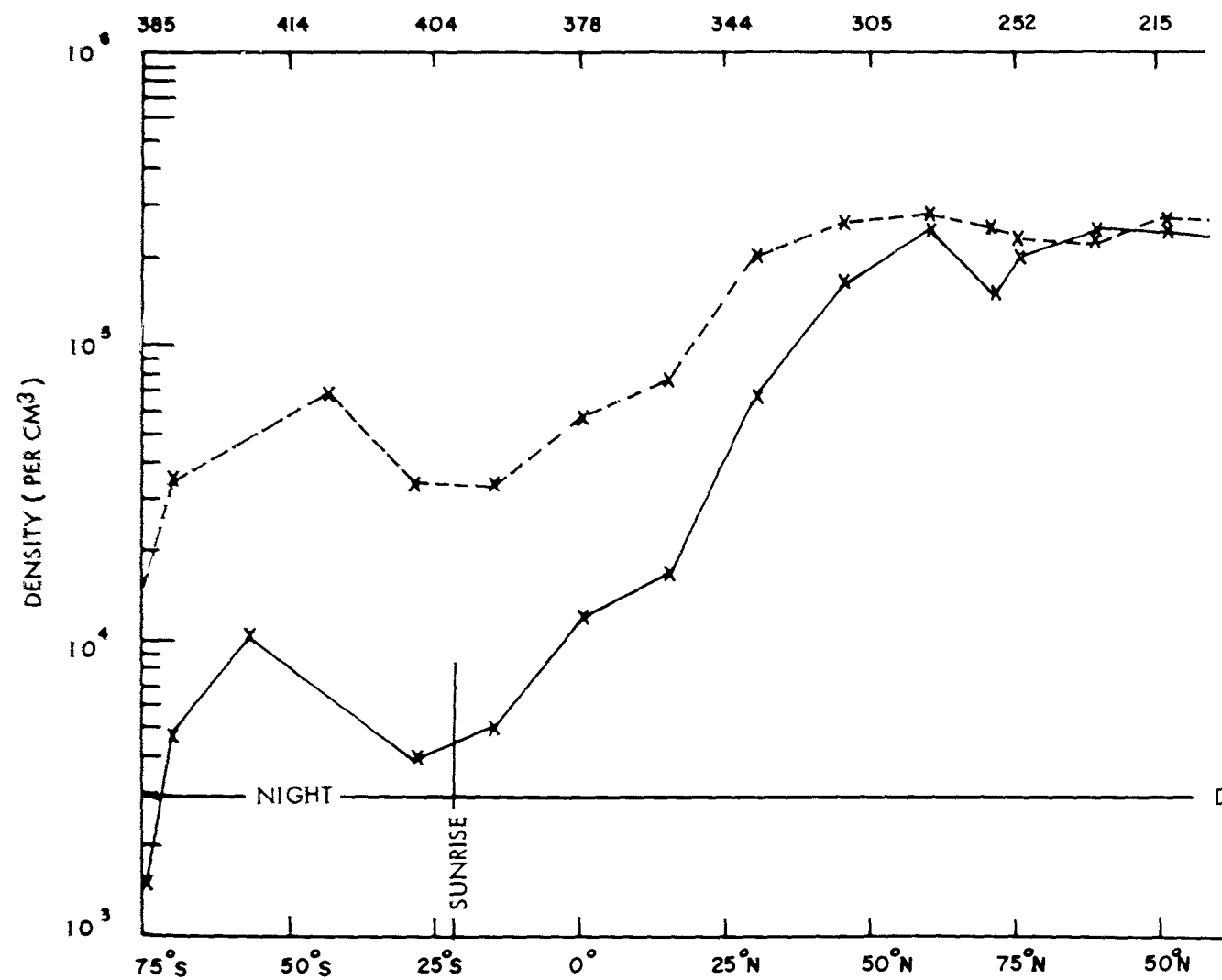


Figure 5.1 Block diagram of ion trap experiment.





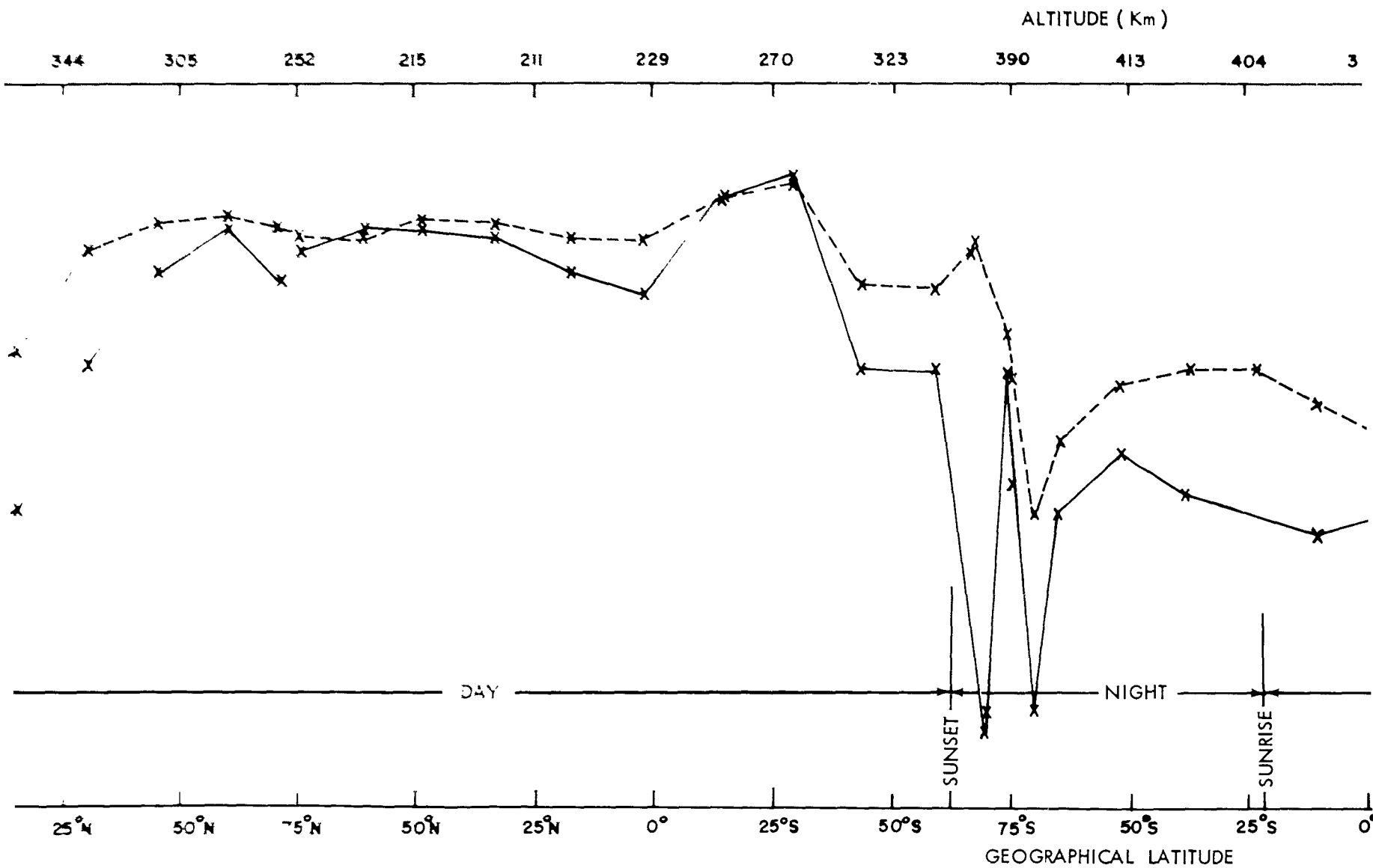
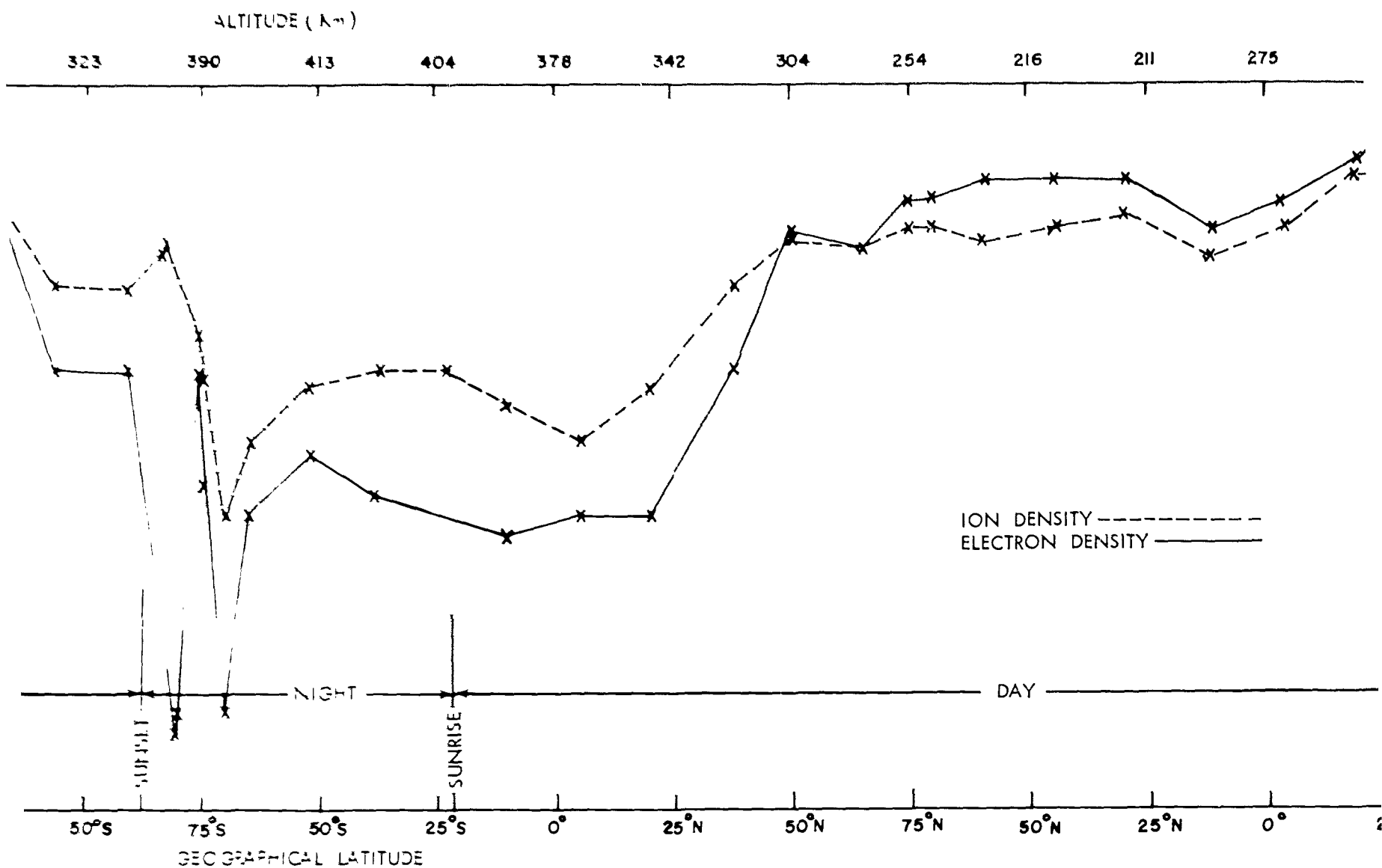


Figure 5.2 FTV 1127, Orbits 2, 3, and 4, VAFB, recorder playback

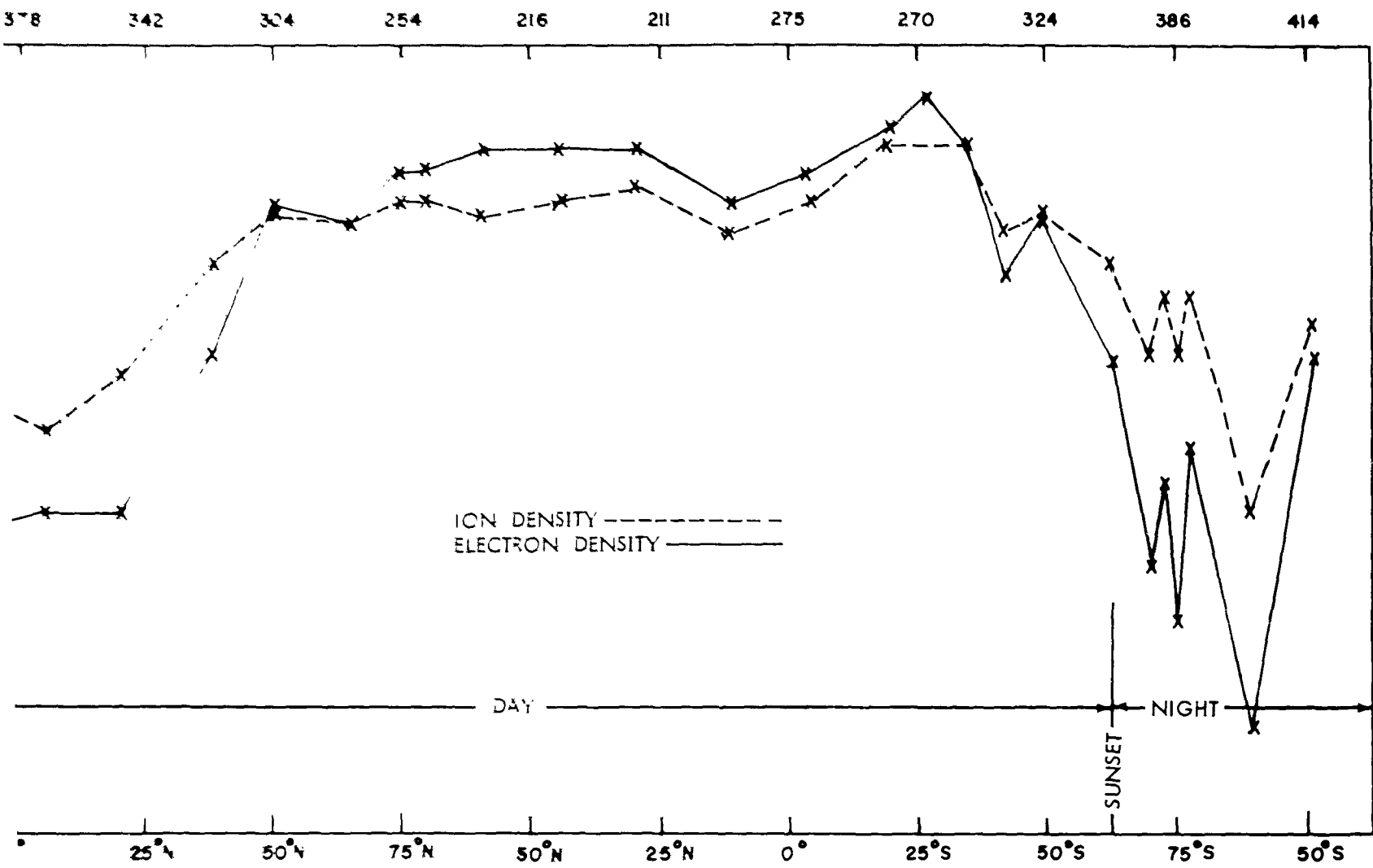


W 1117, Orbits 2, 3, and 4, VAFB, recorder playback data.

171-172

SECRET

3



: data.

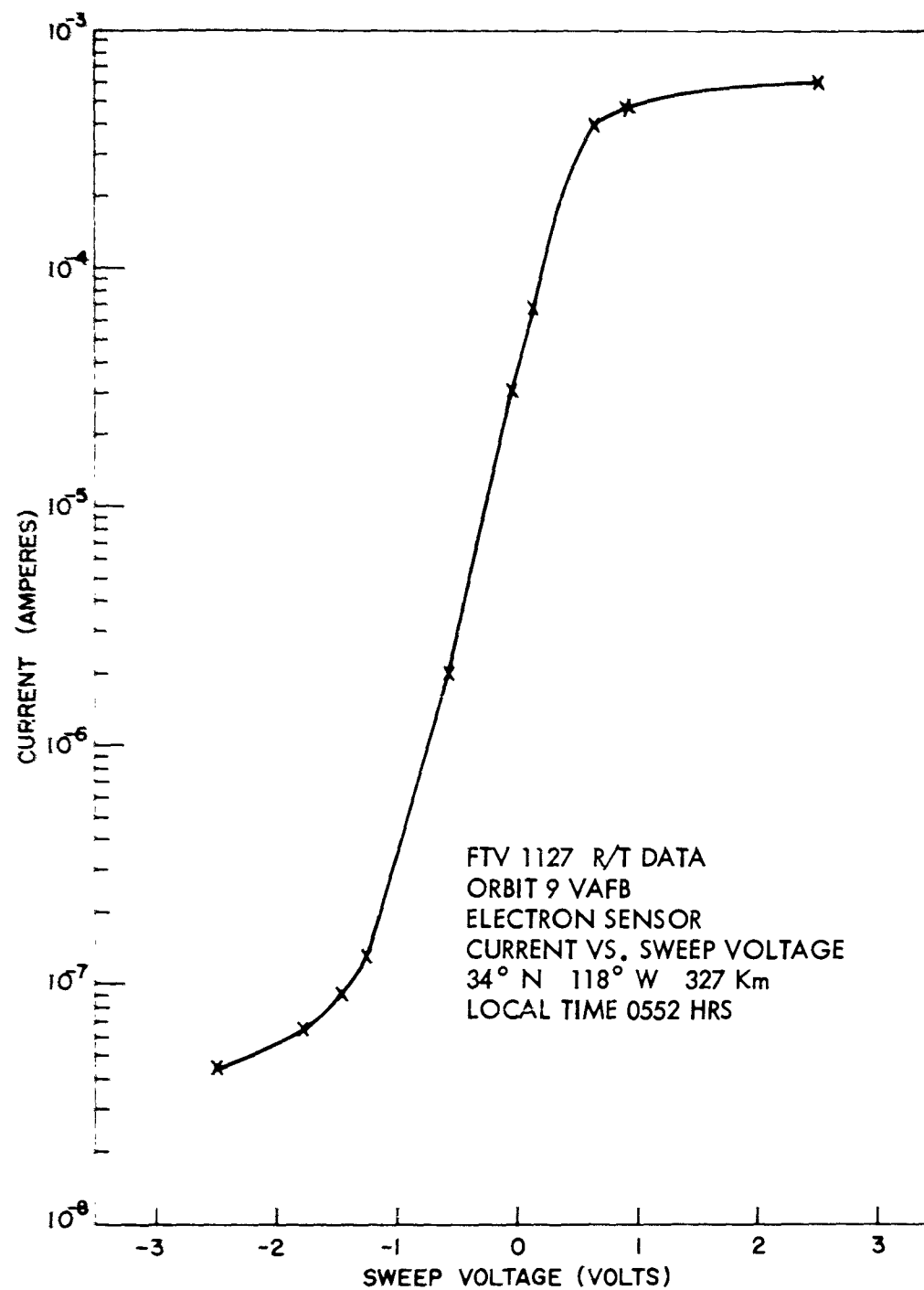


Figure 5.3 FTV 1127, sensor current versus sweep voltage.

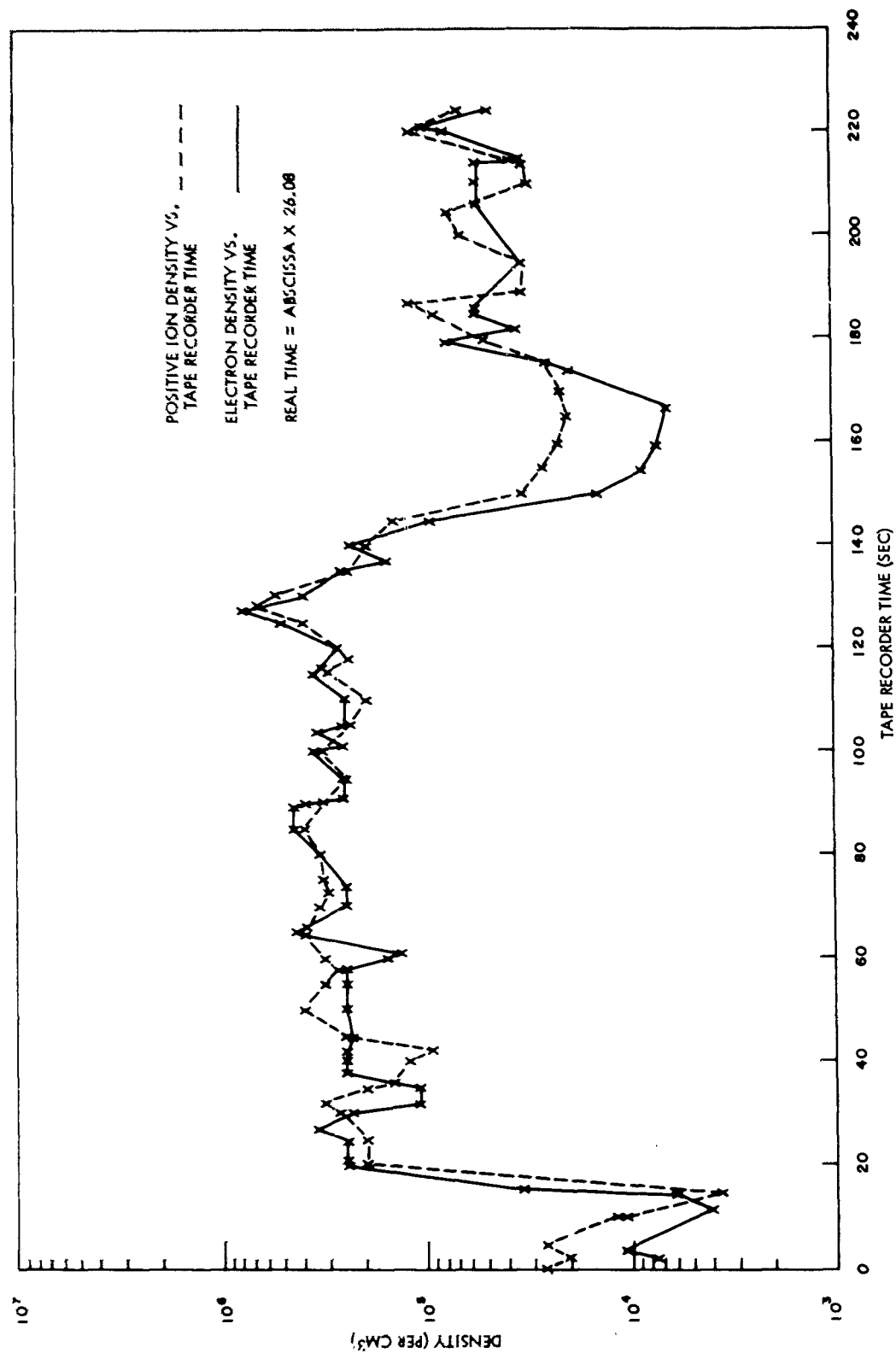
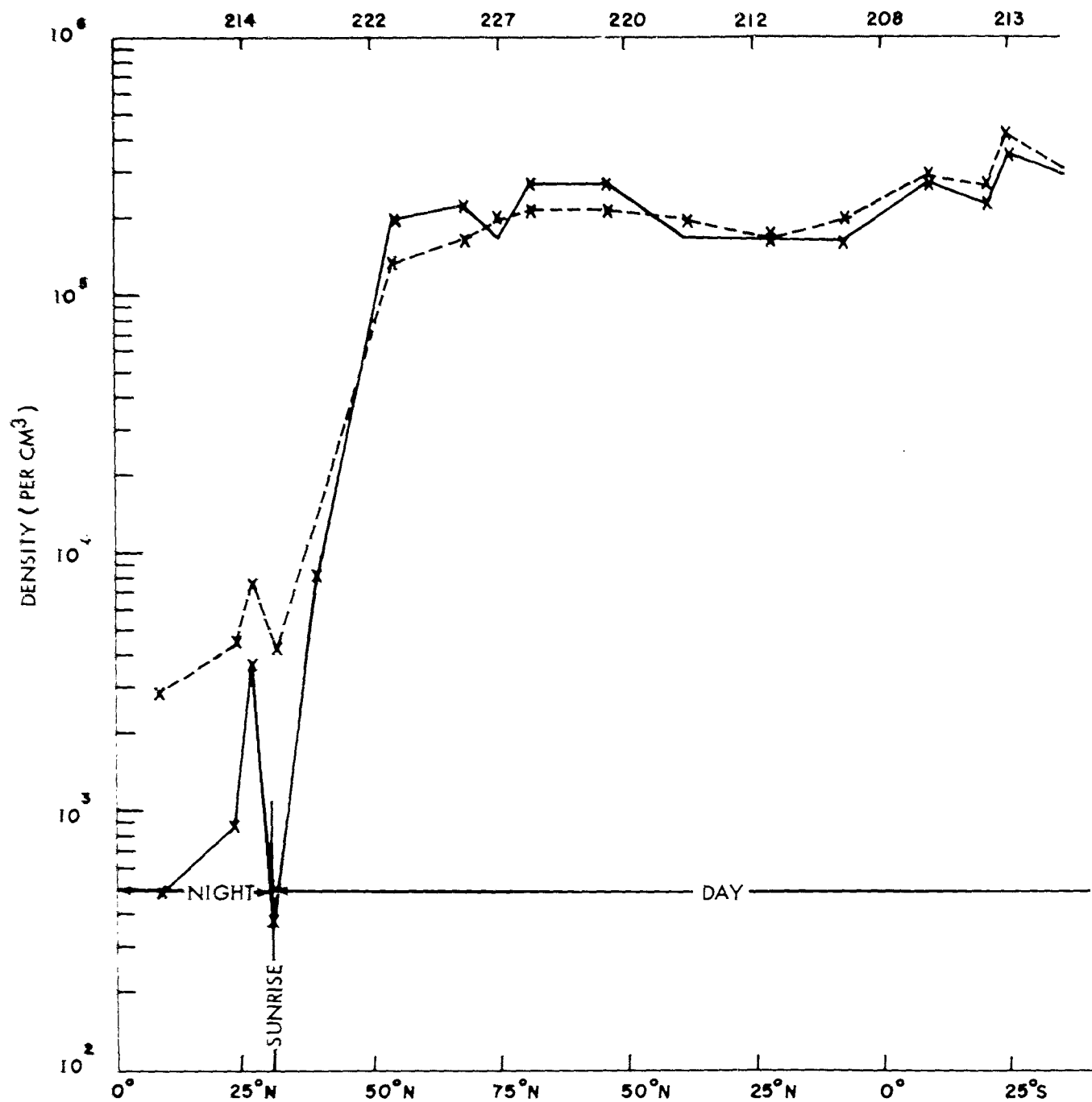


Figure 5.4 FTV 1128, Orbit 65, VAFB, recorder playback data.



1

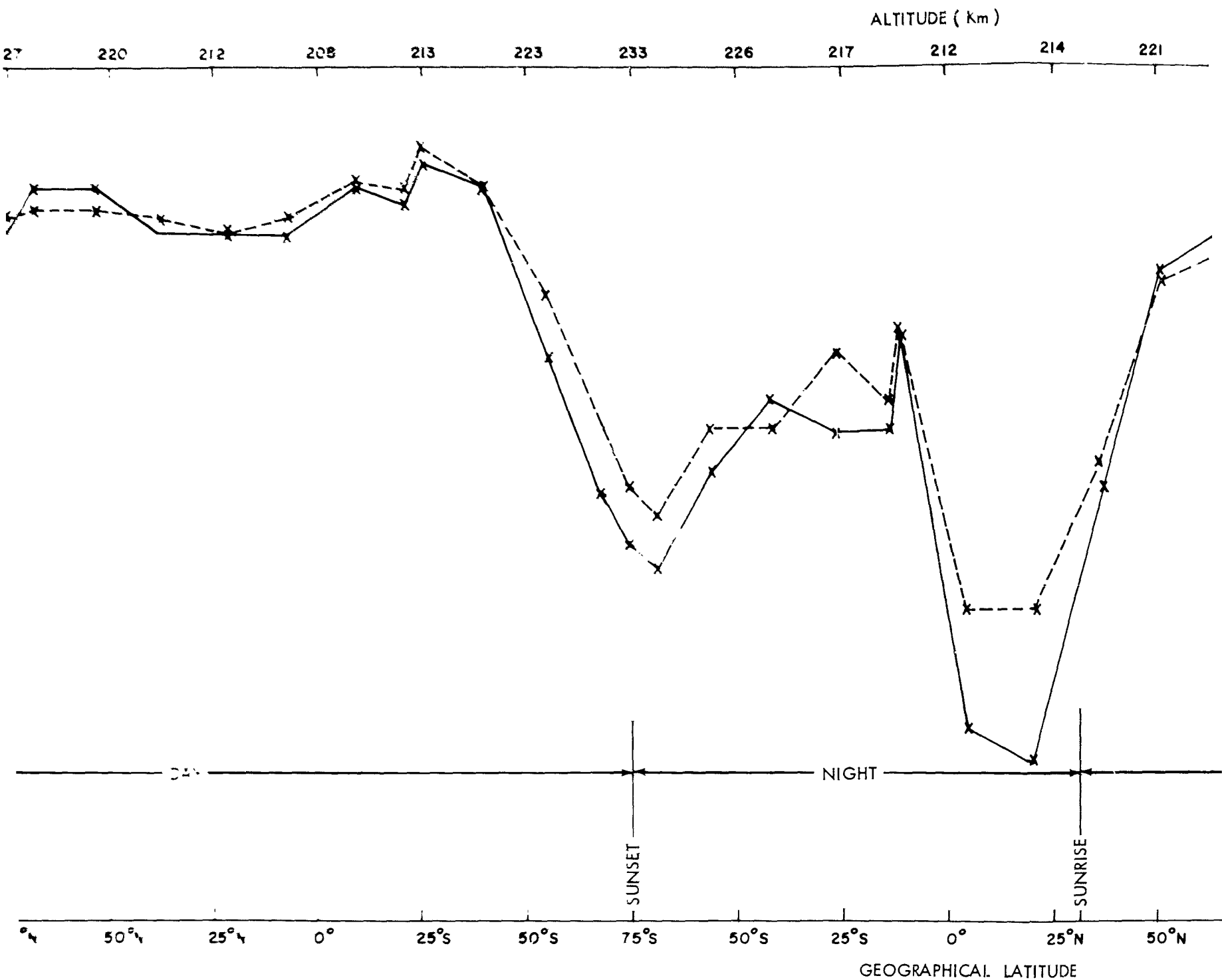
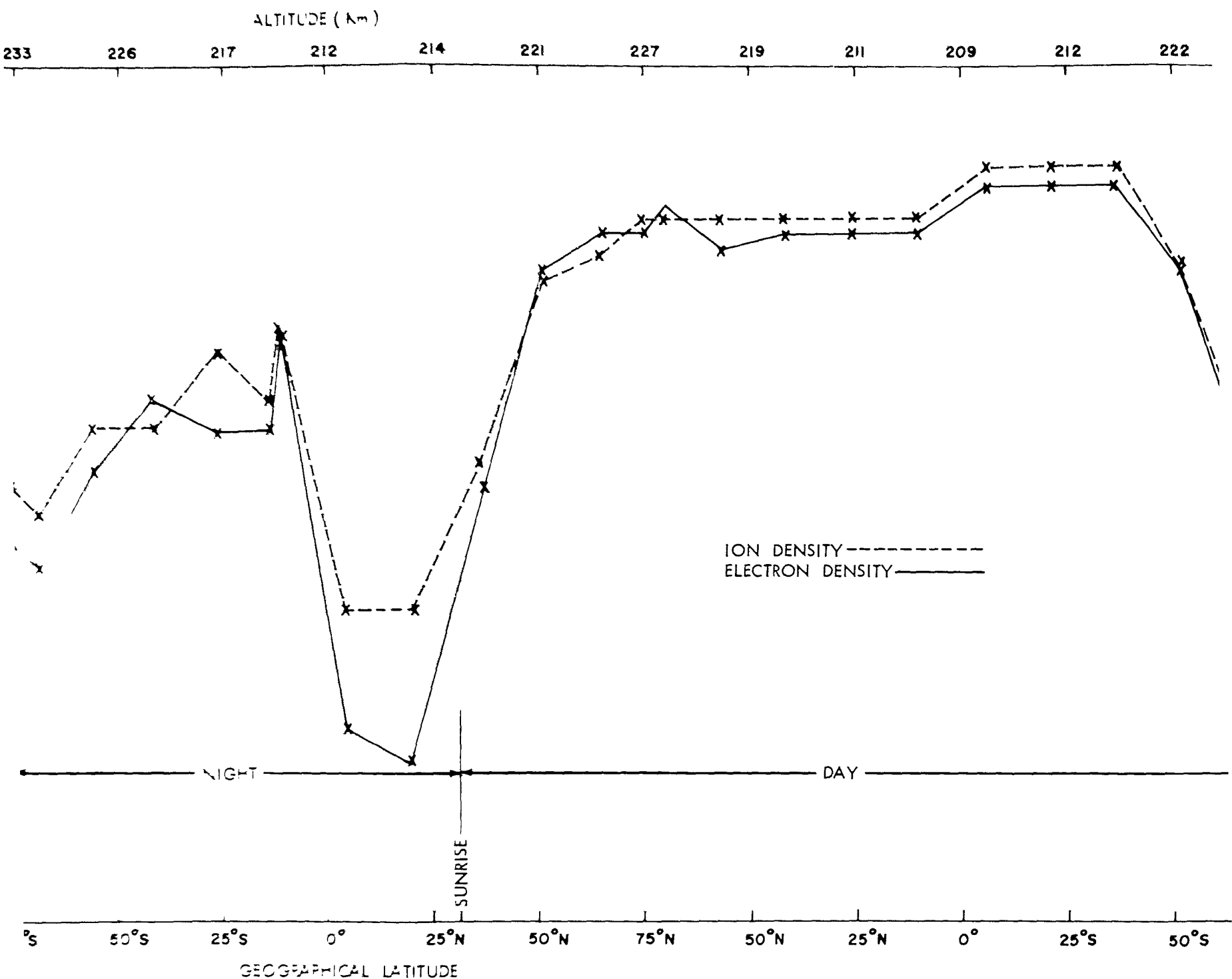


Figure 5.5 FTV 1129, Orbits 177 and 178, VAFB, recorder playback da

2

175-176

SECRET



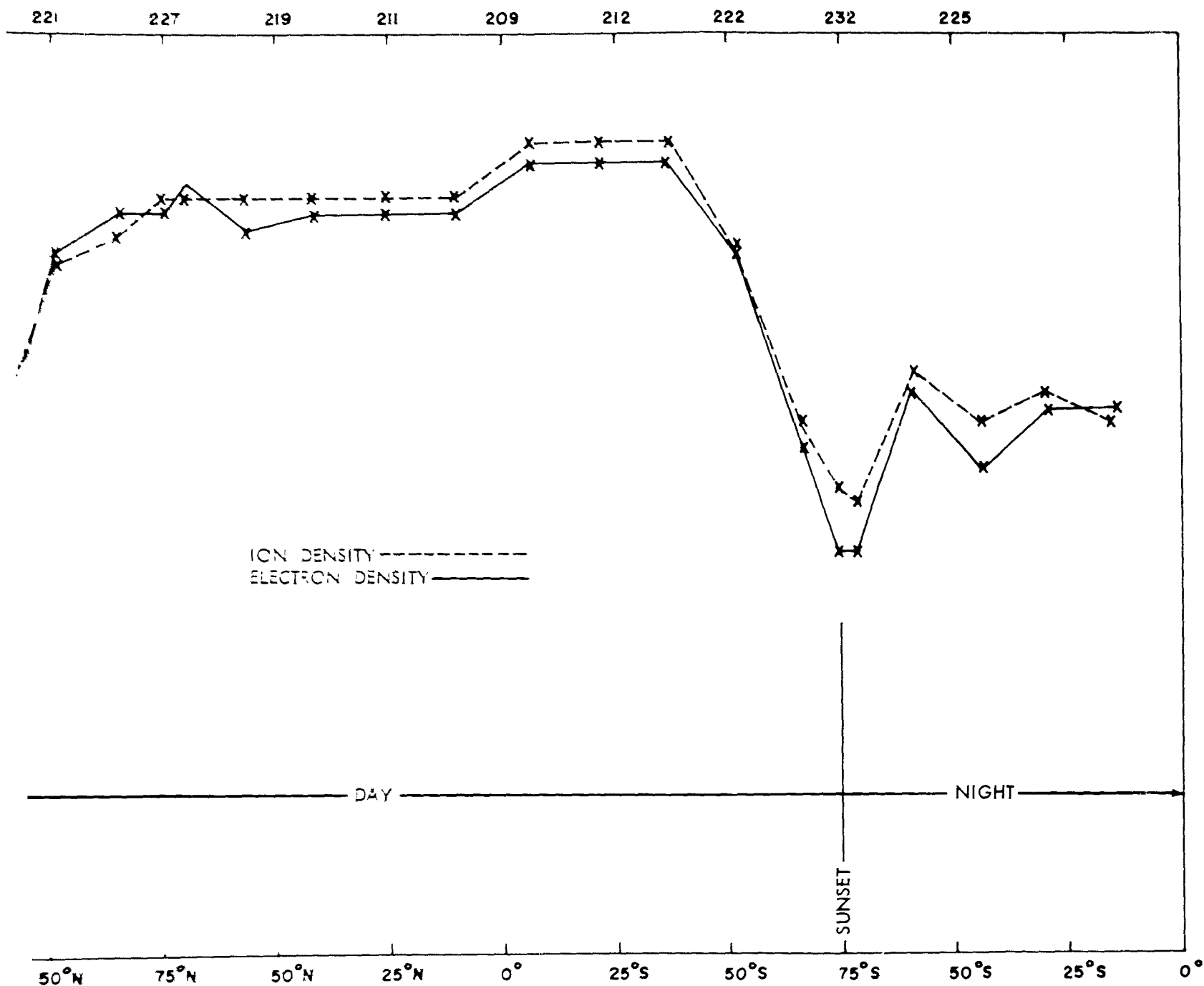
3.3 FTV 1129, Orbits 177 and 178, VAFB, recorder playback data.

173-178

SECRET

3





apbach data.

4

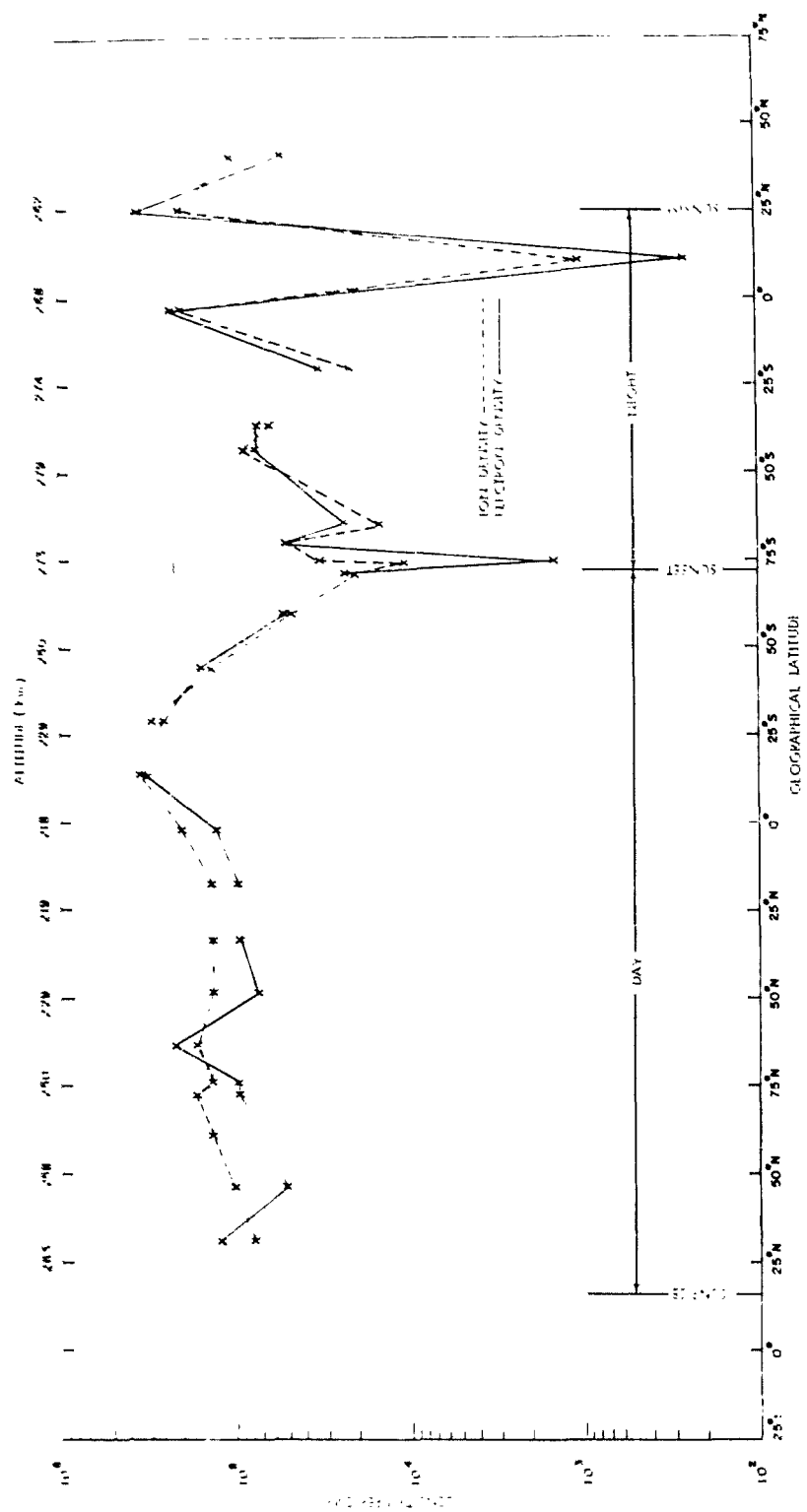


Figure 5.6 FTV 1.29, Orbit 97, HTS, recorder playback data.

SECRET

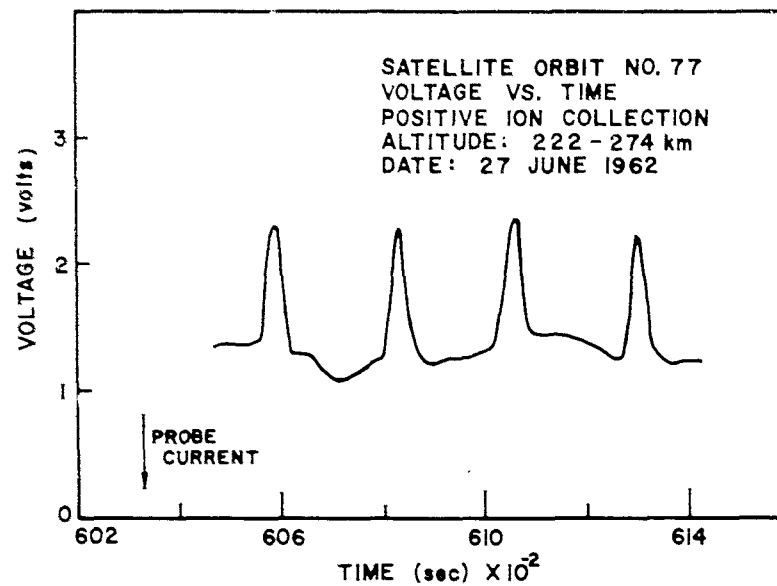


Figure 5.7 Voltage versus time, Orbit 77, FTV 1129.

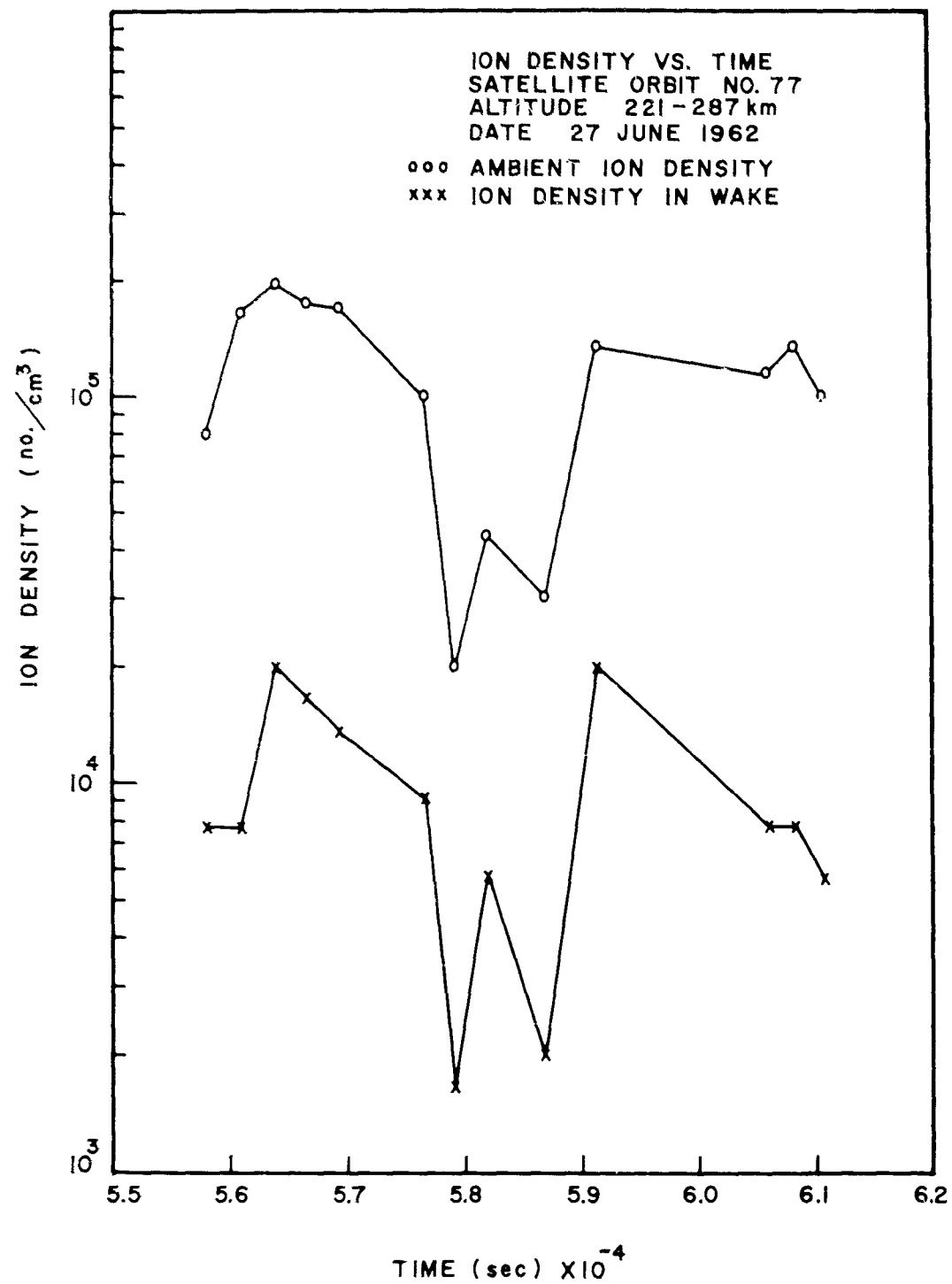


Figure 5.8 Ion density versus time, Orbit 77, FTV 1129.

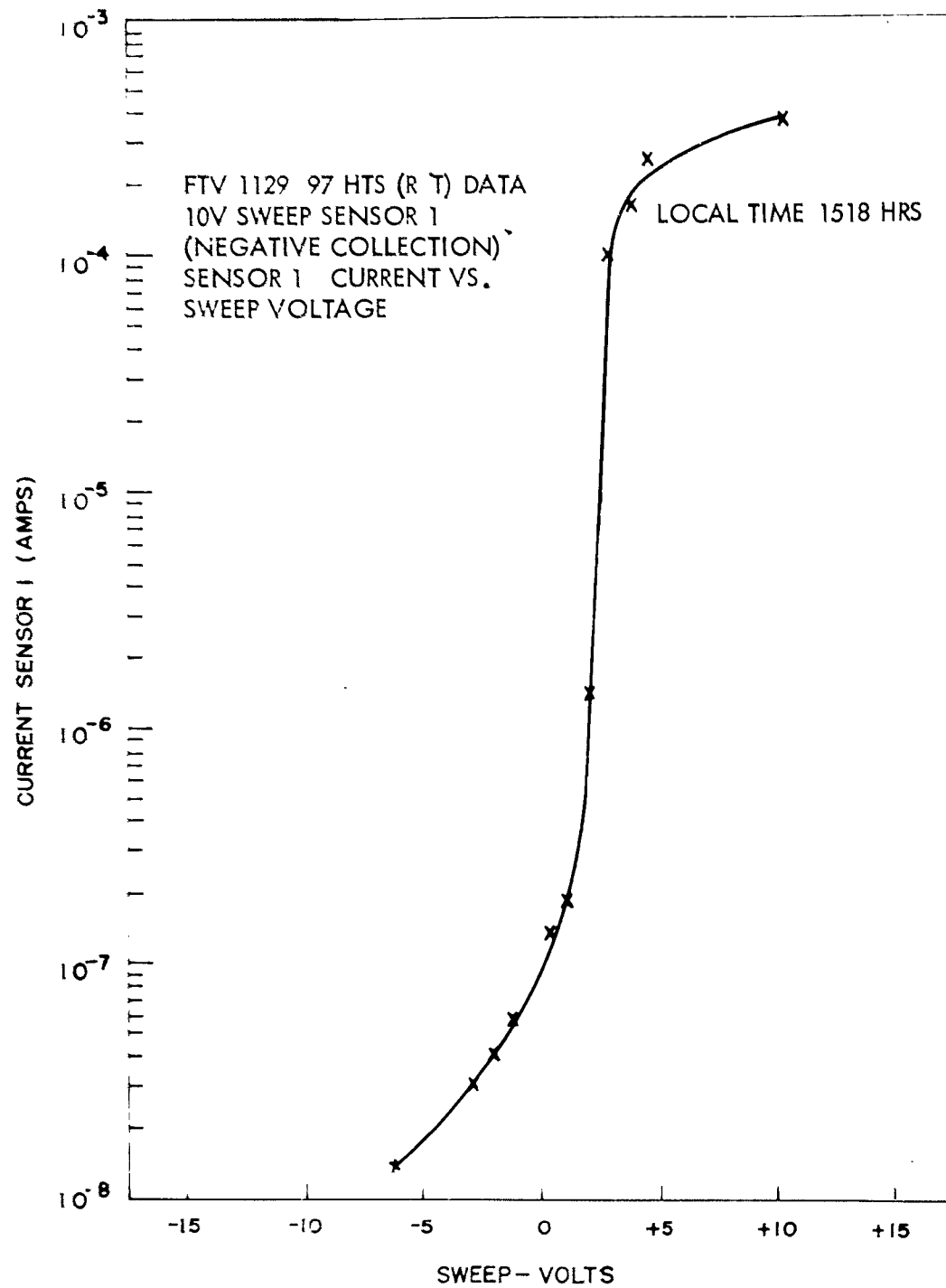


Figure 5.9 FTV 1129, Sensor 1, current versus sweep voltage, 1518 hours.

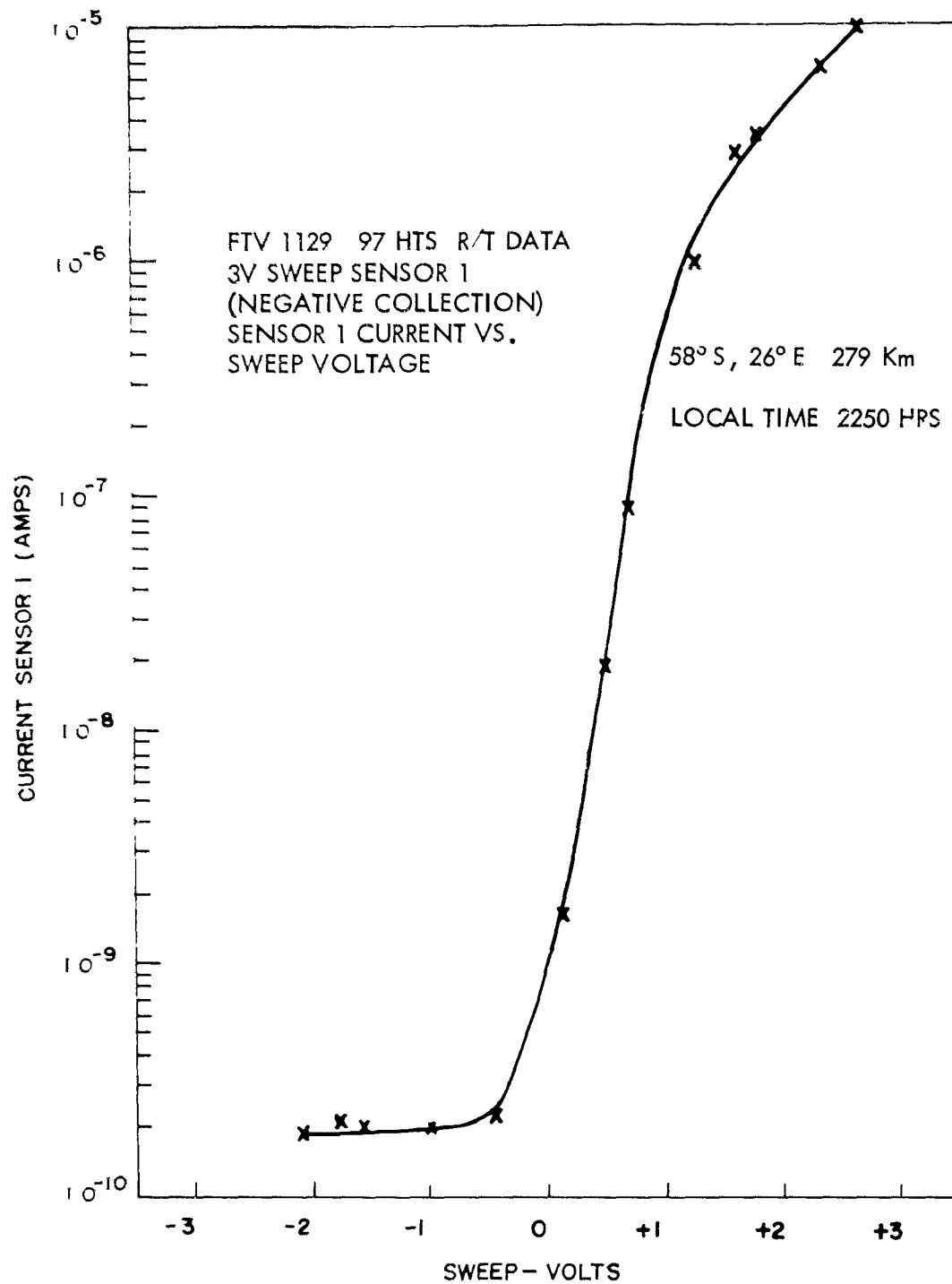


Figure 5.10 FTV 1129, Sensor 1, current versus sweep voltage, 2250 hours.

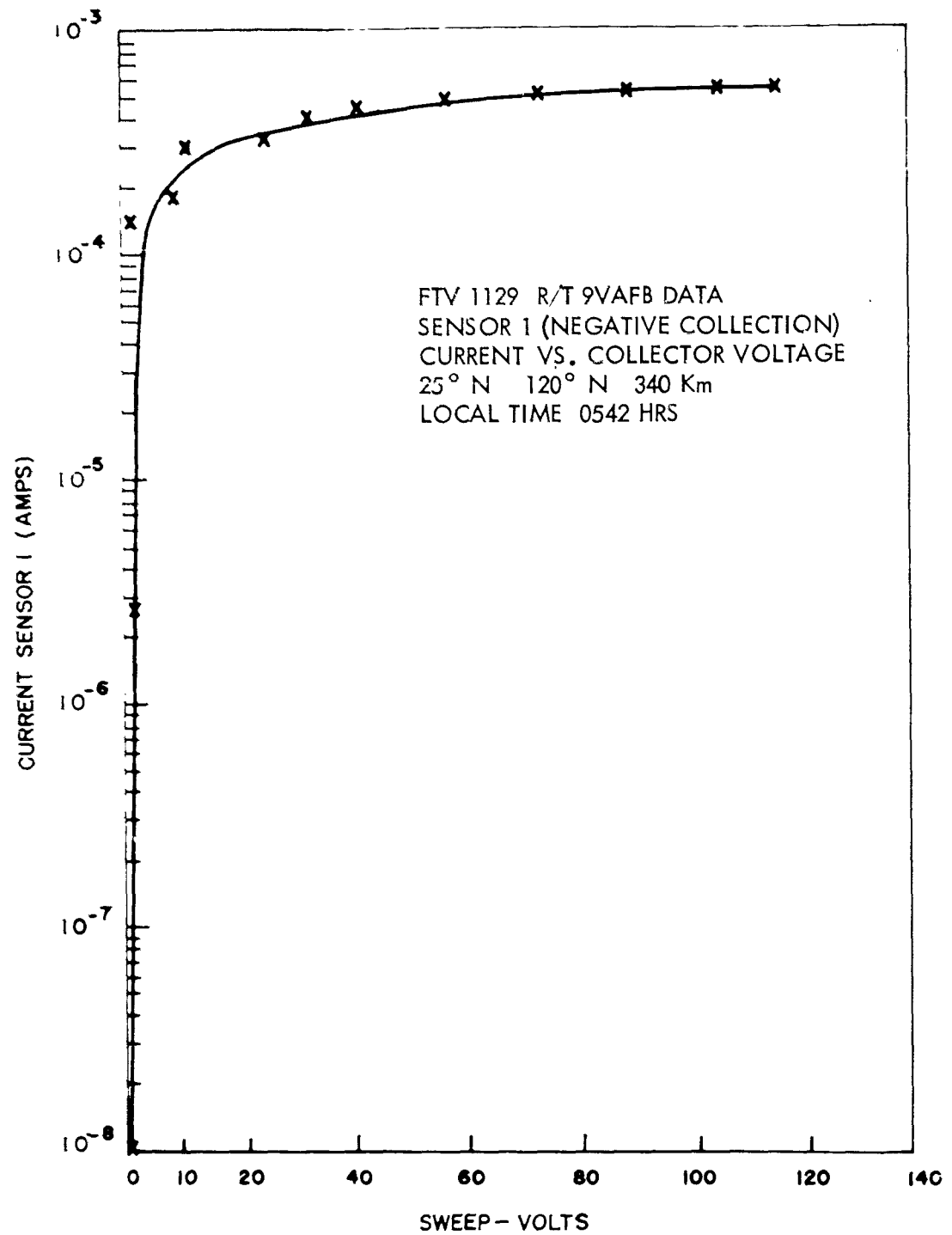


Figure 5.11 FTV 1129, Sensor 1, current versus collector voltage.

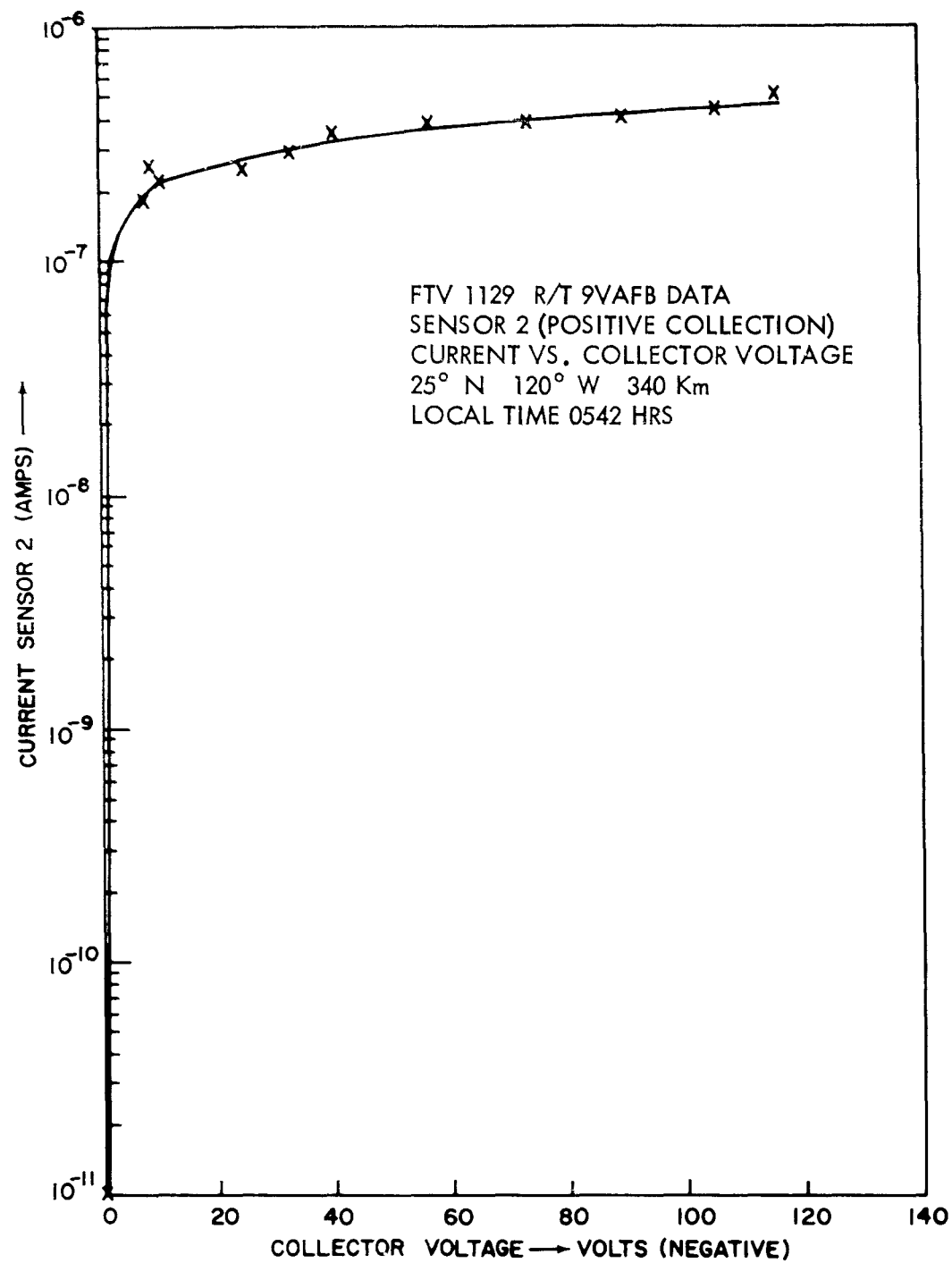


Figure 5.12 FTV 1129, Sensor 2, current versus collector voltage.



## CHAPTER 6

### RETARDING-POTENTIAL ANALYZER

#### 6.1 OBJECTIVE

The objective of this experiment was to acquire information of the explosive effects on characteristics of the ion-electron medium by direct local measurement with a retarding-potential analyzer. In specific, it was to explore on a global basis any measurable characteristic disturbances (as a function of the time after the explosion as well as the global location) in comparison with reference measurements of the same experimental quantities before the explosion.

The interpretation of the raw data obtained is expected to be meaningful not only in general terms of total ion (electron) density and some effective temperature, but also as a determination of the non-Maxwellian tail in the energy distribution, symmetric or asymmetric deviations from isotropic velocity distributions, and a reasonably well resolved separation of ion species. Besides operating as an environmental ion-electron analyzer, the instrument was programmed to accomplish an occasional photoelectron analysis.

## 6.2 BACKGROUND AND THEORY

Vehicle-borne charged-particle sampling devices, with or without retarding-potential discrimination and/or analysis, have become most important tools of direct probing in recent studies of the ion-electron medium throughout the E- and F-regions, the outer ionosphere (magnetosphere), and interplanetary space. Various expressions such as "ion trap", "three-electrode charged-particle trap" and "sheath current monitor" (Bourdeau's group, NASA), "Langmuir probe" (Bourdeau, Spencer), "retarding-potential analyzer" (Hinteregger, GRD), "Faraday Cup" (Rossi, MIT), and other names, have appeared in the literature with rather loosely defined distinctions among them.

The experimental art in this field is still in an exploratory state. Some fundamental questions on the physical interpretation of existing measurements (e.g., those from Sputnik III) have been clarified only recently. Much of the overall theory may still be considered to be in a state of debate. (A monograph, based on informally circulated work by Hinteregger with the benefit of several conferences with Bourdeau's group of NASA, is being prepared for publication.) In spite of certain remaining controversies as to details, however, the general soundness of

using electrostatic retarding-potential discrimination and analysis is considered to be well proven experimentally.

The use of planar geometry for the analyzer structure has been approached most closely in the design of the GRD and NASA instruments (Aerobee Hi 1959, MIDAS 1961, Aerobee 1959, Explorer VIII, respectively). Realization of nearly one-dimensional sampling and retarding conditions not only affords the least complicated theoretical evaluation but also appears to be most advisable in cases of established or suspected symmetric and particularly unsymmetric anisotropies of the particle-velocity distributions. Therefore, more than one planar retarding-potential analyzer of different orientations was provided for the satellite experiment.

In spite of the basic simplicity of the sensor, shown schematically in Figure 6.1, an intelligible yet proper theory cannot be given briefly. Therefore, it may suffice here to state that the instrument rejects (within certain limits) charged particles of one polarity and operates as a normal-energy analyzer for those of the other polarity. Normal energy here is defined as the quantity  $\frac{1}{2} m \underline{v}_n^2$  (see Figure 6.1), i.e., the energy associated with the velocity component of the approaching particle in the normal direction relative to the aperture plate. From the current-voltage

diagrams obtained from two or more detectors with different orientations of their detector axes (see Figure 6.1), it is possible to determine anisotropy and asymmetry of velocity distributions. The diagrams from a single detector already allow (1) inference of ion density (electron density); (2) calculation of effective electron temperature, as well as determination of non-Maxwellian tail in the electron-energy distribution up to the instrumental scanning limit— $E_{R_{\max}}$  (see Figure 6.1); and (3) mass-spectrometric identification of ion species to the extent determined by ratio of the vehicle-velocity component  $V_x$  to the average (thermal) ion speed and by the difference in mass number of the major constituents involved.

Elements of the theory of measurements with planar retarding-potential analyzers have been published.<sup>12</sup> A more complete analysis of the various problems of ion density and velocity-distribution measurements from space vehicles is presently available only as an informal report for limited distribution.<sup>13</sup>

### 6.3 INSTRUMENTATION

Two identical retarding-potential analyzers (Model 6D, Comstock and Wescott, Cambridge, Mass.) with associated automatic range-switching and polarity-switching amplifiers, program unit, and regulated power supplies (Adcole Corporation, Cambridge, Mass.) (see Figure 6.2) were used in the experiment.

The analyzers or sensors were mounted as far apart as possible. Due to physical limitations of the allocated space, they were mounted looking out radially from the vehicle with an angular separation of  $101^\circ$  (see Figure 6.3.)

The instrument was programmed such that both sensors were operated simultaneously in any one of three modes. Mode I was the measurement of photoelectrons leaving the tungsten sensor cathode or target due to incident extreme ultra-violet radiation; Mode II was the measurement of environmental positive ions; and Mode III was the measurement of environmental electrons.

The mode program sequence was II, II, III, II, II, III, I. Each mode consisted of 25 measurements, and each measurement was synchronized with the 0.4-rps telemetering commutator. Two measurements were made on each revolution of the commutator. Therefore, the time between each measurement was 1.25 seconds, and the time duration of each mode was 31.25 seconds. The complete program required 218.75 seconds.

A schematic diagram of the sensor elements and connections is shown in Figure 6.4. A tabulation of element voltages as a function of mode and measurement number is shown in Table 6.1.

The sensor target currents were measured with separate automatic range-switching and polarity-switching amplifiers. The amplifiers had eight ranges of sensitivity. The adjacent range sensitivity ratio was four. Full scale on the most sensitive range was  $2.45 \times 10^{-10}$

ampere. Full-scale for the least sensitive range

was  $2.45 \times 10^{-10} \times 4^7 = 4.0 \times 10^{-6}$  ampere.

When measuring positive currents, the amplifier output at zero input current was 5.0 volts, and at full-scale input current it was 0.0 volt. When measuring negative currents, the output voltage at zero input current was 0.0 volt, and at full-scale input current it was 5.0 volts. This was accomplished in the amplifier by offsetting the amplifier output voltage 5 volts when a polarity change was detected.

Range sensitivities were automatically decreased by a factor of four at full scale for increasing signals and increased by a factor of four at 17% of full scale for decreasing signals.<sup>14</sup>

The system outputs which were telemetered were as follows (see Table 6.2):  $VR_1$  and  $VR_2$  indicated measurement step number. Each output was a five-step staircase between 0 and 5 volts.  $VR_1$  advanced one step for each commutator synchronizing pulse.  $VR_2$  advanced one step for each five  $VR_1$  steps.

$E_{01}$  was the amplifier output voltage for sensor S1 and represented % full-scale of that amplifier.

$E_{T1}$  was the amplifier scale factor and polarity indicator for sensor S1. It consisted of 16 discrete levels corresponding to the eight sensitivity ranges in both polarities.

$E_{O2}$  was the amplifier output for sensor S2.

$E_{T2}$  was the amplifier scale factor and polarity indicator for sensor S2.

$E_D$  was a mode indicator. It consisted of three discrete levels and varied according to the mode program.

Mon #1 and Mon #2 were outputs monitoring the regulated supplies used throughout the instrument.

Synch was used as a means for synchronizing the measuring program with the commutator. The closing of this commutator segment to ground through the telemetering input impedance was used as an input to the program unit.

The program was advanced one measurement step at the end of a read-out period (see commutator pin assignments, Table 6.2.), allowing approximately 0.2 second for transients to settle out before the next read-out.

#### 6.4 DATA REQUIREMENTS

The Ring B commutator had 60 segments at 0.4 rps. Seventeen informational segments were assigned to the retarding-potential analyzer. The assignments are shown in Table 6.2.

For quick-look information, three copies of the stripout are required for the informational segments shown in Table 6.3. For analysis,

two copies are required of the Midwestern record or equivalent of the various acquisition times. The paper speed should be adjusted so that it can be read manually.

Informational segments are to be digitalized and placed on low-density magnetic tape in floating-point binary form. The tape format should be of the form shown in Table 6.4. Each commutator revolution should be one record. Two copies of the binary-coded decimal listing are requested and also a binary tape of the format shown in Table 6.4.

For trajectory information, the following is required:

(1) low-density magnetic tape of the ephemeris; (2) two-ply listing of the data on binary tape or tapes; (3) a write-up of the format of the binary tape (length of record, file, and number of files); and (4) a tape log containing a complete list of the orbits, stations, times, etc., at which the acquisitions were made.

The following is a description of format of the data received from Lockheed Missiles and Space Division. Low-density floating-point binary tapes were received with all experimenters' data merged on one tape. Each file on the tape contained an experimental parameter which consisted of one or more points on the commutator. The format was the following: TIME (1), DATA (1), TIME (2), DATA (1), etc.



Upon receiving the tape, a binary-coded listing of the parameters given in Table 6.2 was produced from the binary input tape.

Plots of voltage versus time were also received for each experimental parameter. A tabular listing of the ephemeris was also supplied.

The current and the logarithm of the current was computed from the  $E_0$  and  $E_t$  value on an IBM 7090 computer.

## 6.5 RESULTS

Retarding-potential analyzers were included in the instrumentation of only two of the satellites: FTV 1128 and FTV 1127. No data was obtained from FTV 1128. Data was obtained from FTV 1127 for a period of 72 minutes or 4/5 of an orbit.

One of the possible reasons for this failure can be traced to the power supply. While the design voltage of the instrument was in the range of 26 to 31 volts, the power supply of the satellite payload was an unregulated 28-volt supply dropping down to a plateau of 26 volts after a few orbits. The same design error may be responsible for the poor performance of detector S1. Another reason is the unusually low temperature as measured in the radio noise instrument. Therefore, only data from detector S2 is being presented.

The data was taken during orbit No. 2 when the attitude of the satellite was stabilized with respect to the vertical and the direction of motion. That means that during this orbit both detectors

were side detectors looking perpendicular to the direction of motion. In this case Mode II data cannot be readily interpreted in terms of positive ion densities.

Mode I was designed for the measurement of photoelectrons. During the useful life of the instrument, both detectors were in the shadow and never looked toward the sun. Two samples of the current-voltage curve for Mode I are shown in Figures 6.5 and 6.6. They were measured in the range of the higher northern latitudes. However, most of the time no current was measured.

Samples of Mode II measurements are shown in Figures 6.7, 6.8, and 6.9. The scale used for the current is logarithmic above  $10^{-10}$  ampere and below minus  $10^{-10}$  ampere. Between these points it is linear, keeping the transition smooth. For high-retarding potentials the current is found to be negative. This is caused most likely by secondary electrons created at the auxiliary grid by ion bombardment. There appears to be a correlation between the ion saturation current and the amplitude of the negative current.

The general behavior of the voltage-current curve as a function of the position on the orbit is represented in Figure 6.10.

The curves show currents versus time for different retarding voltages.

Samples of measurements on Mode III are given in Figures 6.11, 6.12, 6.13, and 6.14 for different positions on the orbit. It should be mentioned that in the plots of current versus retarding potential a correction had been incorporated. The original plots showed a tendency toward a staircase shape in line with the range-switching voltages. The current data points were corrected by subtracting a constant current ( $35 \times 10^{-10}$  amp in range - 5) on all the odd ranges. This can be justified by a drift in the amplifier front end when the temperature drops below the tolerance of the circuit elements. A similar correction was applied for the Mode II data where the constant current had to be added. At southern latitudes (Figure 6.11) the electrons generally follow a thermal distribution with a linear slope in the chosen representation. From the slope an apparent temperature  $T_a$  can be derived using the relation

$$I = I_0 \exp \left[ - \frac{eV}{KT_a} \right].$$
 This apparent temperature is used primarily to

describe the measured data and would represent the actual temperature of the electrons only if the instrument would work according to a simple ideal theory. Unfortunately, we do not have data points in the area of lower retardation. It is possible that the slope in this area could be higher. Under the given circumstances the slope was

constructed from the section between 1 and 4 volts and extrapolated toward higher positive voltages in order to obtain at  $V_{R_1}$  the intersection with the horizontal line given by the saturation current  $I_o$ .  $V_{R_1}$  is found to be in the neighborhood of 7 volts. In the design of the instrument it was anticipated that the current drop would occur in the vicinity of 0 volt. This explains the lack of data points in the critical region of the retarding-voltage curve. At the equator and northern latitudes (Figures 6.12, 6.13, 6.14) a trail of hyperthermal electrons can be observed. It starts sharply at  $V_{R_2}$  and falls off exponentially until about -20 volts where it reaches the threshold of sensitivity.

The variations of the essential features of the retarding-voltage curves for Mode III are shown in Figure 6.15. All the measured values of  $I_o$ ,  $T_a$ ,  $V_{R_1}$  and  $V_{R_2}$  are plotted as a function of time and latitude. The highest value the instrument was able to measure is  $4 \times 10^{-6}$  amp. During part of the orbit the current was above this value.

As mentioned before, detector S1 is not believed to have worked properly according to its design. Nevertheless, the saturation current appears to be a correct measurement both in Mode II and in Mode III operation. The result in this case is only slightly different from the measurements of detector S2. However, the slope of

the retarding-potential curve in Mode II is much smaller than measured with detector S1. On the other hand, in Mode III between +8 volts and +5 volts the current drops from its saturation value to its minimum value. The electron temperature  $T$  can be found from the slope of the current-versus-voltage curve.

In spite of the fact that the detector flown on satellite FTV 1127 is not ideal in the sense mentioned before, the formula was used for determining electron densities.  $I_0$  and  $T_a$  were taken from Figure 6.15 and  $5 \text{ cm}^2$  for  $A$ . The result is shown in Figure 6.16 together with the electron-density plot from the impedance probe.

The agreement is better than might be expected from the use of an unreasonable value as  $T_a$  for the electron temperature. However, the compensation lies in the fact that the collecting area  $A$  should have been measured not at the detector but at the outer edge of the ion sheath.

A qualitative interpretation of the measured  $I - V_R$  curves can be given as follows: the key to the curves is the high voltage of +10 volts on the aperture grid. This value had been chosen to enable the collection of electrons in the case of high-negative vehicle potentials. (Occasional vehicle potentials as high as -10 volts had been reported.) However, in the present flight the vehicle potential was low and probably never went more negative than -1 volt which can be concluded from the Mode II data and which also is confirmed by the ion-trap data. The high aperture voltage causes off-perpendicular

gradients of the potential outside of the detector. However, the detector analyzes the electrons only in terms of the perpendicular components of the gradient. This causes the current to drop off at a higher positive voltage because some of the electrons entering the aperture have not gained a perpendicular velocity as high as indicated by the +10 volts of the aperture grid. Another consequence is a slope less steep than produced by a detector of ideal geometry which explains the high apparent temperature. Finally, more electrons are collected into the aperture, thus increasing the effective area of the aperture.

A way of analyzing the present data quantitatively in terms of electron temperature has not yet been worked out. In any case, the high potential of the aperture with respect to space potential prohibits the determination of an accurate electron temperature.

The tail in the energy distribution of the electrons found on part of the orbit is interesting and believed to be real. It conceivably could be produced in the immediate vicinity of the vehicle if it is not a characteristic of the ionosphere. Production of the tail inside the detector appears very unlikely. On the other hand, the orbit occurred on a magnetically quiet day, and hyperthermal electrons can hardly be visualized to exist in the particular parts of the ionosphere.

## 6.6 DISCUSSION

According to previous experience with retarding-potential analyzers of planar design in satellite vehicles, such an instrument

is well suited to measure positive ion densities, provided it is orientated in the flight direction. It also is a good indication of the mass of the major ions and their number density. When the detector is orientated at an angle with the flight direction, the analysis becomes complicated, and the mass resolution is reduced. In fact, no satisfactory way of analysis has been found so far for this case. Since, in the present program, data was collected only while the detectors were looking sideways, an analysis of Mode II data in terms of ion densities has not been attempted at the present time.

Only limited experience is available for an analysis of Mode III data of the planar retarding-potential analyzer. In an environment of thermal electrons the direction of the detector should have little influence on the measurements. For an ideal detector of plane geometry with the aperture grid at space potential (to eliminate any distortion of the geometry outside of the detector) the formula for the electron density is

$$N = \frac{I_o}{A \cdot e} \sqrt{\frac{m}{kT}}$$

$I_o$  is the saturation current

$A$  is the area of the aperture

$e$  is the charge of the electron

$m$  is the mass of the electron

## 6.7 CONCLUSIONS

In spite of the limited amount of data collected by the instrument the experience gained from the flight is very valuable. Of primary importance is the information obtained on the performance of the instrument itself. It is very helpful for improvements in the design of the retarding-potential analyzer. Some of the more elementary shortcomings can be easily corrected in future flights. Of more fundamental nature is the achievement of a better or more defined geometry of the potentials outside the detector. It is important, however, that the advantage of the planar geometry for detecting and measuring the anisotropic velocity distribution of hyperthermal electrons is maintained. Such electrons appear to be present even in the F-layer of the normal ionosphere and certainly are to be found in the nuclear disturbed ionosphere.

Based on the latest experiences a modified version of the retarding-potential analyzer has been constructed and will be flown in a satellite vehicle in the near future. It is extended on an arm from the vehicle and primarily works in Mode III. In addition to the sweep of the retarding potential a sweep of the voltage on the aperture grid is incorporated. There is every reason to believe that such an arrangement will measure accurately vehicle potential and electron temperature.



If successful, the next step in the development is a device which automatically adjusts the voltage on the aperture grid to the space potential.

TABLE 6.1 SENSOR ELEMENT VOLTAGES AS FUNCTION OF MODE  
MEASUREMENT NUMBER

Measurement Step No.	Mode I		Mode II		Mode III	
	V <sub>O</sub>	V <sub>A</sub>	V <sub>O</sub>	V <sub>A</sub>	V <sub>O</sub>	V <sub>A</sub>
	19.5V	10.0V	-29.8V	-2.99V	19.5V	10.0V
	V <sub>R</sub>	V <sub>K</sub>	V <sub>R</sub>	V <sub>K</sub>	V <sub>R</sub>	V <sub>K</sub>
1	-26.5V*	-29.9V	-24.9V	-4.9V	14.8V	12.2V
2	-28.5	-29.9	-23.3	-3.3	11.2	12.2
3	-28.5	-29.9	-22.2	-2.2	7.9	12.2
4	-28.6	-29.9	-21.4	-1.4	4.7	12.2
5	-28.9	-29.9	-20.2	-0.2	4.07	12.2
6	-29.3	-29.9	-19.3	0.7	3.48	12.2
7	-29.9	-29.9	-18.5	1.5	2.94	12.2
8	-30.6	-29.9	-17.7	2.3	2.43	12.2
9	-31.5	-29.9	-17.0	3.0	1.94	12.2
10	-32.7	-29.9	-16.5	3.5	1.47	12.2
11	-26.5*	-29.9	-15.9	4.1	1.01	12.2
12	-33.7	-29.9	-15.5	4.5	0.58	12.2
13	-34.3	-29.9	-15.1	4.9	0.16	12.2
14	-35.1	-29.9	-14.8	5.2	-0.26	12.2
15	-36.1	-29.9	-14.5	5.5	-0.66	12.2
16	-37.2	-29.9	-14.4	5.6	-1.08	12.2
17	-38.4	-29.9	-13.3	6.7	-1.48	12.2
18	-39.8	-29.9	-12.3	7.7	-1.88	12.2
19	-41.5	-29.9	-11.5	8.5	-2.30	12.2
20	-43.4	-29.9	-10.9	9.1	-2.71	12.2
21	-45.6	-29.9	-10.2	9.8	-3.14	12.2
22	-26.5*	-29.9	6.7	26.7	-8.80	12.2
23	-55.2	-29.9	22.8	42.7	-15.1	12.2
24	-62.4	-29.9	40.2	60.2	-43.4	12.2
25	-74.8	-29.9	57.3	77.3	-74.8	12.2

\*Mode I Saturation Measurements.

TABLE 6.2 TELEMETRY PIN ASSIGNMENTS FOR RETARDING-  
POTENTIAL ANALYZER

<u>Informational Segments</u>	<u>Parameter</u>
01	ZERO (Cal)
06	VR1
07	VR2
08	ET1
09	EO1
10	ET2
11	EO2
12	Sync
25	ED
26	MON1
27	MON2
30	5.0 V (Cal)
35	VR1
36	VR2
37	ET1
38	EO1
39	ET2
40	EO2
41	Sync
57	2.5 V (Cal)

VR, voltage on retarding grid  
ET, voltage that indicates range sensitivity  
ED, voltage that indicates type of mode  
EO, voltage indicating detector current  
MON, monitor for input to voltage detector  
1, indicates Detector 1  
2, indicates Detector 2

TABLE 6.3 QUICK-LOOK SEGMENTS FOR RETARDING-POTENTIAL ANALYZER

<u>Informational Segments</u>	<u>Parameter</u>
06	VR1
07	VR2
08	ET1
09	EO1
10	ET2
11	EO2
Time	

TABLE 6.4 TAPE FORMAT FOR RETARDING-POTENTIAL ANALYZER

<u>Time 1</u>	<u>Time 2</u>
<u>Informational Segments</u>	<u>Informational Segments</u>
01	01
06	06
07	07
etc.	etc.
↓	↓
57	57

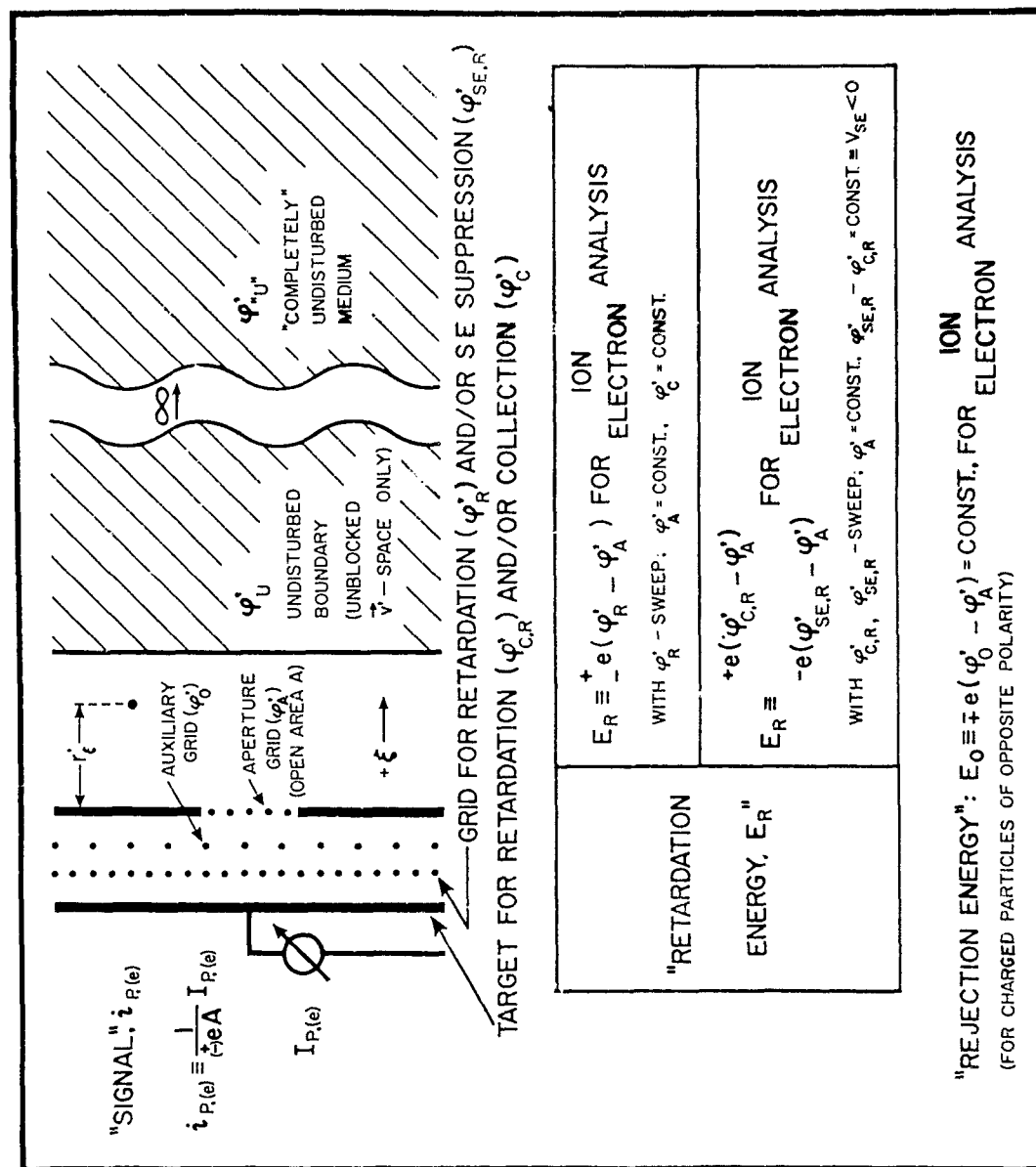


Figure 6.1 Schematic of retarding-potential analyzer.



Figure 6.2 Detector with the antiperturbation shield removed showing the shroud and  $V_0$  grid. The cylindrical cover for the electronics is also removed exposing the three electronic cords.

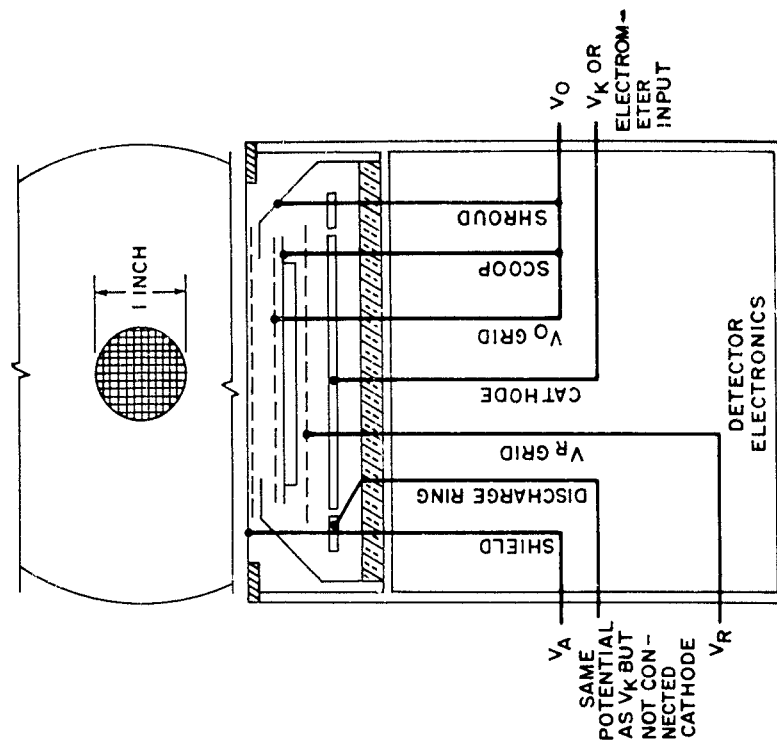


Figure 6.4 Scale drawing of retarding-potential analyzer detector.

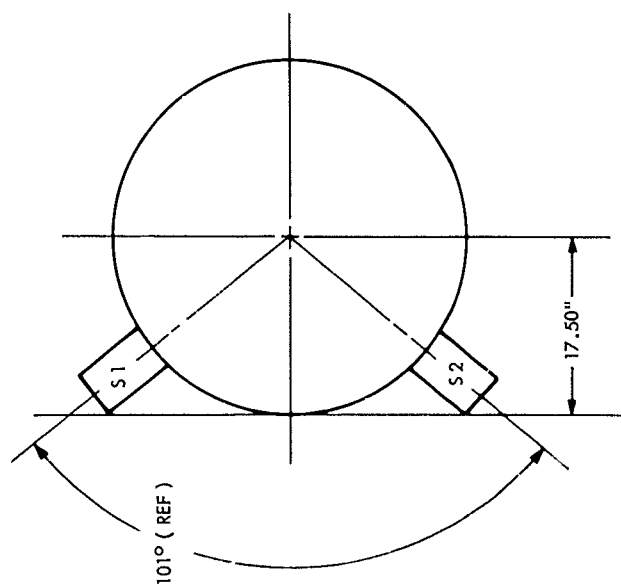
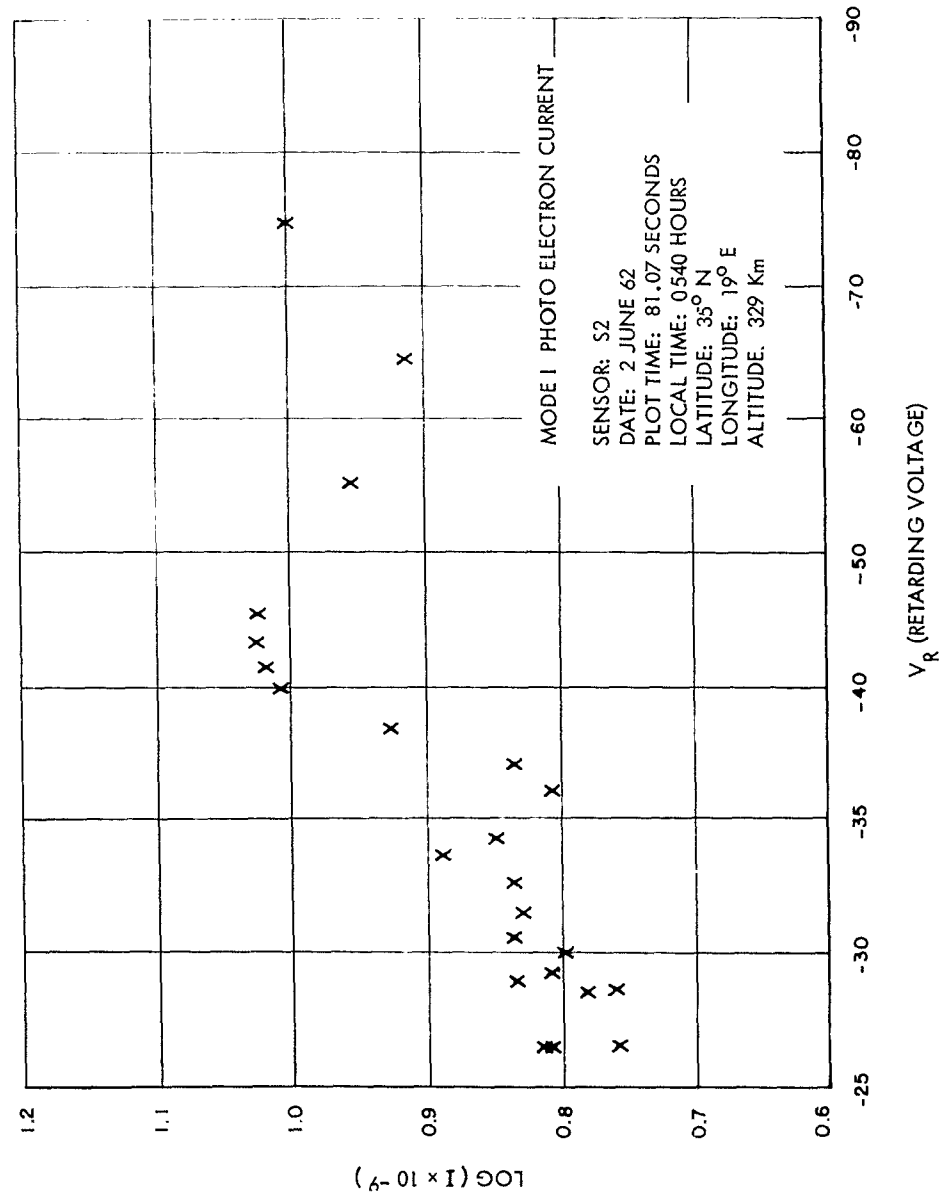


Figure 6.3 Positions of retarding-potential analyzer detectors.





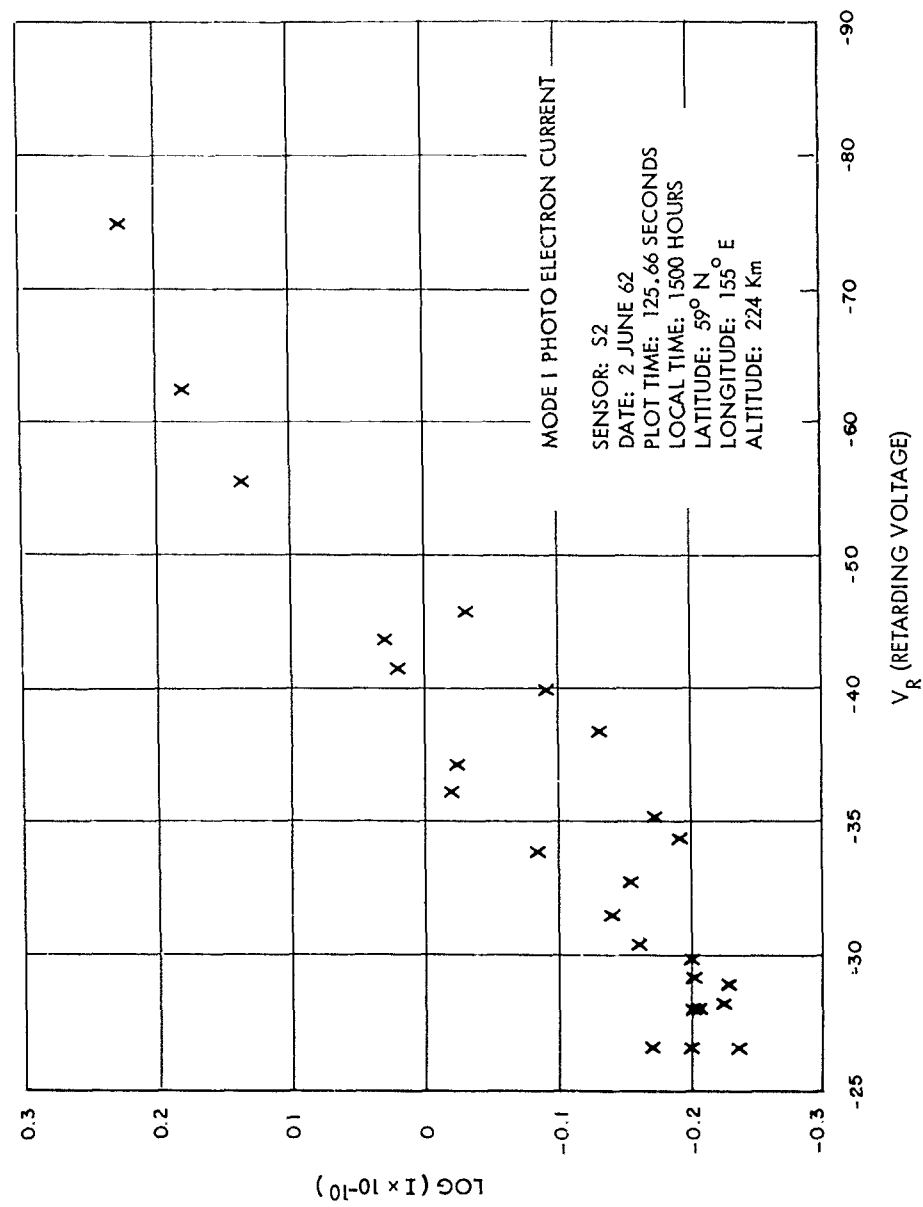


Figure 6.6 Sample of Mode I measurement, 125.66 seconds.

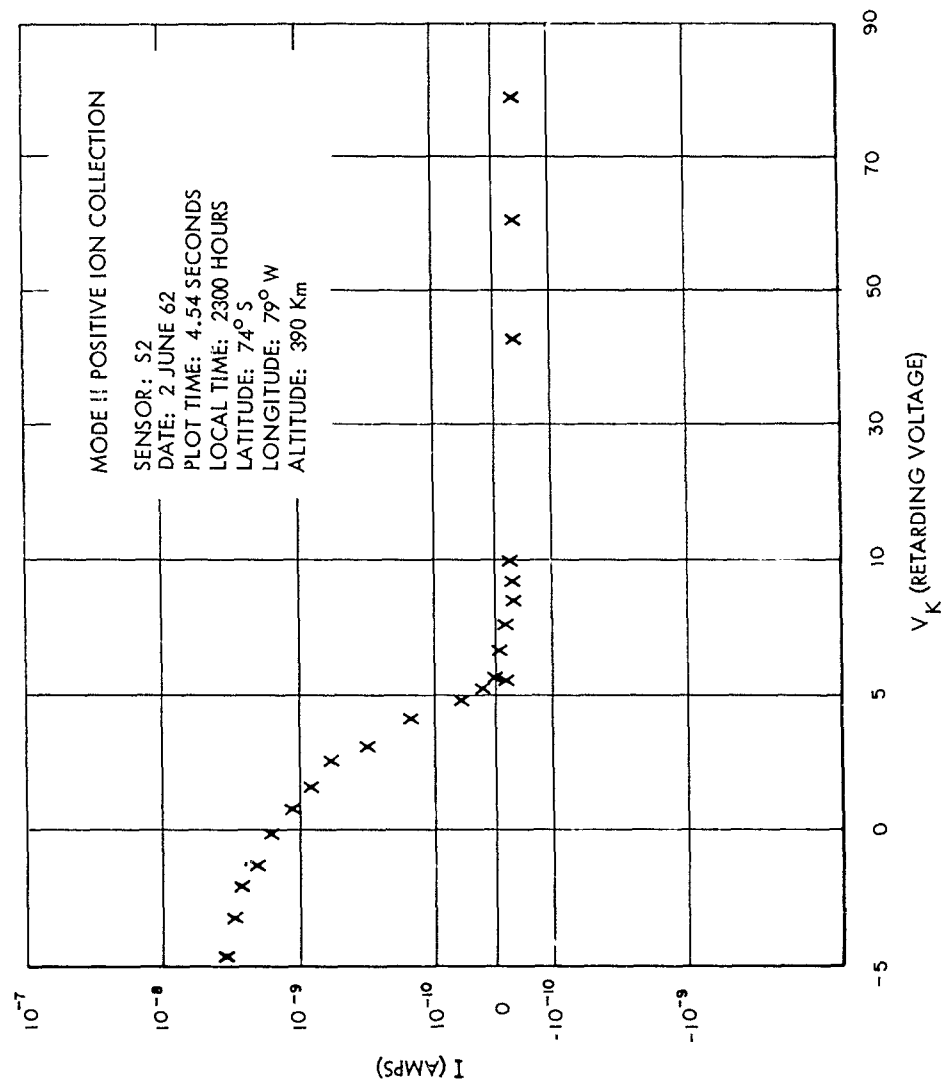


Figure 6.7 Sample of Mode II measurement, 4.54 seconds.

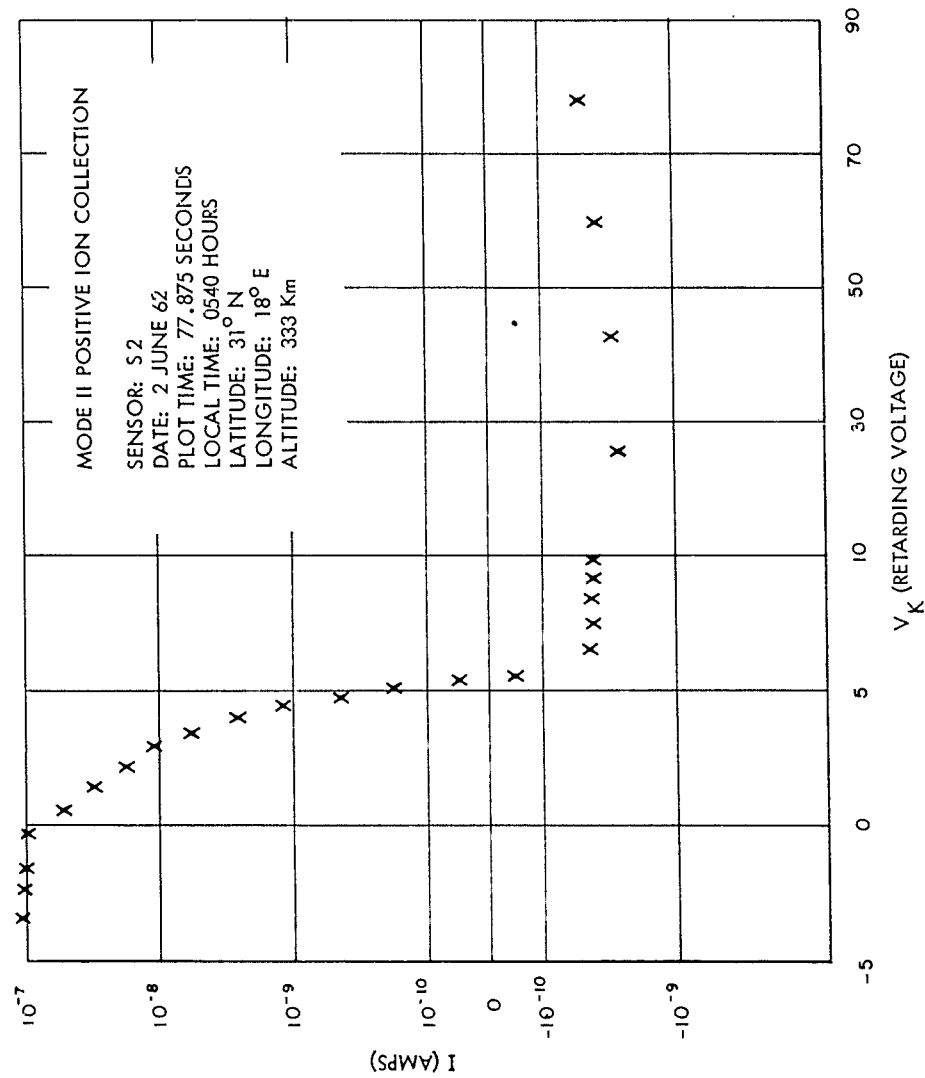


Figure 6.8 Sample of Mode II measurement, 77.875 seconds.

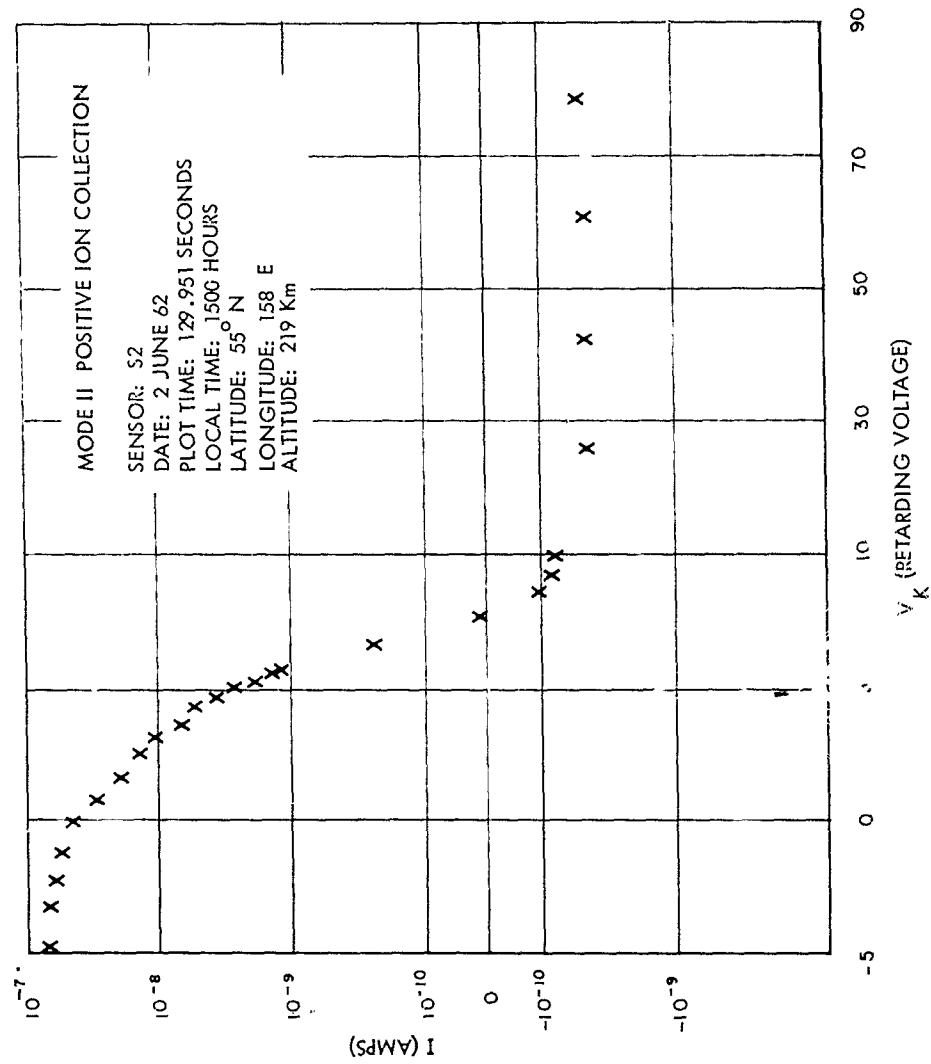


Figure 6.9 Sample of Mode II measurement, 129.951 seconds.

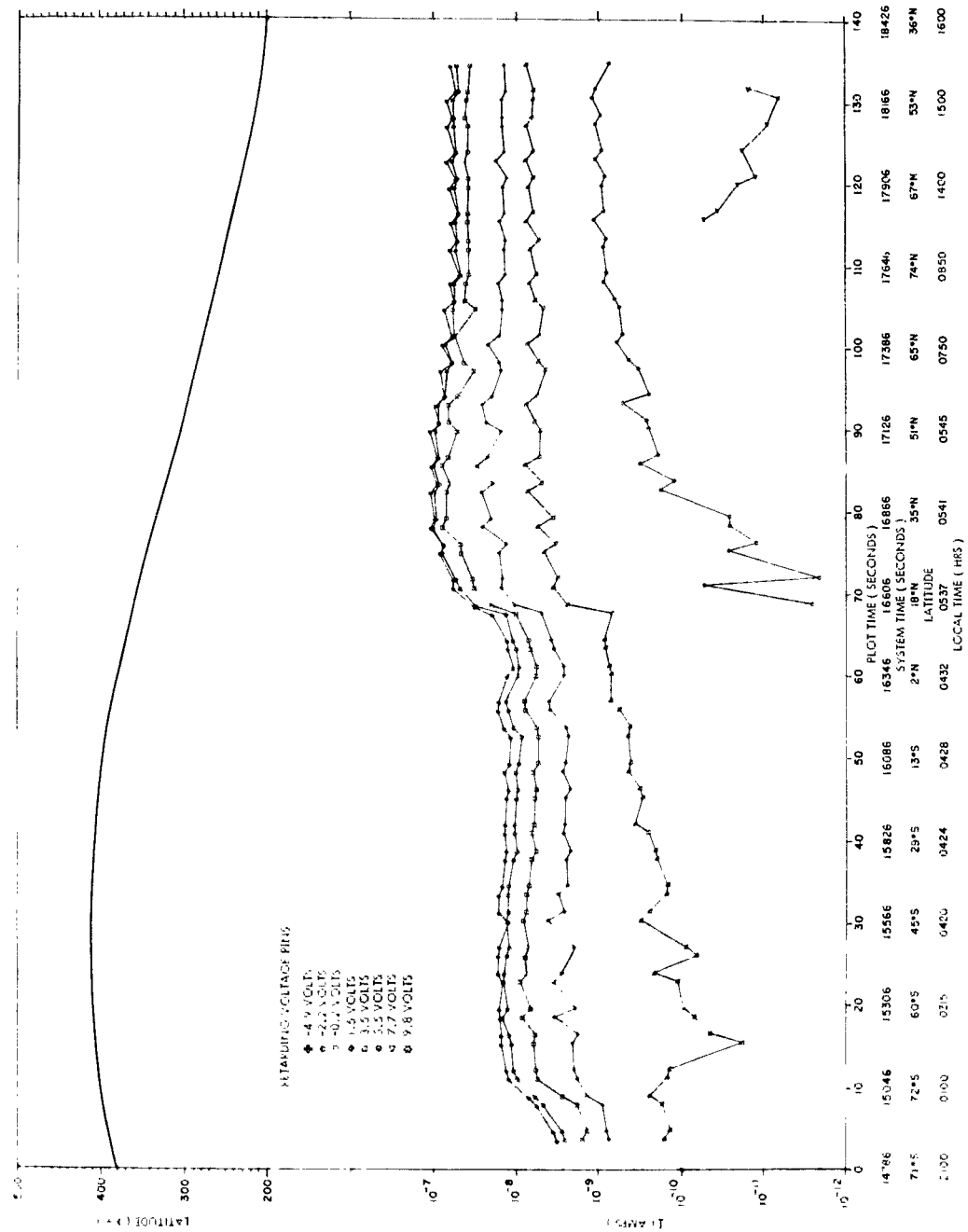


Figure 6.10 Total Mode II measurements.

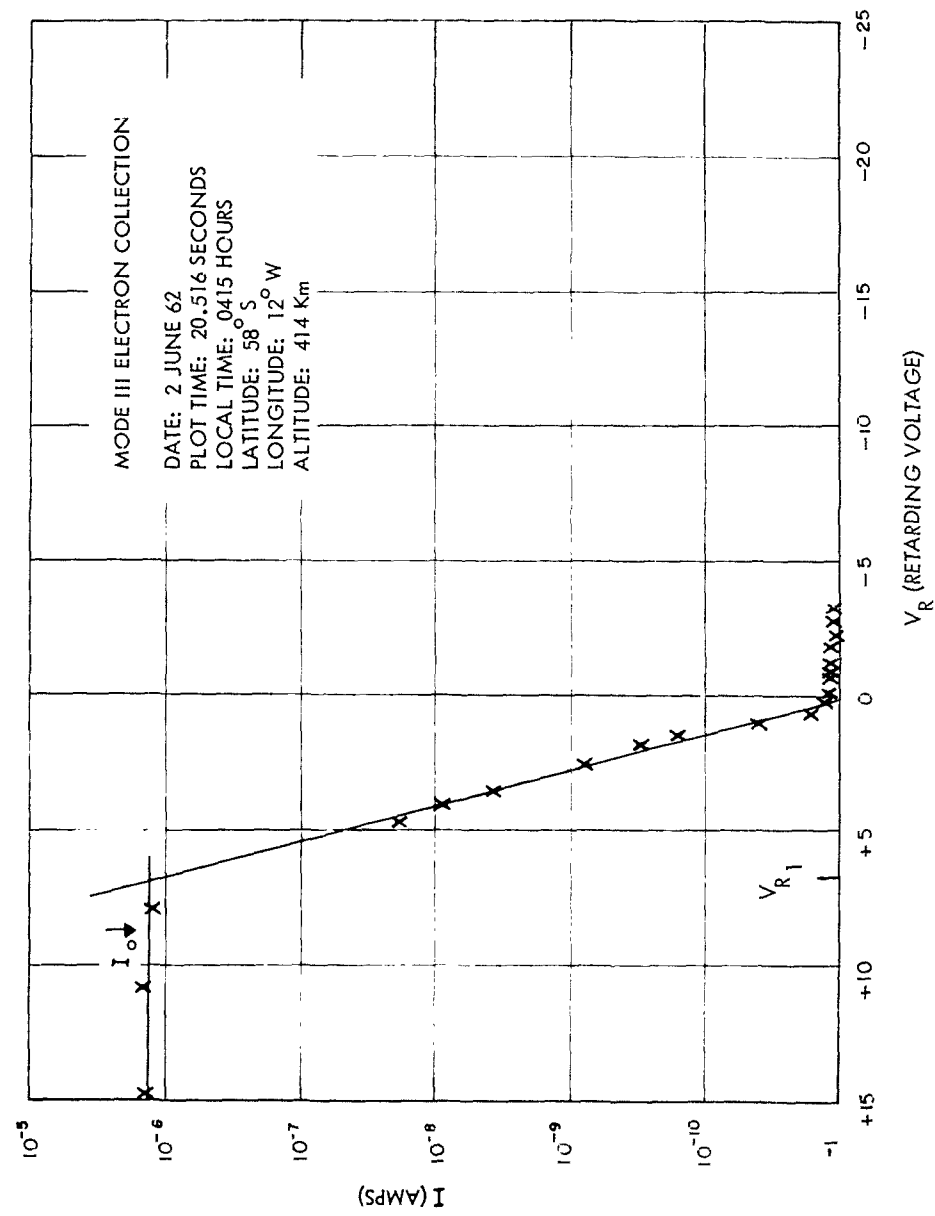


Figure 6.11 Sample of Mode III measurement, 20.516 seconds.

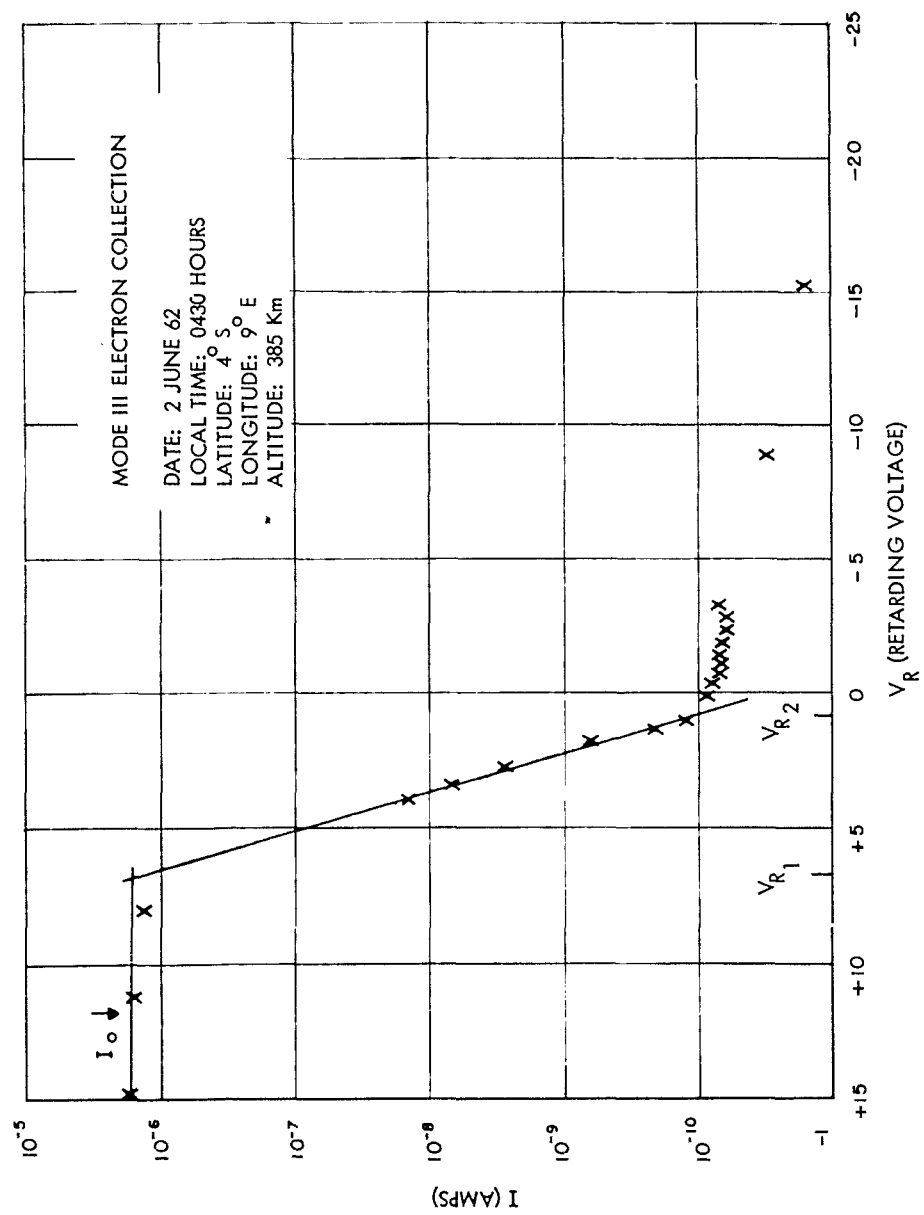


Figure 6.12 Sample of Mode III measurement, 0430 hours.

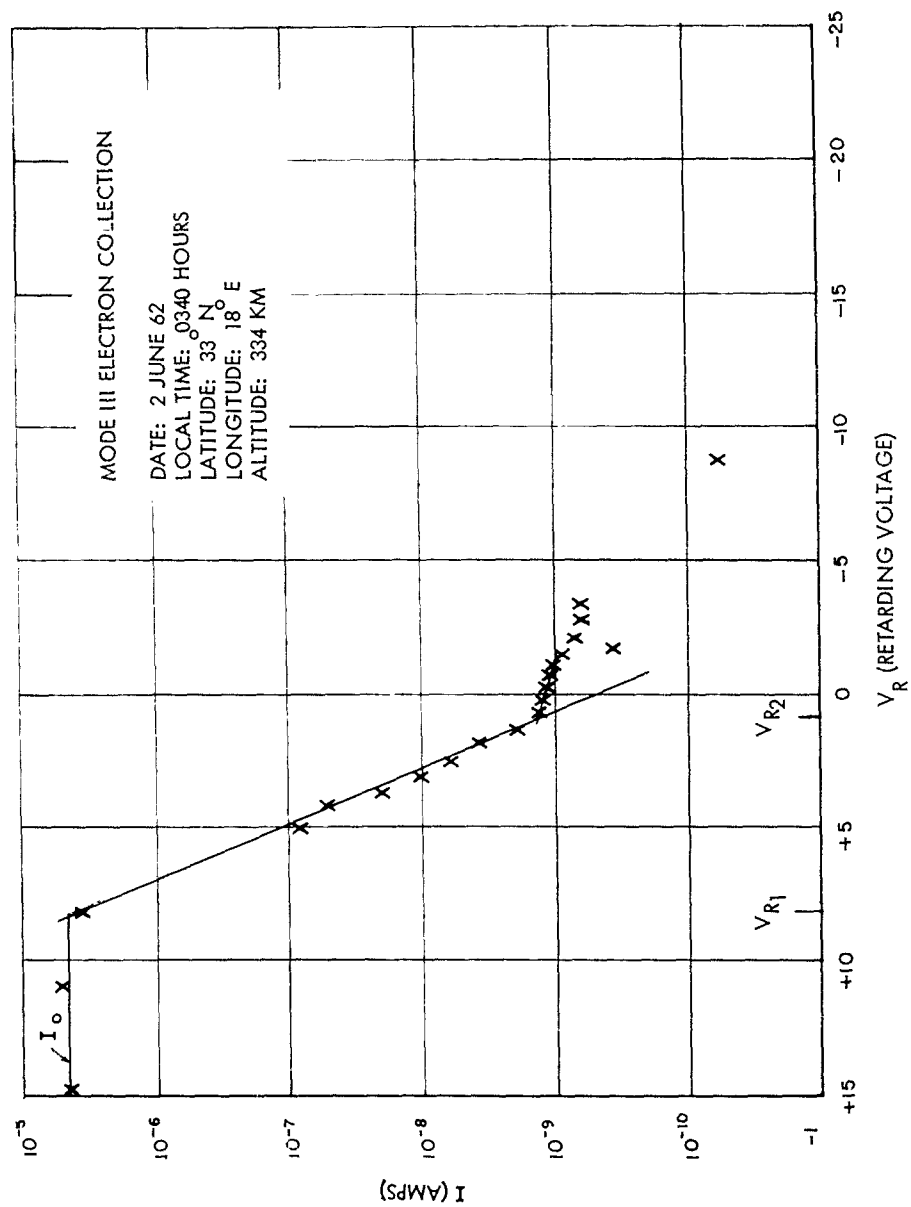


Figure 6.13 Sample of Mode III measurement, 0340 hours.



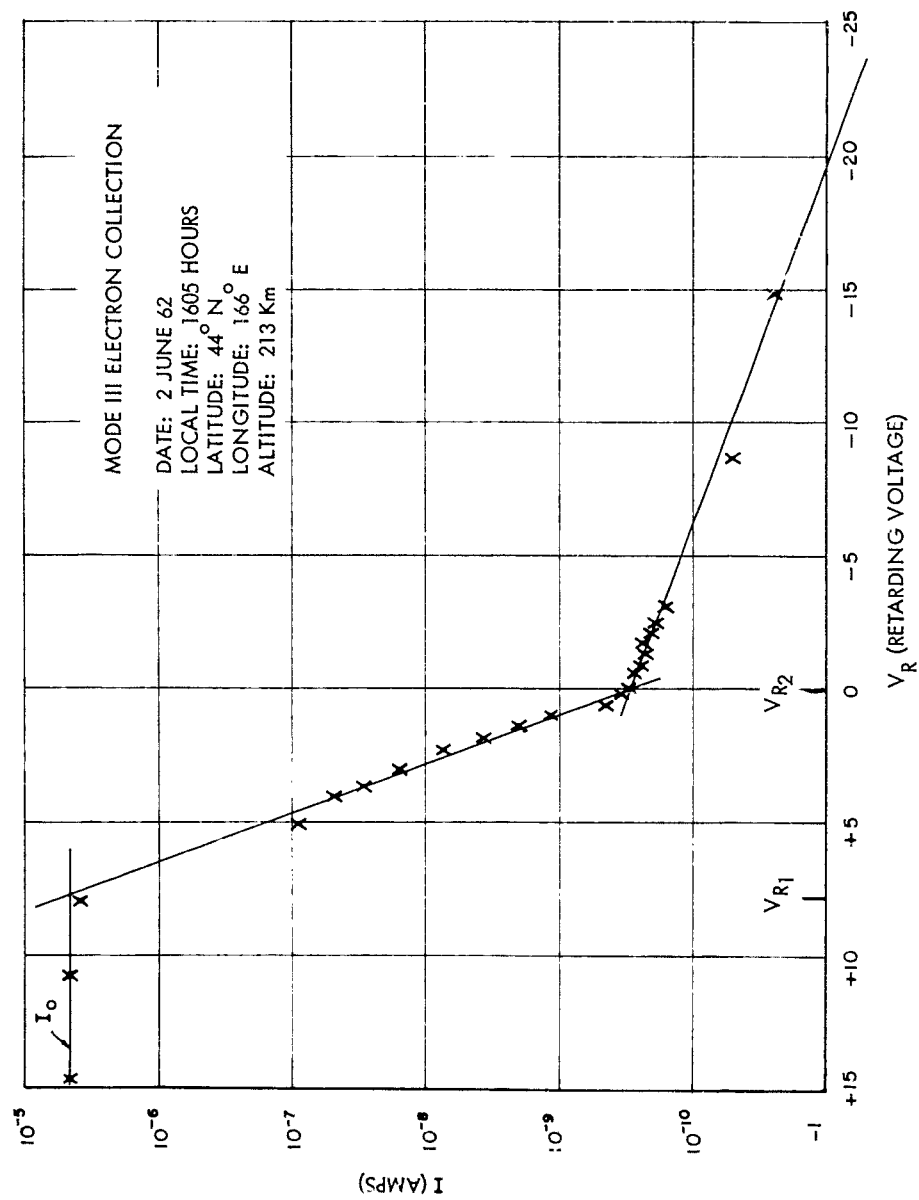


Figure 6.14 Sample of Mode III measurement, 1605 hours.

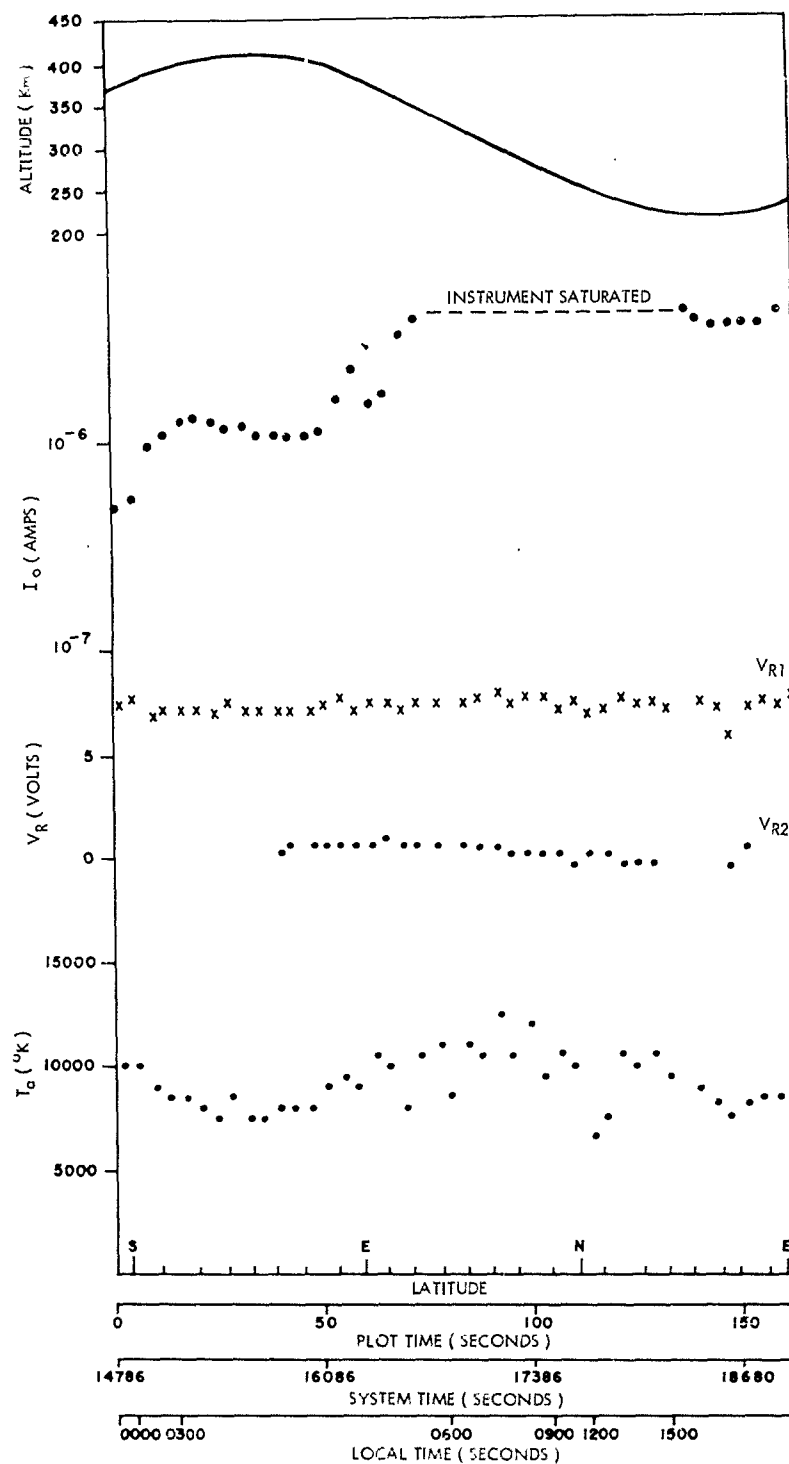


Figure 6.15 Total Mode III measurements.

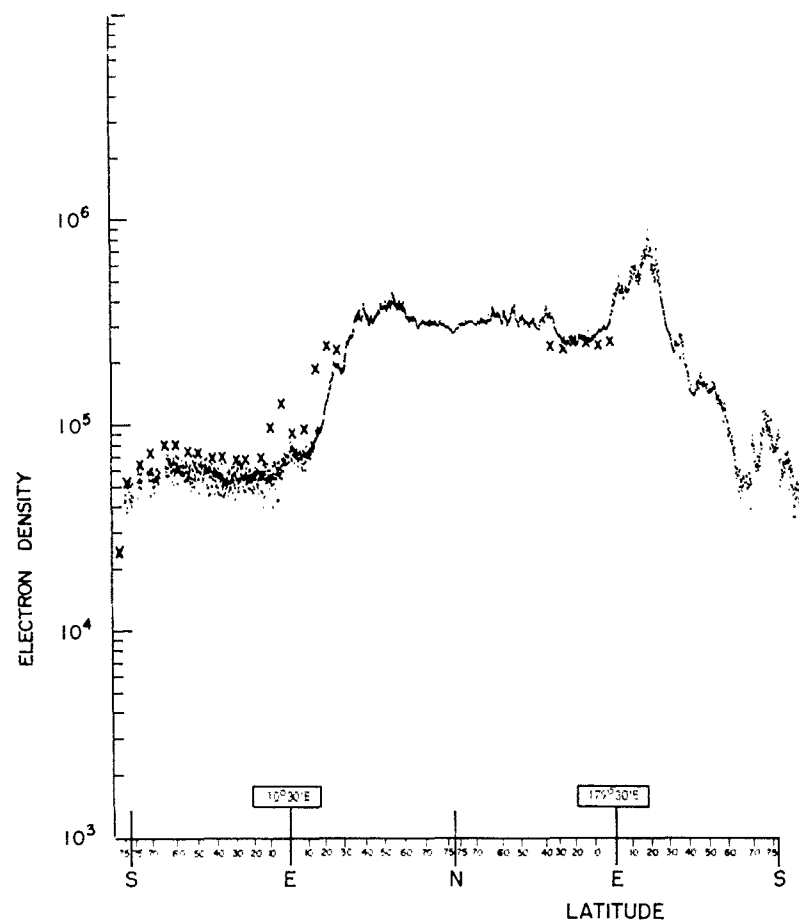


Figure 6.16 Comparison of retarding-potential analyzer and impedance probe data.

## CHAPTER 7

### SUMMARY AND CONCLUSIONS

The original objective of Project 6.12 was to investigate the spread of fission debris around the globe and its effects on ionization and radio noise. Because of the difficulties and schedule slippages encountered in attempting the nuclear detonation, this project was not able to obtain data during the time of primary interest. A secondary objective, however, the evaluation of the ambient ionospheric environment, was successfully carried out by all experiments on board. Although all experiments did not function perfectly on all vehicles, useful and valuable information was nevertheless obtained from each of the instrumented satellites.

Had a nuclear detonation occurred during the active life time of these payloads, the primary objective would have been obtained. The analysis of the data obtained has enabled the experimenters to evaluate the performance of their particular sensor.

This analysis will be extremely valuable in the design of satellite payloads flown in conjunction with future nuclear test programs. Numerous problems were encountered in attempting to schedule these piggy-back research modules to be in orbit during a nuclear detonation on satellite vehicles which had another prime mission. The two major problems were the inability of the experimenter to control both the satellite

launch dates and orbits. If in future tests scheduled events are more closely met, piggyback flights of this nature can accomplish their primary objective. However, a more desirable method to accomplish these satellite missions would be to have the satellite under the direct control of the Defense Atomic Support Agency (DASA). In this manner the launch dates and orbits could be selected to satisfy the requirements of the DASA mission.

Appendix A  
ENGINEERING CHANGE PROPOSAL TO INCORPORATE "N"  
PAYLOADS INTO DISCOVERER SYSTEM

18 January 1962

In reply refer to:  
LWSC/A003162  
D/62-62

Subject: Contract AF 04(647)-673  
ECP-LH-673-15  
Discoverer GRL "N" Detector Payload

To: AFSSD (SS7DK)  
Attn: Mr. E. Pauley  
Air Force Unit Post Office  
Los Angeles 45, California

Thru: Air Force Plant Representative  
Lockheed Missiles & Space Company  
Sunnyvale, California

Enclosure: (a) Seven (7) copies of ECP-LH-673-  
Discoverer GRL "N" Detector Payload

1. Enclosure (a) is transmitted herewith for review, recommendation and necessary follow-up action.

2. The Contractor requires a complete go ahead by 24 January 1962 in order to accommodate special payloads from the Geophysics Research Directorate and the associated support for the three (3) FTV's requested, i.e. FTV 1127 thru FTV 1129. Should additional information or clarification be required, the Contractor will be pleased to provide an oral presentation.

LOCKHEED MISSILES & SPACE COMPANY

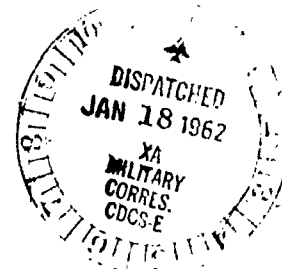
*J. A. Devine*  
J. A. Devine, Manager  
Space Systems Contracts

GAD:HL:bw

cc: AFSSD (SS7D)  
Attn: Col. Battle

AFSSD (SS7D)  
Attn: Capt. A. W. Johnson

Air Force Plant Representative  
Sunnyvale, California



SECRET

WS-1171

# ENGINEERING CHANGE PROPOSAL

1	ECP NUMBER <b>W-673-15</b>	DATE <b>1-12-62</b>	CONTRACT NUMBER <b>AF 04(647)-673</b>	ARTICLE IN PRODUCTION <input checked="" type="checkbox"/> YES <input type="checkbox"/> NO	PRIORITY <b>A</b>
2	TITLE OF CHANGE <b>Discoverer ORD "N" Detector Payload</b>				
3	NATURE OF CHANGE (INCLUDES DESCRIPTION, OR BY EXHIBIT) Reference (A) ECP-LM-673-2 dated 10-18-61 and approved by Amendment #24 The Contractor recommends that the Discoverer Statement of Work, AFM Exhibit 60-6 be supplemented to conduct orbital ORD "N" Detector Tests for a maximum orbital active period of twenty four (24) days on three (3) of thirteen (13) Flight Test Vehicles included by Amendment No. 24. The three (3) recommended Flight Test Vehicles are FTV 1127, FTV 1128 and FTV 1129. The research program will be conducted in accordance with the new work statement paragraphs below and in accordance with ECP-LM-673-2 dated 10-18-61 and approved by Amendment #24. The significant change is to provide extended orbital research tests after Discoverer primary objectives have been accomplished. The program requires a go-ahead prior to 24 Jan. 1962 to assure sufficient time to procure the necessary hardware, design and fabricate the research module, fit and checkout commensurate with FTV 1127 and to install the ground stations in support of the three (3) flights. (continued on Page 2)				
4	REASON FOR CHANGE (INCLUDES EXPLANATION OF ITEMS CHECKED BELOW, OR BY EXHIBIT) Reference (A) ECP-LM-673-2 dated 10-18-61 and approved by Amend.#24 The Contractor recommends that reference (A) ECP be supplemented to provide the system capabilities for a twenty four (24) day active orbit research module life to support the Geophysics Research Directorate "N" Detector Research Payload on three (3) Discoverer FTV's. The additional ground station command and control equipments are included herein and will also be utilized to support the Solar Collector Experiment and the Subsatellite Research efforts proposed on latter FTV's.				
5	ESTIMATED COST OF PROPOSAL (FOR PURPOSES OF FUND ALLOCATION) <b>\$158,000 GFFB Budgetary</b>				
6	ITEMS AFFECTED BY CHANGE (CHECK APPROPRIATE BOX)				
	<input type="checkbox"/> SAFETY	<input type="checkbox"/> PERFORMANCE	<input checked="" type="checkbox"/> SUBSYSTEMS		
	<input type="checkbox"/> SERVICE LIFE	<input type="checkbox"/> TOOLS AND EQUIPMENT	<input checked="" type="checkbox"/> A	<input type="checkbox"/>	
	<input type="checkbox"/> GSE	<input checked="" type="checkbox"/> SPARES	<input type="checkbox"/> B	<input type="checkbox"/> C	
	<input type="checkbox"/> INTERCHANGEABILITY	<input checked="" type="checkbox"/> TEST	<input checked="" type="checkbox"/> C	<input type="checkbox"/> H	
	<input type="checkbox"/> FIXED ASSETS AND FACILITIES	<input checked="" type="checkbox"/> GFP	<input type="checkbox"/> D	<input type="checkbox"/> L	
	<input checked="" type="checkbox"/> WEIGHT AND BALANCE OR CONTRACT WEIGHT		<input type="checkbox"/> E	<input checked="" type="checkbox"/> OTHER	<b>62-62</b>
7	ESTIMATED EFFECTIVITY CHANGE POINT <b>Three (3) Discoverer vehicles - FTV 1127 thru FTV 1129</b>				
8	DOES CONTRACTOR RECOMMEND THAT CHANGE BE MADE RETROACTIVE ON ARTICLES DELIVERED TO PROCURING AGENCY? <input type="checkbox"/> YES <input type="checkbox"/> NO				
SYSTEM/ORGANIZATION MANAGER <b>A.P. Murdaly</b>		DATE <b>1/18/62</b>	TECHNICAL CONTRACTS <b>A.P. Murdaly</b>	MILITARY CONTRACTS <b>J.C. Devine 1/19/62</b>	

FORM LMSC 170-1

SECRET

#### 4. Nature of Change (con't)

The program objective is to make available an extended life (twenty four days) on the Discoverer Agena vehicle for special payloads that the Geophysics Research Directorate will supply.

The following airborne equipments shall be furnished for each of three vehicles.

ITEM NO.	EQUIPMENT	QTY
1	Command Receiver and Decoder	1
*2	Tape Recorder/Reproducer	
	26:1 ratio	1
3	FM/PM T/M Link IV	1
*4	Commutator (0.1 x 60)	1
*5	Time Reference Generator	1
6	Antenna	1
*7	Power Programmer and Control	
	Box	1
8	Battery Type VI	2

The following ground station equipments will be required in each of three (3) stations.

ITEM NO.	EQUIPMENT	QTY
1	VHF Transmitter	1
2	Audio Coder	1
3	Antenna	1

The payload sensors recommended (furnished GFE) for two (2) flights consist of the following:

ITEM NO.	INSTRUMENTS	REQUIRED T/M POINT	WEIGHT (LBS)	POWER (WATTS)
1	Impedance Probe	6	6	2.5
2	Retarding Potential Analyzer	8	5	2.5
3	G.R.F. (Galactic Radio Frequency)	4	5	4.0
4	Ion Trap	12	6	6.0
5	Beta-Gamma Detector	20	13	3.0
	Total	50	35	18.0

The research payload for one (1) flight will consist of equipments to be determined at a later date and supplied as GFE items.

\* These items have been approved and are within scope of Amendment #24 to the -673 Contract.



RECOMMENDED MODIFICATION TO WORK STATEMENT

Add Paragraph 2.11.1.1 ( )

Analysis and Design: The Contractor will perform all the necessary design to integrate a GRD "NN" Detector Payload (furnished GFE) into each of three (3) Discoverer Agena B aft equipment racks, and the installation of the new ground support equipments to support these flights. This design and analysis effort will include the following:

1. On the Vehicle:
  - a. Antenna design and installation
  - b. Command Receiver and Decoder System
  - c. FM/FM Telemeter System
  - d. Power and Programmer System
2. Ground Stations:
  - a. Antenna requirements
  - b. Transmitter and Coder requirements
3. Operational Planning for the conduct of extended orbital life (approximately 24 days activity)

Add Paragraph 2.11.1.2 ( )

Test: The Contractor will direct, coordinate and conduct development and inspection testing of research instrumentation - GRD "NN" Detector Experiment (furnished GFE), Antenna System, Command Receiver and Decoder System, Telemetry System and associated hardware.

Add Paragraph 2.11.2.1 ( )

Fabrication and Assembly: The Contractor will provide the material, procurement, fabrication and assembly of sufficient sets of the following to support three (3) Flight Test Vehicles.

- A. Research Payload - GRD "NN" Detector Experiment Mod. Kit
  1. Command Receiver and Decoder
  2. FM/FM Telemeter Link #4 System
  3. Antenna
  4. Power Supply for 24 days active life

In addition, the Contractor will provide the material, procurement, fabrication, assembly and installation of three (3) ground tracking transmitter systems compatible with the airborne equipments included herein.

### System Description

#### General

The extended life system will consist basically of a tape recorder/telemeter system controlled by a command system. A system block diagram is shown in Figure 1. This system will be passive until after ejection of the recovery capsule, at which time the command receiver is activated. Normal operation of the extended life system is then instituted upon receiving a single momentary ground command signal. The equipments aboard the vehicle are programmed to minimize usage of battery power, thereby extending system life to twenty four (24) days.

#### Typical Orbit Operation

As the vehicle is approaching a tracking station, a ground command transmitter will be used to transmit a single command. The command receiver in the vehicle energizes the telemeter transmitter in an unmodulated mode. The CW signal will persist for approximately two minutes in order to accomplish the dual function of serving as an acquisition beacon and waiting until well within good transmission range before data is transmitted. Upon acquiring of the CW signal, the ground command system may be turned off. After the two minute delay, readout of tape recorded data will be initiated. After readout is accomplished, the telemeter system will shut down and the tape recorder will return to a readin mode until the system is again commanded on.

#### Tracking Station

Figure 2 shows the requirements of a ground tracking station and installation of three (3) such command transmitter system will be provided specifically at VAFB, Hawaii and New Boston.

#### Schedule

The schedule of GRD "N" Detector Payload for FTV 1127 is shown in Figure 3. Using the schedule of FTV 1127 as a base, FTV 1128 follows by (8) calendar days and 1129 follows by (9) calendar days.

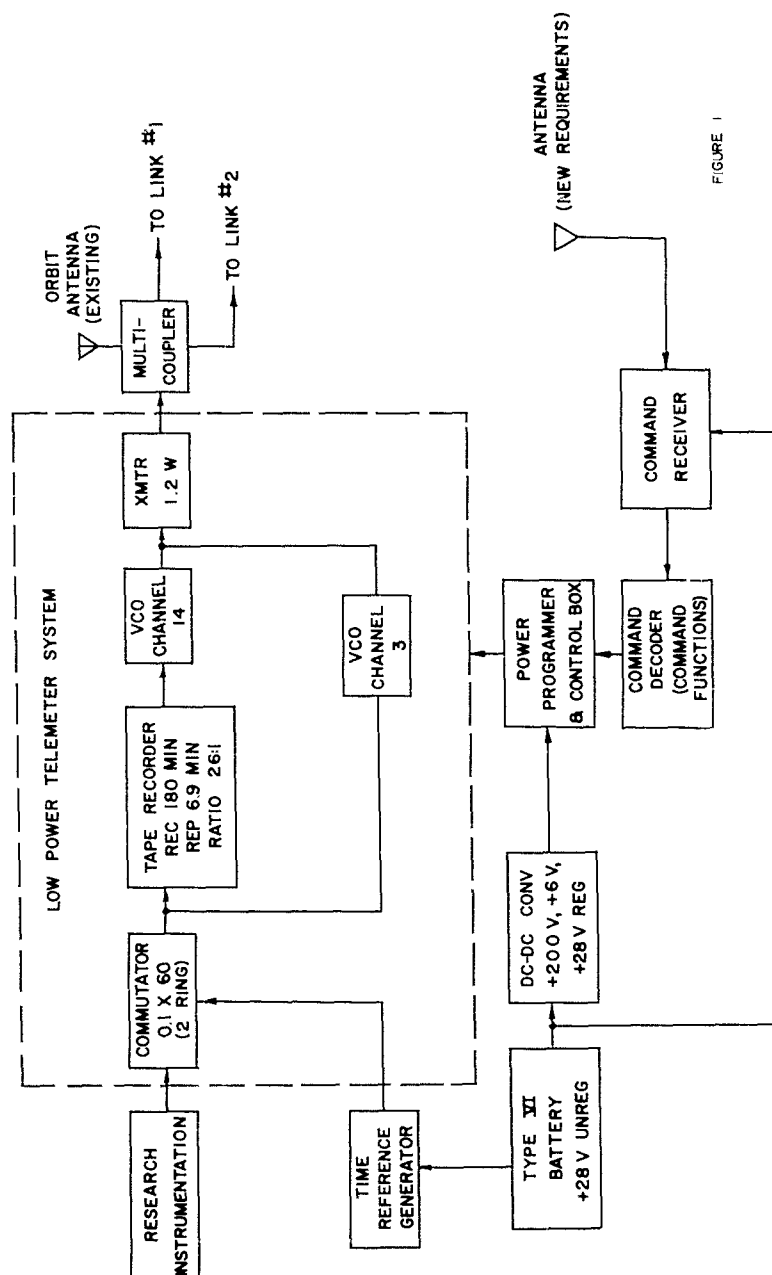


FIGURE 1



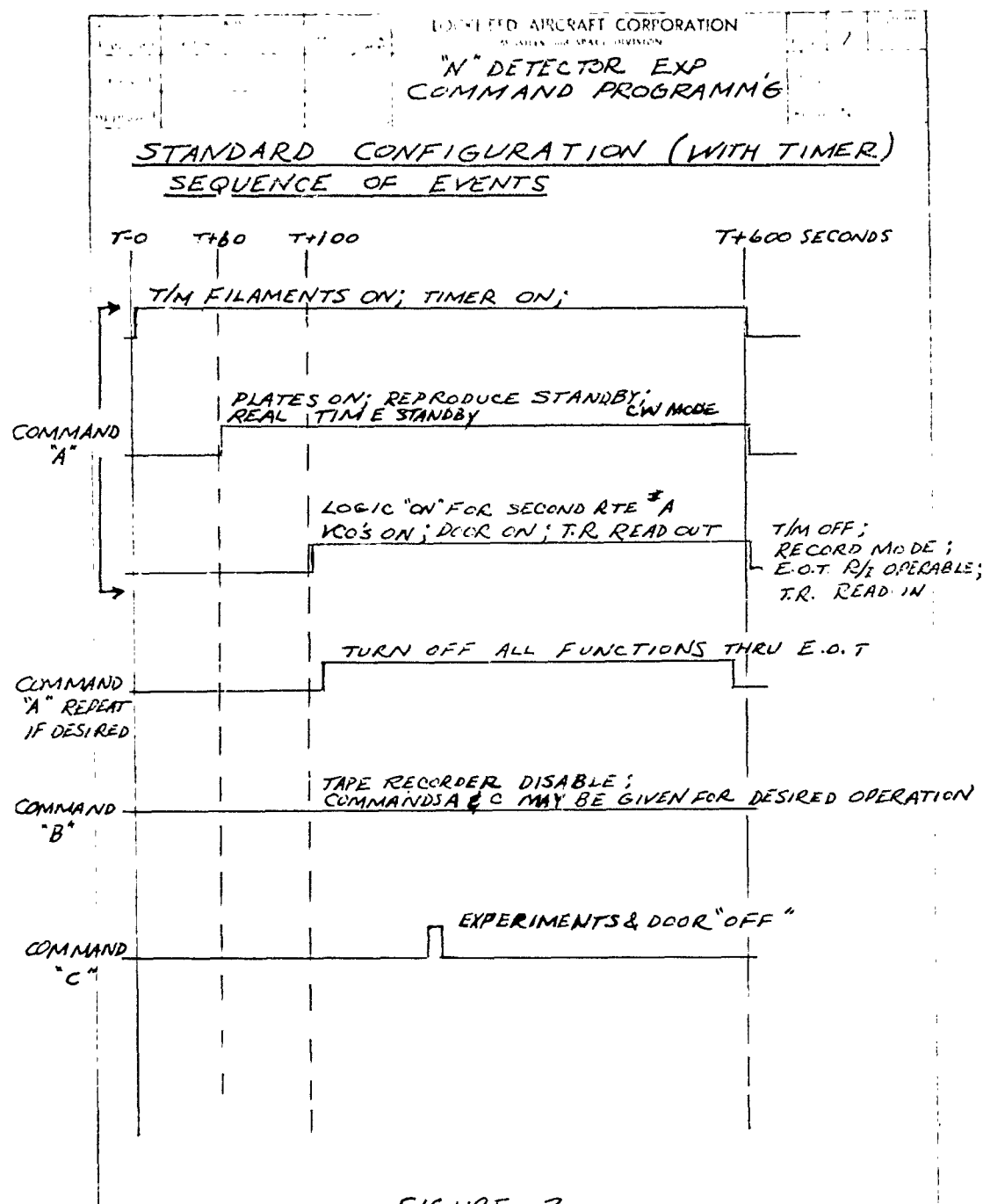
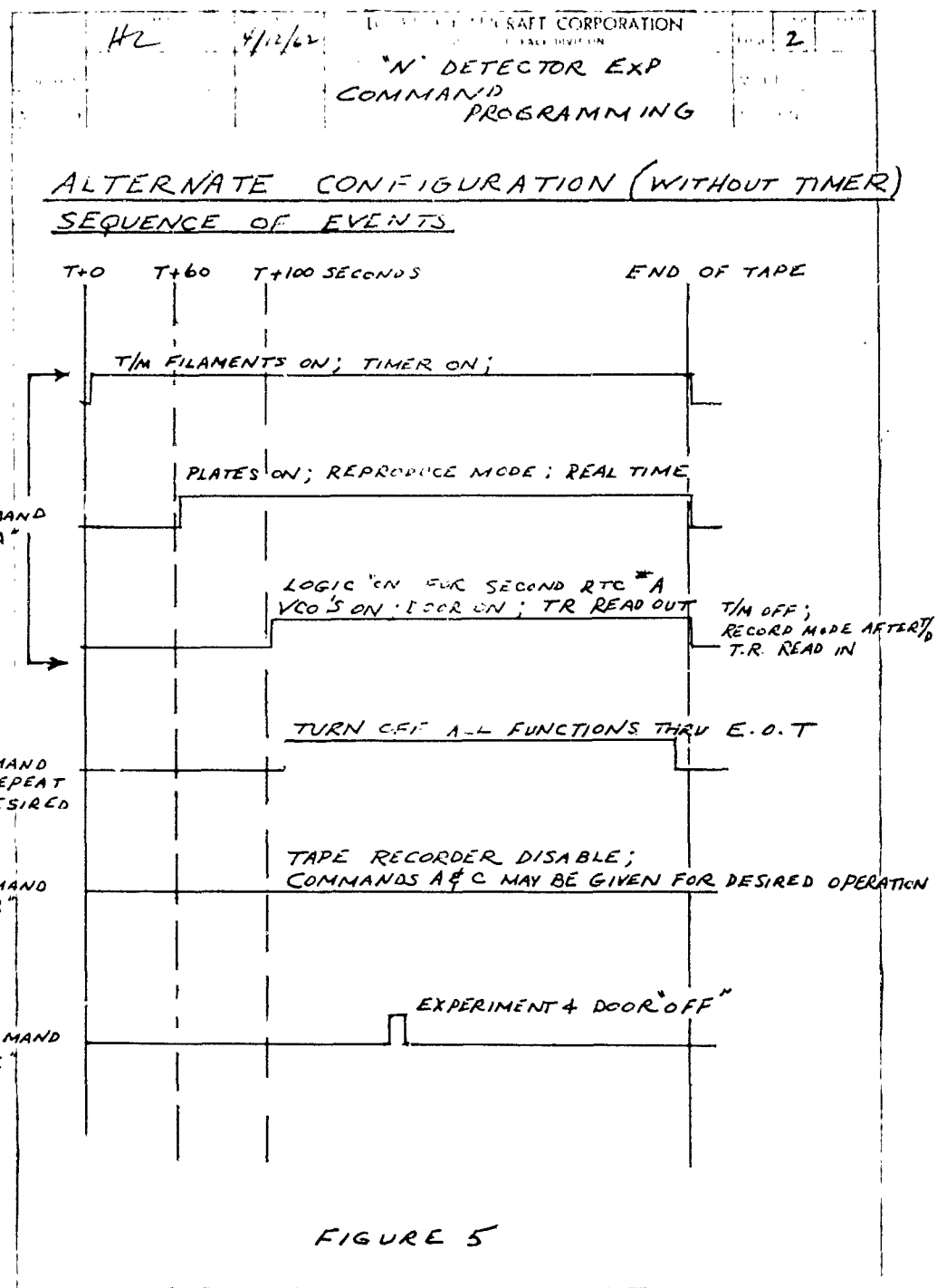


FIGURE 3



Appendix B


CHECKOUT TEST PROCEDURES


REVISIONS			
SYM	DESCRIPTION	DATE	APPROVAL
"A"	Revised paragraphs 3.8.4.2, 4.2.2, 4.2.4, 4.3.5, 4.3.6, 4.3.7, 4.3.10, 4.5.3, 4.5.6, 4.3.8, 4.3.9, 4.3.13. Deleted paragraphs 4.4 and 4.5.7.7	4/24/62	JFP


S337655	6205
NEXT ASSY	USED ON
APPLICATION	

DATE 3/7/62	TEST PROCEDURE	 <p>LOCKHEED AIRCRAFT CORPORATION MISSILES and SPACE DIVISION SUNNYVALE, CALIFORNIA</p>
DR C. F. Wright	(Approval Sheet)	
CHK BY J. W. Brown	GRD DOOR	
ENGRS R. J. Guyote	MODULE 116	
ENGRS H. M. Rapstad	TEST	
ENGRS J. Talley	(6205) 1127 & Up	
APPROVED	SCALE	
	NONE	
	424178	S414126
		CODE 06887

<b>TITLE</b> GRD DOOR MODULE 116 TEST	 LOCKHEED MISSILES & SPACE COMPANY <small>A LOCKHEED COMPANY</small>	<b>TEST PROCEDURE</b> 5411126 <b>SHEET 2 OF 17 SHEETS</b>
<p>1.0 SCOPE - This Procedure details the checkout of GRD Module 116.</p> <p>2.0 APPLICABLE DOCUMENTS -</p> <p>Drawing 1414126 - Specification GRD Module 116          Drawing 1342931 - Wiring Diagram, Module 116          Drawing 1342572 - Instrumentation Schedule, Link II, Vehicle 1127</p> <p>3.0 REQUIREMENTS</p> <p>3.1 <u>Equipment</u></p> <p>DRP Master Control          "I" Detector Test Cables - SP2103, SP2106, SP2107, SP2108          "N" Detector Magnetometer Simulator - SP2104          Command Receiver and Decoder Simulator - SP2148          C.E.C. Recorder or Equivalent</p> <p>3.2 <u>Power</u></p> <p>Equipment - 110V AC 60 CPS          Test Specimen - +28V DC</p> <p>3.3 <u>Environmental</u></p> <p>This procedure may be used under standard test area conditions.</p> <p>3.4 <u>Special Personnel</u> - NONE</p> <p>3.5 <u>Safety</u></p> <p>Normal safety precautions shall be observed to prevent damage to test specimen and equipment or hazard to personnel.</p> <p>3.6 <u>Controlled Functional Equipment</u> -</p> <p>During this test a record of the running time or the number of cycles of each Limited Life Item shall be maintained as per conditions and instructions listed in drawings and/or Controlled Functional Equipment List. The Serial Numbers of the Limited Life Items shall be entered and "START" and "STOP" Times for each entered item shall be indicated as explained on the Operation Record. When the limitation factor is specified as maximum cycles, and "X" shall be placed in the appropriate column for each cycle.</p> <p>"A" Rev. 4/24/62</p>		



<b>TITLE</b>  GRD DCR MODULE 116 TEST	 LOCKHEED MISSILES & SPACE COMPANY <small>A LOCKHEED COMPANY</small>	<b>TEST PROCEDURE</b> 5444126  SHEET 3 OF 17 SHEETS
---	---	--

Check List

3.0 REQUIREMENTS (continued)

3.6 (continued)

At the conclusion of the tests, the run times and/or cycles shall be totaled for each item listed and entered in the appropriate Operation Record.

3.7 Calibration

Check the calibration stickers of the test equipment to verify that the calibration is current.

3.8 Special

3.8.1 Patch Panel Program - Make the following patches on the DRP Master Control Patch Panel:

J1 PATCHES						
			PATCH	TO	PATCH	
X236	TEC-1 SIG	J1-A	Z-1		J-17	Jack 51
X237	TEC-2 SIG	J1-B	Z-2		J-18	Jack 52
X196	CLOCK TEMP	J1-C	Z-3		J-29	Jack 63
X262	RPA-8	J1-D	Z-4		H-33	Jack 33
X263	RPA-9	J1-E	Z-5		H-34	Jack 34
X264	RPA-10	J1-F	Z-6		H-35	Jack 35
	BOOM MON.	J1-G	Z-7		J-33	Jack 67
X248	GRF TEMP (L)	J1-H	Z-8		H-16	Jack 16
J15J1	+28 SQUIP	J1-J	Z-9		L-13	Jack 115
J15J1	+28 SQUIP	J1-K	Z-10		L-14	Jack 116
J15J1	RET SQUIP	J1-L	Z-11		L-15	Jack 122
J15J1	RET SQUIP	J1-M	Z-12		L-21	Jack 123
J15J2	+28 SQUIP	J1-N	Z-13		L-15	Jack 117
J15J2	+28 SQUIP	J1-P	Z-14		L-16	Jack 118
J15J2	RET SQUIP	J1-R	Z-15		L-22	Jack 124
J15J2	RET SQUIP	J1-S	Z-16		L-23	Jack 125
J16J1	+28 SQUIP	J1-T	Z-17		L-17	Jack 119
J16J1	+28 SQUIP	J1-U	Z-18		L-25	Jack 127
J16J1	RET SQUIP	J1-V	Z-19		L-24	Jack 126
J16J1	RET SQUIP	J1-W	Z-20		L-32	Jack 134
J16J2	+28 SQUIP	J1-X	Z-21		L-26	Jack 128
J16J2	+28 SQUIP	J1-Y	Z-22		L-27	Jack 129


"A" Rev. 4/24/66



TITLE		LOCKHEED		TEST PROCEDURE	
GUN DOOR MAINTENANCE TEST		LOCKHEED MISSILES & SPACE COMPANY		0411176	
				SHEETS 5 OF 17 SHEETS	
3.0 REQUIREMENTS (continued)					
3.8 <u>Special</u> (continued)					
3.8.1 (continued)					
J2 PATCHES (continued)					
	PATCH	TO	PATCH		
SQUIB PWR SHIELD	J2-d	W-18	A-12	DC RET	
ADAPT. SER. CTR.	J2-e	V-19	A-17	+28V (SW-12)	
RET. SQUIB PWR	J2-f	X-19	B-6	DC RET	
SQUIB PWR (+28V)	J2-g	W-20	B-11	+28V (SW-5)	
RET. SQUIB PWR	J2-h	V-21	A-6	DC RET	
SQUIB PWR +28V	J2-j	W-22	A-11	+28V (SW-5)	
LOCKOUT SWITCH	J2-k	V-23	W-24	LOCKOUT SWITCH (J2-n)	
SQUIB PWR SHIELD	J2-p	V-25	C-6	DC RET	
J3 PATCHES					
	PATCH	TO	PATCH		
J3-y	S-23	H-14	Jack 14	X238 GRF (4.01)	
J3-TE	Q-27	H-15	Jack 15	X240 GRF (4.01)	
J3-TE	I-26	H-17	Jack 17	X239 GRF (6.9)	
J3-H	S-15	H-18	Jack 18	X247 GRF (6.9)	
J3-H	Q-7	H-19	Jack 19	X109 IMP PROBE	
J3-P	S-7	H-20	Jack 20	X110 IMP PROBE	
J3-E	R-8	H-21	Jack 21	X111 IMP PROBE	
J3-S	T-5	H-22	Jack 22	X112 IMP PROBE	
J3-T	Q-9	H-23	Jack 23	X113 IMP PROBE	
J3-U	S-9	H-24	Jack 24	X114 IMP PROBE	
J3-V	R-10	H-25	Jack 25	X115 IMP PROBE	
J3-E	Q-3	H-26	Jack 26	X251 R.P.A.	
J3-F	S-3	H-27	Jack 27	X252 R.P.A.	
J3-G	R-4	H-28	Jack 28	X253 R.P.A.	
J3-I	I-4	H-29	Jack 29	X254 R.P.A.	
J3-J	Q-5	H-30	Jack 30	X255 R.P.A.	
J3-K	S-5	H-31	Jack 31	X256 R.P.A.	
J3-L	R-6	H-32	Jack 32	X261 R.P.A.	
J3-n	R-16	J-2	Jack 36	X221 Beta-Gamma Detector	
J3-I	I-16	J-3	Jack 37	X222 B-G D	
J3-S	I-20	J-4	Jack 38	X223 B-G D	
J3-J	Q-17	J-5	Jack 39	X224 B-G D	
J3-t	Q-21	J-6	Jack 40	X225 B-G D	
J3-k	S-17	J-7	Jack 41	X226 B-G D	
J3-u	S-21	J-8	Jack 42	X227 B-G D	
J3-n	R-18	J-9	Jack 43	X228 B-G D	

"A" Rev. 4/24/62

TITLE	LOCKHEED MISSILES & SPACE COMPANY A DIVISION OF LOCKHEED CORP.	TEST PROCEDURE 9411126 SHEET 6 OF 13 SHEETS
3.0 REQUIREMENTS (continued)		
3.8 <u>Special</u> (continued)		
3.8.1 (continued)		
J3 PATCHES (continued)		
PATCH	TO	PATCH
J3-n	T-18	J-10 Jack 44 X229 B-G D
J3-p	Q-19	J-11 Jack 45 X230 B-G D
J3-q	S-19	J-12 Jack 46 X231 B-G D
J3-v	R-22	J-13 Jack 47 X232 B-G D
J3-w	T-22	J-14 Jack 48 X233 B-G D
J3-r	R-20	J-15 Jack 49 X234 B-G D
J3-x	Q-23	J-16 Jack 50 X235 B-G D
J3-A	Q-1	J-19 Jack 53 X241 ION TRAP
J3-B	S-1	J-20 Jack 54 X242 ION TRAP
J3-C	R-2	J-21 Jack 55 X243 ION TRAP
J3-a	T-12	J-22 Jack 56 X244 ION TRAP
J3-D	T-2	J-23 Jack 57 X245 ION TRAP
J3-M	T-6	J-24 Jack 58 X246 ION TRAP
J3-W	T-10	J-25 Jack 59 X192 CLOCK
J3-X	Q-11	J-26 Jack 60 X193 CLOCK
J3-Y	S-11	J-27 Jack 61 X194 CLOCK
J3-Z	R-12	J-28 Jack 62 X195 CLOCK
J3-a	R-24	J-30 Jack 64 X081 MAGNETOMETER
J3-AA	T-24	J-31 Jack 65 X082 MAGNETOMETER
J3-BE	Q-25	J-32 Jack 66 X083 MAGNETOMETER
J3-GC	S-25	J-34 Jack 68 +28V MON
J3-c	S-13	K-1 Jack 69 SYNC
J3-ED	R-26	K-2 Jack 70 CAL +
J3-b	C-13	K-3 Jack 71 CAL 1/2
J3-d	R-14	K-4 Jack 72 CAL 2
J4 PATCHES		
PATCH	TO	PATCH
J4-A	T-28	K-7 Jack 75 LINK 2 200V MON
J4-B	Q-29	K-11 Jack 79 LINK 2 OFF MON
J4-C	S-29	K-8 Jack 76 VEH. BATT. INPUT MON
J4-D	R-30	K-5 Jack 73 +28 REG MON (LINK 2)
J4-E	T-30	K-9 Jack 77 2 MIN TIMER COM. MON
J4-F	Q-31	K-10 Jack 78 10 MIN TIMER COM. MON
J4-G	S-31	K-13 Jack 81 SIG RET
J4-H	R-32	K-6 Jack 74 6.3V MON (LINK 2)
J4-J	T-32	K-12 Jack 80 DOOR OFF MON.
"A" Rev. 4/24/62		

<b>TITLE</b>  GRD DOOR MODULE 116 TEST	 LOCKHEED MISSILES & SPACE COMPANY	<b>TEST PROCEDURE</b> SH44126  SHEET 7 OF 17 SHEETS
--	---	--

3.0 REQUIREMENTS (continued)


3.8 Special (continued)

3.8.2 Test Jack Identification - The following is an identification of the DRP Mater Control Test Jacks for this test only:

Jack No.	Identification
1	+28V REG MONITOR (LINK 2)
2	200V MONITOR (LINK 2)
3	6.3V MONITOR (LINK 2)
4	+28V (SWITCHED) TO LINK 2
5	+28V RETURN TO LINK 2
6	+28V (SWITCHED) TO LINK 2
7	28V RETURN TO LINK 2
8	+28V BATT. TO LINK 2
9	+28V BATT. TO LINK 2
10	TIMER START TO LINK 2
11	NOT USED
12	NOT USED
13	NOT USED
14	X238 (4.01 MC GRF SIG NO. 1)
15	X240 (4.01 MC GRF SIG NO. 2)
16	X248 (4.01 MC GRF SIG NO. 3)
17	X239 (6.9 MC GRF SIG OUT)
18	X247 (6.9 MC GRF CAL MON)
19	X109 (IMP. PROBE SIG NO. 1)
20	X110 (IMP PROBE SIG NO. 2)
21	X111 (IMP PROBE SIG NO. 3)
22	X112 (IMP PROBE SIG NO. 4)
23	X113 (IMP PROBE SIG NO. 5)
24	X114 (IMP PROBE SIG NO. 6)
25	X145 (IMP PROBE TEMP)
26	X251 (RPA 1, VR)
27	X252 (RPA 2, VR 2)
28	X253 (RPA 3, ET 1)
29	X254 (RPA 4, EO 1)
30	X255 (RPA 5, ET 2)
31	X256 (RPA 6 EO 2)
32	X261 (RPA SYNC)
33	X262 (RPA ED)
34	X263 (RPA MONITOR 1)
35	X264 (RPA MONITOR 2)
36	X221 (R-3 DET OUTPUT NO. 1)

"A" REV. 4/24/66

TITLE	LOCKHEED MISSILES & SPACE COMPANY	TEST PROCEDURE
GRD DDM MODULE 110 TEST	LOCKHEED MISSILES & SPACE COMPANY	S411126
		SHEET 8 OF 17 SHEETS
3.0 REQUIREMENTS (continued)		
3.8 <u>Special</u> (continued)		
3.8.2 (continued)		
<u>Jack No.</u> 37 38 39 40 41 42 43 44 45 46 47 48 49 50 51 52 53 54 55 56 57 58 59 60 61 62 63 64 65 66 67 68 69 70 71 72 73	<u>Identification</u> X222 (R-G DET OUTPUT NO. 2) X223 (R-G DET OUTPUT NO. 3) X224 (R-G DET OUTPUT NO. 4) X225 (R-G DET OUTPUT NO. 5) X226 (R-G DET OUTPUT NO. 6) X227 (R-G DET OUTPUT NO. 7) X228 (R-G DET OUTPUT NO. 8) X229 (R-G DET OUTPUT NO. 9) X230 (R-G DET OUTPUT NO. 10) X231 (R-G DET OUTPUT NO. 11) X232 (R-G DET OUTPUT NO. 12) X233 (R-G DET OUTPUT NO. 13) X234 (R-G DET OUTPUT NO. 14) X235 (R-G DET OUTPUT NO. 15) X236 (TEC SIG NO. 1) X237 (TEC SIG NO. 2) X241 (ION TRAP AMP 1) X242 (ION TRAP AMP 2) X243 (ION TRAP BIAS 1) X244 (ION TRAP BIAS 2) X245 (ION TRAP SWEEP MON) X246 (ION TRAP O.P. MON) X192 (CLOCK SIG NO. 1) X193 (CLOCK SIG NO. 2) X194 (CLOCK SIG NO. 3) X195 (CLOCK SIG NO. 4) X196 (CLOCK TEMP) Y081 (MAGNETOMETER SIG NO. 1) X082 (MAGNETOMETER SIG NO. 2) X083 (MAGNETOMETER SIG NO. 3) BOOM MONITOR +28V MON (DOOR) SYNCH CAL + CAL 1/2 CAL Z LINK 2 +28V REG MON TO LINK 1	
"A" Rev. 4/24/62		

<b>TITLE</b> GRD DOOR MODULE 116 TEST	 LOCKHEED MISSILES & SPACE COMPANY <small>A SPACE &amp; MISSILE SYSTEMS COMPANY</small>	<b>TEST PROCEDURE</b> S111126 SHEET 9 OF 15 SHEETS
--	---	--

3.0 REQUIREMENTS (continued)

3.8 Special (continued)

3.8.2 (continued)

<u>Jack No.</u>	<u>Identification</u>
74	LINK 2 6.3V MON TO LINK 1
75	LINK 2 200V MON TO LINK 1
76	VEH BATT INPUT MON TO LINK 1
77	2 MIN TIMER COMM TO LINK 1
78	10 MIN TIMER COMM TO LINK 1
79	LINK 2 OFF MON TO LINK 1
80	DOOR OFF MON TO LINK 1
81	SIG RET

<u>Shielded Jack No.</u>	<u>Identification</u>
1	CHANNEL 8 OUTPUT
2	CHAN. EL 9 OUTPUT
3	CHANNEL 'E' OUTPUT
4	CHANNEL 'C' OUTPUT
16	RETURN


Check  
List

3.8.3 Squib Monitor Set-Up - Insert Fuse Holders with 1/10 to 1/5 AMP fuses between the following Test Jacks on the DRP Master Control:

- Between Jack 115 and Jack 122
- Between Jack 116 and Jack 123
- Between Jack 117 and Jack 124
- Between Jack 118 and Jack 125
- Between Jack 119 and Jack 126
- Between Jack 127 and Jack 134
- Between Jack 128 and Jack 135
- Between Jack 129 and Jack 136
- Between Jack 130 and Jack 137
- Between Jack 131 and Jack 138
- Between Jack 132 and Jack 139
- Between Jack 133 and Jack 140

"A" Rev. 4/24/62

<b>TITLE</b> GRD DOOR MODULE 116 TEST	 LOCKHEED MISSILES & SPACE COMPANY <small>A SPACE DIVISION OF LOCKHEED CORP.</small>	<b>TEST PROCEDURE</b> SH4126 SHEET 10 OF 17 SHEETS
--	---	--

Check List

3.0 REQUIREMENTS (continued)

3.8 Special (continued)

3.8.4 Test Set-Up

3.8.4.1 Connect the 'N' Detector Test Set-Up as shown in Figure 1.

NOTE: For this test, +28V DC is used on the following DRP Master Control Power inputs:

+28V REG, +28V UNREG, -28V, 2KC.

3.8.4.2 Label the following DRP Master Control Switches as shown:

SW3 - T/M DISABLE  
 SW5 - SQUIE POWER  
 SW12 - ADAPT. SEP.  
 SW18 - ORBIT MODE  
 SW20 - BRUSH 11  
 SW21 - BRUSH 12  
 SW22 - DOOR ON AND T/R READ-IN  
 SW23 - DOOR ON AND T/R READ-OUT  
 SW24 - BRUSH 5

3.8.4.2 Adjust the output of the +28V supply so that +28 ± 0.3V DC is measured at the DRP Master Control Power Input.

3.9 Test Data Recording -

All required data taken as a result of this test shall be recorded on the Appendix.

Verify that contractor Quality Assurance personnel are present and are adequately equipped to monitor all performance data generated during the accomplishment of this test procedure.

"A" Rev. 4/24/66



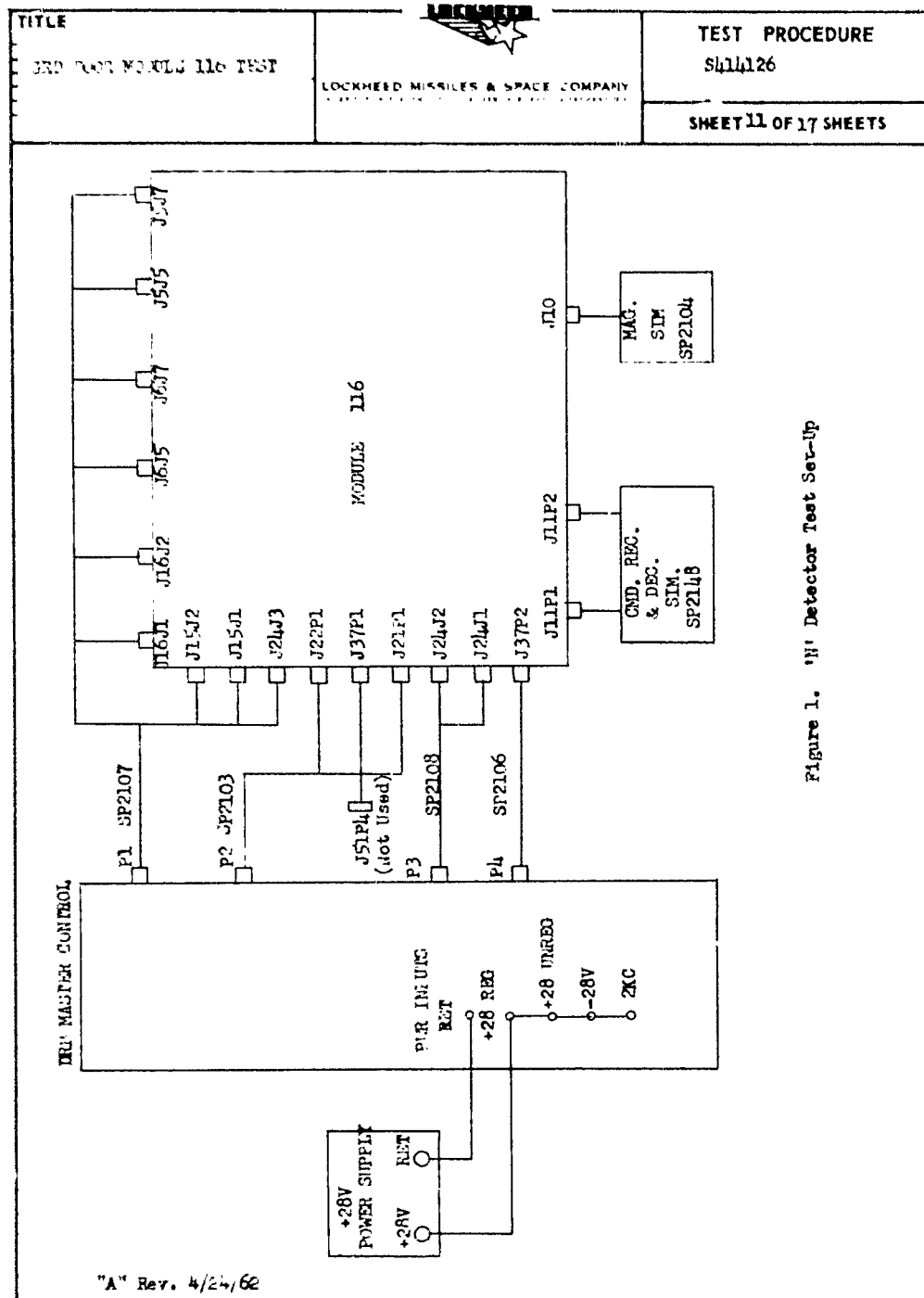



Figure 1. 'H' Detector Test Set-Up

TITLE		TEST PROCEDURE SH44126
GRD DOOR MODULE 116 TEST	LOCKHEED MISSILES & SPACE COMPANY	SHEET 12 OF 17 SHEETS
4.0 TEST		<u>Check List</u>
4.1 <u>Squib Firing Circuit Test</u>		
4.1.1	Position the following DRP Master Control Console Switches to "ON";  SW-1 (DOOR POWER) SW-5 (SQUIB POWER)	_____
4.1.2	Position SW-18 (ORBIT MODE) to "ON", and verify that all Squib Monitor fuses are blown. (Ref. Para. 3.8.3)	_____
4.1.3	Position Switches SW-5 and SW-18 to "OFF".	_____
4.2 <u>Adapter Separation Test</u>		
4.2.1	Position the following switches to "ON":  SW-1 (+28V ) SW-12 (Adapt. Sep.)	_____
4.2.2	Verify that +28V is not present at the following Module Harness Pin :  J12P1 - Pin A	_____
4.2.3	Position SW-12 to "OFF".	_____
4.2.4	Verify that +28V is present at the following Module Harness Pin :  J12P1 - Pin A	_____

"A" Rev. 4/24/62

<b>TITLE</b>  GRD DOOR MODULE 116 TEST	 LOCKHEED MISSILES & SPACE COMPANY <small>LOCKHEED MISSILES &amp; SPACE COMPANY</small>	<b>TEST PROCEDURE</b> S444126  SHEET 13 OF 17 SHEETS
--	---	---

Check List

4.0 TEST (continued)

4.3 Instrumentation Check

4.3.1 Position the following switches to "ON":

SW-1 (+28V Power)  
 SW-18 (Orbit Mode)

4.3.2 Momentarily depress SW-24 (Brush 5, Door ON)

4.3.3 Connect a DC Ammeter between DRP Master Control Power Monitor Jacks +28V Reg "C-1" and "C-2".

4.3.4 Position SW-2 (+28V REG Current Monitor) to "ON", and record in Appendix I the current indicated by the DC Ammeter connected in paragraph 4.3.3.

4.3.5 Momentarily depress SW-20 (Brush 11, I/R OFF) and record in Appendix I the current indicated by the DC Ammeter connected in paragraph 4.3.3.


4.3.6 Momentarily depress SW-21 (Brush 12, ALL OFF) and, record in Appendix I the current indicated by the DC Ammeter connected in paragraph 4.3.3.

4.3.7 Momentarily depress SW-24 (Brush 5, Door ON) and SW-22 (Door ON and T/R READ-IN), and disconnect tape recorder plug J10P2.

4.3.8 Measure and record in Appendix I the voltages present at the following test jacks: (Ref. paragraph 3.8.2 for test jack identification)

Test Jack	Required Voltage
14	0 to 5V DC
15	0 to 5V DC
16	0 to 5V DC
17	0 to 5V DC
18	0 to 5V DC
19	0 to 5V DC
20	0 to 5V DC

"A" Rev. 4/24/62

TITLE GRD DOOR MODULE 116 TEST	 LOCKHEED MISSILES & SPACE COMPANY <small>A DIVISION OF LOCKHEED CORP.</small>	TEST PROCEDURE S411126
		SHEET 14 OF 17 SHEETS


L.O. TEST (continued)

4.3 Instrumentation Check (continued)

4.3.3 (continued)

<u>Test Jack</u>	<u>Required Voltage</u>
21	0 to 5V DC
22	0 to 5V DC
23	0 to 5V DC
24	0 to 5V DC
25	0 to 5V DC
26	-0.2 to +5.0V DC
27	0 to 5V DC
28	0 to 5V DC
29	0 to 5V DC
30	0 to 5V DC
31	0 to 5V DC
32	0 to 5V DC
33	0 to 5V DC
34	0 to 5V DC
35	0 to 5V DC
36	0 to 5V DC
37	0 to 5V DC
38	0 to 5V DC
39	0 to 5V DC
40	0 to 5V DC
41	0 to 5V DC
42	0 to 5V DC
43	0 to 5V DC
44	0 to 5V DC
45	0 to 5V DC
46	0 to 5V DC
47	0 to 5V DC
48	0 to 5V DC
49	0 to 5V DC
50	0 to 5V DC
51	0 to 5V DC
52	0 to 5V DC
53	0 to 5V DC

A. Rev. 4/24/62

<b>TITLE</b> GED DOOR MAINTLY 116 TEST	 LOCKHEED MISSILES & SPACE COMPANY <small>LOCKHEED MISSILES &amp; SPACE COMPANY</small>	<b>TEST PROCEDURE</b> Sh44126
		<b>SHEET 15 OF 17 SHEETS</b>

4.0 TEST (continued)

4.3 Instrumentation Check (continued)

4.3.8 (continued)

<u>Test Jack</u>	<u>Required Voltage</u>
54	0 to 5V DC
55	0 to 5V DC
56	0 to 5V DC
57	0 to 5V DC
58	0 to 5V DC
59	0 to 5V DC
60	0 to 5V DC
61	0 to 5V DC
62	0 to 5V DC
63	0 to 5V DC
64	3.7 ± 0.3V DC
65	2.5 ± 0.3V DC
66	1.2 ± 0.3V DC
68	4.0 ± 0.4V DC
69	5.2 ± 0.05V DC
70	5.0 ± 0.03V DC
71	2.5 ± 0.03V DC
72	0 ± 0.03V DC
76	4.0 ± 0.4V DC
79	4.0 ± 0.4V DC
80	4.0 ± 0.4V DC

4.3.9 Measure and record in Appendix I the voltages present at Test Jack 67 for the following Sensor Boom conditions:


<u>Condition</u>	<u>Required Voltage</u>
Booms Nos. 1 and 2 DOWN	3.7 to 4.4V DC
Boom No. 1 UP, Boom No. 2 DOWN	3.1 ± 0.2V DC
Boom No. 2 UP, Boom No. 1 DOWN	1.9 ± 0.2V DC
Booms Nos. 1 and 2 UP	0.6 ± 0.2V DC

4.3.10 Disconnect tape recorder plug J10P2 and momentarily depress SW-23 (Door ON and T/R Read-Out). Measure and record in Appendix I the voltage at Test Jack 77. This voltage shall be 4.0 ± 0.4V DC.

TA Rev. 4/24/66

TITLE	LOCKHEED	TEST PROCEDURE
DND DOOR MODULE TEST	LOCKHEED MISSILES & SPACE COMPANY	S. 11111
		SHEET 16 OF 17 SHEETS
		<u>Check List</u>
4.0 TEST (continued)		
4.3 <u>Instrumentation Check</u> (continued)		
4.3.11 Momentarily depress SW-22 (Door ON and T/R READ-IN). Measure and record in Appendix I the voltage at Test Jack 75. This voltage shall be $4.0 \pm 0.4V$ DC.		
4.3.12 Position SW-3 to "ON", and momentarily depress SW-21.		
4.3.13 Verify that +28V DC is present at the following test jacks:		
<u>Test Jack</u>	<u>Return</u>	
8	7	
9	7	
10	7	
4.3.14 Verify that continuity exists between the following test jacks:		
Between Test Jack 1 and Test Jack 73		
Between Test Jack 2 and Test Jack 75		
Between Test Jack 3 and Test Jack 74		
4.3.15 Momentarily depress SW-20, and position SW-3 to "OFF".		
4.4 <u>Commutator and Tape Recorder Test</u>		
4.4.1 Disconnect Module Harness Connectors J24P1, J24P2, and J24P3 from the Test Cable and connect them to their mating receptacles on the commutator.		
4.4.2 Depress SW-24 (BPUSH 5) and SW-22 (Door ON and T/R READ-IN) and verify that the commutator and tape recorder are operating.		
4.4.3 After $30 \pm 5$ MIN depress SW-21 (BPUSH 12).		
4.4.4 Connect 4 channels of a C.E.C. Recorder to shielded jacks 1, 2, 3, and 4. (Return on Shielded Jack 5.)		
4.4.5 Set the C.E.C. Recorder speed to 150 inches per second.		
4.4.6 Momentarily depress SW-24 (BPUSH 5) and SW-23 (Door ON and T/R READ-OUT.)		

REV. 1/2/60

<b>TITLE</b> GRD DOOR MODULE 110 TEST	 LOCKHEED MISSILES & SPACE COMPANY	<b>TEST PROCEDURE</b> S414120 SHEET 17 OF 17 SHEETS
4.0 TEST (continued) 4.4 <u>Commutator and Tape Recorder Test</u> (continued) 4.4.7 Position the C.E.C. Recorder Chart Drive Switch to "ON" for 4 ± 1 seconds. 4.4.8 Depress SW-21 (BRUSH 12) and position SW-1 to "OFF". 4.4.9 Data Reduction 4.4.9.1 Verify that all data points recorded in paragraph 4.4.7 are in accordance with Instrumentation Schedule 1342572. 4.4.9.2 Verify that all data points on Channel C and Channel E outputs are flat within ± 0.5V DC.		<b>Check List</b>

781-110-1/24/52

# Appendix C

## "N" DETECTOR PAYLOAD COMMAND SYSTEM CONCEPT

### INTERDEPARTMENTAL COMMUNICATION

TO Distribution DATE 24 April 1962

(Note: Only Table I and Figures 1, 3, and 5 are included in this appendix.)

FROM G. P. Minalga DATE 62-62 104 1 20232

### "N" DETECTOR EXPERIMENT SYSTEM CONCEPT

To acquaint those concerned with the various parameters of this program, the following is a brief description of the Ground and Vehicle systems and its operational plans (Figure 1 is a simplified block diagram of the overall system).

In order that experiments could benefit from the advantages contained in the ability to make measurements at the time of interest, the use of "real-time" command capability in addition with the "pre-programmed" type of command will be used.

#### Ground Command Tracking System

The tracking stations at WAFB, Hawaii, New Boston and Kodiak, have been equipped with single-helix antennas which are slaved to the normal tracking antennas. These helices are driven by crystal-controlled transmitters, which are in turn, modulated by audio tones originating from an audio coder. This coder consists of four audio oscillators, each tuned to a preselected frequency. Originally this unit had a push-button for each audio frequency. Pushing any one button provided a path from the cathode follower output to a push-pull amplifier, which in turn, modulated the transmitter. In order to lessen the possibility of a vehicle accepting a misdirected command, an arrangement has been incorporated into the system which requires that each command shall in reality consist of two discrete frequencies: an Address tone followed by a Command tone. The requirement is such that a master tone must first be transmitted followed by a command tone within one (1) second after termination of master tone termination. In order to facilitate operational sequences at the ground stations, and to eliminate possible difficulty in selecting two tones in the allocated time span, a slight modification of the audio coder was made. The ground support agency has provided a panel in the control area. This panel has three buttons located on the front panel. Engaging any button, provides +28 volts to the audio coder which is located at the remote transmitter site. The coder, upon receiving the +28 command from Button "A" will provide an Address tone having a duty cycle of one (1) second, followed immediately by a Command tone having a duty cycle of one (1) second. This sequence will have a repetition rate of four (4) seconds. The same sequence occurs when buttons "B" and "C" are engaged. In conjunction with this, there is also a four (4) position switch located on the front of the audio coder. Referring to Table I, it is shown that by selecting any of the four positions, a combination of the Address and Command tones can be employed.

#### Vehicle System

The vehicle will contain a narrow-band FM receiver, operating in the 100-150 mc spectrum. This receiver is fed by a dipole antenna which is excited by the tone-modulated signals originating from the ground stations. The audio output of the receiver feeds the Decoder. This Decoder has four audio filters, each sharply tuned to one of the preselected audio frequencies. (See Table I) The output of each filter is fed to a DC amplifier which, in turn, drives a relay. These relays, upon excitation, provide a ground closure to the proper slave relay in the system program. One of the relay driver amplifiers in the Decoder, has a time-delay drop-out circuit. This circuit, upon receipt of the proper tone (Address tone) holds a relay closed for the duration that the signal is present, and upon cessation of the signal, holds the relay closed for



Vehicle System (cont'd)

one (1) second,  $\pm .5$  second. During this time, the altered relay switches it to the remaining relay driver amplifiers, allowing any one of the three remaining tones to be sent through to perform its function.

Three commands (four tones) are available to command and control the functions of the "M" Detector Experiment. Each command is composed of two (2) tones, one of which is a signature or identification. This arrangement will lessen the possibility of a vehicle accepting a misdirected command. Assignment of the tone command combination will be issued prior to the launch of the vehicle. These commands will be transmitted from command system located at each of the tracking stations.

The following is a description of the sequence of events of the vehicle during any "active" mode.

Standard Configuration (with timer) with reference to ~~Figure 4~~ and Figure 3

- A. Command A (Brush 5) initiates the timer-programmer at which time the following sequence of operation occurs: at time-zero, the filaments of the T/M are turned on; timer on.

At time plus 30 seconds, the plates of the T/M are turned on; tape recorder energized to the reproduce mode; real-time data readout.

At time plus 60 seconds, VOG's are on; the equipment on the Door "ON"; tape recorder starts to read out data.

At time plus 300 seconds, telemetry "OFF"; record signal to tape recorder; tape recorder in the record mode; programmer logic in the state to accept another command.

- B. Command B (Brush 14) initiates the tape recorder by pass. This function is given in the event of a tape recorder malfunction and real time data is required for completion of mission.

- C. Command C (Brush 17) initiates the experiment's "OFF" and Door "OFF" functions.

Alternate Configuration (w/ built timer) with reference to ~~Figure 4~~ and Figure 5

The commands initiate the functions as described in the operations for the standard configuration with exception of having the end of tape sensor of the tape recorder to turn the functions "OFF" and place the system logic in the state to accept another command.

This system will be used as a back up to the timer programmer.

End-of-Tape

The end-of-tape function of the tape recorder is used to control certain sequence of operations and is as follows (Reference ~~Figure 4~~ and Figure 5).

1. During a record mode and at the end of 5 hours of read-in, the E.O.T. sensing returns the related circuitry to turn the instrumentation "OFF" and to place the system logic in the state to accept another command.
2. During a reproduce mode and at the end of 7 minutes of readout, the E.O.T. sensing activates a 30 seconds time delay circuit to place the tape recorder in the record mode and read in data. After 30 seconds, K-2 (record mode) is actuated which drops power to K-11 thus in turn energizes K-9 and K-8 to accept a signal to turn door off upon completion of the recording sequence. The system is now placed in the state of logic to accept another command.

#### Operational Plan

During the active phase of the Discoverer's primary mission, the "N" Detector Experiment will have the following sequence of operations:

1. Monitoring only during the orbit mode.
2. Confirm "N" Detector Payload operation prior to recovery. During this period, the "N" Timer is programmed to acquire data for one (1) complete orbit and to play out data at the first good acquisition prior to going into the passive mode.
3. Achieving completion of the primary mission and after L.B. exercise, the vehicle power and U.P. antenna is transferred for the exclusive use of the "N" Detector Experiment.
4. The vehicle will remain in a passive mode of operation, until such time that "activation" of the experiment is deemed necessary. (System "OFF" with the exception of the command receiver and decoder)
5. Operational checks of the experiment are planned for every 49 hours interval.
6. Upon receipt of instructions from Dept. 62-62 to commence with the "active" phase of the experiment, the "N" Detector Experiment is turned "ON" for a period of days until depletion of batteries and/or "ON" and "OFF" for specific times to be determined by Dept. 62-62. The desired command sequence will be sent to all tracking stations.

For purposes of clarity, an example of a typical operational sequence is given: Refer Figure I. It is necessary to activate the experiment for real-time and stored data receipt. TWR is directed to instruct the vehicle at a time based on ephemeris information; the "remote site" operator puts the selector switch on the audio reader to position 1. (See Table I) The control operator, at the predicted time of vehicle acquisition, depresses button "1", which according to Table I, will turn on all equipment.

(Note: the operator will continue to send this command until notified of telemetry transmission verification from the receiving station) The vehicle, upon receipt of one proper Address 100 and 00 and tone, will go into a CW mode of transmission for thirty, (30) seconds. This will allow the receiving and slave antennas to get "locked-on" before the tape recorder begins reading out. If there are no further operational requirements for TWR during this orbit, then upon completion of the acquisition, the telemetry will turn off, the instruments will stay on, and the tape recorder will begin operating in the read-in mode. (Refer to Table II, definition of Commands.)

*G. P. Minolga*  
G. P. Minolga, Manager  
Discoverer Recovery Payloads

GPX:HL:bw

cc: E. E. Crowther/S. I. Weiss  
J. Peckenberry  
G. M. Flynn  
I. Ganning  
G. P. Minolga  
R. J. Watson  
R. E. Meyer  
H. Loebe  
J. Wiley  
D. Porter  
R. Macdonald

N. N. Epstein  
T. O. Harshbarger  
M. D. Loncke  
P. Warrick  
D. Peiffer  
L. I. I. I.  
R. L. Weller  
G. Lanza  
J. Chapman  
R. Waller

Table I

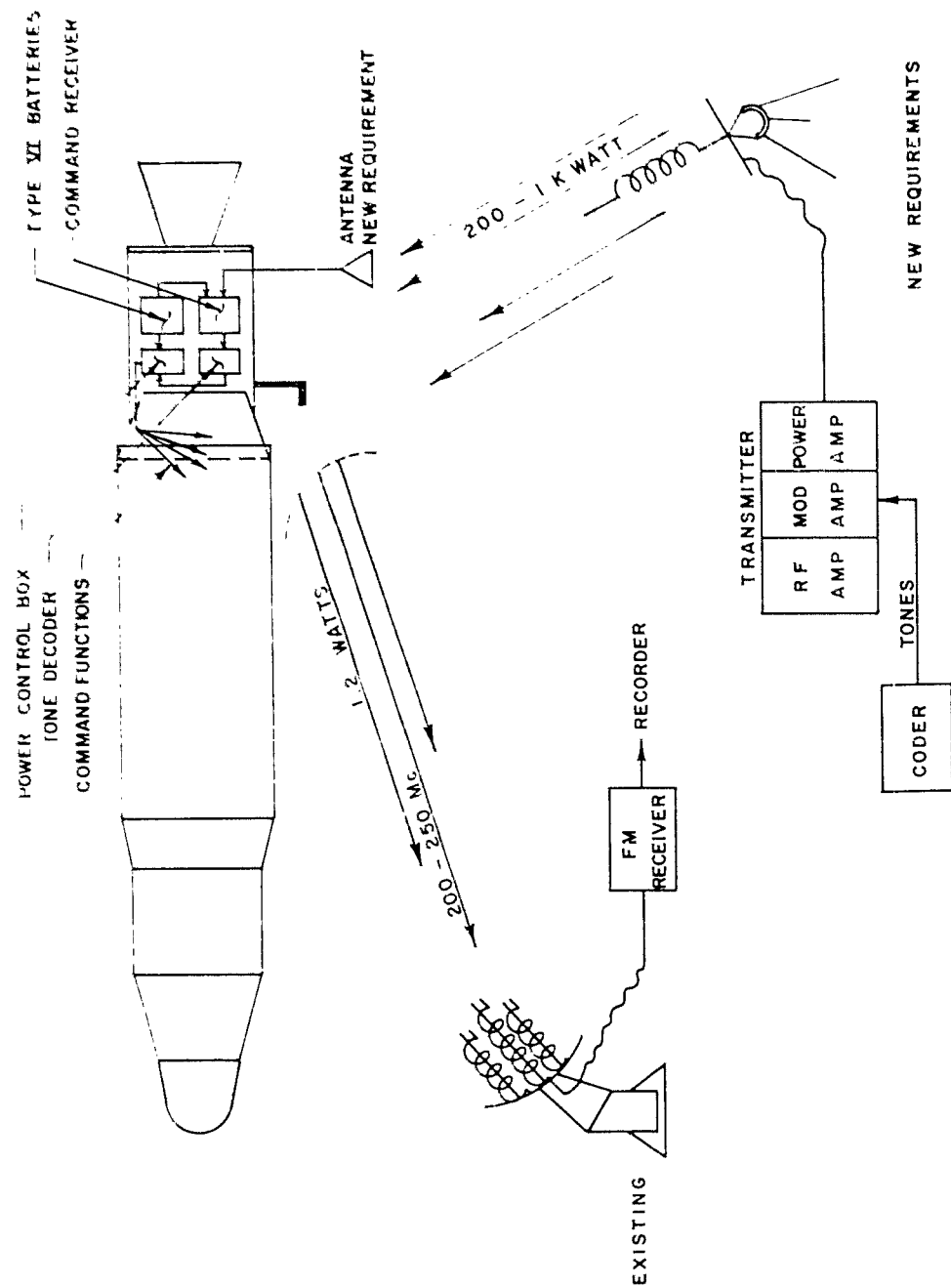
Selector Switch Position	Control Position	Address and Command Frequency	
#1	"A"	6.0	5.1
#1	"B"	6.0	5.4
#1	"C"	6.0	5.7
#2	"A"	5.7	5.4
#2	"B"	5.7	6.0
#2	"C"	5.7	5.1
#3	"A"	5.4	5.1
#3	"B"	5.4	5.7
#3	"C"	5.4	6.0
#4	"A"	5.1	6.0
#4	"B"	5.1	5.7
#4	"C"	5.1	5.4

Table II

## Definition of Command

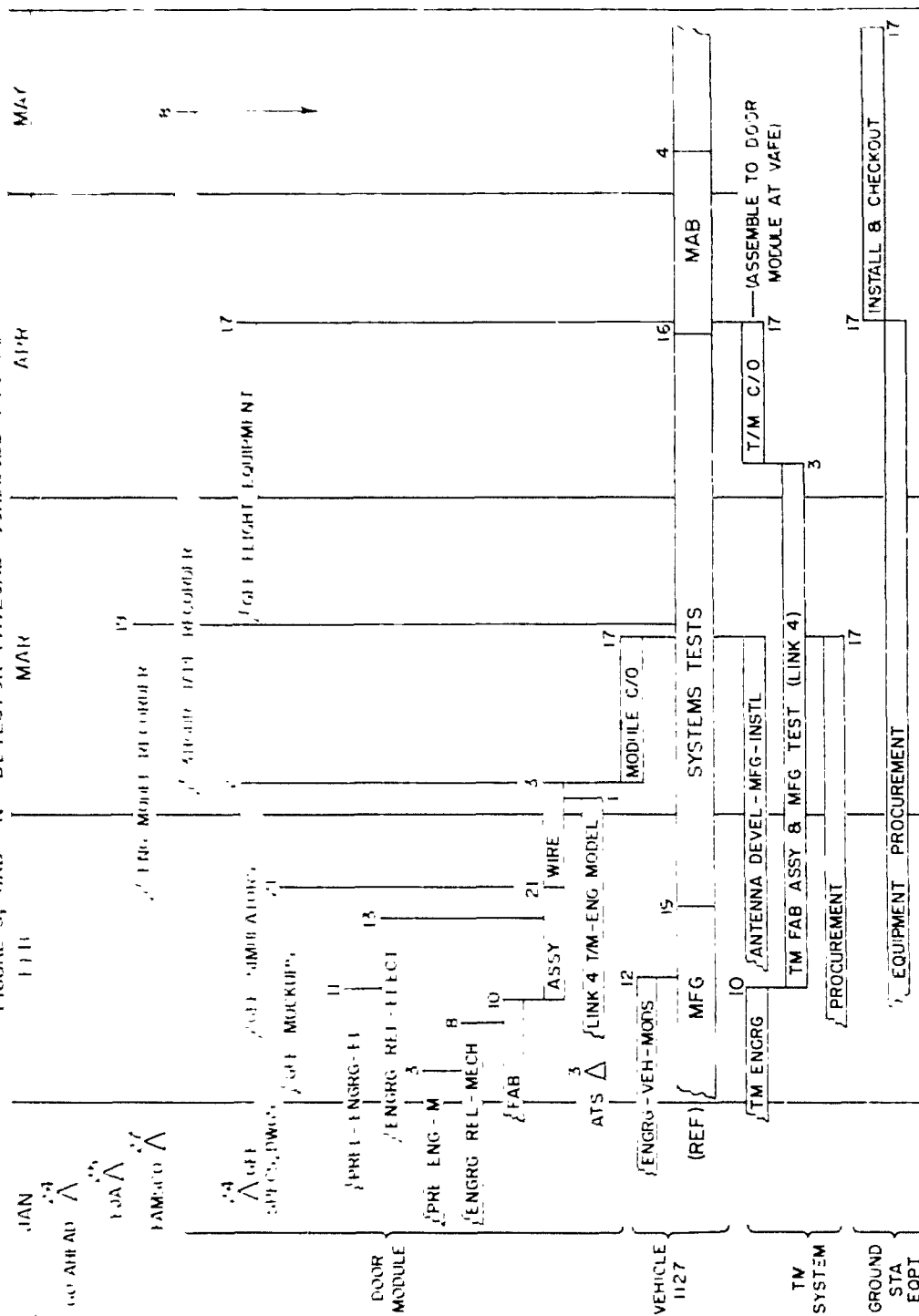
Command "A" = Filaments/ON

T+50 seconds = Plates/ON  
Face Recorder/Readout PositionT+60 seconds = Core/ON  
Type Recorder/ONT+610 seconds = T/A Off  
Port/ON  
Type Recorder = ON/Read-In Mode



TRACKING STATION REQUIREMENTS

FIGURE 3, GRD "N" DETECTOR PAYLOAD SCHEDULE FTV 1127



Appendix D

INSTRUMENTATION SCHEDULE, FTV 1127

This Specification describes the Instrumentation Requirements and minimum standard of performance for the telemeter system.

Revision Status of Sheets on Dates Noted

Approved	Date	1	2	3	4	5	6	7	8	9	10	11	12	13	14	15	16	17	18	19	20	21	EJT
<i>[Signature]</i>	4-28-62	X	X	R	R	R	R	R	R	R	R	R	R	R	R								

ND-1, ND-2, incorporated

	NAME	DATE
PREPARED	<i>E.H. Lasse</i>	4-28-62
APPROVED	<i>[Signature]</i>	5-1-62
APPROVED	<i>[Signature]</i>	

REVISED:	LOCKHEED AIRCRAFT CORPORATION MISSILES and SPACE DIVISION SUNNYVALE, CALIF.	TITLE INST. REQD. WILM LINK II (205 T.M. 1127)	1348572
			SHEET I OF 1

CONTINUOUS CHANNELS EXCEPT AS NOTED										MODEL	6205	LOCATED
LINK NO.	1	VEHICLE NO.	1127	T/N PART NO.	VOLTAGE SOURCE		OSCILLATOR	AUXILIARY	SLOT			
MEASUREMENT	MEAS	NO.	RANGE	VOLTS	TRANSDUCER	TYPE	TYPE	TYPE	TYPE	TYPE	TYPE	TYPE
OR KYNOS	OR KYNOS	OR KYNOS	OR KYNOS	OR KYNOS	OR KYNOS	OR KYNOS	OR KYNOS	OR KYNOS	OR KYNOS	OR KYNOS	OR KYNOS	OR KYNOS
1												
2												
3												
4												
5												
6												
7												
8	Spare											
9												
10												
11	Spare											
12												
13												
14												
15	IRP Status Data	5 x 60	Commutator									
16												
17												
18												

REVISED: LOCKHEED AIRCRAFT CORPORATION MISSILES and SPACE DIVISION BUNNYVALE, CALIF.

TITLE: INST. SCHED. UTLN LINK II 6205 VEH. 1127

1342572  
SHEET 2 OF 14





CONTINUOUS CHANNELS EXCEPT AS NOTED														
LINK NO. 2		VEHICLE NO. 1127		T/N PART NO.		MODEL 6255		LOCATED						
REVISED	OR KTHC BIR	MEASUREMENT	HEAS NO.	OSG RANGE VOLTS	TRANSDUCER RANGE	VOLTAGE SOURCE		OSCILLATOR TYPE DAO NO (REF)	AUXILIARY EQUIPMENT (REF)	SLOT NO.	OSC INPUT FLAG	SALON		
						OK	TYPE							
1														
2														
3														
4														
5														
6														
7														
8		N Detector Module .4 x .60 Commutator Real Time Ring B												
9		N Detector Module .4 x .60 Commutator Real Time Ring A												
10														
11														
12														
13														
14		Link I Status Data												
15														
16		N Detector Module .4 x .60 Commutator 26 to 1 tape recorder Ring B												
17														
18		N Detector Module .4 x .60 Commutated 26 to 1 Tape Recorder Ring A												

LOCHEED AIRCRAFT CORPORATION  
MISSILES and SPACE DIVISION  
BURBANK, CALIF.

TITLE  
INST. SCHED. UTILM LINK II  
6255 VEH. 1127

1342572

SHEET 4 of 14

Ring COMPUTED CHANNEL NO. 3 LINK NO. 2 COM. TYPE 5D NO. 3 RATE 4 RPS POINT 60											
COM POS	MEASUREMENT	STBY	IS LOC (FET)	MEAS NO.	RANGE VOLTS	XDCR RANGE	VOLT SOURCE OR XDCR TYPE	AUXILIARY EQUIPMENT (REF)	INPUT PLUG J24F2	IS LOC	IS LOC
1	Cal 0				0 V				31		
2	ES-1			X241	0-5V				32		
3	ES-2			X242					33		
4	ES-3			X243					34		
5	ES-4			X244					35		
6	RPA-1			X251					36		
7	RPA-2			X252					37		
8	RPA-3			X253					38		
9	RPA-4			X254					39		
10	RPA-5			X255					40		
11	RPA-6			X256					41		
12	RPA-7			X261					42		
13	IP-1			X213					43		
14	IP-2			X214					44		
15	IP-3			X215					45		
16	IP-4			X216					46		
17	IP-5			X217					47		
18	IP-6			X218					48		
19	ES-1			X241					49		
20	ES-2			X242					J24F3		
21	ES-3			X243					5		
22	TEC-1			X235					6		
23	TEC-2			X237					7		
24	Clock Temp			X196					8		
25	RPA-8			X262					9		
26	RPA-9			X263					10		
27	RPA-10			X264					11		
28	Boom Mot. ERECT				Boom Up 3.1V 1&2 Up .6V Boom Down 1.9V 1&2 Down 1.2V				12		
29	ES-4			X244	0-5V				13		
30	Cal +				5.0V				14		
LOCKHEED AIRCRAFT CORPORATION MISSILES and SPACE DIVISION SUNNYVALE, CALIF.		TITLE INSTRUMENTATION SCHEDULE UTM LINK II 6205 VEHICLE 1127							1342572 SHEET 5 of 4		

Ring COMPUTATED CHANNEL NO. <u>3</u> LINK NO. <u>2</u> CORN. TYPE <u>5D</u> NO. <u>B</u> H <sup>2</sup> K <u>4RPS</u> POINT <u>GO</u>											
COR POS	MEASUREMENT	SYS ID	MEAS NO.	RANGE VOLTS	XDGR RANGE	VOLT SOURCE OR XDGR TYPE	AUXILIARY EQUIPMENT (REF)	INPUT PLUG J24P4	ECT	ECT	ECT
31	ES-1		X241	0-5V				1			
32	ES-2		X242					2			
33	ES-3		X243					3			
34	ES-5		X245					4			
35	RPA-1		X251					5			
36	RPA-2		X252					6			
37	RPA-3		X253					7			
38	RPA-4		X254					8			
39	RPA-5		X255					9			
40	RPA-6		X256					10			
41	RPA-7		X261					11			
42	ES-5		X245					12			
43	ES-1		X241					13			
44	ES-2		X242					14			
45	ES-4		X244					15			
46	IR-1		X213					16			
47	IR-2		X214					17			
48	IR-3		X215					18			
49	IR-4		X216					19			
50	IR-5		X217					20			
51	IR-6		X218					21			
52	IR-7		X219					22			
53	Clock 1		X192					23			
54	Clock 2		X193					24			
55	Clock 3		X194					25			
56	Clock 4		X195	0-5V				26			
57	Cal 4			2.5V				27			
58	Sync			5.25V				28			
59	Sync			5.25V				29			
60	Sync			5.25V				30			
REVISION:	LOCKHEED AIRCRAFT CORPORATION MISSILE and SPACE DIVISION BURNINGALE, CALIF.		TITLE INSTRUMENTATION SCHEDULE UTM LINK II 6205 VEHICLE 1127						1342572 SHEET 6 of 14		

COMPUTATED CHANNEL NO. 9 LINK NO. 2 CORR. TYPE 50										RINO		NO. A		RATH 4		RPS POINT 60	
CON	POS	MEASUREMENT	ST226	IO.10	(227)	MEAS NO.	RANGE VOLTS	XDGR RANGE	VOLT SOURCE OR XDGR TYPE	HFU	AUXILIARY EQUIPMENT (REF)	INPUT PLUG J24P	SCALE				
1		Cal 1					0.7					1					
2		RT-1				X221	0-5V					2					
3		RT-2				X222						3					
4		RT-3				X224						4					
5		RT-4				X226						5					
6		RT-8				X228						6					
7		RT-9				X229						7					
8		RT-10				X230						8					
9		RT-11				X231						9					
10		RT-12				X231						10					
11		RT-5				X223						11					
12		RT-5				X225						12					
13		RT-7				X227						13					
14		RT-12				X232						14					
15		RT-13				X233						15					
16		RT-15				X235						16					
17		GRP-1				X238						17					
18		GRP-2				X239						18					
19		GRP-3				X240						19					
20		RT-1				X221						20					
21		RT-2				X222						21					
22		RT-4				X224						22					
23		RT-6				X226						23					
24		RT-8				X228						24					
25		RT-9				X229						25					
26		RT-10				X230						26					
27		RT-11				X231						27					
28		RT-12				X234	0-5V					28					
29		Cal 2					0V					29					
30		Cal +					5.0V					30					

REVISED	LOCHEED AIRCRAFT CORPORATION MISSILES & SPACE DIVISION BURNINGALE, CALIF.	TITLE INST. SCHED. WTM LINK II 6205 VER. 1127	1342572
	SHEET 7 OF 14		

COMPUTED CHANNEL NO. 0 LINK NO. 2 CORR. TYPE 5D RING NO. A RATE 14 MPS POINT 60										
CHN POS	MEASUREMENT	STDS	IS. LG (REF)	MEAS NO.	RANGE VOLTS	XDGR RANGE	VOLT SOURCE OR XDGR TYPE	AUXILIARY EQUIPMENT (REF)	INPUT PLUG J24P2	ECTE
31	Par - 1 + X			X081	0-5V				31	
32	Par - 2 + Y			X082	0-5V				32	
33	Par - 3 + Z			X083	0-5V				33	
34	Cal 1				0 V				34	
35	Cal +				5.0V				35	
36	GRF 4			X247	0-5V				36	
37	Test Pon 5 + 28V Batt.				0-5V				37	
38	TEC 1			X236					38	
39	TEC 2			X237					39	
40	BT-1			X221					40	
41	BT-2			X222					41	
42	BT-4			X224					42	
43	BT-6			X226					43	
44	BT-8			X228					44	
45	BT-9			X229					45	
46	BT-10			X230					46	
47	BT-11			X231					47	
48	BT-14			X234					48	
49	GRF-1			X238					49	
50	GRF-2			X239					23	
51	RF-3			X240					24	
52	RF-5 Temp			X248					25	
53	Clock 1			X192					26	
54	Clock 2			X193					27	
55	Clock 3			X194					28	
56	Clock 4			X195	0-5V				29	
57	Cal 1/2				2.5V				30	
58	Sync.				5.25V				31	
59	Sync.				5.25V				32	
60	Sync.				5.25V				33	

REVISED	LOCOMED AIRCRAFT CORPORATION ROCKET AND SPACE DIVISION SUNNYVALE, CALIF.	TITLE INST. SCHED. UTM LINK II 6205 VER. 1127	1342572
			SHEET 8 OF 14

COMPUTED CHANNEL NO. C		LINK NO. 2		CONF. TYPE		5D		Ring		NO. B		NPS POINT		60	
CH	MEASUREMENT	SYS	LOC (277)	MEAS NO.	RANGE VOLTS	XDCR RANGE	VOLT SOURCE OR XDCR TYPE	WFO	AUXILIARY EQUIPMENT (REF)	INPUT PLUG	PLUG	PLUG	PLUG	PLUG	PLUG
1	Cal 0				0. V								31		
2	ES-1			X241	0-5V								32		
3	ES-2			X242									33		
4	ES-3			X243									34		
5	ES-4			X244									35		
6	RPA-1			X251									36		
7	RPA-2			X252									37		
8	RPA-3			X253									38		
9	RPA-4			X254									39		
10	RPA-5			X255									40		
11	RPA-6			X256									41		
12	RPA-7			X257									42		
13	ES-1			X213									43		
14	ES-2			X214									44		
15	ES-3			X215									45		
16	ES-4			X216									46		
17	ES-5			X217									47		
18	ES-6			X218									48		
19	ES-1			X241									49		
20	ES-2			X242									024P3		
21	ES-3			X243									5		
22	ES-4			X236									6		
23	ES-2			X237									7		
24	Clock Temp 1			X196									8		
25	RPA-1			X262									9		
26	RPA-9			X263									10		
27	RPA-10			X264									11		
28	Boom Temp 1												12		
29	ES-4			X244	0-5V								13		
30	Cal +				5.0V								14		

LOCKHEED AIRCRAFT CORPORATION  
MISSILE and SPACE DIVISION  
BUNTINGVILLE, CALIF.

TITLE INSTRUMENTATION SCHEDULE UTM LINK II  
6205 VEHICLE 1127

1342572

SHEET 9 OF 14

Ring COMPUTED CHANNEL NO. C LINK NO. 2 CORR. TYPE 5D NO. B HATK 4 RPS POINT 60											
CORR POS	MEASUREMENT	STDS 10.100 (ACT)	MEAS NO.	RANGE VOLTS	XDCH RANGE	VOLT SOURCE OR XDCH TYPE INFO	AUXILIARY EQUIPMENT (REF)	INPUT PLUG J24P2	ECT2	ECT1	
31	ES-1		X241	0-5. V				1			
32	ES-2		X242					2			
33	ES-3		X243					3			
34	ES-5		X245					4			
35	RPA-1		X251					5			
36	RPA-2		X252					6			
37	RPA-3		X253					7			
38	RPA-4		X254					8			
39	RPA-5		X255					9			
40	RPA-6		X256					10			
41	RPA-7		X257					11			
42	ES-6		X246					12			
43	ES-1		X241					13			
44	ES-2		X242					14			
45	ES-4		X244					15			
46	IP-1		X213					16			
47	IP-2		X214					17			
48	IP-3		X215					18			
49	IP-4		X216					19			
50	IP-5		X217					20			
51	IP-6		X218					21			
52	IP-7		X219					22			
53	Clock 1		X192					23			
54	Clock 2		X193					24			
55	Clock 3		X194					25			
56	Clock 4		X195	0-5. V				26			
57	Cal 1			2.5 V				27			
58	Sync.			5.25V				28			
59	Sync.			5.25V				29			
60	Sync.			5.25V				30			
REVISED:	LOCKHEED AIRCRAFT CORPORATION ROCKWELL and SPACE DIVISION BUNTVILLE, CALIF.		TITLE INSTRUMENTATION SCHEDULE UPLINK LINK II 6205 VEHICLE 1127					1342572 SHEET 10 OF 14			

COMPUTED CHANNEL NO. <u>18</u> LINK NO. <u>2</u> COM. TYPE <u>5D</u> RING NO. <u>A</u> WAVE <u>LNPS POINT 60</u>										
CH	MEASUREMENT	SYMBOL	UNIT	MEAS NO.	RANGE VOLTS	DCR RANGE	VOLT SOURCE OR DCR TYPE	AUXILIARY EQUIPMENT (REF)	INPUT PLUG J24P1	NOTES
1	CH-1				0 V				1	
2	CH-2			X221	0-5V				2	
3	CH-2			X222					3	
4	CH-4			X224					4	
5	CH-5			X226					5	
6	CH-6			X228					6	
7	CH-9			X229					7	
8	CH-10			X230					8	
9	CH-11			X231					9	
10	CH-11			X231					10	
11	CH-3			X223					11	
12	CH-5			X225					12	
13	CH-7			X227					13	
14	CH-12			X232					14	
15	CH-13			X233					15	
16	CH-15			X235					16	
17	CH-1			X233					17	
18	CH-2			X239					18	
19	CH-3			X240					19	
20	CH-1			X221					20	
21	CH-2			X222					21	
22	CH-4			X224					22	
23	CH-6			X226					23	
24	CH-9			X229					24	
25	CH-9			X229					25	
26	CH-10			X230					26	
27	CH-11			X231					27	
28	CH-11			X234	0-5V				28	
29	Cal 2				0V				29	
30	Cal +				5.0V				30	

REVISED:	LOCKHEED AIRCRAFT CORPORATION AERIAL FI and SPACE DIVISION BURBANK, CALIF.	TITLE INST. SCHED. UTLN LINK II 6205 VER. 1127	1342572 SHEET 11 OF 14
----------	--	--	---------------------------

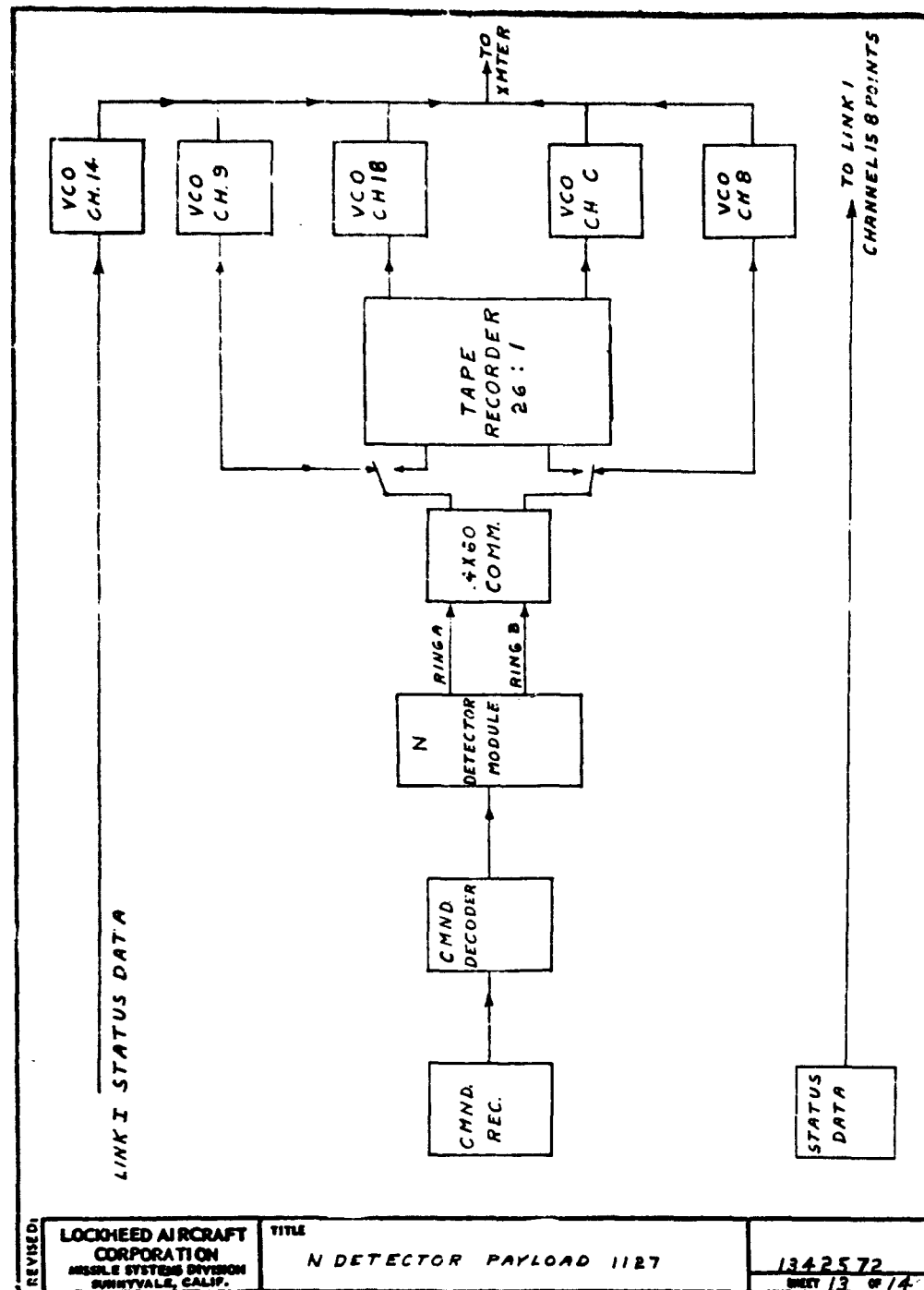


COMPUTED CHANNEL NO. <u>18</u> LINK NO. <u>2</u> CORR. TYPE <u>5D</u> RING NO. <u>A</u> DATA <u>INPS POINT 50</u>		MEAS. NO.	RANGE VOLTS	XDCR RANGE	VOLT SOURCE OR XDCR TYPE	AUXILIARY EQUIPMENT (REF)	INPUT PLUG	OUTPUT
31	100 - 2 + X	X281	0-5V				31	
32	100 - 2 + Y	X282	0-5V				32	
33	100 - 3 + Z	X283	0-5V				33	
34	0-5V		0 V				34	
35	0-5V		5.0V				35	
36	0-5V	X287	0-5V				36	
37	0-5V		0-5V				37	
38	0-5V	X286					38	
39	0-5V	X237					39	
40	0-5V	X221					40	
41	0-5V	X222					41	
42	0-5V	X223					42	
43	0-5V	X224					43	
44	0-5V	X225					44	
45	0-5V	X226					45	
46	0-5V	X227					46	
47	0-5V	X228					47	
48	0-5V	X229					48	
49	0-5V	X230					49	
50	0-5V	X231					50	
51	0-5V	X232					51	
52	0-5V	X233					52	
53	0-5V	X234					53	
54	0-5V	X235					54	
55	0-5V	X236					55	
56	0-5V	X237					56	
57	0-5V	X238					57	
58	0-5V	X239					58	
59	0-5V	X240					59	
60	0-5V	X241					60	
61	0-5V	X242					61	
62	0-5V	X243					62	
63	0-5V	X244					63	
64	0-5V	X245					64	
65	0-5V	X246					65	
66	0-5V	X247					66	
67	0-5V	X248					67	
68	0-5V	X249					68	
69	0-5V	X250					69	
70	0-5V	X251					70	
71	0-5V	X252					71	
72	0-5V	X253					72	
73	0-5V	X254					73	
74	0-5V	X255					74	
75	0-5V	X256					75	
76	0-5V	X257					76	
77	0-5V	X258					77	
78	0-5V	X259					78	
79	0-5V	X260					79	
80	0-5V	X261					80	
81	0-5V	X262					81	
82	0-5V	X263					82	
83	0-5V	X264					83	
84	0-5V	X265					84	
85	0-5V	X266					85	
86	0-5V	X267					86	
87	0-5V	X268					87	
88	0-5V	X269					88	
89	0-5V	X270					89	
90	0-5V	X271					90	
91	0-5V	X272					91	
92	0-5V	X273					92	
93	0-5V	X274					93	
94	0-5V	X275					94	
95	0-5V	X276					95	
96	0-5V	X277					96	
97	0-5V	X278					97	
98	0-5V	X279					98	
99	0-5V	X280					99	
100	0-5V	X281					100	

LOCKHEED AIRCRAFT CORPORATION  
MISSILES and SPACE DIVISION  
BURNINGWATER, CALIF.

TITLE: INST. SCHED. UTIL. LINK II  
6205 YTH. 1127

1342572  
SHEET 12 OF 14



### PROGRAMMING

Separation:	Turns on clock, receiver and decoder. Three ground commands will perform the following functions.
Command A:	T/M filaments on. 60 sec time delay starts and initiates T/M plate voltage. 1.5 min time delay starts tape recorder readout. 10 min time delay turns tape recorder and T/M off. Tape recorder switched to read in mode.
Command B:	Tape recorder bypass
Command C:	All equipment off except receiver, decoder and clock
Brush 11:	T/M filaments on. 60 sec time delay starts and initiates T/M plate voltage. 1.5 min time delay starts tape recorder readout. 10 min time delay turns tape recorder and T/M off. Tape recorder switched to read in mode.
Brush 5:	Tape recorder bypass
Brush 12:	All equipment off except receiver, decoder and clock.
Brush 25:	T/M filaments on, door disable
Brush 26:	T/M plates and VCO on
Brush 23:	Spare
Brush 24:	Spare

## REFERENCES

1. C. McIlwain; J. Geophys. Res. 64, 923, (1959).
2. J.D. Mikhalow, D.D. Elliott, S.C. Freden, F.S. Mozer, G.D. Pavlikas, and A.L. Vampols; Trans. Am. Geophys. Union, 43, 461, (1962).
3. F.D. Seward, F.C. Gilbert, H.N. Kornblum, and R.S. White; Bull. Am. Phys. Soc. 7, (2), (1962).
4. H.L. West, L.G. Mann, and S.D. Bloom; Bull. Am. Phys. Soc. 7, (2), 62, (1962).
5. B.J. O'Brien; J. Geophys. Res. 67, 3637, (1962).
6. J.W. Chamberlain; Physics of the Aurora and Airglow Academic Press, N.Y., (1962).
7. J.R. Winckler, P.D. Bhavsar, K.A. Anderson; J. Geophys. Res. 67, 3717, (1962).
8. C.D. Anger, J.R. Barcus, R.R. Brown and D.S. Evans; J. Geophys. Res. 68, 1023, (1962).
9. D.C. Haycock and K.D. Baker; "Measuring Antenna Impedance in the Ionosphere"; Electronics, vol. 34, pp 88-92, January 1961.
10. W. Pfister, J.C. Ulwick and R.P. Vancour; "Some Results of Direct Probing in the Ionosphere"; Journal of Geoph. Res., vol. 66, pp 1293-1297, April 1961.
11. J.C. Ulwick and W. Pfister; "Spatial and Temporal Variations of Electron Density from an Orbiting Satellite"; Cospar, Third International.
12. H.E. Hinteregger; "Combined Retarding Potential Analysis of Photoelectrons and Environmental Charged Particles up to 234 km"; 1960; Space Research I, p. 394, edited by Hilde Kalhmann Bijl; North Holland Publishing Company, Amsterdam; Unclassified.
13. H.E. Hinteregger; "Analysis of Problems Associated with Ion Density and Velocity - Distribution Measurements from Space Vehicles"; 1961; GRD-CRZA working copy mimeographed; Air Force Cambridge Research Laboratories, Bedford, Massachusetts; Unclassified.
14. "Automatic Range and Polarity Switching Amplifier"; Adcole Corporation, Cambridge, Massachusetts.

Military sites, installations, and contractors requesting changes of address or distribution requirements should forward their requests through established channels to the Chief, Defense Atomic Support Agency, Washington, D. C. 20301

## DISTRIBUTION

### Military Distribution Category 1

#### ARMY ACTIVITIES

- 1 CHIEF OF R & D DA
- 2 AC OF S INTELLIGENCE DA
- 3 CHIEF OF ENGINEERS DA
- 4 ARMY MATERIAL COMMAND
- 5 CHIEF SIGNAL OFFICER DA
- 6- 7 U S ARMY COMBAT DEVELOPMENTS COMMAND
- 8 U S ARMY CDC NUCLEAR GROUP
- 9 U S ARMY ARTILLERY BOARD
- 10 U S ARMY AIR DEFENSE BOARD
- 11 U S ARMY AVIATION BOARD
- 12 U S ARMY AIR DEFENSE SCHOOL
- 13 U S ARMY CDC ARMOR AGENCY
- 14 U S ARMY CDC ARTILLERY AGENCY
- 15 U S ARMY CDC INFANTRY AGENCY
- 16 U S ARMY CDC CBR AGENCY
- 17 U S ARMY SIGNAL SCHOOL
- 18- 19 ENGINEER RESEARCH & DEV LAB
- 20 WATERWAYS EXPERIMENT STATION
- 21 PICATINNY ARSENAL
- 22 DIAMOND ORDNANCE FUZE LABORATORY
- 23 BALLISTIC RESEARCH LABORATORY
- 24 FRANKFORD ARSENAL
- 25- 27 REDSTONE SCIENTIFIC INFORMATION CENTER
- 28- 29 WHITE SANDS MISSILE RANGE
- 30 U S ARMY MOBILITY COMMAND
- 31 U S ARMY AMMUNITION COMMAND
- 32 U S ARMY MUNITIONS COMMAND
- 33 ELECTRONICS COMMAND
- 34 U S ARMY ELECTRONIC PROVING GROUND
- 35- 38 U S ARMY ELECTRONIC R & D LABORATORY
- 39- 42 U S ARMY CDC COMBAT SERVICE SUPPORT GROUP
- 41 THE RESEARCH & ANALYSIS CORP
- 42- 43 WHITE SANDS SIGNAL SUPPORT AGENCY
- 44 U S ARMY NUCLEAR DEFENSE LABORATORY
- 45 U S ARMY CDC AIR DEFENSE AGENCY
- 46 UNITED STATES CONTINENTAL ARMY COMMAND
- 47 U S ARMY CDC COMBINED ARMS GROUP
- 48 U S ARMY ENGINEER RSD LABS ENGR-EP
- 49- 50 U S ARMY ENGR, RES. & ENGR LABS.
- 51 PROJECT MGR, NIXE X PROJECT OFFICER

#### NAVY ACTIVITIES

- 52- 53 CHIEF OF NAVAL OPERATIONS OPO3EG
- 54 CHIEF OF NAVAL OPERATIONS OP-05E5
- 55 CHIEF OF NAVAL OPERATIONS OP-75
- 56 CHIEF OF NAVAL OPERATIONS OP-922G1
- 57 CHIEF OF NAVAL OPERATIONS OP-94
- 58 CHIEF OF NAVAL OPERATIONS OP-922F2
- 59- 61 CHIEF BUREAU OF NAVAL WEAPONS CLI-3
- 62 CHIEF BUREAU OF SHIPS CODE 423
- 63 CHIEF BUREAU OF YARDS & DOCKS CODE 74
- 64 DIR, U S NAVAL RESEARCH LAB.
- 65- 66 U S NAVAL ORDNANCE LABORATORY
- 67 NAVY ELECTRONICS LABORATORY
- 68 U S NAVAL RADIOLOGICAL DEFENSE LAB
- 69 U S NAVAL CIVIL ENGINEERING LABORATORY
- 70 U S NAVAL SCHOOLS COMMAND U S NAVAL STATION
- 71 U S NAVAL POSTGRADUATE SCHOOL
- 72 AIR DEVELOPMENT SQUADRON 5 VX-5
- 73 U S NAVAL AIR DEVELOPMENT CENTER
- 74 U S NAVAL WEAPONS EVALUATION FACILITY
- 75 U S NAVAL MEDICAL RESEARCH INSTITUTE
- 76 DAVID M TAYLOR MODEL BASIN
- 77- 80 U S MARINE CORPS CODE A03H

#### AIR FORCE ACTIVITIES

- 81- 83 HQ USAF AFTAC-TO
- 84 HQ USAF AFRDPF

- 85 HQ USAF AFXPDS
- 86 HQ USAF AFCEKA
- 87 HQ USAF AFDOA
- 88- 92 HQ USAF AFNINDE
- 93 BALLISTIC SYSTEMS DIVISION
- 94 SPACE SYSTEMS DIVISION SSTDS
- 95 TACTICAL AIR COMMAND
- 96 AIR DEFENSE COMMAND
- 97 AIR FORCE SYSTEMS COMMAND
- 98 AF COMMUNICATIONS SERVICE
- 99 RADC-RAALD, GRIFFISS AFB
- 100-101 AF CAMBRIDGE RESEARCH CENTER
- 102-104 AFWL WLL-3 KIRTLAND AFB
- 105 SCHOOL OF AVIATION MEDICINE
- 106-108 AERONAUTICAL SYSTEMS DIVISION
- 109-110 USAF PROJECT RAND
- 111 ELECTRONIC SYSTEMS DIV ESAT
- 112 AIR TECHNICAL INTELLIGENCE CENTER
- 113 HQ USAF AFORD
- 114 HQ USAF AFXPDK

#### OTHER DEPARTMENT OF DEFENSE ACTIVITIES

- 115 DIRECTOR OF DEFENSE RESEARCH AND ENGINEERING
- 116 ASST TO THE SECRETARY OF DEFENSE ATOMIC ENERGY
- 117-118 ADVANCE RESEARCH PROJECT AGENCY
- 119 WEAPONS SYSTEM EVALUATION GROUP
- 120-123 DEFENSE ATOMIC SUPPORT AGENCY
- 124 FIELD COMMAND DASA
- 125 FIELD COMMAND DASA FCTG
- 126-127 WEAPONS TEST DIV., DASA, SANDIA, WTW-TI
- 128 DEFENSE COMMUNICATIONS AGENCY
- 129 JOINT TASK FORCE-8
- 130 COMMANDER-IN-CHIEF PACIFIC
- 131 COMMANDER-IN-CHIEF ATLANTIC FLEET
- 132 STRATEGIC AIR COMMAND
- 133 CINCONAD
- 134 DIR, DEFENSE INTELLIGENCE AGENCY
- 135-154 DEFENSE DOCUMENTATION CENTER

#### POB CIVILIAN DIST. CAT. B 1

- 155 AEROSPACE CORPORATION
- 156 AEROJET GENERAL NUCLEONICS SAN RAMON CALIF
- 157 FORD MOTOR CO NEWPORT BEACH CALIF ATTN TECH LIBRARY
- 158 AEROSPACE CORP EL SEGUNDO CALIF
- 159 ALLIED RESEARCH ASSOC. INC CNCORD MASS
- 160 AMER. SCIENCE GENG CO CAMBRIDGE MASS
- 161 IIT RESEARCH INSTITUTE CHICAGO ILL.
- 162 AVCO CORP EVERETT MASS
- 163 AVCO CORP WILMINGTON MASS ATTN TECH. LIBRARY
- 164 BMI COLUMBUS OHIO ATTN DEFENDER INFO CENTER
- 165 BELL TEL LAB. WHIPPANY NEW JERSEY
- 166 BENDIX CORP. SOUTHFIELD, MICH.
- 167 BOEING COMPANY SEATTLE WASHINGTON ATTN TECH LIBRARY
- 168 COLLINS RADIO CO CEDAR RAPIDS IOWA
- 169 COLUMBIA UNIV ELEC RESEARCH LAB NEW YORK
- 170 CORNELL AERONAUTICAL LAB INC BUFFALO NY
- 171 DEFENSE RESEARCH CORP SANTA BARBARA ATTN WEITZ
- 172 DOUGLAS AIRCRAFT CORP SANTA MONICA CALIF
- 173 EDGERTON GERMESHAUSEN & GRIER INC BOSTON
- 174 E H PLESSET ASSOC INC LOS ANGELES ATTN TECH. LIBRARY
- 175 ELECTRO-OPTICAL SYSTEMS PASADENA CALIF
- 176 SPERRY RAND CORP LONG ISLAND N Y
- 177 GEN DYNAMICS ASTRO DIV SAN DIEGO ATTN HAMLIN
- 178 GEN DYNAMICS GEN ATOMIC DIV SAN DIEGO ATTN T I S
- 179 GEN DYNAMICS CORP FT WORTH TEXAS
- 180 GEN ELEC CO ADVANCED ELEC CENTER ITHACA N Y
- 181 GEC TECH MIL PLANNING OPER SANTA BARBARA ATTN DASA
- 182 SYLVANIA DIV ELEC DEF LAB MT VIEW CALIF

# SECRET

182 GEOPHYSICS CORP OF AMER BEDFORD MASS  
184 H R B SINGER INC STATE COLLEGE PA  
185 SECURE-ENTRY SYSTEMS DEPT ATTN TECH INFO CENTER  
186 MOHLS AIRCRAFT CO CULVER CITY CALIF ATTN HANSCOME  
187 INST FOR DEFENSE ANALYSIS WASHINGTON  
188 INTER TEL & TELER CORP MURLEY N J  
189 J HOPKINS UNIV APPL PHYSICS LAB SILVER SPRING  
190 ARMAN NUCLEAR COLORADO SPRINGS ATTN SMELTON  
191 LOCKHEED AIRCRAFT CORP PALO ALTO CALIF ATTN MEYROTT  
192 MARTIN MARITIME CO DENVER COLORADO  
193 LINCOLN LABORATORY ATTN TECH LIBR PANNELL  
194 MITRE CORP BEDFORD MASS ATTN TECH LIBRARY  
195 MITCHELL RESEARCH ASSOC INC  
196 N AMERICAN AVIATION DOWNEY CALIF  
197 NORTHROP AIRCRAFT INC PALMDALE CALIF  
198 RCA DEFENSE & COMM PRODUCTS MOUNTAIN VIEW ATTN ENGR. LHM  
199 RCA DAVID SARNOFF RES CENTER PRINCETON NJ  
200 THOMPSON SUBMORPHONE CALIF ATTN TECH LIBRARY  
201 RAND CORP SANTA MONICA CALIF  
202 RANT-TECH CO MISSILE & SPACE DIV BEDFORD MASS  
203 REPUBLIC AVIATION FARMINGDALE LI NY

204 SPACE GEN CORP EL MONTE CALIF  
205 SP-TECH LAB LOS ANGELES CALIF  
206 STANFORD RESEARCH INST ATTN TECH LIBR  
207 STANFORD RESEARCH INST ATTN RADIO PHYSICS LAB  
208 TECH OPER INC BURLINGTON MASS ATTN RICHARDS  
209 UNIV OF MICHIGAN ANN ARBOR MICH ATTN BAHIRAC LIBR  
210 VITRO CORP OF AMERICA WEST ORANGE N J  
211 WESTINGHOUSE RESEARCH LAB PITTSBURGH PA  
212 WESTINGHOUSE ELEC CORP WASH DC ATTN PRYTULA  
213 NATIONAL BUREAU OF STANDARDS BETHESDA MD  
214 GENERAL ELECTRIC CO DEF ELEC DIV

## ATOMIC ENERGY COMMISSION ACTIVITIES

215-217 AEC WASHINGTON TECH LIBRARY  
218-219 LOS ALAMOS SCIENTIFIC LAB  
220-234 SANDIA CORPORATION  
235-244 LAWRENCE RADIATION LAB LIVERMORE  
245 NEVADA OPERATIONS OFFICE LAS VEGAS  
246 DTIC OAK RIDGE MASTER  
247-276 DTIC OAK RIDGE SURPLUS

# SECRET